



# Gravitational Dynamical Systems

Alicia Simon-Petit

## ► To cite this version:

Alicia Simon-Petit. Gravitational Dynamical Systems. Dynamical Systems [math.DS]. Université Paris Saclay (COMUE), 2018. English. NNT : 2018SACL021 . tel-01997477

**HAL Id: tel-01997477**

**<https://pastel.hal.science/tel-01997477>**

Submitted on 2 Apr 2019

**HAL** is a multi-disciplinary open access archive for the deposit and dissemination of scientific research documents, whether they are published or not. The documents may come from teaching and research institutions in France or abroad, or from public or private research centers.

L'archive ouverte pluridisciplinaire **HAL**, est destinée au dépôt et à la diffusion de documents scientifiques de niveau recherche, publiés ou non, émanant des établissements d'enseignement et de recherche français ou étrangers, des laboratoires publics ou privés.

# THÈSE DE DOCTORAT

de

L'UNIVERSITÉ PARIS-SACLAY

École doctorale de mathématiques Hadamard (EDMH, ED 574)

*Établissement d'inscription :* École nationale supérieure de techniques avancées

*Laboratoire d'accueil :* Unité de mathématiques appliquées, ENSTA-CNRS-INRIA

*Spécialité de doctorat :* Mathématiques aux interfaces

**Alicia SIMON-PETIT**

Systèmes dynamiques gravitationnels

*Date de soutenance :* 10 Décembre 2018

*Après avis des rapporteurs :* JULIEN LARENA (University of Cape Town)  
JEAN-PIERRE MARCO (Université Pierre et Marie Curie)

	PIERRE-HENRI CHAVANIS	(Université Paul Sabatier) Examinateur
	ALAIN CHENCINER	(Université Paris VI) Examinateur
	GUILLAUME DUVAL	(INSA Rouen) Invité
	JACQUES FEJOZ	(Université Paris-Dauphine) Examinateur
<i>Jury de soutenance :</i>	ERIC GOURGOULHON	(Observatoire de Paris-Meudon) Examinateur
	CHRISTOPH KOPPER	(Ecole Polytechnique) Président
	JULIEN LARENA	(University of Cape Town) Rapporteur
	JEAN-PIERRE MARCO	(Université Pierre et Marie Curie) Rapporteur
	JÉRÔME PEREZ	(ENSTA ParisTech) Directeur de thèse



A ma sœur Marie,

à ma mère.







# Acknowledgment

---

À Jérôme Perez pour ces années de recherche parcourues ensemble. Merci pour ces heures paraboliques dédiées aux isochrones, ton regard éclairé d'astrophysicien, ta bienveillance naturelle. A Guillaume Duval et Guillaume Plum, pour toutes nos rencontres et discussions mathématiques et informatiques, lesquelles se concrétisent par cette thèse.

Je tiens à remercier particulièrement Jean-Pierre Marco, maître de conférences à l'Université Pierre et Marie Curie, pour avoir suivi mon travail avec un intérêt et un enthousiasme constant, et Julien Larena, maître de conférences à l'Université du Cap, pour sa grande disponibilité et sa prompte attention à ma recherche. Je les remercie tous deux de me faire l'honneur d'être rapporteurs de ma thèse. Mes remerciements s'adressent également à Pierre-Henri Chavanis, directeur de recherche CNRS à l'Université Paul Sabatier, pour ses échanges sincères et avisés, à Alain Chenciner, professeur émérite de mathématiques à l'Université Paris VI et à l'Observatoire de Paris, et Jacques Féjoz, professeur de mathématiques à l'Université Paris-Dauphine et à l'Observatoire de Paris, pour m'avoir inspirer par leur engagement et authenticité la vocation de chercheur, à Ericourgoulhon, directeur de recherche CNRS à l'Observatoire de Paris-Meudon, pour sa sollicitude et son intérêt immédiat pour mon travail, à Christoph Kopper, enseignant-chercheur et président du Département de Physique de l'Ecole Polytechnique, pour son écoute attentive et son enseignement clair en physique mathématique. Je les remercie de me faire l'honneur de participer à mon jury de thèse. Leurs recherches et enseignements sont autant de modèles exemplaires et éducateurs que je souhaite à chacun de rencontrer.

Ma plus profonde gratitude s'adresse à l'Unité de Mathématiques Appliquées de l'ENSTA ParisTech et l'ensemble de ses membres pour leur accueil au sein de leur équipe. L'interdisciplinarité est une richesse inestimable qui pare ce laboratoire, qu'ils trouvent ici ma vive reconnaissance pour l'abondant enseignement et l'attention qu'ils m'ont prodigués.

Merci à Marc Lenoir, Davide Boschetto, Jérôme Perez, Guilhem Gallot et Christoph Kopper pour m'avoir proposé d'enseigner dans leurs cours et département, et pour leur confiance.

Aux professeurs et chercheurs qui ont semé leur graine sur ma route, merci à Mme Faillard, Sallet Kalité, Pascale Dekker, André Füzfa, Stéphane Mathis, Pierre Jacquemin. Un immense merci à l'ensemble de l'Institut de Mécanique Céleste et Calcul des Ephémérides de l'Observatoire de Paris, qu'ils trouvent ici l'expression de ma profonde sympathie, et une pensée spéciale pour les membres de l'équipe Astronomie et Systèmes Dynamiques. Merci à Alain Albouy pour sa grande ouverture et son partage scientifique, historique et humain inestimable.

Aux lecteurs assidus de ce manuscrit et amis, Faisal, Laure et Rafael, merci pour votre dévouement et votre patience. Pour nos échanges scientifiques, linguistiques, interludes musicaux et simplement notre amitié, merci à Laure, Rafael, Faisal, Dmitry, Maryna, Geoffrey, Nicolas, Marc, Antoine, Emile, Félix, Théodore, Nicolas, Lucien, Léandre, Samuel, Sandrine, Yohanes, Damien, Clément, Maria, Hervé, Gwenaël, Frédéric, Abed, Farida, Nathan, Jessica, Alexandre, Thibaut, Alexis, Léo, Timothée, Arthur, Lucas, Anne, Maud et bien d'autres encore. Merci à Sofya, Arnaud, Damien, Luca, Achille, Han-Hoe des "co-bureaux" inoubliables.

A ma famille pour leurs encouragements et soutien fidèle. A la famille Spindler, dont l'esprit, l'amitié et la sympathie m'ont accompagnée jusqu'à là, qu'ils trouvent ici un hommage à leur précieux travail du bois. A ma grand-mère et ma grande-tante, pour leur affection et bonne humeur. A ma mère et à ma sœur, pour leur amour et leur patience, toute mon affection.

Un grand merci à tous pour votre accompagnement dans cette aventure.



## Résumé

---

L'HISTOIRE séculaire des systèmes dynamiques puise ses origines dans le développement du cadre mathématique en astronomie. L'objet de cette thèse est l'étude de propriétés de la gravitation de ce point de vue de la dynamique à différentes échelles cosmologiques.

Dans la théorie du potentiel, l'isochronie définit généralement le mouvement d'oscillation harmonique de pendules. En 1959, le mathématicien et astronome Michel Hénon étend cette définition afin de caractériser les oscillations orbitales d'étoiles, autour du centre du système à symétrie sphérique auquel elles appartiennent. Dans ce cas, la période d'oscillation peut dépendre de l'énergie de l'étoile. Aujourd'hui, son potentiel isochrone est majoritairement utilisé en simulation numérique pour ses propriétés analytiques d'intégrabilité, mais demeure par ailleurs souvent méconnu. Dans cette thèse, nous revisitons la caractérisation géométrique de l'isochronie comme initiée par Michel Hénon et complétons ainsi la famille des potentiels isochrones en physique. La classification de cet ensemble sous l'action de divers groupes mathématiques met en évidence une relation privilégiée entre les isochrones. Nous montrons alors la nature keplérienne intrinsèque aux isochrones, laquelle est au cœur de la nouvelle relativité isochrone que nous présentons.

Les conséquences de cette relativité en mécanique céleste, à savoir la généralisation de la troisième loi de Kepler, celle de la transformation de Bohlin ou Levi-Civita, et le théorème de Bertrand, conduisent à l'analyse du résultat d'un effondrement gravitationnel. Une analyse isochrone est développée pour caractériser un état de quasi-équilibre de systèmes auto-gravitants isolés, comme certains amas stellaires ou galaxies dynamiquement jeunes, à partir de propriétés orbitales de leurs étoiles ou contenu physique.

A l'échelle cosmologique, la dynamique de l'univers dépend de sa composition énergétique. Elle peut s'exprimer sous forme d'un système dynamique conservatif, bien connu en écologie pour décrire la dynamique de populations variées. Ce modèle dit de Lotka-Volterra est exploité pour décrire un espace-temps globalement homogène et isotrope, dont les composantes peuvent être en interaction non uniquement gravitationnelle. Dans cet univers jungle, des comportements dynamiques effectifs à grande échelle peuvent alors se développer.

**Mots clefs** Gravitation, mécanique céleste, relativité isochrone, systèmes auto-gravitants, galaxies : évolution, amas globulaires, dynamique, cosmologie : énergie noire.





# Abstract

---

*D*YNAMICAL systems have a centuries-long history with roots going back to the mathematical development for astronomy. In the modern formalism, the present thesis investigates dynamical properties of gravitation at different astrophysical or cosmological scales.

In potential theory, isochrony often refers to harmonic oscillations of pendulums. In 1959, the mathematician and astronomer Michel Hénon introduced an extended definition of isochrony to characterize orbital oscillations of stars around the center of the system which they belong to. In that case, the period of oscillations can depend on the energy of the star. Today, Michel Hénon's isochrone potential is mainly used for its integrable property in numerical simulations, but is not widely known. In this thesis, we revisit his geometrical characterization of isochrony and complete the family of isochrone potentials in physics. The classification of this family under different mathematical group actions highlights a particular relation between the isochrones. The actual Keplerian nature of isochrones is pointed out and stands at the heart of the new isochrone relativity, which are presented together.

The consequences of this relativity in celestial mechanics — a generalization of Kepler's Third law, Bohlin or Levi-Civita transformation, Bertrand's theorem — are applied to analyze the result of a gravitational collapse. By considering dynamical orbital properties, an isochrone analysis is developed to possibly characterize a quasi-stationary state of isolated self-gravitating systems, such as dynamically young stellar clusters or galaxies.

At a cosmological scale, the dynamics of the universe depends on its energy content. Its evolution can be expressed as an ecological dynamical system, namely a conservative generalized Lotka-Volterra model. In this framework of a spatially homogeneous and isotropic spacetime, named Jungle Universe, the dynamical impact of a non-gravitational interaction between the energy components is analyzed. As a result, effective dynamical behaviors can arise.

**Keywords** Gravitation, celestial mechanics, isochrone relativity, self-gravitating systems, galaxies: evolution, globular clusters, dynamics, cosmology: dark energy.





# Contents

---

Acknowledgment	5
Résumé - Abstract	7
List of figures and tables	13
Introduction	16
<b>I Isochrony</b>	<b>21</b>
<b>1 Isochrony in physics</b>	<b>23</b>
1.1 Isochronous potentials, a widely spread notion . . . . .	23
1.2 Isochrony as defined by Michel Hénon . . . . .	25
<b>2 Hénon's isochrony</b>	<b>29</b>
2.1 Hénon's isochrony in potential theory . . . . .	29
2.2 Geometric characterization of isochrony . . . . .	32
2.3 Classification of isochrone potentials . . . . .	35
2.3.1 The space of isochrone parabolas . . . . .	35
2.3.2 Isochrone parabolas and potentials' congruity . . . . .	37
2.3.3 The space of isochrone potentials . . . . .	41
2.4 Physics of isochrone potentials . . . . .	42
2.4.1 Isochrone physical systems . . . . .	42
2.4.2 Isochrone orbits . . . . .	44
2.4.3 The Bertrand theorem . . . . .	46
2.5 Isochrones' relationships, on the road to isochrone relativity . . . . .	47
<b>3 Isochrone relativity</b>	<b>49</b>
3.1 From Hooke to Kepler . . . . .	49
3.2 Isochrone transformations . . . . .	51
3.2.1 The BOLST transformation . . . . .	51
3.2.2 The $\mathbf{i}$ -BOLST transformation . . . . .	52
3.3 The essence of isochrony . . . . .	54
3.3.1 Isochrone structure of the affine plane . . . . .	54
3.3.2 Relativity of isochrone orbits . . . . .	55
3.3.3 Dictionary for isochrone and special relativity . . . . .	57
3.4 Generalization of Kepler's Third Law . . . . .	57
3.5 Conclusion . . . . .	61



<b>4</b>	<b>Isochrony and evolution of self-gravitating systems</b>	<b>63</b>
4.1	Isolated self-gravitating systems . . . . .	63
4.1.1	Overview of isolated self-gravitating systems evolution . . . . .	63
4.1.2	Modeling isolated self-gravitating systems . . . . .	64
4.2	Description of the numerical simulations . . . . .	65
4.2.1	Initial conditions . . . . .	65
4.2.2	Numerical integrator . . . . .	66
4.3	Numerical experiments . . . . .	67
4.3.1	Density profiles and simulation observables . . . . .	67
4.3.2	Isochrone analysis of the simulated dynamics . . . . .	67
4.4	An isochrone stage for isolated self-gravitating systems . . . . .	72
4.5	Isochrony in astrophysics . . . . .	75
4.5.1	Isochrony in self-gravitating systems . . . . .	75
4.5.2	Loss of isochrony . . . . .	76
4.5.3	Conclusion and perspectives . . . . .	76
<b>II</b>	<b>Cosmology</b>	<b>81</b>
<b>5</b>	<b>Universe description</b>	<b>83</b>
5.1	Equations of the dynamics . . . . .	83
5.1.1	A curved spacetime . . . . .	83
5.1.2	Einstein's equations . . . . .	85
5.2	The expanding Universe . . . . .	90
5.2.1	Constraining the geometry . . . . .	90
5.2.2	Describing the energy content . . . . .	91
5.2.3	Friedmann - Lemaître equations . . . . .	92
5.3	The Universe as a gravitational dynamical system . . . . .	93
<b>6</b>	<b>Jungle interaction in the Universe</b>	<b>97</b>
6.1	Lotka-Volterra systems . . . . .	97
6.2	An ecological framework for the standard model of cosmology . . . . .	98
6.3	Jungle interactions enrich the standard model . . . . .	100
6.4	Camouflage in the Jungle . . . . .	102
6.5	Questioning the nature of dark energy . . . . .	105
	<b>Conclusion and Perspectives</b>	<b>109</b>
	<b>Bibliography</b>	<b>111</b>
	<b>Annexe</b>	<b>121</b>
	<b>French Summary</b>	<b>127</b>
	<b>Complement: Isochrony in 3D central potentials (SPD)</b>	<b>130</b>



# List of Figures

---

1.1	Isochronous oscillation. Galileo Galilei observes the chandelier in the Cathedral of Pisa . . . . .	24
1.2	Huyghens' isochronous pendulum clock . . . . .	25
1.3	Asymmetric isochronous potentials . . . . .	26
1.4	The globular cluster NGC362 . . . . .	26
2.1	Effective potential . . . . .	30
2.2	Orbital characteristics of PROS . . . . .	32
2.3	Geometric view of Hénon's variables . . . . .	33
2.4	Transvection action on tilted isochrone parabolas . . . . .	37
2.5	Classes of equivalence of isochrone parabolas . . . . .	38
2.6	Canonical isochrone parabolas . . . . .	39
2.7	Isochrone parabolas and potentials correspondence . . . . .	41
2.8	Mass repartition in isochrone potentials . . . . .	43
2.9	Rotation and transvection of the Kepler parabola to a Hénon one . . . . .	47
3.1	Two special BOLSTS . . . . .	52
3.2	General BOLST transformation . . . . .	53
3.3	Potentials relativity . . . . .	53
3.4	Isochrone-relativistic structure of the affine plane . . . . .	62
4.1	Evolution of observables in simulations . . . . .	68
4.2	Mass density comparison: simulation result, King and isochrone models . . . . .	69
4.3	Diverse types of orbits in the simulations of a gravitational collapse . . . . .	70
4.4	3D representation of an orbit in a King model . . . . .	71
4.5	Isochrone test of a King model and a collapsed Hénon sphere . . . . .	73
4.6	Second isochrone test of a King model and a collapsed Hénon sphere . . . . .	74
4.7	Evolution of the density in a Hénon sphere of initial virial ratio $\kappa = -0.5$ . . . . .	75
5.1	Light propagation and equivalence principle . . . . .	85
5.2	Standard cosmological model . . . . .	93
6.1	Evolution of three coupled fluids in the Jungle . . . . .	101
6.2	Interaction between three dark matter fluids with effective dark energy . . . . .	106





## List of Tables

---

3.1	Special - isochrone relativities dictionary . . . . .	58
4.1	Statistical analysis for the sets $[\ln(a), \ln(\tau_r)]$ in the simulations K and H. . . . .	72





# Introduction

---

**D**YNAMICAL systems stem from abundant studies in mechanics and astronomy. Their mathematical theory is probably born with the reports “Sur les courbes définies par les équations différentielles” — “On the curves defined by the differential equations” — by Henri Poincaré in 1881 [30]. Its purpose consists in accurately describing the asymptotic (over large time scales) behavior of the solutions of differential equations. For that, a phase space contains all possible positions and momentum (velocities) for a system. The modelization of physical laws then constrain the dynamics of the system to evolve in a determined way in the phase space, following an evolution law.

In the present thesis, we address the modeling of dynamical systems in which gravitation plays a crucial role due to their relative large sizes. This long-range interaction has an impact on small, astrophysical and cosmological scales.

What does gravitation teach us about gravitational dynamical systems? What is the role of gravitation in their evolution? These are crucial questions for better understanding their behavior in classical or relativistic gravitation theories.

## Isochrony and the $N$ –body problem

Remarkably, the fundamental ideas for the theory of dynamical systems rely on the study of few but crucial problems of mechanics. The three-body problem in celestial mechanics or oscillators in various domains of physics is one such example. The first aims at understanding the evolution of a system of  $N = 3$  point masses interacting only by gravitational forces. As shown by Poincaré, there is no closed-form solutions for this problem and solutions are said to be non-analytic, that is they cannot be written as a mathematical expression that can be evaluated in a finite number of operations. The problem is said to be non integrable, but some persistent properties of the dynamics can be understood thanks to the investigation of periodic solutions for instance.

When the number  $N$  of bodies becomes much larger or tends to infinity, the number of degrees of freedom, which completely determines all occupied spatial positions in a system, and thus the number of differential equations to solve, increases as  $3N$  for three-dimensional physical systems. Nevertheless, the study of their symmetries as well as the usage of statistical laws or continuous models as in potential theory provide fair descriptions for the dynamics.

The second example of dynamical system problems we mentioned above deals with oscillators. We will focus on particular oscillation dynamics. In classical mechanics, isochrony often characterizes equal-period oscillations. In 1959, the mathematician and astronomer Michel Hénon introduced an extended definition for isochrony, for oscillations with energy-dependent periods. This dynamical property can actually arise for “oscillating” (see chapter 1) trajectories of stars in spherically symmetric stellar clusters. Such systems are defined by so-called isochrone potentials.

In potential theory, we adopt an original geometrical approach initiated by Michel Hénon. The investigation of the isochrone property in orbital differential equations leads to the completion of

the family of isochrone potentials (chapter 2). Consequently, relationships between isochrone systems can be developed, by generalizing the well-known Levi-Civita or Bohlin transform (chapter 3). The subsequent new isochrone relativity, by analogy with special relativity, allows a better comprehension of the notion of isochrony in relation with the Kepler potential of the two-body problem.

## Isochrony in the dynamics of self-gravitating systems

Self-gravitating systems define objects which are retained by their own gravitational field. In the 1960's, the observational data of luminosity profiles suggested the possibility for special self-gravitating systems, such as certain globular clusters, to be isochrone as noticed by Michel H  non.

Globular clusters are stellar systems composed of  $10^3$  to  $10^6$  stars. Our Galaxy contains about 200 globular clusters spherically distributed in its halo around its bulge. These spherical or quasi-spherical and ancient objects are generally thought to be born along with their host galaxies, and are thus relatively stable. Their masses lie in-between  $10^3$  and  $5.10^6 M_\odot$ . Apparently, they do not contain interstellar dust nor gas, and dark matter appears not to be necessary to account for their dynamics. In addition, these very dense systems (with a mean density of  $10^4 M_\odot.\text{pc}^{-3}$  compared with  $0.05 M_\odot.\text{pc}^{-3}$  in the solar neighborhood) can generally be considered as isolated in their environment and thus evolve quite independently of their galactic neighborhood in the first stages of their life. Therefore, globular clusters are almost perfect self-gravitating systems for the  $N$ -body problem [78] p.30. Their relatively small sizes (about 1/1000 of the size of the host galaxy) make them stand as points in the galactic potential. Over long intervals of time (typically the age of the universe) they undergo a slow gravitational relaxation which affects their internal repartition of mass. In some cases, when they are hosted by a spiral galaxy, they are periodically harassed when they pass through the galactic plane. Such effects have to be taken into account in a long term analysis of such clusters. We are interested in the present work in the quasi-steady state which emerges after their formation process which could be summarized by the violent relaxation model.

Another example of almost isolated self-gravitating systems are Low Surface Brightness (LSB) galaxies. LSB galaxies are dark-matter dominated galaxies where the stellar populations contribute much less to their observed rotation curves than dark-matter does [39]. These galaxies have a low star formation rate and are therefore of low surface brightness, even though their pronounced blue color suggests the current formation of stars [155, 106]. Their visible structures are often contained in a disc, but show various morphologies [40]. These discs are much more stable than for high surface brightness (HSB) galaxies. LSB galaxies are very common, may be located either in field or in cluster environment [58], and appear to be more isolated than normal HSB galaxies [133]. What makes them special from a dynamical point of view is their dark matter halos, which can present a spherical symmetry and play crucial regulating roles in the stability of the discs [58]. Hence, they dynamically behave as if they were almost isolated and not much influenced by their environment. Then, they evolve more quietly than HSBs and provide an insight into the evolution of galaxies in unperturbed environments.

As fundamental bricks for dating astrophysical systems for example, the evolution of these self-gravitating systems is deeply investigated with several approaches. In statistical physics, they can be described by distribution functions which contain all the reachable position and momentum in the phase space of the system and satisfy the gravitational Boltzmann equation that sets the evolution law. Its collisionless version (Vlasov-Poisson equation) is commonly adopted in

the context of the gravitational  $N$ -body problem because the time for two-body encounters or collisions (two-body relaxation time) is much larger than the time for a star to cross the system (dynamical time). There exist then several possible approaches to choose the equilibrium distribution functions: from thermodynamics as the result of a violent relaxation (isothermal spheres or polytropic systems) and through stability analysis. Self-gravitating systems have a particular thermodynamics, initially described by Antonov, and then Lynden-bell and Wood ([78]). Their main specificity resides in their negative specific heat, i.e. the more they expand the hotter they become, and the more they collapse the colder they are, which leads to the unequivalence between usual statistical ensembles. With a temperature related to velocity dispersion, this means that regions losing heat will actually increase their density, possibly leading to the so-called gravothermal catastrophe (and core collapse for globular clusters see chapter 4) in this unstable thermodynamics. Kinetic models are additionally (gravitational Boltzmann equation also known as Vlasov-Poisson equation) under active investigation [112]. After Jeans' first works, principal stability studies have been carried out by Antonov and successive researchers [4, 121, 60, 156]. To summarize, the accepted evolution of gravitational systems as globular clusters over long intervals of time (typically the age of the universe) is a slow gravitational relaxation which affects their internal repartition of mass.

However, the formation process of these self-gravitating systems remains an open problem. Taking into account analytical and observational constraints several spherical models are possible (see [78], especially Plummer or other polytropic models, de Vaucouleur's law  $r^{1/4}$ , King model and Hénon's isochrone, Hernquist for spherical isotropic systems, Ossipko-Meritt for the anisotropic or generalized polytropes). Nevertheless, none of them can be taken for sure as the initial condition for the following evolution since they only characterize global luminosity profiles but no physically-justified stellar dynamics. The isochrone relativity we have constructed and the generalization of the Third Kepler law are employed to analyze the numerical results of gravitational collapses (chapter 4). We are then able to determine whether the violent relaxation process leads to an isochrone quasi-stationary state for isolated self-gravitating systems.

## Cosmology

The evolution of the precedent gravitational dynamical systems also has to be considered in a cosmological context. In the context of the general theory of relativity, the universe is itself a dynamical system. In the universe, classical properties of gravitation are still influential but are completed by new possibilities. The isotropic and homogeneous universes of Friedmann, Lemaître and Einstein date back to the first part of the XX<sup>th</sup> century. Numerous solutions of Einstein's equations for the general theory of relativity have then been exhibited. They are all described by systems of differential equations with various properties and need very modern analyses, e.g. [158, 138].

The dynamics of the universe can be formulated in terms of dynamical systems. The universe evolution law depends on its energy content. In the standard model of cosmology, with the  $\Lambda$ CDM model which is in concordance with several experimental, observational as well as theoretical constraints, the universe is assumed to be filled by ordinary matter, dark matter and a cosmological constant. As dark energy the latter should cause the observed accelerated expansion of the universe. This notion of expansion is introduced and developed in three short movies which we have done to present its historic origin and meaning in cosmology [125]. Understanding the theoretical grounds of this model enables one to consider late- or early-time cosmological solutions (illustrated in chapter 5). The natural dynamics in the standard model is actually similar to the one in an ecological predator-prey model (chapter 6). This particular



framework allows us to enrich the idealized isotropic and homogeneous universe model through so-called Jungle interactions and highlight emergent effective behaviors.

The annexe contains an introduction to differential geometry, detailed for the needs of the derivation of Einstein's equations in chapter 5.

In the complement, the original paper on isochrone relativity is attached and referred to as SPD. It contains useful detailed proves as well as a diverse constructive approach as the one presented in part I.

Part I

Isochrony





# Isochrony in physics

---

*I*SOCHRONY commonly refers to events that occur at the same time or with the same period. For example, two clocks are generally isochronous in Newtonian physics. In astrophysics, stellar isochrones are curves where each point represents a star of a given age whatever its mass. They are used for a theoretical determination of age and derive ages and metallicities, especially for stellar clusters.

In this chapter and the following ones, we will consider the definition of isochrony in the context of the potential theory. As we will see, isochrony is then often synonymous with oscillations of constant period but can also be extended to some properties of self-gravitating systems.

## 1.1 Isochronous potentials, a widely spread notion

According to tradition, it is by observing the chandelier of the cathedral in Pisa that Galileo noticed an important feature of its pendulum behavior, see figure 1.1. It was oscillating with different amplitudes but always with the same period! After several experiments with pendulums of varying masses, made of lead and cork for instance, he asserted that the period of a pendulum is always the same: it does not depend on the amplitude of its oscillations, which decrease in time because of friction. Moreover, he also clarifies its determination: “The length of the pendulums are proportional to the square of their period”, as explained in *Dialogo intorno ai due massimi sistemi del mondo, Tolemaico e Copernicano*, published in 1632.

A few years later, the French priest Marin Mersenne pointed out in his book *Nouvelles pensées de Galilée* a mistake in Galileo’s remarks and explained that his conclusions are only valid when the oscillations of the pendulum are of small amplitudes. Otherwise, the period is longer and depends on the maximum height that is reached by the masses.

This behavior of equal-period oscillations has been progressively called isochronous.

In 1658, the physicist, mathematician and astronomer Christiaan Huyghens built on this notion to solve a mechanical problem for the construction of clocks. At that time, measuring latitudes was relatively easy by comparing meridian passages of stars. But measuring longitudes, which was of vital importance for sea navigations, was a difficult task because it demanded a very accurate measurement of time. Huyghens constructed a pendulum clock which improved the accuracy of time measurements, but this was not enough to guarantee a safe measurement of longitude. Since he knew that the simple pendulum gave equal periods only for small amplitudes, he started to look for an isochronous pendulum, with the objective of improving maritime chronometers. So that they would not change the period of oscillation even if their amplitudes changed due to a rough sea.

For that, he needed to put lateral obstacles of appropriate shape near a simple pendulum but was not able to find empirically the exact shape. By chance, he participated in a contest organized by Blaise Pascal at the same time. There, Pascal proposed six problems stemming



Figure 1.1: Galileo Galilei observes the chandelier in the Cathedral of Pisa. Affresco di Luigi Sabatelli, 1840 (Museo di Storia Naturale di Firenze - Sezione di Zoologia “La Specola” - Tribuna di Galileo).

from some problems he received from Mersenne, which he solved and deepened, see [149] and references therein for more details on the history. They dealt with the curve traced by a point on the circumference of a rolling circle, namely the cycloid. Once Huyghens became familiar with the cycloid, he decided to test whether this would help him solve the isochronous pendulum problem.

In his work *Horologium oscillatorium*, published in 1673, he showed that the cycloid is a tautochrone curve — a curve on which a particle, sliding without friction and under the action of a constant gravitational force, would have a period that is independent of the height from which it was released. But he still needed to find the shape of the lateral obstacles that would make a pendulum follow a cycloidal trajectory. Fortunately, he tried again the cycloid and was successful, since the evolute of the cycloid is itself. The introduction of an arc of cycloid made the oscillations isochronous whatever their amplitude, see figure 1.2. His pendulum clock did not succeed as a marine chronometer because of its remaining sensitivity to sea perturbations. The preferred mechanism for marine chronometers, which went through centuries up to the introduction of electronic aids, relies on a fast-beating balance wheel controlled by a temperature-compensated spiral spring. It was proposed in 1761 by the cabinet-maker John Harrison, who then won the prize published by the British government in 1714 for elaborating such an accurate time-keeper. However, the tautochrone problem played an important role in the history of classical mechanics of the XVII<sup>th</sup> century, and gave rise to the development of curves analysis with many applications in differential geometry.

The tautochrone problem was solved during the second part of the XVIII<sup>th</sup> century by Lagrange who used a variational method. This piece of work constitutes the beginning of mathematical studies for the calculus of variations. In 2006, the paper [149] pointed out other

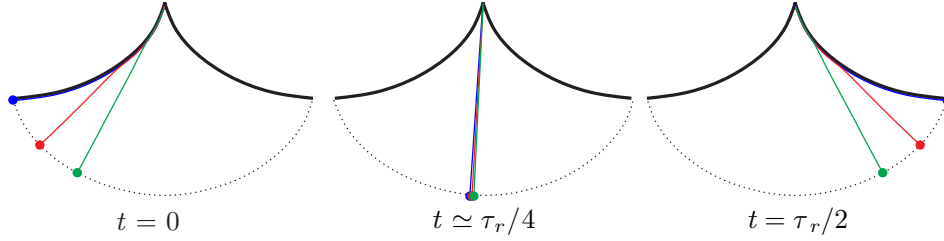


Figure 1.2: Huyghens' isochronous pendulum clock. Whatever their initial amplitudes, the three pendulums reach the center and their maximum height at the same time.

solutions besides the simple cycloid. These are related to sheared potentials introduced hereafter.

In modern classical mechanics, the one-dimensional motion of an oscillator or small oscillations of a pendulum are characterized by harmonic potentials

$$\psi_{\text{ha}}(q) = \frac{1}{2}\omega^2 q^2, \quad (1.1)$$

where  $q$  translates the amplitude of the oscillations and  $\omega$  gives their pulsation. Their periods only depend on the energy-independent pulsation  $\omega$ , hence the harmonic appellation. In the scientific literature, isochronous potentials are often synonymous with this harmonic potential but can also be more general. As a matter of fact, the harmonicity can be broken in so-called isochronous potentials which are obtained by shearing the parabolic well of  $\psi_{\text{ha}}$  in such a way that, at fixed energy, the distance between two turning points of the oscillation is preserved [44, 119, 3], see figure 1.3. From this shearing procedure, there is an infinite number of such isochronous potentials [90]. The analysis of the non-linear equation of motion and the isochrony condition lead to a generic construction of such isochronous potentials, giving an interpolation between them and the harmonic potential, as formulated by Bolotin and MacKay [20]. These potentials and their associated physical systems are asymmetric. The oscillations are said to be anharmonic but they all share the same period.

These isochronous potentials are abundantly studied in classical mechanics and quantum physics, although the energy quantum spectrum they create is not always equispaced as one might have expected from the analogy with a harmonic potential [44, 147, 24]. Physically, they can describe some symmetric or asymmetric molecular structures and can be used to account for dynamical properties such as resonances. Eventually, since they provide analytic material to explore these dynamical systems, an oscillatory behavior near some equilibria can obviously be described by the dynamics near isochronous equilibria, namely isochronous centers in phase space [29].

## 1.2 Isochrony as defined by Michel Hénon

Michel Hénon extended the definition of isochrony in the potential theory while he was working on the dynamics of globular clusters. Through the observation and first simulations of these stellar systems depicted in figure 1.4, he noticed two special orbital properties. He noticed that stars confined to the homogeneous center behave as in a harmonic oscillator, and that stars confined to the outer parts feel a Kepler potential, which characterizes the motion of a point mass distribution.

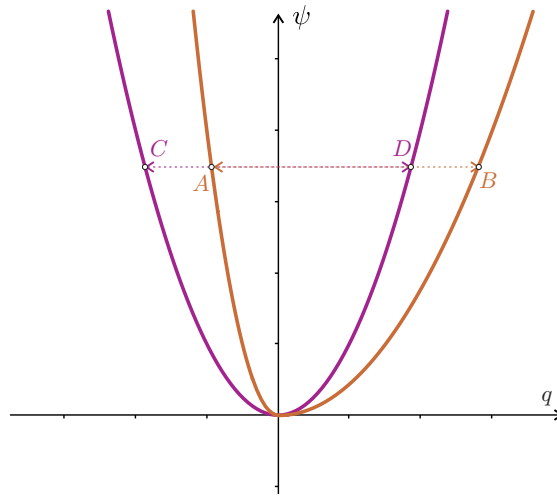


Figure 1.3: Asymmetric isochronous potentials. The harmonic potential is plotted in purple. In brown is plotted a sheared potential, such that the distance between the two turning points,  $A$  and  $B$  on the sheared parabola, and  $C$  and  $D$  on the harmonic parabola, is preserved. The period of oscillations between these points is then the same, whatever their ordinate heights.

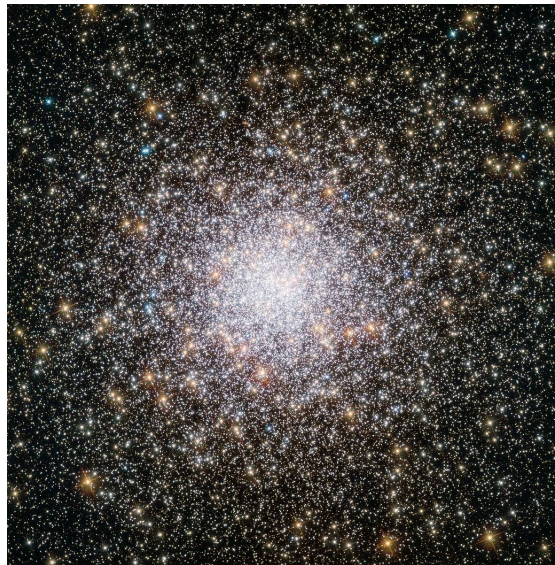


Figure 1.4: The globular cluster NGC362 — Source: ESA/Hubble & NASA. The dense central region can be approximated by a sphere of constant density, described by a harmonic potential. From the outer parts or the reader point of view, the cluster can be approximated by a sphere of small spatial extension, characterized by the Kepler potential.

The orbits are ellipses in both cases, and the associated orbital periods present common features. In a harmonic potential, stars share the same constant period

$$T = \frac{2\pi}{\omega}, \quad (1.2)$$

where  $\omega$  is related to the mass contained in the central region of the cluster, while in the Kepler potential, stars obey the third Kepler law

$$T = \frac{2\pi\mu}{|2\xi|^{3/2}}, \quad (1.3)$$

where  $\mu$  is also related to the central mass and  $\xi$  is the specific energy of the star. Remarkably, the periods are constant or only depend on  $\xi$ , but not on the angular momentum, the second degree of freedom which characterizes the orbit along with  $\xi$ . Michel Hénon then proposed looking for a general potential which could be characterized by this property. In other words, a potential in which all stars would move closer and away from the central region with a period, called radial period, that is independent from the angular momentum of the stars. The result was his famous isochrone potential.

Hénon's isochrone gives a mass density in good agreement with some of the observed globular clusters, as those available in 1959 when he published his seminal paper in French [68, 69, 70] (for an English translation see [77]). Afterwards, his model among others was praised because of its stability under small perturbations associated with its analyticity [78, 18]. It has been used to investigate the general dynamical mechanism that shapes galaxies [81, 97, 34, 113, 16]. Furthermore, it has been subject to many proofs with various distribution functions that preserve its mass density radial profile [87]. When expressed in flattened coordinates, with an anisotropic velocity distribution, it can account for general galactic shapes [54].

Its integrability in the Liouville sense [7], i.e. the existence of a maximal number of first integrals induced by the symmetries of the system, is of particular interest for analytic analyses. Its orbits can be integrated in terms of elementary functions no worse than inverse trigonometric functions, and the dynamics can be expressed in terms of angle-action variables [17, p.316]. For this reason, this model has been actively used in numerical simulations, e.g. [78, 107, 140] or much recently [66].

However, aside from its numerical advantages, Hénon's isochrone model has been progressively forgotten. In his conclusion, Michel Hénon proposed a mechanism based on resonances to explain the possibility of forming an isochrone stellar cluster. This scenario needed to be considered with respect to other processes, such as Lynden-Bell's violent relaxation, and proved more rigorously, but it has not been further investigated. In addition, the observational data refinement and the development of numerical simulations revealed a great variety of density profiles for self-gravitating systems, making Hénon's isochrone one among many.

Nevertheless, a conference in honor of Michel Hénon was organized in 2014. There, his isochrone model was revisited. With Guillaume Duval, who noticed a miss in the analytic derivation of Hénon's potential, and Jérôme Perez, who co-organized the conference and introduced Guillaume Duval to [68], we looked at Hénon's isochrone more closely. In the spirit of Michel Hénon, I have adopted a geometrical approach which easily highlights a miss in [68]. This point of view actually provides a larger family of isochrone potentials presented in chapter 2.

Chapter 3 is devoted to the isochrone relativity that stems from the physical relations between isochrone systems. The initial research and proofs have been published in [144]. This paper is attached to the present document in the complement page 131.



In light of these results, we investigate in chapter 4 whether isochrony could in fact be inherited from the formation process of isolated self-gravitating systems.



## Hénon's isochrony

---

*H*ÉNON'S isochrony defines specific properties of trajectories in three-dimensional spherically symmetric systems. Inside them, stars or particles of identical energy can share the same oscillation period, whatever the shape of their orbits for example.

In the present chapter, we introduce the new complete family of Michel Hénon's isochrone systems. As for the harmonic potential already presented, a geometrical characterization relates isochrones to specific curves in the affine plane. Then natural geometrical transformations, based on dynamical and mass repartition characteristics, enlighten a classification of isochrones. The physics that takes place in isochrone systems is considered and yields to revisiting a classical theorem of celestial mechanics. Opening the road to isochrone relativity, the relationships between isochrone systems are eventually investigated.

Hereafter the acronym SPD will refer to the article [144]. This detailed article is attached as a complement at the end of the present document. It contains useful detailed proves for the following two chapters as well as a diverse constructive approach.

### 2.1 Hénon's isochrony in potential theory

Let us first define the particular set of orbits (PROs) of particles that do not definitely escape a reasonable neighborhood of a gravitational system in a finite time. We may then rigorously define isochrone potentials.

We consider a spherically-symmetric stellar system described by a gravitational potential

$$\psi(\mathbf{r}) = \psi(r), \quad (2.1)$$

where  $\mathbf{r}$  is the position vector of a test particle of mass  $m$  confined in this system. By symmetry, the potential only depends on the distance  $r$  between the star and the center of mass of the cluster. The orbit of this test particle is contained in a plane, where the two parameters of this orbit are its energy  $E = m\xi$  and the norm of its angular momentum  $L = m\Lambda$ . These two degrees of freedom along with the potential  $\psi(\cdot)$  enables one to determine the radial distance  $r$  at each instant  $t$ . It is summarized in the definition of the energy of the star

$$\xi = \frac{1}{2} \left( \frac{dr}{dt} \right)^2 + \frac{\Lambda^2}{2r^2} + \psi(r) = \text{cst}, \quad (2.2)$$

which defines a differential equation for  $r : t \mapsto r(t)$ . The gravitational interaction is characterized by increasing potentials, since they satisfy Gauss' theorem in a spherical symmetry

$$\frac{d\psi}{dr} = \frac{GM(r)}{r^2} \quad (2.3)$$

with positive masses. Then, we may look for increasing potentials  $\psi(r)$  for which the ODE (2.2) admits periodic solutions, named hereafter Periodic Radial Orbits (PROs). The effective potential

$$\psi_e(r) = \frac{\Lambda^2}{2r^2} + \psi(r) \quad (2.4)$$

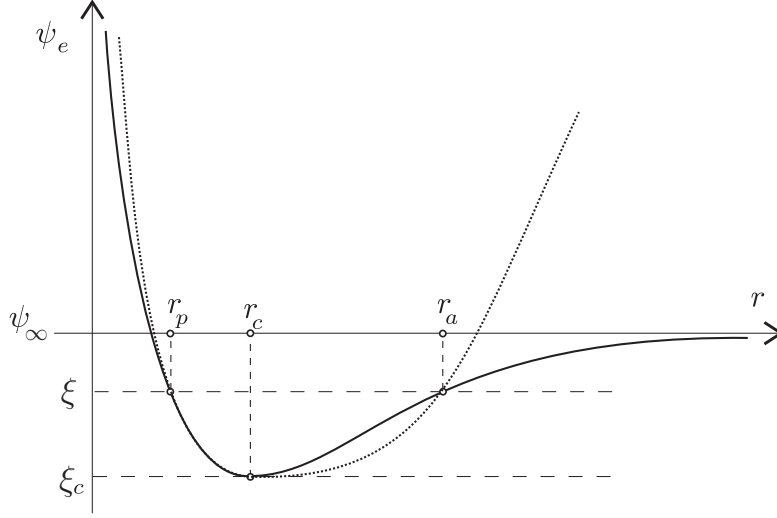


Figure 2.1: Physical effective potentials that allow Periodic Radial Orbits. The solid curve corresponds to a finite  $\psi_\infty$  and the dashed curve corresponds to an infinite  $\psi_\infty$ .

then reaches a global minimum and diverges to  $+\infty$  when  $r \rightarrow 0$  as shown in lemma 2.1 and figure 2.1. When they exist, the apoastron at distance  $r_a$  and periastron at  $r_p$  of a PRO are given by the two intersections of the graph of  $\psi_e$  with constant  $\xi$ -lines. For a given energy  $\xi_c$  corresponding to the minimum of  $\psi_e$ , the distance  $r_a = r_p$  and the orbit is circular. Lemma 2.1 specifies the behavior of the potential  $\psi$  when  $r \rightarrow 0$ , assuring the existence of a global minimum.

**Lemma 2.1.** *If for some  $\Lambda \geq 0$ , the effective potential  $\psi_e(r) \rightarrow +\infty$  when  $r \rightarrow 0$ , then  $\lim_{r \rightarrow 0} r^2 \psi(r) = \ell < \infty$ . Conversely, if  $\lim_{r \rightarrow 0} r^2 \psi(r) = \ell < \infty$ , then for any  $\Lambda \geq 0$  the effective potential  $\psi_e(r) \rightarrow +\infty$  when  $r \rightarrow 0$  provided that  $\ell > -\Lambda^2$ .*

*Proof.* The converse claim is obvious since  $\lim_{r \rightarrow 0} r^2 \psi_e(r) = \Lambda^2 + \ell > 0$  if  $\ell > -\Lambda^2$ . For the first claim, let us assume that  $\lim_{r \rightarrow 0} r^2 \psi(r)$  is infinite. Then  $\lim_{r \rightarrow 0} \psi(r)$  is also infinite. But since  $r \mapsto \psi(r)$  is increasing we must have  $\lim_{r \rightarrow 0} \psi(r) = -\infty$ . So for any  $\Lambda > 0$ , by choosing  $r$  close enough to 0, we would get

$$r^2 \psi(r) < -\Lambda^2 \implies \psi(r) < -\frac{\Lambda^2}{r^2} \implies \psi_e(r) < -\frac{\Lambda^2}{2r^2}$$

which implies  $\lim_{r \rightarrow 0} \psi_e(r) = -\infty$ . The claim follows by contraposition.  $\square$

We can then define the set of periodic radial orbits.

**Definition 2.1.** (PRO) When  $\ell = \lim_{r \rightarrow 0} r^2 \psi(r)$  is negative and finite, the set of radially periodic orbits of a gravitational radial potential  $\psi$  is defined by

$$\begin{aligned} \mathbb{O}_\psi &= \{(\xi, \Lambda) \in \mathbb{R}^2, \text{ s.t. } r(\cdot) \text{ solving (2.2) is periodic}\} \\ &= [\xi_c, \psi_\infty) \times [\sqrt{-\ell}, +\infty), \text{ with } \psi_\infty = \lim_{r \rightarrow +\infty} \psi(r). \end{aligned} \quad (2.5)$$

Such PROs admit finite radial periods, even when the total and/or the central mass of the systems is infinite. These periods correspond to the total duration of the transfer from farthest distances of the orbit at their apocenters  $r_a$  to the nearest ones at their pericenters  $r_p$  and back. They can be defined from the radial equation of motion (2.2) or through  $\xi$ -derivatives of the radial action  $\mathcal{A}_r$ , which also gives the precession of the orbits as defined in definition 2.2 or [78] p. 221. These orbital parameters are illustrated in figure 2.2.

**Definition 2.2.** Let  $\psi$  be a gravitational<sup>1</sup> radial potential. If  $(\xi, \Lambda) \in \mathbb{O}_\psi$ , then the radial action

$$\mathcal{A}_r = \frac{1}{\pi} \int_{r_p}^{r_a} \sqrt{2[\xi - \psi(r)] - \frac{\Lambda^2}{r^2}} dr \quad (2.6)$$

defines the radial period  $\tau_r$  and radial pulsation

$$\Omega_r^{-1} = \frac{\tau_r}{2\pi} = \frac{\partial \mathcal{A}_r}{\partial \xi}, \quad (2.7)$$

as well as the increment of the azimuthal angle  $\Delta\varphi$  during the transfer between two successive apocenters

$$\frac{\Delta\varphi}{2\pi} = n_\varphi = -\frac{\partial \mathcal{A}_r}{\partial \Lambda}. \quad (2.8)$$

In particular, if  $(\xi, \Lambda) \in \mathbb{O}_\psi$ , then we may derive the expression of the radial period as

$$\tau_r(\xi, \Lambda) = 2 \int_{r_p}^{r_a} \frac{dr}{\sqrt{2(\xi - \psi(r)) - \frac{\Lambda^2}{r^2}}} < \infty, \quad (2.9)$$

and increments  $n_\varphi$  as

$$n_\varphi = \frac{1}{\pi} \int_{r_p}^{r_a} \frac{\Lambda}{r^2 \sqrt{2[\xi - \psi(r)] - \frac{\Lambda^2}{r^2}}} dr. \quad (2.10)$$

Both  $\tau_r$  and  $\Delta\varphi$  are clearly two functions of the two variables  $\xi$  and  $\Lambda$ . Yet, in Michel Hénon's isochrone potentials, the radial periods only depend on  $\xi$ .

**Definition 2.3.** The set  $\mathbb{I}_{\text{pot}}$  of isochrone potentials is defined by

$$\mathbb{I}_{\text{pot}} = \left\{ \psi : \mathbb{R}_+ \rightarrow \mathbb{R}, \psi \in \mathcal{C}^2, \text{ s.t. } \mathbb{O}_\psi \neq \emptyset \text{ and } \forall (\xi, \Lambda) \in \mathbb{O}_\psi, \tau_r(\xi, \Lambda) \equiv \tau_r(\xi) \right\}. \quad (2.11)$$

The formulation in terms of the radial action enables us to complete this characterization of isochrony by an equivalent property on the azimuthal angle in theorem 2.1. This will be of particular interest for studying some orbital characteristics in section 2.4.3.

**Theorem 2.1.** Consider a central potential  $\psi$ . Then the following properties are equivalent:

1. For any orbit  $(\xi, \Lambda)$  in  $\mathbb{O}_\psi$ ,  $\tau_r$  only depends on  $\xi$ .
2. For any orbit  $(\xi, \Lambda)$  in  $\mathbb{O}_\psi$ ,  $n_\varphi$  only depends on  $\Lambda$ .
3. There exist two functions  $f$  and  $g$  such that, for any  $(\xi, \Lambda)$  in  $\mathbb{O}_\psi$ , the radial action is  $\mathcal{A}_r(\xi, \Lambda) = f(\xi) + g(\Lambda)$ .

---

<sup>1</sup>From now on, we only consider gravitational, i.e. increasing, potentials. The same analysis remains valid for decreasing potentials.

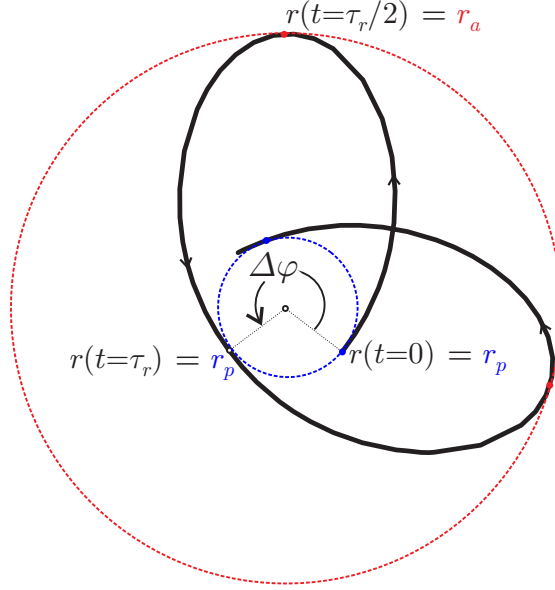


Figure 2.2: The radial distance of a PRO oscillates between pericenters  $r_p$  and apocenter  $r_a$  with a radial period  $\tau_r$ . These extremal distances present a precession characterized by the increment of the azimuthal angle  $\Delta\varphi$ .

*Proof.* The separation of variables in the radial action expressed in 3 implies the two properties 1 and 2 by direct differentiation with respect to  $\xi$  for 1 and  $\Lambda$  for 2.

Assume 2 is true for any orbit in the central potential  $\psi$ . Then  $\frac{\partial \mathcal{A}_r}{\partial \xi} = \frac{\tau_r(\xi)}{2\pi}$  and by integration there exists a function  $g$ , constant with respect to  $\xi$ , such that  $\mathcal{A}_r(\xi, \Lambda) = f(\xi) + g(\Lambda)$ , where  $f$  is a primitive of  $\frac{\tau_r}{2\pi}$ . We thus recover 3.

In the same way, assuming 2 implies 3.  $\square$

**Corollary 2.1.** *The set  $\mathbb{I}_{\text{pot}}$  of isochrone potentials is characterized by*

$$\mathbb{I}_{\text{pot}} = \left\{ \psi : \mathbb{R}_+ \rightarrow \mathbb{R}, \psi \in \mathcal{C}^2, \text{ s.t. } \mathbb{O}_\psi \neq \emptyset \text{ and } \forall (\xi, \Lambda) \in \mathbb{O}_\psi, n_\varphi(\xi, \Lambda) \equiv n_\varphi(\Lambda) \right\}. \quad (2.12)$$

Michel Hénon has pointed out the two fundamental Keplerian and harmonic potentials as two members of  $\mathbb{I}_{\text{pot}}$  and he has adjoined his isochrone. We propose in the next section to complete and classify his result.

## 2.2 Geometric characterization of isochrony

Instead of studying the radially periodic orbits by effective potentials, we may concentrate on the nature of the potentials that we search through a change of variables. We introduce Hénon's variables,

$$x = 2r^2 \quad \text{and} \quad Y(x) = x\psi\left(\sqrt{x/2}\right), \quad (2.13)$$

which modify the radial equation of motion as

$$\frac{1}{16} \left( \frac{dx}{dt} \right)^2 = \xi x - \Lambda^2 - Y(x). \quad (2.14)$$

Hereafter we will draw the graph of  $Y$  in the Hénon plane of coordinates  $(x, y)$ . The first coordinate  $x$  either refer to Hénon's first variable or a simple abscissa coordinate. The second coordinate  $y$  is the generic other coordinate for the plane, while  $Y$  contains the definition of a potential  $\psi$  according to (2.13). These variables also simplify the integral expression of the radial period when  $(\xi, \Lambda) \in \mathbb{O}_\psi$  as

$$\tau_r(\xi, \Lambda) = \frac{1}{2} \int_{x_p}^{x_a} \frac{dx}{\sqrt{\xi x - \Lambda^2 - Y(x)}}, \quad (2.15)$$

and enable one to determine orbits by visualizing the graph of  $Y$  as we will see below. The isochrone condition  $\tau_r(\xi, \Lambda) = \tau_r(\xi)$  strongly constrains it and the isochrone potentials set can then be geometrically characterized with the following

**Theorem 2.2.** *A radial potential  $\psi$  is isochrone if and only if the graph of  $Y$  in Hénon's variables is a parabola.*

*Proof.* We summarize here the original proof of Michel Hénon [68].

Let  $\psi$  be a radial potential. In Hénon's variables, one can see that the  $x$ -values of the periastron and apoastron of a PRO  $(\xi, \Lambda) \in \mathbb{O}_\psi$ , namely  $x_a$  and  $x_p$ , are the roots of the equation  $Y(x) = \xi x - \Lambda^2$ . Graphically, they correspond to the intersection abscissas of the lines

$$\mathcal{L} : y = \xi x - \Lambda^2 \quad (2.16)$$

with the graph  $\mathcal{C}$  of  $Y$ . When they coincide in a single repeated root  $x_c$ , the orbit  $(\xi, \Lambda)$  is circular, while no PRO exist if the line  $\mathcal{L}$  does not intersect the graph  $\mathcal{C}$ , i.e. if  $(\xi, \Lambda) \notin \mathbb{O}_\psi$ . As it is detailed in figure 2.3, for a fixed value  $\xi$  of the energy, the set of all points  $(P_{a,i}; P_{p,i})$  on the lines  $y = \xi x - \Lambda_i^2$  with corresponding abscissas  $x_{a,i}$  and  $x_{p,i}$  form the graph of  $Y$ . For a given orbit  $(\xi, \Lambda_i) \in \mathbb{O}_\psi$ , the solution of (2.14) is contained in the graph of  $Y$  located under  $\mathcal{L}_i$ . Moreover the time needed to reach an apocenter  $P_{a,i}$  from a pericenter  $P_{p,i}$  is half of its radial period. This strongly constrains the graph of  $Y$  when  $\psi$  is isochrone.

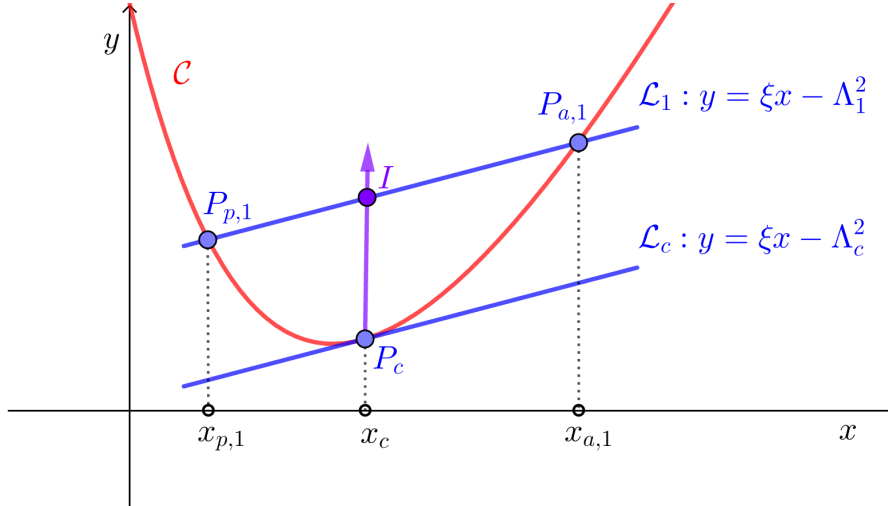


Figure 2.3: Geometric view of Hénon's variables.

As a matter of fact, using a clever analysis, Michel Hénon shows that  $\tau_r$  only depends on  $\xi$  if and only if  $P_c I$  is proportional to  $(x_{p,1} - x_{a,1})^2$  when  $\Lambda_1^2$  is varying. Let us summarize his proof.

We assume  $\psi$  is isochrone. All couples  $(x_p, x_a)$ , obtained from a bundle of parallel chords for each energy  $\xi$ , enable one to define the potential. On the first hand, we define

$$-u^2 = \xi x - \Lambda_c^2 - Y(x) \quad (2.17)$$

the algebraic distance from  $\mathcal{C}$  to the line  $\mathcal{L}_c : y = \xi x - \Lambda_c^2$ , that is tangent to  $\mathcal{C}$  at  $P_0$  of abscissa  $x_c$ , with  $u < 0$  if  $x < x_c$  and  $u > 0$  if  $x > x_c$ . On the other hand, we define the distance between  $\mathcal{L}_c$  and the lines  $\mathcal{D} : y = \xi x - \Lambda^2$  with fixed energy  $\xi$  by

$$\lambda^2 = \Lambda_c^2 - \Lambda^2. \quad (2.18)$$

Let us parametrize the length  $u^2$  by

$$u = \lambda \sin \theta, \text{ with } \theta \in \left[-\frac{\pi}{2}, \frac{\pi}{2}\right] \quad (2.19)$$

since the two distances coincide at the intersection points  $(P_p, P_a)$  of  $\mathcal{L}$  and  $\mathcal{C}$ . This parametrization once again simplifies the expression of the radial period as

$$\tau_r(\xi, \Lambda^2) = \int_{-\frac{\pi}{2}}^{\frac{\pi}{2}} F(\lambda \sin \theta) d\theta \quad (2.20)$$

where  $F(u) = \frac{dx}{du}$ , see [68, 77]. The condition for the radial period to only depend on  $\xi$  is equivalent to constraining this integral (2.20) not to depend on  $\Lambda^2$ , and thus on  $\lambda$ . A series expansion of the function  $F$  and its integration shows that it must decompose into a  $\tau_r$ -proportional constant term and an odd function  $g$  of  $u$ , i.e.  $F(u) = \frac{\tau_r}{\pi} + g(u)$ . With the definition of  $F$ , the constrain  $\tau_r \equiv \tau_r(\xi)$  is equivalent to  $x(u) = \frac{\tau_r}{\pi}u + G(u^2)$ , where  $G$  is an even function of  $u$ . We can then deduce the relation

$$x_a - x_p = \frac{2\tau_r}{\pi}\lambda. \quad (2.21)$$

Finally, the equation of the curve  $\mathcal{C}$  can be made explicit. The derivation with respect to  $\xi$  and  $\Lambda^2$  of the definition of  $x_p$  and  $x_a$  gives

$$\begin{cases} \xi x_p - \Lambda^2 - Y(x_p) = 0, \\ \xi x_a - \Lambda^2 - Y(x_a) = 0, \end{cases} \quad (2.22)$$

and the new condition

$$\tau_r = \tau_r(\xi) \Leftrightarrow (x_a - x_p)^2 = \frac{4\tau_r(\xi)^2}{\pi^2}(\Lambda_0^2(\xi) - \Lambda^2) \quad (2.23)$$

to get an equation, e.g.  $[2x - (x_p + x_p)]^2 = (x_a - x_p)^2$ , where  $x_p$  et  $x_a$  are solutions. After a much more involved analysis on the derivatives of the equation of motion (2.14), Michel Hénon was able to provide an equation for  $Y(x)$  at all possible values of  $x_a$  et  $x_p$ , namely

$$\left[ \frac{2}{3s} \frac{ds}{d\xi} Y(x) - \left( 2 + \frac{2\xi}{3s} \frac{ds}{d\xi} \right) x + \left( \frac{2\Lambda_0^2}{3s} \frac{ds}{d\xi} + 2 \frac{d\Lambda_0^2}{d\xi} \right) \right]^2 = s [Y(x) - \xi x + \Lambda_0^2], \quad (2.24)$$

with  $s = \frac{4\tau_r^2}{\pi^2}$  and which characterizes a parabola. The converse claim is almost direct.  $\square$

As this original proof is very technical, we propose a new version of it in the appendix B of SPD by highlighting the analytical property of the potentials, independently of the equation of motion.

**Definition 2.4.** We call isochrone parabolas a parabola that contains an isochrone potential, according to theorem 2.2.

**Definition 2.5.** We call  $\mathbb{I}_{\text{par}}$  the set of isochrone parabolas in  $\mathbb{R}^2$ .

**Corollary 2.2.** *The set of isochrone potentials,  $\mathbb{I}_{\text{pot}}$ , is in bijection with the set of isochrone parabolas,  $\mathbb{I}_{\text{par}}$ .*

Remarkably, each feature of the parabolas relies on the attributes of their associated potentials. We propose to step on this equivalence to classify the two sets  $\mathbb{I}_{\text{pot}}$  and  $\mathbb{I}_{\text{par}}$  in the next section.

## 2.3 Classification of isochrone potentials

The construction of the classification of isochrone potentials is presented in SPD sections 2.2, 2.3 and 2.5. We specify here the main results and emphasize the geometrical point of view to classify  $\mathbb{I}_{\text{par}}$  and  $\mathbb{I}_{\text{pot}}$ .

### 2.3.1 The space of isochrone parabolas

Let us first introduce the definition of some transformations of the real two-dimensional affine space.

**Definition 2.6.** Let  $\epsilon$  and  $\lambda$  be two real parameters. An  $\epsilon$ -transvection is defined by

$$\begin{aligned} \mathbb{R}^2 &\rightarrow \mathbb{R}^2 \\ (x, y) &\mapsto (x, y + \epsilon x). \end{aligned} \quad (2.25)$$

We call  $\lambda$ -gauge a vertical translation

$$\begin{aligned} \mathbb{R}^2 &\rightarrow \mathbb{R}^2 \\ (x, y) &\mapsto (x, y + \lambda). \end{aligned} \quad (2.26)$$

We call  $\mathbb{A}$  the set of  $\epsilon$ -transvections and  $\lambda$ -gauge compositions  $J_{\epsilon, \lambda}$  given by

$$J_{\epsilon, \lambda} : \begin{aligned} \mathbb{R}^2 &\rightarrow \mathbb{R}^2 \\ (x, y) &\mapsto (x, y + \epsilon x + \lambda). \end{aligned} \quad (2.27)$$

The set  $\mathbb{A}$  is a subgroup of affine transformations of the real plane with the composition law

$$J_{\epsilon, \lambda} \circ J_{\epsilon', \lambda'} = J_{\epsilon + \epsilon', \lambda + \lambda'} \in \mathbb{A}. \quad (2.28)$$

It is isomorphic to  $(\mathbb{R}^2, +)$ , and generates an equivalence relation  $\sim$  on the set of isochrone parabolas  $\mathbb{I}_{\text{par}}$  as:  $\forall (\mathcal{P}, \mathcal{P}') \in \mathbb{I}_{\text{par}}$ ,

$$\mathcal{P} \sim \mathcal{P}' \Leftrightarrow \exists (\epsilon, \lambda) \in \mathbb{R}^2, \mathcal{P} = J_{\epsilon, \lambda}(\mathcal{P}'). \quad (2.29)$$

These transformations in Hénon's variables correspond to physical transformations on the potentials which preserve the isochrone property and the dynamical properties in the potentials. They lead to a geometrical classification of isochrone parabolas that will be used for a classification of  $\mathbb{I}_{\text{pot}}$ , as stated in the following propositions.



**Proposition 2.1.** *The set  $\mathbb{I}_{\text{par}}$  of isochrone parabolas is partitioned by the  $\mathbb{A}$ -group action in four classes of equivalence with the following canonical representatives:*

- the parabola  $\mathcal{P}_{\text{ha}}$ , a straight parabola with a vertical symmetry axis and a horizontal tangent at the origin ( $x \mapsto x^2$ );
- the parabola  $\mathcal{P}_{\text{ke}}$ , a parabola with a horizontal symmetry axis and a vertical tangent at the origin ( $x \mapsto \pm\sqrt{x}$ );
- the parabola  $\mathcal{P}_{\text{he}}$ , a right-oriented parabola with a horizontal symmetry axis and a vertical tangent of negative abscissa;
- the parabola  $\mathcal{P}_{\text{bo}}$ , a left-oriented parabola with a horizontal symmetry axis and a vertical tangent of positive abscissa.

*They all possess an aperture that is defined up to a factor.*

*Proof.* First of all, we can choose the origin of the  $x$ -axis so that it coincides with that of the physical system described by  $Y$ . In that case, the  $y$ -axis intersects the associated parabola at least once. When its symmetry axis is not vertical, we parametrize the abscissa of its vertical tangent by  $x_t = \pm 2b^2$ , depending on the location of the tangent that is completely determined by the physical characteristics of the system, such as mass or size. In Hénon's variables, the general equation for the parabola is written as

$$(ax + gY)^2 + cx + dY + e = 0. \quad (2.30)$$

The expression of the constants  $a, g, c, d$  and  $e$  depend on the physical problem parameters, as given by (2.24) or the original Hénon paper [68]. For the following discussion on the parabolas, we may consider a given aperture width of the parabolas.

The few following remarks enable us to delimitate  $\mathbb{I}_{\text{par}}$ . The variable of the potential is the radial distance, a positive real number. Each isochrone potential is then included in the  $x$ -positive half-plane. This remark excludes left-oriented laid parabolas from  $\mathbb{I}_{\text{par}}$ . For any non-straight parabolas, there are two functions  $x \mapsto y_1(x)$  and  $x \mapsto y_2(x)$  into which the  $x$ -positive part of the graph of the parabola can be decomposed. The slope of the chord between the origin and a point  $M$  of abscissa  $x > 0$  on the graph of  $y_1$  or  $y_2$  is given by the ratio  $\frac{y_1(x)}{x}$  or  $\frac{y_2(x)}{x}$  which is precisely the definition of the potential  $\psi$ . This remark shows that  $\psi$  is an increasing (resp. decreasing) function if the graph of  $y$  is convex (resp. concave), i.e. the chord between two points is above (resp. below) the function. As we look for increasing potentials in order to have PRO's, we have to consider the convex part of the parabola graph. This part is named  $y_1$ . It therefore excludes bottom-oriented straight parabolas ( $y \propto -x^2$ ) from  $\mathbb{I}_{\text{par}}$ .

Geometrically, an  $\epsilon$ -transvection adds the constant  $\epsilon$  to the slope of any straight line. In particular, it modifies the orientation of the parabolas by swiveling their symmetry axes. But it keeps invariant vertical directions and the  $y$ -axis. Consequently, laid ( $y \propto \pm\sqrt{x}$ ) and tilted parabolas are morphed as illustrated on figure 2.4, while straight parabolas ( $y \propto x^2$ ) have their apices translated, by  $\left(-\frac{\epsilon}{2}, -\frac{\epsilon^2}{4}\right)$  for  $x \mapsto x^2$ .

The composition of  $\epsilon$ -transvections and  $\lambda$ -gauges therefore engender any straight or laid parabola and any tilted parabola of  $\mathbb{I}_{\text{par}}$  from one of those four parabola types, see the proof in SPD pp.7-11. This action of  $\mathbb{A}$  on  $\mathbb{I}_{\text{par}}$  is depicted in figure 2.5.

Nevertheless, one can neither jump from a left-oriented parabola to a right-oriented one using an affine transformation, nor reach a straight or laid parabola from a tilted one, and vice versa. This is due to the limit values of  $\epsilon \in \mathbb{R}$  that can only make the slope of the symmetry axes

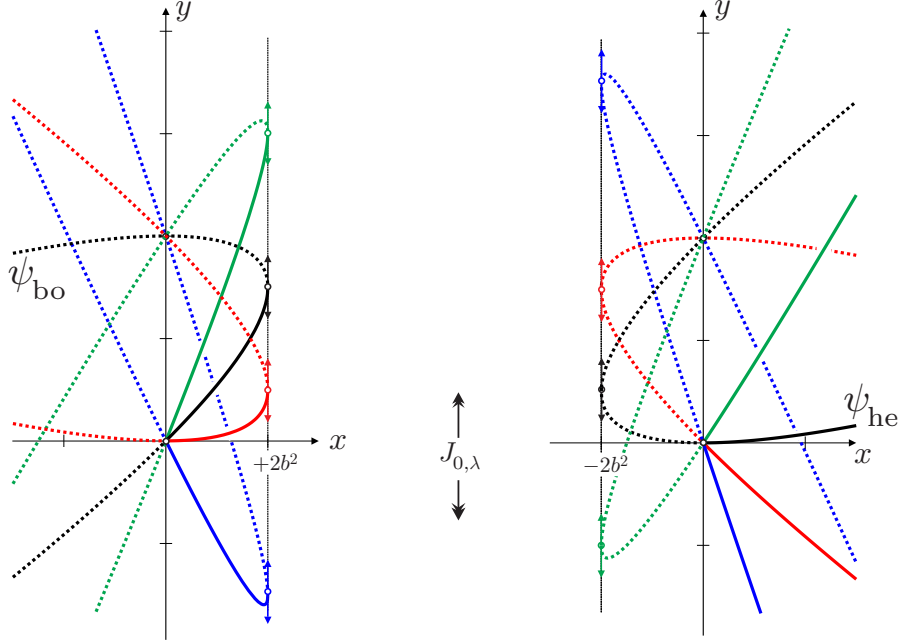


Figure 2.4: Transvection action on tilted isochrone parabolas.

vary from  $-\infty$  to  $+\infty$  for tilted parabolas and that leave invariant the one of straight parabolas. In addition, no affine transformation of  $\mathbb{A}$  can shift the parabolas to get two from a unique intersection with the  $y$ -axis. In fact, the action of  $\mathbb{A}$  splits the set  $\mathbb{I}_{\text{par}}$  into the four classes of equivalence of straight, laid, right- or left-oriented parabolas.

The four canonical isochrone parabolas are chosen so that they present vertical or horizontal symmetry axes. They are drawn in figure 2.6. Their associated isochrone potentials will be made explicit later in the section.  $\square$

### 2.3.2 Isochrone parabolas and potentials' congruity

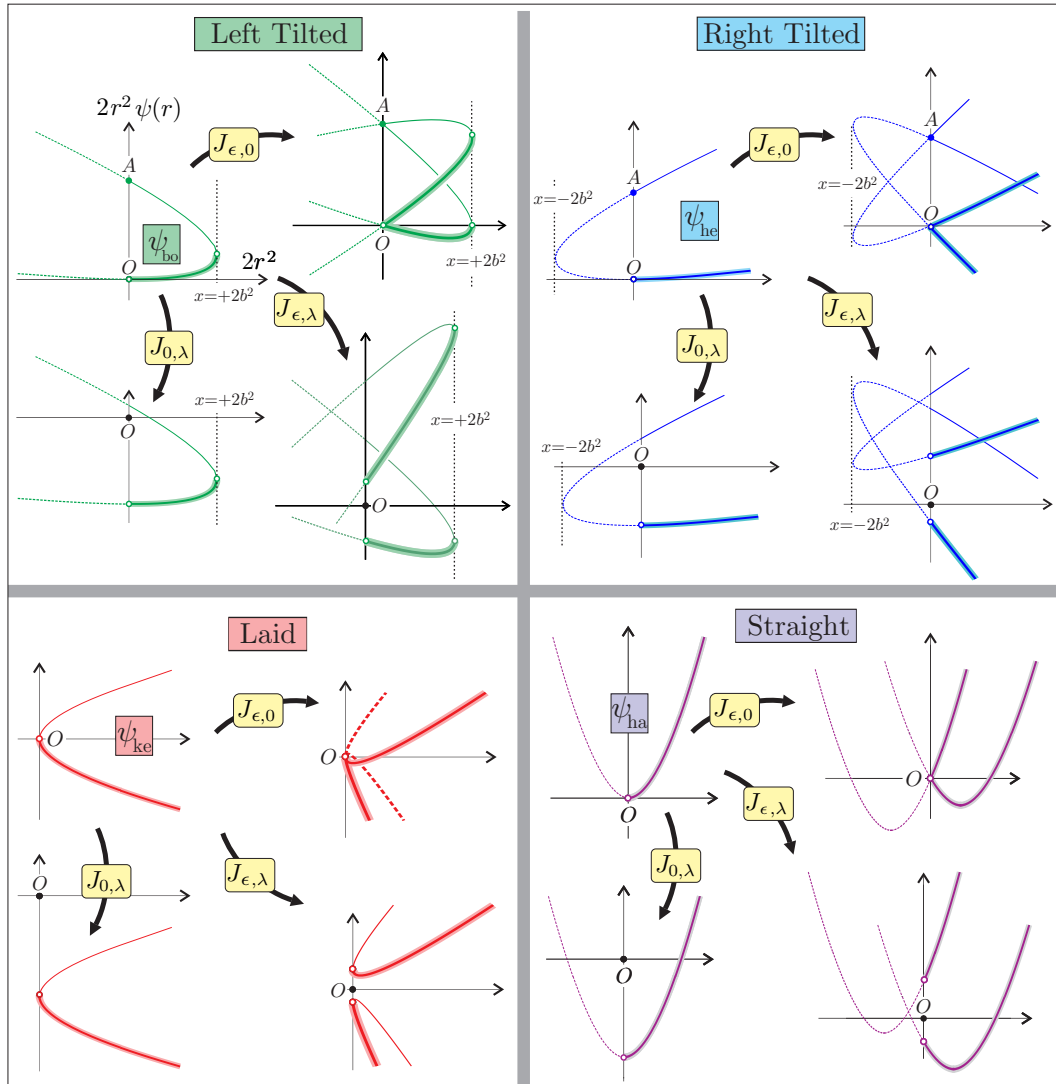
**Proposition 2.2.** *The partition of  $\mathbb{I}_{\text{par}}$  by the  $\mathbb{A}$ -group action characterizes four different types of isochrone potentials.*

*Proof.* First, we note that the affine characteristic of the transformations  $J_{\epsilon, \lambda}$  preserves isochrony, since it preserves the property of the graph of  $Y$  to be a parabola.

For convenience, we recall the equation of motion of a particle in Hénon's variables (2.14):

$$\frac{1}{16} \left( \frac{dx}{dt} \right)^2 = \xi x - \Lambda^2 - Y(x). \quad (2.31)$$

The action of  $\mathbb{A}$  corresponds to physical transformations on the potentials. As a matter of fact, in physics, any potential is defined up to a constant  $\epsilon$ , then the type of an isochrone potential is left unchanged under the transformation  $\psi \mapsto \psi + \epsilon$ . Geometrically, in the Hénon plane  $(x, y)$ , this corresponds to an  $\epsilon$ -transvection. Similarly, one can redefine the origin for the angular momentum values by mapping  $\Lambda^2 \mapsto \Lambda^2 + \lambda > 0$  without altering the dynamical properties in (2.31). Provided that  $\Lambda^2 + \lambda > 0$ , this corresponds to vertically translating the parabola in the Hénon plane. When  $\Lambda^2 + \lambda < 0$ , there is no PRO. We may call gauged potential the result

Figure 2.5: The four classes of equivalence of isochrone parabolas under the action of the group  $\mathbb{A}$ .

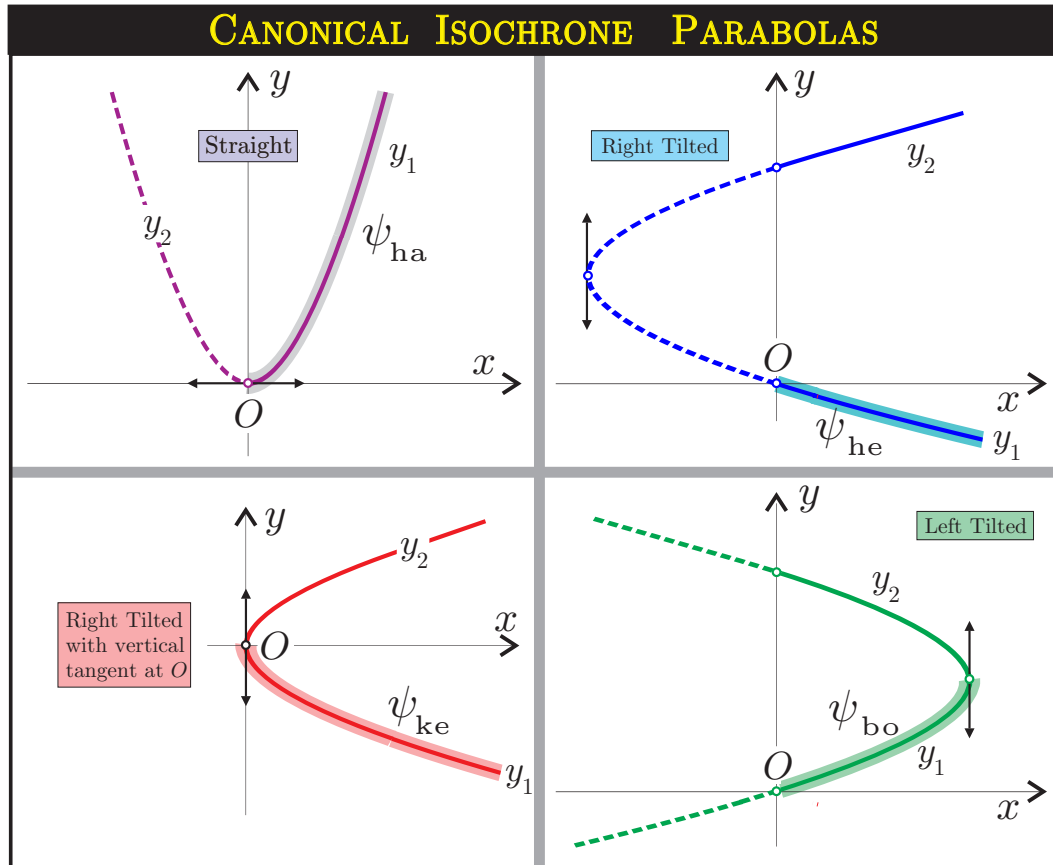


Figure 2.6: Canonical isochrone parabolas. The parts of the parabolas associated with increasing potentials are highlighted ( $y_1$ ). The dashed parts of the parabolas correspond to potentials with an imaginary distance argument ( $x < 0$ ). The unhighlighted solid line parts of the parabolas ( $y_2$ ) in the  $x$ -positive half-plane correspond to decreasing potentials.

of this transformation  $\psi^*(r) = \psi(r) + j_\lambda(r)$  where  $j_\lambda(r) = \frac{\lambda}{2r^2}$ . This gauged potential is then of the same isochrone type as  $\psi(r)$ . As a result, the partition of  $\mathbb{I}_{\text{par}}$  settled in proposition 2.1 characterizes four types of isochrone potentials, each one associated to a parabola in the four classes of equivalence of  $\mathbb{I}_{\text{par}}$ .  $\square$

The correspondence between isochrone potentials and parabolas results in a tight relation between the features of the parabolas and the physical attributes of the potentials. The precedent reduction of isochrone parabolas enables us to gather these relations in the following proposition and synthesize them in figure 2.7, after two brief definitions.

**Definition 2.7.** Let  $\mathcal{D}_\psi \subset \mathbb{R}^+$  be the domain on which the potential is defined physically. Then, we denote by

$$\mathcal{R} = \sup_{\mathbb{R}} [\mathcal{D}_\psi], \quad (2.32)$$

the size of the domain  $\mathcal{D}_\psi$ . *A priori*  $\mathcal{R}$  is finite and positive if  $\mathcal{D}_\psi$  is bounded, otherwise  $\mathcal{R} = +\infty$ .

**Definition 2.8.** We denote by

$$\psi_\infty = \lim_{r \rightarrow \mathcal{R}} \psi(r) \quad (2.33)$$

the value of the potential at the boundary of its domain.

**Proposition 2.3.** *The attributes of isochrone parabolas and potentials are related as follows:*

- *the parabola aperture width is determined by the mass repartition of the physical system;*
- *the slope of the symmetry axis of the parabola is given by the value of the potential at infinity;*
- *when the parabola crosses the  $y$ -axis twice, the abscissa of its vertical tangent gives a characteristic size of the physical system;*
- *the ordinate of the intersection point between the convex branch for the parabola and the  $y$ -axis gives the  $\lambda$ -gauge associated to the isochrone potential.*

*Sketch of the proof.* The affine transformations of the  $\mathbb{A}$ -group can be used to reduce the equation of a parabola. The exhaustive analysis is settled in lemmas 2 to 4 in SPD. The first step consists in reducing the parabola by the action of  $\mathbb{A}$  to parabolas that show a vertical or horizontal tangent at the origin. This allows to distinguish four reduced parabolas (actually six but two of them are in the equivalence classes of the four others).

Their equations are written as

$$(A + B\psi)^2 = \frac{C\psi + D}{2r^2}. \quad (2.34)$$

When  $B = 0$ , the potential is infinite at infinity, the parabola is straight and actually corresponds to a harmonic potential. Reciprocally, an infinite value of  $\psi$  at infinity implies that  $B = 0$ , see lemma 3 in SPD. When  $\psi_\infty = \lim_{r \rightarrow 0} \psi(r)$  is finite, then the right member in (2.34) vanishes while the left one gives the slopes of the symmetry axes in terms of  $-\frac{B}{A} = \psi_\infty$ .

Left-oriented parabolas correspond to spatially bound systems. Their radii are given by the abscissas of the vertical tangents. Right-oriented parabolas also present a characteristic length related to the abscissa of their vertical tangents. As we will see later, the density of the associated system is almost constant up to this parameter before it decreases with the radial distance.

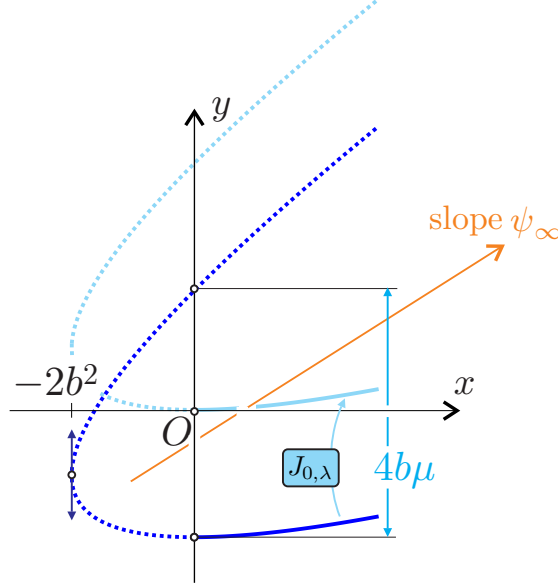


Figure 2.7: Correspondence between isochrone parabolas and potentials attributes.

Since the convex branches of the parabolas contain the increasing isochrone potentials and given that  $\psi(x) = \frac{Y}{x}$ , a strictly negative lower  $y$ -intersection corresponds to a non-finite value of the potential which thus contains a gauge term. Then the convex branch of non-gauged parabolas pass through the origin.

This gauge or the analytic expression of the potential (see SPD section 4.1) determine the distance between the two  $y$ -intersections of the parabola as a function of the mass content of the system, and thus condition the aperture width of the parabola.

The same analysis can be done with the canonical parabolas. For all other parabolas, the correspondence can be derived from the inverted action of  $\mathbb{A}$ .  $\square$

### 2.3.3 The space of isochrone potentials

We are now ready to state the main result for the classification of the isochrone potentials.

**Theorem 2.3.** *The isochrone potentials are classified by the two following properties.*

*There are four canonical types of isochrone potentials:*

- the harmonic potential  $\psi_{\text{ha}}$ , which parabola is straight with a horizontal tangent at the origin;
- the Keplerian potential  $\psi_{\text{ke}}$ , which parabola has a horizontal symmetry axis and a vertical tangent at the origin;
- the Hénon potential  $\psi_{\text{he}}$ , which parabola is right-oriented with a vertical tangent line parametrized by  $x = -2b^2 < 0$  and a horizontal symmetry axis;
- the bounded potential  $\psi_{\text{bo}}$ , which parabola is left-oriented with a vertical tangent line parametrized by  $x = 2b^2 > 0$  and a horizontal symmetry axis.

Any isochrone potential  $\psi$  is in the group orbit of one of the four previous potentials under the group action of  $\mathbb{A} = \{\epsilon - \text{transvections}, \Lambda - \text{translations}\}$ . That is to say, there exist two constants  $\epsilon$  and  $\lambda$  and some canonical potential  $\psi_{\text{can}} \in \{\psi_{\text{ke}}, \psi_{\text{ha}}, \psi_{\text{he}}, \psi_{\text{bo}}\}$  such that for all  $r \in \mathbb{R}_+$ ,  $\psi(r) = \psi_{\text{can}}(r) + \epsilon + \frac{\lambda}{2r^2}$ .

*Proof.* The partition of  $\mathbb{I}_{\text{pot}}$  by the equivalence relation generated by the action of the group  $\mathbb{A}$  stems from its bijection with  $\mathbb{I}_{\text{par}}$ , according to proposition 2.1 and corollary 2.2.

The expressions of the four canonical isochrone potentials can be extracted from the study of the four canonical parabolas equations and are completely derived in the proof presented in SPD pp.7-14.  $\square$

The four canonical isochrone potentials generate four classes of equivalence that cover all isochrone potentials. We set their names and analytic expressions in the following definition.

**Definition 2.9.** 1. We call the four canonical isochrone potentials

$$\begin{aligned} \psi_{\text{ke}}(r) &= -\frac{\mu}{r}, & \psi_{\text{ha}}(r) &= \frac{1}{2}\omega^2 r^2, \\ \psi_{\text{he}}(r) &= -\frac{\mu}{b + \sqrt{b^2 + r^2}}, & \text{and } \psi_{\text{bo}}(r) &= \frac{\mu}{b + \sqrt{b^2 - r^2}}, \end{aligned}$$

the Kepler, the harmonic, the Hénon and the bounded potential, respectively.

2. We call *reduced isochrone* potentials  $\psi_{\text{iso}}^{\text{red}}$  one of the four potentials

$$\psi_{\text{ke}}, \psi_{\text{ha}}, \psi_{\text{he}}^{\text{red}} = J_{\frac{\mu}{2b}, 0}(\psi_{\text{he}}) = \frac{\mu}{2b} + \psi_{\text{he}} \text{ or } \psi_{\text{bo}}^{\text{red}} = J_{-\frac{\mu}{2b}, 0}(\psi_{\text{bo}}) = -\frac{\mu}{2b} + \psi_{\text{bo}}.$$

3. We call *physical isochrone* potentials  $\psi_{\text{iso}}^{\text{phy}}$  the result of a transvection applied to a canonical isochrone:  $\psi_{\text{iso}}^{\text{phy}} = J_{\epsilon, 0}(\psi_{\text{iso}}^{\text{can}}) = \psi_{\text{iso}}^{\text{can}} + \epsilon$ .

4. We call *gauged isochrone* potentials  $\psi_{\text{iso}}^{\text{gau}}$  the result of a vertical translation applied to a physical isochrone:  $\psi_{\text{iso}}^{\text{gau}} = J_{0, \lambda}(\psi_{\text{iso}}^{\text{phys}}) = \psi_{\text{iso}}^{\text{phys}} + \frac{\lambda}{2r^2}$ .

Our reduction to four families of parabolas and their corresponding potentials has enabled us to obtain the whole set of isochrone potentials. The reduced isochrones are used to infer the parabola classification in SPD, the first three reduced isochrones are the ones obtained by Michel Hénon in [68]. In his historical study, Michel Hénon did not remark on the crucial role of these affine transformations. He dismissed out-of-origin parabolas and forgot left-oriented tilted ones.

## 2.4 Physics of isochrone potentials

### 2.4.1 Isochrone physical systems

Physical isochrones possess interesting physical properties. They all confine a finite mass in a finite radius  $r < \mathcal{R}$  but are distinguished by their repartitions, plotted in figure 2.8. Two of them are very well known: the Kepler potential  $\psi_{\text{ke}}$  is associated with a Dirac density distribution and the harmonic potential  $\psi_{\text{ha}}$  is sourced by a constant density distribution of matter in the considered volume. In a Hénon one, the mass is equally distributed up to a characteristic length settled by the parameter  $b$ , and in a less concentrated decreasing power law repartition after

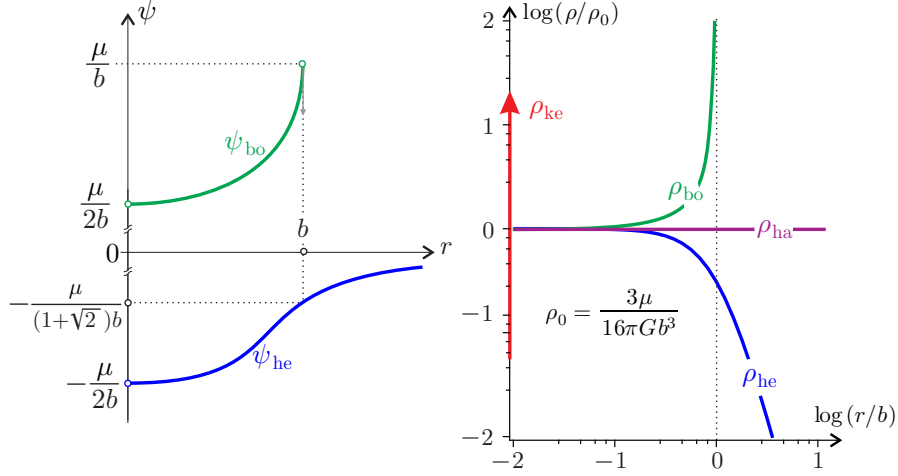


Figure 2.8: The bounded and the Hénon isochrone potentials (left). The mass density of isochrones (right).

this characteristic radius. When  $b$  increases, the first dense harmonic part grows and the Hénon potential eventually behaves like a harmonic potential with

$$\psi_{\text{he}}^{\text{red}} \underset{b \rightarrow \infty}{\sim} \frac{\mu}{8b^3} r^2, \quad (2.35)$$

i.e. the physical Hénon isochrone is changed into the physical harmonic when  $b \rightarrow +\infty$ . This property can be easily seen on the mass density distribution in the right panel of the figure 2.8. Subsequently, with

$$\psi_{\text{bo}}^{\text{red}} \underset{b \rightarrow \infty}{\sim} \frac{\mu}{8b^3} r^2, \quad (2.36)$$

we can say in a converse manner that the bounded potential concentrates the infinite mass of the unbounded harmonic into a finite domain of size  $b$ . Both are harmonic near their center, and Keplerian when  $r \rightarrow \infty$ .

The Hénon potential  $\psi_{\text{he}}$  has important physical properties in gravitational stellar dynamics. In chapter 4, we will show that it appears to be a fundamental equilibrium state where stellar systems settle down after violent relaxation. The corresponding density is a core-halo structure: the typical size of the core is the length  $b$  and the surrounding halo falls like a  $r^{-4}$  power law. This property ensures that the mass  $M_{\text{he}}(r)$  contained in any ball of radius  $r$  in a Hénon potential is finite. As a matter of fact, by Gauss' theorem, we have

$$GM_{\text{he}}(r) = r^2 \frac{d\psi_{\text{he}}}{dr} \quad (2.37)$$

and

$$\lim_{r \rightarrow \infty} GM_{\text{he}}(r) = \mu. \quad (2.38)$$

Recalling definition 2.9, this finite mass property is trivially conserved for all physical Hénon's  $\psi_{\text{he}}^{\text{phy}} = \psi_{\text{he}} + \epsilon$  for any real  $\epsilon$ . However, the gauged Hénon  $\psi_{\text{he}}^{\text{gau}} = \psi_{\text{he}}^{\text{phy}} + \frac{\lambda}{2r^2}$  contains an infinite mass in its center and has poor physical meaning. Nevertheless, this latter potential is still isochrone.



The properties of systems associated with the  $\psi_{\text{bo}}$  potential are more unusual and do not seem to have appeared in the literature before. When they are considered on its whole domain

$$\mathcal{D}_{\psi_{\text{bo}}} = [0, b], \quad (2.39)$$

the systems have an infinite total mass. As a matter of fact,

$$GM_{\text{bo}}(r) \sim \mu \sqrt{\frac{b}{2(b-r)}} \quad (2.40)$$

when  $r \rightarrow b$ . This property holds for any physical bounded potential. In fact these systems are self-confined because there exists an infinite repulsive force at their boundaries in  $r = b$ . Perhaps  $\psi_{\text{bo}}$  potentials might be used as classical models for structurally confined systems like, for example, quarks in the nucleon. Indeed, such fundamental particles are confined in the nucleon (here of size  $b$ ) and are characterized by asymptotic freedom, i.e. they do not feel any force at the center of the nucleon. Gauged bounded potentials are even more unusual with their infinite central mass!

When the  $\lambda$ -gauge  $J_{0,\lambda} : \psi \rightarrow \psi + \frac{\lambda}{2r^2}$  is applied to a physical potential, it makes it divergent as  $r^{-2}$  when  $r \rightarrow 0$ . As we said in section 2.3.2, such transformations correspond to a change of the value of the angular momentum in the corresponding isochrone orbit. Due to their  $r^{-2}$  divergence when  $\lambda \neq 0$ , gauged isochrone potentials have an infinite mass at their center and thus possess poor physical meaning. However, they are essential to the completeness of the isochrone set and the dynamics can be described as the one in physical isochrones seen from some rotating frame [117].

### 2.4.2 Isochrone orbits

As any bound orbit in a radial potential, isochrone orbits generally (except collapsing orbits) oscillate between apo- and peri-centers. These are determined by chords on isochrone parabolas. Once more, this parabolic definition constrains the associated radial periods. Proposition 2.4 gathers the properties  $\tau_r$  and  $n_\varphi$  of isochrone orbits and reveals the interesting similarities of isochrone radial periods. Their form in  $\psi_{\text{he}}$  and  $\psi_{\text{bo}}$  is the same as in the Keplerian potential. We will use this remark to generalize Kepler's third law in the next chapter. In a harmonic potential,  $\tau_r$  is the same regardless of the energy of the massive particles. Moreover, in  $\psi_{\text{ke}}$  and  $\psi_{\text{ha}}$ ,  $n_\varphi$  is rational and all orbits are closed.

**Proposition 2.4.** *Given a PRO  $(\xi, \Lambda)$  in an isochrone potential, its radial and azimuthal periods are*

	$\psi_{\text{ke}}$	$\psi_{\text{ha}}$	$\psi_{\text{he}}$	$\psi_{\text{bo}}$
$\tau_r$	$2\pi\mu  2\xi ^{-3/2}$	$\pi\omega^{-1}$	$2\pi\mu  2\xi ^{-3/2}$	$2\pi\mu  2\xi ^{-3/2}$
$n_\varphi$	1	$\frac{1}{2}$	$\frac{1}{2} + \frac{\Lambda}{2\sqrt{4b\mu + \Lambda^2}}$	$\frac{1}{2} - \frac{\Lambda}{2\sqrt{4b\mu + \Lambda^2}}$

(2.41)

The dynamics is unchanged when adding constants to potentials, i.e.  $\psi \rightarrow \psi + \epsilon$ . However, the expression of the periods are modified and can be deduced from propositions 2.4 and 2.5 for the reduced, physical and gauged isochrones.

**Proposition 2.5.** *Let  $\psi$  and  $\psi^*$  be two potentials related by an affine transformation such that they satisfy*

$$\psi^* = J_{\epsilon, \lambda}(\psi) = \psi + \epsilon + \frac{\lambda}{2r^2}. \quad (2.42)$$

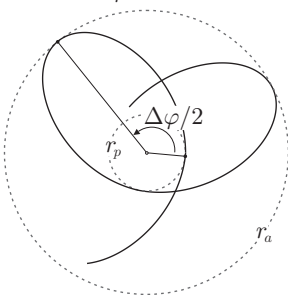
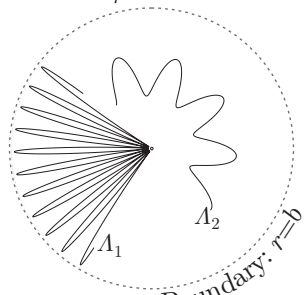
*An orbit defined in  $\psi$  and its affine transformation in  $\psi^*$  share the same orbital properties  $\tau_r$  and  $n_\varphi$ .*

*Provided that  $\lambda + \Lambda^2 > 0$ , the radial action and its derivatives are transformed as follows:*

1.  $\mathcal{A}_r^*(\xi; \Lambda) = \mathcal{A}_r(\xi - \epsilon; \sqrt{\lambda + \Lambda^2})$ ,
2.  $\tau_r^*(\xi; \Lambda) = \tau_r(\xi - \epsilon; \sqrt{\lambda + \Lambda^2})$ ,
3.  $n_\varphi^*(\xi; \Lambda) = n_\varphi(\xi - \epsilon; \sqrt{\lambda + \Lambda^2}) \frac{\Lambda}{\sqrt{\lambda + \Lambda^2}}$ .

Eventually, the radially periodic orbits are rosettes, [78] sect. 3. The number  $n_\varphi$  of revolutions to reach a periastron from the preceding one can be greater or lower than for a harmonic or Keplerian potential. A gauge introduces orbits that spiral into the origin [98], as it happens for orbits of the extremal line defining an imaginary radial distance on its parabola at the pericenter. The gauged harmonic presents a similarity with  $\psi_{\text{he}}$  and  $\psi_{\text{bo}}$ , as described in proposition 2.6. The precession of orbits that emerge when adding a  $\frac{1}{r^2}$ -term to the potential corresponds to the one described in Proposition XLIV of Newton's *Principia* [117] for the Kepler force.

**Proposition 2.6.** *Bounded, Hénon and gauged harmonic PRO's are rosettes with azimuthal precessions  $n_\varphi$  such that:*

$\psi_{\text{he}}$ and $J_{0, \lambda}(\psi_{\text{ha}})$ with $\lambda > 0$	$\psi_{\text{bo}}$ and $J_{0, \lambda}(\psi_{\text{ha}})$ with $\lambda < 0$
<p style="text-align: center;"><math>n_\varphi &gt; 1/2</math></p> 	<p style="text-align: center;"><math>n_\varphi &lt; 1/2</math></p> 

*Proof.* All the proofs of the preceding propositions can be found in SPD section 4.2. □

Let us remark that the extension ( $r_a$  and  $r_p$ ) of an isochrone orbit is controlled by its energy (for an evidence see the expressions of the isochrone radial actions in SPD section 4.2) while the thickness of its oscillation is governed by its angular momentum. More precisely, radial (thin) orbits are obtained when  $\Lambda \rightarrow 0$  and circular (fat) orbits when  $\Lambda = \Lambda_c$ , the largest possible value of the angular momentum for the considered energy.

The period and precession properties of periastron for isochrones combined with the completeness of  $\mathbb{I}_{\text{pot}}$  enables us to simply prove a well-known theorem of celestial mechanics in the next section.

### 2.4.3 The Bertrand theorem

In 1873, J. Bertrand published a fascinating theorem: *There are only two central potentials for which all orbits with an initial velocity below a certain limit are closed, namely the Keplerian and the harmonic potentials.* While this fascinating result was proved more than 140 years ago, the proof of this theorem has been retaining attention. According to the most recent reviews [32] and works on this topic [1, chap. 3], it has been proven using very different techniques: [13, 6, 88, 79, 26], using global methods, sometimes stemming from the analysis of the precession rate as initiated in proposition XLV of [117]; [21, 65, 163, 55], developing perturbative expansions; [151, 64, 141], using inverse transformations methods; [132], by searching for additional constants of motion; and [56], mainly using Birkhoff invariants along circular orbits in a generic potential. Furthermore, the original proof does not mention the case of collision orbits. We will therefore consider the result of Bertrand's theorem under the hypotheses of orbits that are bounded in position and bounded away from 0. We propose here to show that, in fact, Bertrand's theorem is a refined property of the isochrone one.

**Theorem 2.4.** *In a given radial potential  $\psi$ , if all non-circular orbits that are bounded in position and bounded away from 0 are closed, then  $\psi$  is isochrone.*

*Proof.* In a given radial potential  $\psi$ , if all bounded and bounded away from 0 orbits are closed, the increment of the azimuthal angle  $\Delta\varphi$  during the transfer from  $r_a$  to  $r_p$  is a fractional multiple of  $2\pi$ , i.e. the quantity  $n_\varphi = \frac{\Delta\varphi}{2\pi} \in \mathbb{Q}$ . But, for a given radial potential  $\psi(r)$ , we have that

$$n_\varphi = -\frac{\partial \mathcal{A}_r}{\partial \Lambda} = \frac{1}{\pi} \int_{r_p}^{r_a} \frac{\Lambda}{r^2 \sqrt{2[\xi - \psi(r)] - \frac{\Lambda^2}{r^2}}} dr \quad (2.43)$$

is a continuous mapping  $(\xi, \Lambda) \mapsto n_\varphi(\xi, \Lambda)$ . By continuity, if there are only closed orbits in the potential, then the function  $n_\varphi$  has to be constant,  $n_\varphi = \text{cst} \in \mathbb{Q}$ , as it is well-known for a continuous function of  $\mathbb{R}$  into  $\mathbb{Q}$ , since the set  $\mathbb{R} \setminus \mathbb{Q}$  is dense in  $\mathbb{R}$ . Under these conditions we then have

$$\frac{\partial n_\varphi}{\partial \xi} = 0. \quad (2.44)$$

This characterizes an isochrone potential according to theorem 2.1. The potentials of the form  $-\frac{\mu}{r^\alpha}$  with  $\alpha > 2$  are excluded because all orbits that are bounded in position either collide at the origin or are circular.  $\square$

Using the completeness of  $\mathbb{I}_{\text{pot}}$  that we have obtained through a geometric description, we can go deeper into the consequences of theorem 2.4. More specifically, we have obtained in table (2.41) the explicit value of  $n_\varphi$  for all isochrone potentials. The completeness of our description and that table enable us to claim that Bertrand's theorem is a corollary of theorem 2.4.

**Corollary 2.3.** *The Bertrand theorem! There are only two central potentials for which all non-circular orbits that are bounded in position and bounded away from 0 are closed, namely the Keplerian and the harmonic potentials.*<sup>2</sup>

*Proof.* As the quantities  $\frac{\Lambda}{2\sqrt{4b\mu+\Lambda^2}}$  and  $\frac{\Lambda}{\sqrt{\lambda+\Lambda^2}}$  in proposition 2.4 and 2.5 cannot be rational for each value of  $\Lambda$ , among all isochrone potentials, only  $\psi_{\text{ke}}$  and  $\psi_{\text{ha}}$  have rational  $n_\varphi$  for all orbits, i.e. for all values of  $(\xi, \Lambda)$ .  $\square$

In a given potential, the fact that all bounded orbits are closed, namely Bertrand's property, is then a supplementary restriction to the isochrone one.

<sup>2</sup>We thank Alain Albouy and Jean-Baptiste Fouvry who contributed to this new proof of Bertrand theorem.

## 2.5 Isochrones' relationships, on the road to isochrone relativity

To summarize, the two sets  $\mathbb{I}_{\text{pot}}$  and  $\mathbb{I}_{\text{par}}$  are in bijection and theorem 2.3 states that, from a mathematical point of view, they are four-dimensional manifolds. As a matter of fact, each isochrone potential is uniquely determined by four real parameters  $(\mu, b, \epsilon, \lambda)$  with  $\mu > 0$ ,  $b \geq 0$  and  $(\epsilon, \lambda) \in \mathbb{R}^2$  — n.b. for  $\psi_{\text{bo}}$ ,  $b > 0$ .

We have also seen that the two-dimensional affine group  $\mathbb{A} \simeq (\mathbb{R}^2, +)$ , generated by the affine transformations  $J_{\epsilon, \lambda}$  with  $(\epsilon, \lambda) \in \mathbb{R}^2$ , acts on both sets, either on potentials or on the corresponding parabolas. Since the dimension of  $\mathbb{A}$  is less than the dimension of  $\mathbb{I}_{\text{pot}}$  and  $\mathbb{I}_{\text{par}}$  ( $2 < 4$ ), the action is not transitive and each group orbit  $\mathbb{A} \cdot \psi$  or  $\mathbb{A} \cdot \mathcal{P}$  for corresponding potential  $\psi$  or parabola  $\mathcal{P}$  is a two-dimensional sub-manifold of  $\mathbb{I}_{\text{pot}}$  or  $\mathbb{I}_{\text{par}}$ .

Besides, we note that relations exist between the isochrone potentials. As a matter of fact,  $\psi_{\text{ke}}$  and  $\psi_{\text{ha}}$  come from  $\psi_{\text{he}}$  when  $b \rightarrow 0$  and  $b \rightarrow +\infty$ , respectively. Furthermore, known relations exist between  $\psi_{\text{ke}}$  and  $\psi_{\text{ha}}$ , such as the Bohlin or Levi-Civita transformation ([19], [8], [99], see also chapter 3) which maps the harmonic orbits onto Keplerian ones and vice versa. All these relations are not in the scope of the affine group action and do not affect the parameters  $(\mu, b)$  or  $\omega$  of the concerned potentials.

Nevertheless, making use of rotations  $R_\theta$  of an angle  $\theta$  in the Hénon plane and starting for instance from the laid Kepler parabola, we can obtain a new parabola with an arbitrarily oriented axis of symmetry. Then, acting with  $J_{\epsilon, \lambda}$ , we can recover the corresponding reduced parabola in one of the four families. This operation is graphically illustrated in figure 2.9 in the case of the morphing from the Kepler isochrone to the Hénon isochrone.

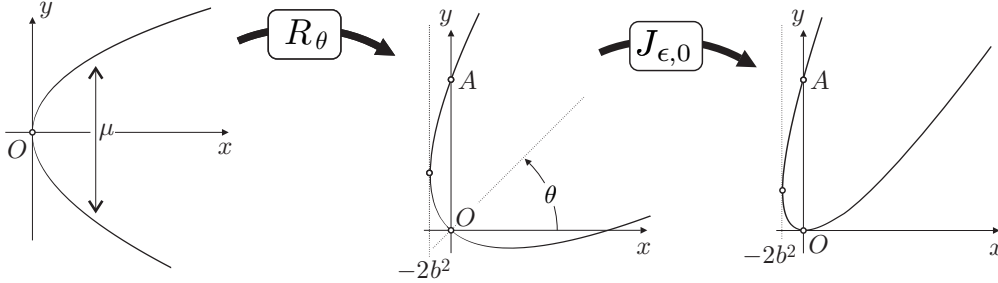


Figure 2.9: Rotation and transvection of the Kepler parabola to a Hénon one.

Additionally varying the unique parameter  $\mu$  of the Kepler potential, written as

$$y_{\text{ke}}(x) = -\mu\sqrt{2x} \quad (2.45)$$

in Hénon's variables, the aperture of its laid parabola varies and produces a variation of the  $b$  parameter of the Hénon potential corresponding to the negative part of the rotated parabola. Using this process one can easily understand that when  $\theta \in (-\frac{\pi}{2}, +\frac{\pi}{2})$ , we recover a Hénon potential  $\psi_{\text{he}}$ ; when  $\theta \in (\frac{\pi}{2}, +\frac{3\pi}{2})$ , we recover the bounded potential  $\psi_{\text{bo}}$ ; and for  $\theta = +\frac{\pi}{2}$ , we obtain the harmonic  $\psi_{\text{ha}}$  from the Kepler potential  $\psi_{\text{ke}}$ . More generally, any isochrone potential is contained in the group orbit of a Kepler potential under the action of the group  $\text{SO}(2) \ltimes \mathbb{A}$ .

The affine group action on the isochrone sets is thus restricted, we investigate other possible

relations between isochrone systems in the next chapter. We will see that relevant isochrone rotations are not Euclidian but hyperbolic.



## Isochrone relativity

---

SPECIAL relativity was introduced to write the laws of physics in the same way in any inertial referential. A very useful feature at the time of Albert Einstein, when different clocks in the same city possibly indicated different times. In this theory, changes of referentials are achieved through transforms of time and space. As a matter of fact, there also exist preferential frames to describe the motion in isochrone systems.

In this chapter we investigate relations between isochrones and hence get the essence of isochrony. We remind a classical relation between the two fundamental Keplerian and harmonic systems, which we extend to the whole set of isochrones. This reveals the intrinsic Keplerian nature of isochrony. As a result, an isochrone relativity has been developed in SPD, by analogy with special relativity. We geometrically look through this relativity. Eventually, we extend an essential symmetry of Keplerian systems to isochrone ones, namely the third Kepler law.

### 3.1 From Hooke to Kepler

Let us remind here a classical canonical transformation of a harmonic orbit into an elliptic Keplerian one. It creates an opening route from isochronous to isochrone systems.

In the two central potentials

$$\psi_{\text{ha}}(q) = \frac{1}{2}\omega q^2 \quad (3.1)$$

and

$$\psi_{\text{ke}}(r) = -\frac{\mu}{r}, \quad (3.2)$$

bound particles move on planar elliptical orbits, with respectively a center of attraction located at the center or at one of the foci of the ellipses. In the following proposition, we denote by  $p_Q$  the generalized momentum associated to a coordinate  $Q$ .

**Proposition 3.1.** *Let  $q$  and  $\theta$  be polar coordinates for a harmonic system. Let  $\ell \in \mathbb{R}^*$ . The canonical transformation*

$$(q, p_q) \mapsto (r, p_r) = \left( \frac{q^2}{\ell}, \frac{\ell p_q}{2q} \right) \quad (3.3)$$

*maps a harmonic orbit into a Keplerian one. One can further synchronize the two orbits with the unique parameter  $\varphi = 2\theta$ , when the associated generalized momenta are related by  $p_\varphi = \frac{p_\theta}{2}$ .*

*Proof.* Let consider a particle of mass  $m = 1$ , then its hamiltonian corresponds to  $\mathcal{H} = \xi$  and its angular momentum is such that  $L = \Lambda$ . The harmonic hamiltonian is defined by

$$\mathcal{H}_{\text{ha}} = \frac{1}{2} \left( p_q^2 + \frac{p_\theta^2}{q^2} \right) + \frac{1}{2}\omega q^2. \quad (3.4)$$

The momentum of the particle satisfy

$$p_q = \frac{dq}{dt} \text{ and } p_\theta = q^2 \frac{d\theta}{dt}. \quad (3.5)$$

For the transformation to be canonical, it must preserve the symplectic structure of phase space, i.e. the new variables must satisfy

$$\frac{\partial r}{\partial q} \frac{\partial p_r}{\partial p_q} - \frac{\partial r}{\partial p_q} \frac{\partial p_r}{\partial q} = 1. \quad (3.6)$$

By choosing  $r = \frac{q^2}{\ell}$ , the derivative  $\frac{\partial r}{\partial p_q}$  vanishes and one gets  $p_r = \frac{\ell p_q}{2q}$ . In the transformed variables, the hamiltonian can be expressed as

$$\mathcal{H}_{\text{ha}} = \frac{4r}{\ell} \left[ \frac{1}{2} \left( p_r^2 + \frac{p_\theta^2}{4r^2} \right) + \frac{\omega^2 \ell^2}{8} \right], \quad (3.7)$$

where left and some right terms can be exchanged to rewrite it as

$$-\frac{\omega^2 \ell^2}{8} = \frac{1}{2} \left( p_r^2 + \frac{p_\theta^2}{4r^2} - \frac{\ell \mathcal{H}_{\text{ha}}}{4r} \right). \quad (3.8)$$

If one defines  $\mathcal{H}_{\text{ke}} = \xi_{\text{ke}} = -\frac{\omega^2 \ell^2}{8} < 0$  and  $\mu = \ell \mathcal{H}_{\text{ha}}$ , then the equation (3.8) corresponds to the definition of a Keplerian Hamiltonian with a negative energy

$$\mathcal{H}_{\text{ke}} = \frac{1}{2} \left( p_r^2 + \frac{p_\varphi^2}{r^2} \right) - \frac{\mu}{r}. \quad (3.9)$$

By finally setting  $p_\varphi = \frac{p_\theta}{2}$ , and computing  $\frac{dq}{d\theta} = \frac{dq}{d\theta}$  and  $\frac{dr}{d\varphi} = \frac{dr}{d\varphi}$  from their respective hamiltonians, one can synchronize the orbits  $q(\theta)$  and  $r(\varphi)$  with  $2\theta = \varphi$ , as illustrated in the left panel of figure 3.1.  $\square$

This transformation was initiated by Newton in his Principia, and Hooke in their correspondance. Its inverse has been then formalized by C. MacLaurin [102], E. Goursat [63] and G. Darboux [37], by reformulating it in complex coordinates as the transformation  $z \mapsto z^2$ . They were followed by Tullio Levi-Civita for the regularization of the two-body problem [94], mapping a Keplerian into a harmonic ellipse on a zero energy surface. In celestial mechanics, the Bohlin transformation which corresponds to  $z \mapsto \frac{1}{2}z^2$ , [19, 8] corresponds to the choice  $l = \frac{1}{2}$  in the proof above.

This linear mapping of harmonic into Keplerian orbits exchanges the energy and potential terms. Since  $p_\varphi = \Lambda = r^2 \frac{d\varphi}{dt}$ , the harmonic hamiltonian can be expressed in Hénon's variables as

$$\mathcal{H}x = 4x^2 p_x^2 + p_\theta^2 + Y(x), \quad (3.10)$$

with  $x = x_{\text{ha}} = 2q^2$ . The image variables are such that  $x' = x_{\text{ke}} = 2r^2$ . The Bohlin transformation then corresponds to a total exchange of the quantities  $\mathcal{H}x$  and  $Y(x) = x\psi(x)$ , with the conserved orbital energy  $\mathcal{H} = \xi$ . As a matter of fact, it can be written as

$$\begin{bmatrix} \mathcal{H}'x' \\ y' \end{bmatrix} = \begin{bmatrix} 0 & -1 \\ -1 & 0 \end{bmatrix} \begin{bmatrix} \mathcal{H}x \\ y \end{bmatrix}. \quad (3.11)$$

Since isochrone potentials bridge harmonic and Keplerian dynamics (see section 2.4.1, e.g.  $\psi_{\text{he}}$  interpolates between  $\psi_{\text{ha}}$  and  $\psi_{\text{ke}}$ ), is it possible to relate them through a *partial* exchange of the energy and potential terms? The answer is positive and is presented in the next section.

## 3.2 Isochrone transformations

The Bohlin transformation regularizes Keplerian orbits and brings out a direct relation between Keplerian and harmonic systems. We propose now to generalize it to isochrone orbits.

### 3.2.1 The BOLST transformation

Consider a PRO,  $(r, \varphi) \in \mathbb{O}_\psi$ , in a radial potential  $\psi$ . In Hénon's variables

$$x = 2r^2 \text{ and } Y(x) = x\psi(x), \quad (3.12)$$

the dynamics is governed by the ordinary differential equation (2.14), coming from the hamiltonian  $\mathcal{H}$  that satisfies

$$\mathcal{H}x - Y(x) = 4x^2 p_x^2 + p_\varphi^2. \quad (3.13)$$

When the potential is isochrone, the graph of  $Y$  is a parabola. A linear transformation of (3.13) will preserve this property, mapping the initial orbit into another one which is characterized by

$$\mathcal{H}'x' - Y'(x') = 4(x')^2 (p_{x'})^2 + (p_{\varphi'})^2, \quad (3.14)$$

where  $Y'$  contains an isochrone potential  $\psi' \in \mathbb{I}_{\text{pot}}$ , which can be different from  $\psi$ . From now on, we consider that  $\psi \in \mathbb{I}_{\text{pot}}$ , and give the respective conserved energies of the two orbits,  $\xi = \mathcal{H}$  and  $\xi' = \mathcal{H}'$ . In addition, we remind that  $p_\varphi = \Lambda$  and  $p_{\varphi'} = \Lambda'$ .

As suggested in section 3.1 and further discussed in SPD p.19, we propose a partial exchange of energy and potential terms which conserves the differences

$$\mathcal{H}'x' - Y'(x') = \mathcal{H}x - Y(x). \quad (3.15)$$

The more general linear transformation of  $\mathbf{w} = (\xi x, y)^\top$  satisfying the constraint (3.15) is given by

$$\mathbf{w}' = B_{\alpha, \beta}(\mathbf{w}) \text{ with } B_{\alpha, \beta} = \begin{bmatrix} \alpha & \beta \\ \alpha - 1 & \beta + 1 \end{bmatrix}, \quad (\alpha, \beta) \in \mathbb{R}^2. \quad (3.16)$$

We assume  $\det(B_{\alpha, \beta}) = \alpha + \beta \neq 0$  because the corresponding singular transformation leads to constant potentials or not well-defined image orbits. As a consequence,  $B_{\alpha, \beta}$  will be invertible and can be used to change reference frames. In this case we call  $B_{\alpha, \beta}$  a BOLST in the general case or an *i*-BOLST when it is symmetric. Reasons for these names will become clear later.

The BOLSTS generalize the Bohlin transformation, which corresponds to  $B_{0, -1}$  as in (3.11), and unify the isochrone sets  $\mathbb{I}_{\text{pot}}$  and  $\mathbb{I}_{\text{par}}$ . They map isochrone orbits together as settled by the following theorem.

**Theorem 3.1.** *Only the harmonic and Keplerian potentials can exchange their radial orbits with a linear change of polar angle. The transformation of a Kepler system into a scaled Kepler system is given by  $B_{\alpha, 0}$ . On the other hand,  $B_{0, \beta}$  maps a Kepler system onto a harmonic one by fully exchanging the energy and potential. This is the classical Bohlin transformation.*

*Otherwise, when  $\alpha\beta \neq 0$ , the image of a Keplerian PRO by  $B_{\alpha, \beta}$  is an isochrone orbit. Its azimuthal angle is given by*

$$\varphi'(\varphi) = \frac{\varphi}{2} + \frac{\chi}{\sqrt{(1+\chi)^2 - e^2}} \arctan \left[ \sqrt{\frac{1+\chi-e}{1+\chi+e}} \tan \left( \frac{\varphi}{2} \right) \right] \quad \text{with } \chi = \frac{p\alpha|\xi|}{\mu\beta}, \quad (3.17)$$

where  $p$  and  $e$  are respectively the semilatus rectum and excentricity of the primary Keplerian orbit. The expression holds when  $\alpha \rightarrow 0$  and for the neutral BOLST  $B_{\alpha, 0}$  when  $\beta \rightarrow 0$ . The



precession  $\Delta\varphi'$  of the transformed polar angle during the transfer from the periastron to the apoastron and back is given by

$$\Delta\varphi' = \pi \left( 1 + \frac{\chi}{\sqrt{(1+\chi)^2 - e^2}} \right). \quad (3.18)$$

*Proof.* The detailed proof and derivation of orbital parameters of BOLSTED orbits can be found in the complement SPD pp. 20-23. It relies on the investigation of the equations of motion, As for the canonical transformation in section 3.1, the same area law,  $\Lambda = \Lambda'$ , is assumed in a first step. This point and the formulation of the constraints are introduced in SPD pp. 18-20.  $\square$

As we explained before, the special case  $B_{0,-1}$  corresponds to the total exchange between energy and potential, as in the Bohlin transformation. In the other cases, the BOLSTS generalize it. The action of  $B_{\alpha,0}$  and  $B_{0,\beta}$  is delineated in figure 3.1. And the isochrone rosette orbit that results from the BOLST action on a keplerian ellipse is represented in figure 3.2. Notice that the image orbit is not always a PRO.

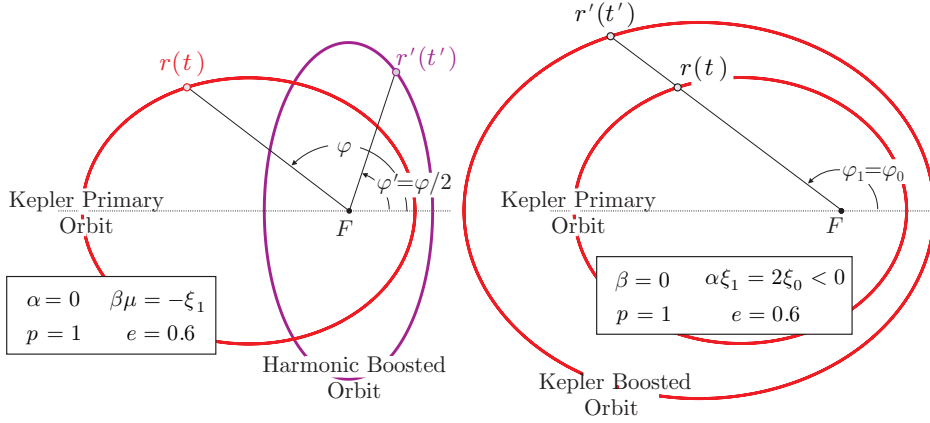


Figure 3.1: The transformation  $B_{0,\beta}$  of a Keplerian PRO gives a harmonic PRO when  $\beta\xi' < 0$ , as represented on the left panel. The transformation  $B_{\alpha,0}$  of a Keplerian PRO gives a Keplerian PRO when  $\alpha > 0$  and  $\xi' < 0$ , as represented on the right panel.

### 3.2.2 The $i$ -BOLST transformation

Afterwards, we favor the case where the matrix of a BOLST is symmetric, for the sake of simplicity. The BOLSTS are then reduced to the following transformations, without loss of generality.

**Definition 3.1.** Let  $\gamma$  be a non-vanishing real parameter. We define an  $i$ -BOLST by the matrix

$$B_\gamma = \frac{1}{2} \begin{bmatrix} \gamma + 1 & \gamma - 1 \\ \gamma - 1 & \gamma + 1 \end{bmatrix}. \quad (3.19)$$

The BOLST matrices can be recovered from  $i$ -BOLSTS through specific transvections, presented in the complement SPD p. 33. The set of  $i$ -BOLSTS form a commutative linear group

$$\mathbb{B} = \{B_\gamma, \gamma \in \mathbb{R}^*\}, \quad (3.20)$$

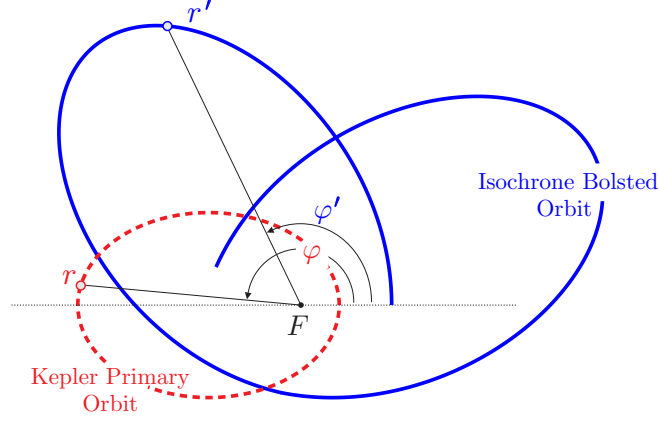


Figure 3.2: The  $\alpha = 1.5$  and  $\beta = 0.6$  BOLST of a Keplerian ellipse ( $e \simeq 0.7$ ;  $p \simeq 0.35$ ) which gives an isochrone orbit with the same energy ( $\xi = \xi' = -1$ ).

with the commutative law

$$\forall (\gamma, \gamma') \in \mathbb{R}^* \times \mathbb{R}^*, \quad B_\gamma \circ B_{\gamma'} = B_{\gamma'} \circ B_\gamma = B_{\gamma\gamma'} \in \mathbb{B}. \quad (3.21)$$

For this multiplicative law,  $B_1$  is an identity element. The inverse of a transformation  $B_\gamma$  for  $\gamma \in \mathbb{R}^*$  is  $B_{\frac{1}{\gamma}}$ . As stated in proposition 3.2, the group action of  $\mathbb{B}$  covers the isochrone sets  $\mathbb{I}_{\text{pot}}$  and  $\mathbb{I}_{\text{par}}$ .

**Proposition 3.2.** *Any isochrone potential is in the group orbit of the Kepler potential — canonical, physical or gauged — under the action of the  $\mathbf{i}$ -BOLST group  $\mathbb{B}$ .*

*Proof.* The explicit formulation of the parameters of the image isochrone potentials can be obtained by direct resolution of quadratic equations. They are made explicit in SPD p. 31, when the primary orbits are keplerian or harmonic. A diagram in figure 3.3 gathers the resulting types of isochrone image potentials.  $\square$

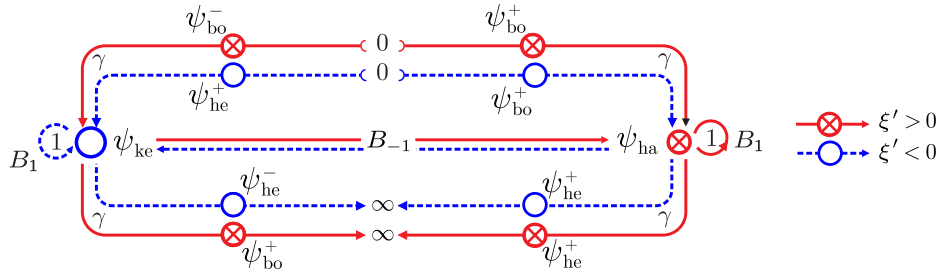


Figure 3.3: Diagram of the  $\mathbf{i}$ -BOLST action on isochrone potentials. The possible  $\mathbf{i}$ -BOLSTED potentials are defined up to an additive constant, symbolized by + or – indices, and analytically defined in the complement SPDp. 31.

In physics, the additive representation of groups often reveals to be even more meaningful. Therefore, after obtaining the generation of isochrones from the Keplerian potential as explained in proposition 3.2 and figure 3.3, we have looked for this and for its consequences. As a matter of

fact, in their additive representation,  $\mathbf{i}$ -BOLSTS can be decomposed as the 1-parameter product of a homothety and a hyperbolic rotation, namely

$$B_\chi = e^\chi \begin{bmatrix} \cosh(\chi) & \sinh(\chi) \\ \sinh(\chi) & \cosh(\chi) \end{bmatrix} \quad (3.22)$$

when  $\gamma = e^{2\chi} > 0$ . The negative case ( $\gamma < 0$ ) can be obtained from the positive one by a supplementary symmetry around the anti-diagonal  $y = -\xi x$ . Then, their action on isochrone parabolas and potentials can be clarified: not only they do gather isochrones in a 1-parameter family, but they do this in a way that is analogous to special relativity. This is the purpose of section 3.3. Noticeably, the group of  $\mathbf{i}$ -BOLSTS is a subgroup of conformal transformations as in relativity. In reference to the generalization of the Bohlin transformation and to the hyperbolic rotations of special relativity — boosts or Lorentz transformations, the name BOLST stands for bohlin boost and  $\mathbf{i}$ -BOLST for symmetric bohlin boost.

### 3.3 The essence of isochrony

Under the  $\mathbf{i}$ -BOLST group action, the isochrone sets  $\mathbb{I}_{\text{pot}}$  and  $\mathbb{I}_{\text{par}}$  coincide with the group orbit of the keplerian class of equivalence that is defined by the  $\mathbb{A}$ -group action. Thus, we can assert that

**Theorem 3.2.** *To be isochrone is essentially to be Keplerian.*

This crucial property reveals the essential nature of isochrony and can be figured out with the isochrone relativity for the reasons we explain in this section.

#### 3.3.1 Isochrone structure of the affine plane

Let us consider that the parameter  $\xi$  is fixed, and defines a PRO of angular momentum  $\Lambda$  in  $\psi_{\text{ke}}$ . We define by  $\mathcal{R} = (\mathbf{i}, \mathbf{j})$  the canonical basis of the plane containing the isochrone parabolas, identified with  $\mathbb{R}^2$ . An  $\mathbf{i}$ -BOLST structures this affine plane where the isochrone parabolas lie, when it is meshed with the system of coordinates  $(\xi x, y)$ , as does the metrics with the affine space in special relativity, which is meshed with  $(ct, x)$ . As a matter of fact, its eigenvectors are defined by

$$\mathbf{k} = \frac{1}{\sqrt{2}} (\mathbf{i} - \mathbf{j}) \text{ and } \mathbf{l} = \frac{1}{\sqrt{2}} (\mathbf{i} + \mathbf{j}), \quad (3.23)$$

such that

$$B_\gamma(\mathbf{k}) = \mathbf{k} \text{ and } B_\gamma(\mathbf{l}) = \gamma \mathbf{l}. \quad (3.24)$$

Then, its eigendirections define an invariant cone  $\mathcal{C} = \mathbb{R}\mathbf{k} \cup \mathbb{R}\mathbf{l}$  which splits the affine plane, as determined in definition 3.2. We use there the Minkowski inner product, for which

$$\forall \mathbf{z} = (z_1, z_2) \in \mathbb{R}^2, \langle \mathbf{z} | \mathbf{z} \rangle = z_1^2 - z_2^2. \quad (3.25)$$

**Definition 3.2.** The radial cone

$$\mathcal{C} = \{ \mathbf{z} \in \mathbb{R}^2, \langle \mathbf{z} | \mathbf{z} \rangle = 0 \}, \quad (3.26)$$

the periodic space

$$\mathcal{P} = \{ \mathbf{z} \in \mathbb{R}^2, \langle \mathbf{z} | \mathbf{z} \rangle < 0 \}, \quad (3.27)$$

and the aperiodic space

$$\mathcal{A} = \{\mathbf{z} \in \mathbb{R}^2, \langle \mathbf{z} | \mathbf{z} \rangle > 0\} \quad (3.28)$$

define invariant domains of the affine plane under the action of  $\mathbf{i}$ -BOLSTS.

The radial cone appellation comes from the fact that  $y = \xi x$  defines a radial orbit ( $\Lambda = 0$ ) of energy  $\xi$ . As its period should be infinite, a radial orbit is not a PRO but we can say that it is a maximal time-bounded orbit. Since the convex  $x$ -positive part of parabolas containing PROs in the coordinate system  $(\xi x, y)$  is delimited by  $\mathcal{C}$  and exactly contained in  $\mathcal{P}$ , the names of  $\mathcal{P}$  and  $\mathcal{A}$  follow.

Furthermore, the  $\mathbf{i}$ -BOLSTS do not preserve a quadratic form as in special relativity but assure the linear exchanges between time and space. By definition, the  $\mathbf{i}$ -BOLST preserves the intervals

$$\xi' x' - y' = \xi x - y. \quad (3.29)$$

However,  $\mathbf{i}$ -BOLSTS are generally not isometries, and the eigenvalue  $\gamma$  leads to the equality

$$\xi' x' + y' = \gamma (\xi x + y). \quad (3.30)$$

Thus, by multiplication of (3.29) and (3.30), one gets

$$(\xi' x')^2 - y'^2 = \gamma \left[ (\xi x)^2 - y^2 \right], \quad (3.31)$$

unlike the preserved space-time intervals of special relativity.

### 3.3.2 Relativity of isochrone orbits

As the Lorentz transformations, the action of  $\mathbf{i}$ -BOLSTS consists in swiveling the parabolas so that the image of their tangents and symmetry axes give the tangents and directions of the symmetry axes of the image parabolas. For example, consider the  $\mathbf{i}$ -BOLST  $B_\gamma \in \mathbb{B}$ . Let  $(\mathbf{u}, \mathbf{v})$  be the resulting image of the canonical basis  $(\mathbf{i}, \mathbf{j})$  by  $B_\gamma$ . When starting from an initial keplerian parabola  $\mathcal{P}$ , of tangent directed by  $\mathbf{i}$  and symmetry axis directed by  $\mathbf{j}$ , the tangent of the  $\mathbf{i}$ -BOLSTED parabola  $\mathcal{P}'$  will be directed by  $\mathbf{u}$  and its symmetry axis by  $\mathbf{v}$ . In other words, in  $(0, \mathbf{u}, \mathbf{v})$ , the parabola  $\mathcal{P}'$  has a vertical tangent at the origin and a horizontal symmetry axis. Therefore,  $\mathcal{P}'$  is of keplerian type in this frame. It is then natural to define  $(O, \mathbf{u}, \mathbf{v})$  as being the reference frame of the isochrone parabola  $\mathcal{P}'$ .

**Definition 3.3.** The reference frame of a given parabola  $\mathcal{P}$  is the frame  $(O, \mathbf{t}, \mathbf{n})$  where the tangent to the parabola at the origin is  $\mathcal{T}_O(\mathcal{P}) = \mathbb{R}\mathbf{t}$  and the symmetry axis is  $\mathcal{S}(\mathcal{P}) = \mathbb{R}\mathbf{n}$ .

In their reference frames, all physical isochrone parabolas are keplerian.<sup>1</sup>

Moreover, in the system of coordinates  $(\xi x, y)$ , PROs are contained in the arcs of parabolas delimited by the intersections of the convex positive parts of the parabolas with the lines

$$y = -X - \Lambda^2, \quad \text{with } X = -\xi x. \quad (3.32)$$

They are all contained in-between the extremal line that is tangent to the parabola and that determines a circular orbit, and the one that crosses the parabola at  $x = 0$ . An initial orbit,

<sup>1</sup>This property holds for gauged potentials, if one defines the reference frame with the tangent at the intersection between the ordinate axis and the  $x$ -positive convex branch of the parabola.

defined by a line  $\Delta$ , has an image that is defined by  $\Delta' = B_\gamma(\Delta)$ . We have plotted an example in figure 3.4 when  $\gamma > 1$ . In that case, the image parabola is of Hénon type. When the energy is kept constant during the mapping, i.e. when  $\xi' = \xi$ , the radial distances of the isochrone PRO, on the arc between  $P'$  and  $A'$  as represented in figure 3.4, are related by the  $\mathbf{i}$ -BOLST to their  $\mathbf{l}$ -parallel projections on the Keplerian parabola. When  $|\xi'| \neq |\xi|$ , the image orbit is shifted along the isochrone parabola, creating spatial distortion when observed from  $(O, \mathbf{i}, \mathbf{j})$ .

In the Keplerian reference frame of the isochrone, the precessing orbit is viewed as a Keplerian ellipse, which center of force is the center of the isochrone. The radial distances, that can be read on the arcs of parabolas, along with the related angles, given by theorem 3.1, allow to define relative frames in which the orbit are either precessing or Keplerian. The relative orbits are illustrated in figure 3.4. In the reference frame of  $\mathcal{P}$  and  $\mathcal{P}'$ , both orbits have the same angular momentum, while the precessing orbit shows the angular momentum  $\Lambda'$  in the Keplerian frame.

The role of the light velocity is played here by the energy. Introducing the proper time  $\tau$  such that  $d\tau = \xi dt$ , the orbital differential equation in the affine coordinate system  $(\xi x, y)$  can be written in the same way in all reference frames. Its expression, given in theorem (3.3), is invariant under the action of  $\mathbf{i}$ -BOLSTS.

**Theorem 3.3.** *An orbit is isochrone if and only if it is the  $\mathbf{i}$ -BOLSTED image of a Keplerian orbit. Let  $(\xi, \Lambda)$  define a PRO. In the affine coordinate system  $(\xi x, y)$ , the vector  $\mathbf{w}$  that points towards the corresponding arc of parabola satisfies the orbital differential equation*

$$\frac{1}{16} \left[ \frac{d}{d\tau} (\mathbf{w}|\mathbf{t}) \right]^2 = (\mathbf{w}|\mathbf{t} - \mathbf{n}) + (\mathbf{w}_\Lambda|\mathbf{n}), \quad (3.33)$$

where  $\mathbf{w}_\Lambda = -\Lambda^2 \mathbf{j}$  and  $(O, \mathbf{t}, \mathbf{n})$  is the reference frame of the parabola.

Hitherto, we have constructed the Hénon-isochrone image of a Keplerian elliptic orbit. Yet, the  $\mathbf{i}$ -BOLST actually deserves to be used in the reverse sense of the mapping, in order to find the Keplerian counterpart of an isochrone orbit as illustrated in figure 3.4. Such construction and isochrone relativity foundations are developed in SPD pp. 24-33. With a constant energy, different values of orbit can be related to Keplerian parabola. For the reader convenience, we gather the admitted values for the angular momentum.

- In the Keplerian potential  $\psi_{\text{ke}}(r) = -\frac{\mu}{r}$ , the existence of a PRO depends on the values of the angular momentum as stated by lemma 2.1. Its allowed values in the Keplerian potential are

$$0 \leq \Lambda^2 \leq \frac{\mu^2}{2|\xi|} \quad (3.34)$$

with  $\xi$  the specific energy of the PRO. In that case, the apo- and pericenters are the roots of the radial velocity:

$$r_{a,p} = \frac{-\mu \pm \sqrt{\mu^2 + 2\xi\Lambda^2}}{2\xi}. \quad (3.35)$$

- In the same way, in the potentials  $\psi(r) = \frac{\mu}{b \pm \sqrt{b^2 + sr^2}}$  with  $\mu \in R$ ,  $b > 0$ , and  $s = \pm 1$ , a PRO exists if

$$4\mu b \leq \Lambda^2 \leq \frac{1}{2} \frac{(4\xi^2 b^2 - 4\xi b\mu + \mu^2)}{s(-\xi)} \quad (3.36)$$

Then, the roots of its radial velocity can be written as

$$r_{a,p} = \frac{1}{2} \sqrt{-\frac{-2s\xi\Lambda^2 - 2\mu^2 + 4\xi b\mu \pm 2\sqrt{\Delta}}{s(\xi)^2}} \quad (3.37)$$

with  $\Delta = 4\xi^2 b^2 \mu^2 + 2s\xi\Lambda^2 \mu^2 - 4\mu^3 \xi b + \mu^4$ .

- In the harmonic potential,  $\psi_{ha}(r) = \frac{1}{2}\omega^2 r^2$ , a PRO exists if

$$0 \leq \Lambda^2 \leq \left(\frac{\xi}{\omega}\right)^2. \quad (3.38)$$

The apo- and pericenters are then given by

$$r_{a,p} = \sqrt{\frac{\xi \pm \sqrt{\xi^2 - \omega^2 \Lambda^2}}{\omega^2}}. \quad (3.39)$$

These relations are then useful for orbital isochrone constructions.

### 3.3.3 Dictionary for isochrone and special relativity

Consider a set of isochrone PROs of energy  $\xi$ . We summarize the precedent analogies between special and isochrone relativities with the following correspondences in table 3.1.

The Keplerian nature of isochrones induces the preservation of Keplerian symmetries. Specifically, the understanding of the way in which lengths can be transformed in the affine space of parabolas enables us to express a generalization of Kepler's Third Law in any isochrone potential.

## 3.4 Generalization of Kepler's Third Law

The Kepler potential  $\psi_{ke}(r) = -\frac{\mu}{r}$  is sourced by a point of mass  $M$  such that  $\mu = \mathcal{G}M$  where  $\mathcal{G}$  is the Newton constant. Radially periodic orbits close after one radial period  $\tau_r$  and form ellipses with semi major axes  $a = -\frac{\mu}{2\xi}$ . In his last major book *Harmonices Mundi* [83], Johannes Kepler proposed in 1619 his third law claiming that  $\tau_r^2 \times a^{-3}$  is constant for all ellipses. Isaac Newton, half a century later, proved this empirical observation using his laws of dynamics and his gravitational force. This law appears to become a cornerstone of celestial mechanics because the Kepler constant appears to be  $\tau_r^2 a^{-3} = \frac{4\pi^2}{\mu}$  and thus gives the mass of the attracting body.

We have shown that Kepler potential generates the isochrone group and we remark that Kepler's third law could be generalized. As a matter of fact, considering the specific energy  $\xi$  associated with a given PRO in an isochrone potential  $\psi \in \{\psi_{ke}, \psi_{he}, \psi_{bo}\}$ , we see that according to proposition 2.4, except for the harmonic potential, all isochrone orbits are such that

$$\tau_r^2 |\xi|^3 = \frac{\pi^2 \mu^2}{2} = \text{cst}. \quad (3.40)$$

Nevertheless, the law (3.40) expressed in terms of the specific energy is not stable under transvections of the potential,  $\psi \mapsto \psi^* = \psi + \epsilon$ , and has to be slightly modified for physical potentials when adding a constant, see SPD p. 38.

Isochrone relativity ( <i>i</i> -SR)	Special relativity (SR)
Preserved isochrone interval $\xi'x' - y' = \xi x - y$ but $\xi'x' + y' = \gamma(\xi x + y)$	Preserved space-time interval $c^2 dt^2 - d\mathbf{r}^2$
orbital energy $\xi$	light velocity $c$
radial cone	light cone
periodic-like vectors	time-like vectors
aperiodic-like vectors	space-like vectors
reference frames with $\varphi'$	inertial frames
proper time for reference observers	proper time for inertial observers
<i>i</i> -BOLST: change of parabola reference frame	Boost: change of inertial frame
time and length distortion when varying the energy $\xi'$ with respect to its Keplerian counterpart $\xi$	length-contraction and time-dilatation when the observer moves with constant velocity with respect to inertial frame

Table 3.1: Special - isochrone relativities dictionary

The formulation of Kepler  $\tau_r^2 \times a^{-3}$  in terms of the geometric parameter  $a$  is more appropriate for conveying the symmetry of the potential. In order to geometrically express Kepler's Third law, we introduce in definition 3.4 "semi major axes", relevant to all isochrone potentials, and directly related to their Keplerian relative description. These characteristic lengths, generally related to specific energies by (3.49), (3.50) and (3.53), provide a method to determine the mass of an isochrone system as mentioned at the end of this section.

**Definition 3.4.** Let  $r_p$  and  $r_a$  be the peri- and apoastron radial distance of a given isochrone periodic orbit. We call the *isochrone semi-major axis* of this orbit by the following lengths:

1. in a Kepler potential,

$$a = \frac{1}{2} (r_a + r_p), \quad (3.41)$$

2. in a homogeneous box of radius  $R$ ,

$$a = \left(\frac{1}{2}\right)^{2/3} R, \quad (3.42)$$

3. in a Hénon potential,

$$a = \frac{1}{2} \left( \sqrt{b^2 + r_a^2} + \sqrt{b^2 + r_p^2} \right), \quad (3.43)$$

4. in a bounded potential,

$$a = \frac{1}{2} \left( \sqrt{b^2 - r_a^2} + \sqrt{b^2 - r_p^2} \right). \quad (3.44)$$

In definition 3.4, we have considered a homogeneous box to include the description of its elliptic trajectories with the Third Law. In fact, the situation of the harmonic potential needs more attention since  $\psi_{\text{ha}}$  is degenerate. In such a potential all test particles share the same period but different specific energies, hence relation (3.40) cannot hold for each specific energy.

The harmonic potential is not exactly representative of a real system because of its constant density and infinite spatial extension, which imply an infinite mass. Instead, the potential associated with a finite homogenous repartition of masses in a ball of radius  $R$  with constant density (while the outside region is empty) does represent a real system and can be written as

$$\psi_{\text{ha}}^R(r) = \begin{cases} \frac{1}{2}\omega^2 r^2 - \frac{3}{2}\omega^2 R^2 & \text{if } r < R \\ -\frac{\mathcal{G}M}{r} & \text{if } r > R. \end{cases} \quad (3.45)$$

We call it a bounded harmonic potential. Additionally, either Gauss' theorem or the continuity of the force at the boundary of the ball leads to the following relation:

$$\mu = \mathcal{G}M = \omega^2 R^3. \quad (3.46)$$

As mentioned on page 43, the harmonic potential corresponds to the limit of an isochrone potential  $\psi_{\text{he}}$  or  $\psi_{\text{bo}}$  when  $b \rightarrow \infty$ . This result holds for the finite harmonic potential  $\psi_{\text{ha}}^R$ . As it will be proven in theorem 3.4, the characteristic length for the finite harmonic also naturally appears in the formulation of Kepler's Third Law.

Now, Kepler's third law can be generalized to all isochrone potentials in theorem 3.4.

**Theorem 3.4.** *For any radially periodic orbit in an isochrone potential, the square of the radial period is proportional to the cube of the isochrone semi-major axis by*

$$\tau_r^2 = \frac{4\pi^2}{\mu} a^3, \quad (3.47)$$

where  $\mu$  is the mass parameter of  $\psi_{\text{ke}}$ ,  $\psi_{\text{he}}$ ,  $\psi_{\text{bo}}$  and  $\mu = \omega^2 R^3$  for  $\psi_{\text{ha}}^R$ .

*Proof.* Using isochrone potential expressions, the radial period (2.7) come from the computation of the radial action

$$\mathcal{A}_r = \frac{1}{\pi} \int_{r_p}^{r_a} \sqrt{2[\xi - \psi(r)] - \frac{\Lambda^2}{r^2}} dr. \quad (3.48)$$

For a Keplerian orbit of energy  $\xi_k < 0$  in  $\psi_{\text{ke}}(r) = -\frac{\mu}{r}$  and a harmonic orbit of energy  $\xi_h > 0$  in  $\psi_{\text{ha}}(r) = \frac{1}{2}\omega^2 r^2$ , we have

$$\mathcal{A}_r^{\text{ke}} = \frac{\sqrt{2|\xi_k|}}{\pi} \int_{r_p}^{r_a} \frac{\sqrt{(r-r_p)(r_a-r)}}{r} dr \text{ with } \begin{cases} r_p + r_a = \frac{\mu}{|\xi_k|} \\ r_p r_a = \frac{\Lambda^2}{2|\xi_k|} \end{cases} \quad (3.49)$$



and

$$\mathcal{A}_r^{\text{ha}} = \frac{\sqrt{\mu}}{2\pi} \int_{r_p^2}^{r_a^2} \frac{\sqrt{(u - r_p^2)(r_a^2 - u)}}{u} du \text{ with } \begin{cases} r_p^2 + r_a^2 = \frac{2\xi_h}{\omega^2} \\ (r_p r_a)^2 = \frac{\Lambda^2}{\omega^2} \end{cases} \quad (3.50)$$

The computation of these radial actions can be done by meticulous integration to recover  $\tau_r$  and  $n_\varphi$  in  $\psi_{\text{ke}}$  and  $\psi_{\text{ha}}$ . Conversely, knowing the radial and azimuthal periods, one recovers the expression of  $\mathcal{A}_r^{\text{ke}}$  and  $\mathcal{A}_r^{\text{ha}}$ . As it is shown in appendix D of the complement SPD, one gets

$$\mathcal{A}_r^{\text{ke}} = \frac{\mu}{\sqrt{2|\xi_k|}} - \Lambda \text{ and } \mathcal{A}_r^{\text{ha}} = \frac{\xi_h}{2\omega} - \frac{\Lambda}{2}. \quad (3.51)$$

For the two non classical isochrones  $\psi_{\text{he}}^{\text{bo}}(r) = \pm \frac{\mu}{b} \left(1 + \sqrt{1 \mp \frac{r^2}{b^2}}\right)^{-1}$ , generalizing [78] p.152, we introduce  $s = 1 + \sqrt{1 \mp \frac{r^2}{b^2}}$ . For the Hénon potential,  $s > 2$  and the PRO has  $\xi_- < 0$  according to its effective potential. In the same way, for the bounded potential,  $2 > s > 0$  and its PRO has positive energy  $\xi^+ > 0$ . Then, for  $s_p < s_a$ , the radial actions are

$$\mathcal{A}_{r,\text{he}}^{\text{bo}} = \mp \frac{b\sqrt{2|\xi^\pm|}}{\pi} \int_{s_p}^{s_a} \frac{(s-1)}{s(s-2)} \sqrt{(s-s_p)(s_a-s)} ds \quad (3.52)$$

with

$$\begin{cases} s_p + s_a = 2 + \frac{\mu}{b|\xi^\pm|} \\ s_a s_p = \frac{4b\mu + \Lambda^2}{2b^2|\xi^\pm|} \end{cases} \quad (3.53)$$

Hence, as it is derived in SPD pp. 35-36, one gets

$$\mathcal{A}_{r,\text{he}}^{\text{bo}} = \mp \frac{\mu}{\sqrt{2|\xi^\pm|}} - \frac{1}{2} \left( \Lambda \mp \sqrt{4b\mu + \Lambda^2} \right). \quad (3.54)$$

So, in  $\psi_{\text{he}}$ , for a PRO of energy  $\xi < 0$ , the radial variable  $s$  satisfies (3.53) as

$$s_a + s_p = 2 - \frac{\mu}{\xi b} = 2 + \sqrt{\left(\frac{r_a}{b}\right)^2 + 1} + \sqrt{\left(\frac{r_p}{b}\right)^2 + 1} \quad (3.55)$$

and

$$\xi = -\frac{\mu}{2a} \text{ with } a = \frac{\sqrt{r_a^2 + b^2} + \sqrt{r_p^2 + b^2}}{2}. \quad (3.56)$$

Inserting this definition of  $\xi$  in (3.40) gives (3.47).

Similarly, in  $\psi_{\text{bo}}$  the variable  $s$  satisfies

$$s_p + s_a = 2 + \frac{\mu}{\xi b} = 2 + \sqrt{1 - \left(\frac{r_p}{b}\right)^2} + \sqrt{1 - \left(\frac{r_a}{b}\right)^2} \quad (3.57)$$

and

$$\xi = \frac{\mu}{2a} > 0 \text{ with } a = \frac{1}{2} = \sqrt{b^2 - r_p^2} + \sqrt{b^2 - r_a^2}. \quad (3.58)$$

By inserting this definition in (3.40), we recover the law (3.47).

In  $\psi_{\text{ha}}$ , all orbits have the same radial period

$$\tau_r = \frac{\pi}{\omega}. \quad (3.59)$$

When a harmonic system is compacted into a ball of radius  $R$  of constant density, then  $\mu = \omega^2 R^3$  according to (3.46). Hence, the period could be related to the radius of the ball through the relation  $\tau_r = \frac{\pi}{\sqrt{\mu}} R^{3/2}$ . Introducing the length  $a = \left(\frac{1}{2}\right)^{2/3} R$ , one has

$$\mu \tau_r^2 = 4\pi^2 a^3. \quad (3.60)$$

□

Thus, Kepler's third law appears to be generalized to the isochrone set. Kepler's third law is mainly used for mass determination, as in, for example, the post-newtonian approximation to estimate the mass of black holes. For a Kepler potential, only one orbit is theoretically necessary to determine the mass of the central attractive body given by  $\mu$ . For other isochrone potentials, using (3.4), only two orbits would be necessary to determine the parameter  $b$  and mass  $\mu$  described by their isochrone potential.

### 3.5 Conclusion

The generalization of the Bohlin transformations through the BOLST transformation has highlighted the Keplerian nature of isochrony. This has been emphasized through adequate reference frames and by the action of the  $\mathfrak{i}$ -BOLST group. Then any isochrone is Keplerian in its reference frame and isochrone orbits are characterized by their Keplerian counterparts. The latter can be graphically deduced from the space of isochrone parabolas.

As in special relativity, all the orbital laws can be written in the same way in all reference frames. But instead of the preservation of a quadratic form as in special relativity,  $\mathfrak{i}$ -BOLSTS assure the linear exchange of energy and potential quantities by preserving isochrone intervals  $\xi x - y$ .

The derivation of the bounded potential and the new demonstration of Bertrand's theorem have been actually the starting point of the above presentation. It is by investigating Lynden-Bell's isochrone transformations that we have looked more closely at isochrone relationships. By then looking for orbital constructions by hand of isochrone trajectories and with our developed affinity with Hénon's parabolas, we have progressively been able to finely understand what adequate structure was needed to describe isochrone relationships, which we have called isochrone relativity.

This global view has led us to the generalization of a symmetry of Keplerian systems to isochrones. Namely, Kepler's third law is a crucial dynamical property of isochrones that we employ in chapter 4 to characterize a quasi-stationary state of isolated self-gravitating systems.

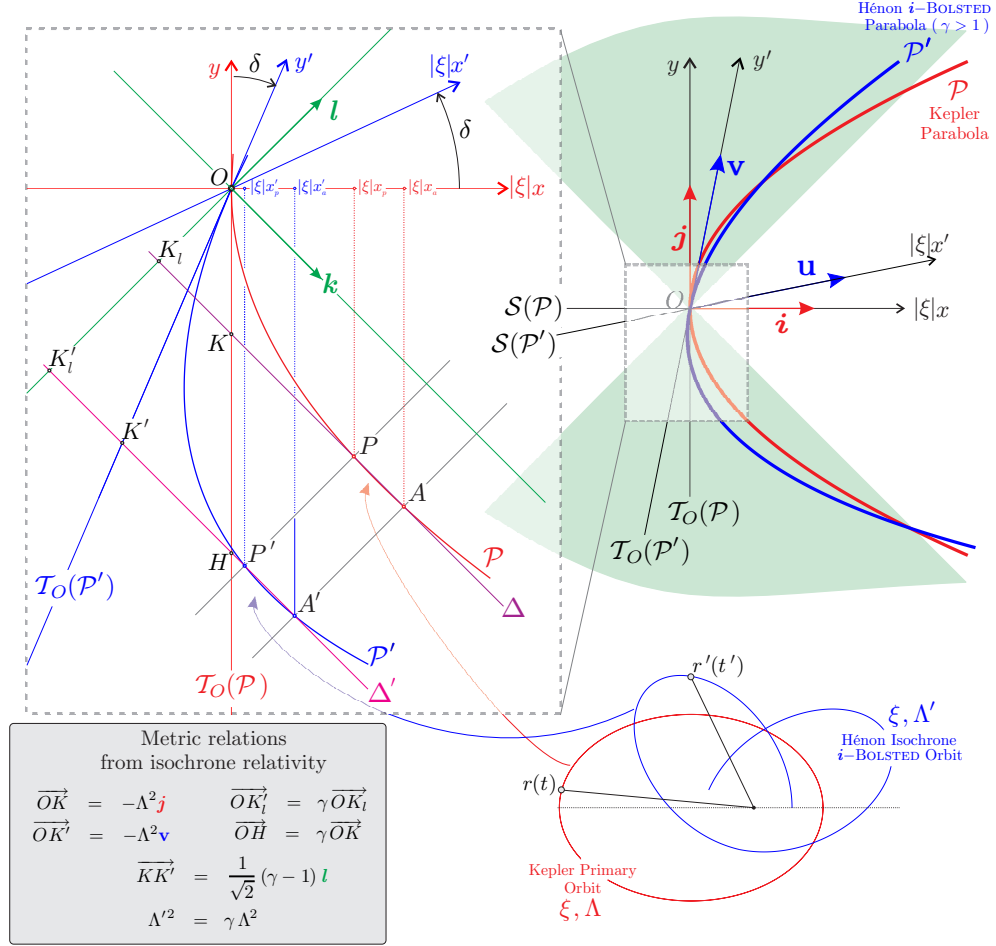


Figure 3.4: The affine plane in the system of coordinates  $(\xi x, y)$  is structured by the radial cone, which delimitates the orange periodic cone  $\mathcal{P}'$  and the white aperiodic cone  $\mathcal{A}'$ . The  $x$ -positive part of the cone  $\mathcal{P}'$  contains the PROs of the Kepler and Hénon parabolas,  $\mathcal{P}$  and  $\mathcal{P}'$ . An isochrone PRO and its Keplerian counterpart in its reference frame are featured bottom-right.



# Isochrony and evolution of self-gravitating systems

---

IN his pioneering paper Michel Hénon [68] proposed that globular clusters can be isochrone. This proposition was based on the fact that, in the late of the fifties, the observed globular cluster mass density distribution looked like the one of the isochrone model. The refinement of the observations has actually revealed a wider diversity!

Is the widely used truncated isothermal core-halo structure the unique specificity of dynamically young isolated self-gravitating systems or does their internal dynamics obey some fundamental criteria? We propose to characterize violently relaxed self-gravitating systems from their internal dynamics, testing whether it agrees with discriminating isochrone properties such as the generalized Kepler's third law. This chapter presents numerical experiments achieved in collaboration with Guillaume Plum (GEPI, Paris Observatory) and submitted for publication in the Monthly Notices of the Royal Astronomical Society.

## 4.1 Isolated self-gravitating systems

### 4.1.1 Overview of isolated self-gravitating systems evolution

First of all, the mass density of globular clusters changes during their dynamical evolution. Although they are characterized by a spherical core-halo structure almost all along their life, the size of their constant density core and the slope of their power law surrounding halo actually change during their evolution. When they are dynamically young, observed or computed globular clusters are mainly characterized by large cores surrounded by steep  $r^{-4}$  halos. This state is generally associated with the result of the so-called violent relaxation which is due to large fluctuations of the gravitational potential of the system ([96] for the original contribution and [78] p. 380-382 for a modern review). The violent character of this process refers to the fact that it spans over a few dynamical times  $T_d$  of the system,  $T_d$  being the time needed for a star to cross the system. From this initial condition, numerous relaxation processes shrink their cores whose density progressively increase and soften their halo toward isothermal  $r^{-2}$  profile. These relaxation processes have been widely investigated during the last decades, they are internal (two body relaxation, small potential fluctuations arising from their finite number of particles e.g. [72]) or external (tidal shocks, galactic potential, etc.). Such processes are sometimes called slow relaxation as they span over much longer times than violent relation, typically  $N \times T_d$  where  $N$  is the number of particles which contribute to the self-gravity of the system.

After decades, the lowered isothermal [84] model and its generalizations (e.g. [78] p. 307-311) appear to be quite universal to describe any state of the evolution of globular clusters. Reasons for such a success in the description of the dynamical properties of globular clusters are physically understandable. When it has been understood that the full gravitational relaxation process leads to a singularity when the system is unlimited in phase space (Singular isothermal problem, e.g. [78] p.305-307), physical improvements have been proposed. These refinements essentially consist in the introduction of some physical cut-off. When this cut-off is crudely introduced by hands in the isothermal model, it produces the original King model [84]. It

is originally justified by spatial limitation corresponding to the tidal cut-off imposed by the surrounding galaxy in which the globular cluster evolves. When the cut-off is included as a parameter of the statistical problem, it produces an isothermal sphere in a box (ISB) which is a trademark problem of the gravitational statistical physics. This fundamental problem has a centennial history and it finally appears to be closely related with the King model (see [28] and reference therein). Studying the stability properties of this ISB in terms of the conditions imposed on the box, theoretical astrophysicists were gradually able to understand the dynamical history of globular clusters through the more and more refined analysis of the so-called gravothermal catastrophe ([100], [82], [120], [27]). The conclusion of this history is now well established concerning the mass density (see for example a very nice synthesis in §7.5 of [78]): after the initial violent relaxation process an isolated  $N$ -body system settles down in a spherical core-halo and quasi-equilibrium state. This state is well described by a lowered isothermal sphere (King Model) and evolves adiabatically to a more concentrated lowered isothermal state under the influence of slow relaxation. When the stability of this lowered isothermal state — governed by its density contrast — is no more possible, the core of the system shrinks. For example in our galaxy, about 20 per cent of the globular clusters possess the steep cusp in their surface-brightness profile (e.g. [43]) that is predicted by models of post-collapse evolution. The complementary set is not yet collapsed and possess a core-halo structure with a slope in the halo fixed by the level of relaxation of the system. When the system is assumed to have a non constant mass function this mechanism is reinforced by mass segregation: the most massive objects become concentrated in the high-density central core.

### 4.1.2 Modeling isolated self-gravitating systems

Mass density profiles can be obtained by an Abel transform of the luminosity profiles, which are generic observational data for sufficiently resolved objects.

Since the “King-fit” scenario is globally accepted for the mass density (at least for globular clusters in our Galaxy, for other hosts the situation is not so clear e.g. [101] for GC in the SMC), the interest of the community progressively moved to the evolution of the globular cluster mass function (see [57] for the more recent review) which is a more complicated and tricky problem, which can be tackled only by observations and simulations. This late interest let the theoretical approach of this problem at rest for a decade.

Additionally, the three parameters of the King model essentially control the relative size of its core and the slope of its halo. Monitoring the evolution of globular clusters using King model seems to be a good idea, but several questions remain posed. What are the physical characteristics of the steep core-halo  $r^{-4}$  structure produced by the violent relaxation? In what sense this initial state of the slow relaxation is a lowered isothermal sphere?

Quite recently, a fine analysis by [167] points out that although King models usually offer a good representation of the observed photometric profiles, they often lead to less satisfactory fits to the kinematic profiles, independently of the relaxation condition of the systems.

The old idea from Michel Hénon to associate globular clusters to the isochrone model has then been progressively forgotten because of the King model ability to reproduce their mass density distribution. It is probably why nobody has verified if the result of the violent relaxation is truly isochrone, i.e. in a kinematic sense checking orbital properties of its components.

By generalizing Kepler’s Third Law we have obtained a way to investigate the isochrone character of an equilibrium steady state of self-gravitating system. We propose in the next section to answer the question of the isochrony status for the initial state of the globular cluster

slow relaxation process.

## 4.2 Description of the numerical simulations

### 4.2.1 Initial conditions

The physical self-gravitating systems we have let evolve are a Hénon sphere and a King model.

The Hénon sphere (e.g. [71]) is particularly suited for our purpose since it is known to preserve well its spherical nature during the course of the dynamics, even in simulations employing a  $N$ -body technique (see for example [139]). In this model the initial phase-space distribution function is isotropic, spatially homogeneous, gaussian distributed in velocity space and given by

$$f_H(r, v, j) = \begin{cases} \rho_0 (2\pi\sigma_v^2)^{-3/2} \exp\left(-\frac{1}{2} \frac{v^2 + j^2/r^2}{\sigma_v^2}\right), & \text{for } r < R, \\ 0 & \text{if } r > R. \end{cases} \quad (4.1)$$

Considering  $E_k = \sum_{i=1}^N \frac{1}{2} m \mathbf{v}_i^2$  and  $E_p = \sum_{i=1, j>i}^N -\frac{m^2}{|\mathbf{x}_i - \mathbf{x}_j|}$  respectively the total kinetic and potential energy of the system, when the initial virial ratio  $\kappa = 2E_k/E_p$  is in the interval  $] -1, 0[$ , the system collapses to an equilibrium state in a few dynamical times (e.g. [139]). Provided that the initial state is not too cold ( $\kappa \in ] -1, -0.25[$ ) the radial orbit instability (see [105] for a review of this fundamental process) does not occur and the equilibrium state is spherical. Its mass density is characterized by a core-halo structure. It is very well established that the core of this structure contains roughly half of the mass of the system and the halo is well approximated by a power law:  $\rho(r) \propto r^{-4}$  (see e.g. [139] or [80]<sup>1</sup>). For our purpose we have studied a Hénon sphere with  $\kappa = -0.5$ , an initial size  $R = 2$  which gives after collapse a typical size  $R_{50} = 1$  see section 4.2.2 for units.

The King model is a stable spherical isotropic equilibrium state of the Vlasov-Poisson equation. It means that if there is no relaxation its distribution function does not change in time. This distribution function is given by

$$f_K(E) = \begin{cases} \rho_0 (2\pi\sigma_\epsilon^2)^{-3/2} \exp\left(-\frac{E_\ell - E}{\sigma_\epsilon^2}\right) - 1, & \text{for } E < E_\ell, \\ 0 & \text{if } E > E_\ell. \end{cases} \quad (4.2)$$

The mean field potential  $\psi(r)$  associated to this distribution function is given by the Poisson equation

$$\Delta\phi(r) = 4\pi m G \rho_0 \left\{ \sqrt{\frac{4\phi}{\pi\sigma_\epsilon^2}} \left(1 + \frac{2\phi}{3\sigma_\epsilon^2}\right) + e^{\frac{\phi}{\sigma_\epsilon^2}} \operatorname{erf}\left(\sqrt{\phi}/\sigma_\epsilon\right) \right\} \quad (4.3)$$

where

$$\phi(r) = E_\ell - m\psi(r) \quad \text{and} \quad \operatorname{erf}(x) = \frac{2}{\sqrt{\pi}} \int_0^x e^{-u^2} du. \quad (4.4)$$

The King model has three free parameters which are:

- the liberation energy  $E_\ell$  which is the cutoff in the energy space introduced to cure the infinite mass problem of the isothermal model;
- the depth of the potential well  $\psi(0)$  at the origin;

<sup>1</sup>The figure 14 of this paper is particularly explicit about this result.

- the energy variance  $\sigma_\epsilon^2$ .

These parameters are gathered in one by introducing  $W_0 = \frac{\phi(0)}{\sigma_\epsilon^2} > 0$ . As said before, King models are core-halo structures (see for example [78] p.308-309): the size of the core is a non trivial function of  $r_c = \sigma_\epsilon(4\pi m G \rho_0)^{-1/2}$  while  $W_0$  controls the steepness of the power law  $r^\alpha$  in the halo of the mass density profile. The slope  $\alpha$  varies from  $\alpha \simeq -2$  (the isothermal value) when  $W_0$  is large, typically greater than 12, to  $\alpha \leq -5$  when  $W_0$  becomes smaller than 3. The large-energy cut-off of the King model introduces a sharp cut-off in the mass density profile for large values of the radius. The slope of the halo we are speaking about concerns the region surrounding the core where the mass density is not less than typically  $\rho_0/10^3$ . This value corresponds to observable and then measurable values of the projected luminosities profiles. For our purpose we have studied a King model with  $W_0 = 9$ . This value corresponds to the best-fit concentration parameter  $c = 2$  proposed in figure 1 of [43] thanks to the correspondence figure 4.9 p. 310 in [78]. The typical size of our King model is  $R_{50} \simeq 1$ .

#### 4.2.2 Numerical integrator

We have performed two accurate  $N$ -body simulations using the latest version of the **Gadget-2** code [146]. This code is appropriate for  $N$ -body simulations on massively parallel computer with distributed memory. It computes gravitational forces with a hierarchical tree algorithm. Only the hierarchical treecode part of treePM algorithm is employed. These simulations contain  $N = 3 \cdot 10^4$  equal mass  $m$  particles in a typical radius of the order of unity in the units of the simulations. These units are such that the gravitational constant  $G = 1$  and the total mass  $M = Nm = 1$ . As shown by [139], this number of particles is sufficient for our purpose of capturing the physics of the problem with reasonable runtimes.

The parameters for **Gadget** runs were adapted to our purpose:

- The softening length of the gravitational force is set to  $\varepsilon = \left(\frac{4\pi}{3N}\right)^{1/3} R_{50}$  with  $R_{50} \simeq 1$  for both simulations. This value corresponds to an estimation of the initial mean interparticle distance, it is a bit larger than the usual value for  $\varepsilon$  in standard simulations. Nevertheless, it is well adapted for our purpose for which we want to minimize the effect of two body relaxation in order to study the properties of orbits in a frozen collisionless equilibrium gravitational potential. This value is also sufficient to solve the collapse problem when the initial virial ratio of the Hénon sphere is not too small and the corresponding collapse is not too violent e.g.  $\kappa = -0.5$  (see [139]).
- In **Gadget**, each particle has its individual time step bounded by  $\delta t = \min \left[ \delta t_{\max}, \sqrt{2\eta\varepsilon/|\mathbf{a}|} \right]$ , where  $\mathbf{a}$  is the acceleration of the particle and  $\eta$  is a control parameter. We choose  $\eta = 0.025$  and  $\delta t_{\max} = 0.01$ . This ensures an energy conservation of the order of 1% for each run.
- The tolerance parameter controlling the accuracy of the relative cell-opening criterion (parameter designed by **ErrTolForceAcc** in the documentation of **Gadget**, see equation 18 of [146]) is set at  $\alpha_F = 0.005$ .

The duration of each simulation is 300 equilibrium dynamical times for the Hénon sphere and 500 equilibrium dynamical times for the King model.

## 4.3 Numerical experiments

### 4.3.1 Density profiles and simulation observables

The evolution of the physical parameters of the simulations are presented on figure 4.1, the left side concerns the Hénon sphere and the right one the King model:

- $R_{90}$ ,  $R_{50}$  and  $R_{10}$  respectively represent the radii containing 90%, 50% and 10% of the total mass of the system. They are plotted in the top two panels. The King model is a stable equilibrium state, so these three quantities remain constant during the dynamical evolution. The initial state of the Hénon sphere with  $\kappa = -0.5$  suffers Jeans' instability and collapses to a steady state in a few dynamical times. The typical size of each system stays of the order of unity.
- Computing the eigenvalues  $\lambda_1 > \lambda_2 > \lambda_3$  of the inertia matrix of the system, the quantities  $a_1 = \lambda_1/\lambda_2$  and  $a_2 = \lambda_3/\lambda_2$  are usually called the axial ratios of the system. Both of these quantities are equal to +1 when the system is a sphere. We can see on the next two panels that our simulations remain spherical all over their dynamical evolution.
- The virial ratio  $\kappa$  is equal to  $-1$  when the system is at equilibrium. We can see on the third line panels that the King sphere remains at equilibrium and that the Hénon sphere quickly joins such a state just after a violent relaxation initial phase.
- For such hamiltonian systems, the total energy  $E_{tot} = E_p + E_k$  is conserved during the time evolution. We observe that in the King model this conservation is properly respected in a mean sense. For the Hénon sphere, this is the same after the warm collapse of the system.

Counting particles in concentric spherical shells, we have computed the radial mass density for our simulation every 10 dynamical times. As expected the mass density of the King sphere does not evolve at all over the 500 dynamical times computed. As expected too, the Hénon sphere initially collapses in a few dynamical times and reaches a steady state characterized by a core-halo structure: the size of the constant mass density core is roughly the radius containing half of the total mass of the system; the slope of the power-law-like surrounding halo is roughly  $-4$ . Once it is formed ( $t \sim 10T_d$ ), this core-halo structure does not evolve at all until the end of our computation at  $t = 300 T_d$ . In figure 4.2, we have plotted these mass densities on the same graph in order to compare them.

A rough analysis does not reveal differences between the results of our warm collapse (H) and simulated King model with  $W_0 = 9$  (K). In addition we note that we can adjust the unique parameter  $b$  of the Hénon potential  $\psi_{he}$  defined in section 2.3.3 to get an isochrone mass density (i) which resembles to the one of (K) or (H). In fact the plots of figure 4.2 clearly show that the density analysis is not conclusive concerning the nature of the equilibrium we obtain after the violent relaxation: it could be fitted by either a King model or an isochrone. Hence, a precise kinetic analysis is needed to reach firm conclusion. The kinematic analysis we propose consists in a fine study of orbits.

### 4.3.2 Isochrone analysis of the simulated dynamics

The isochrone analysis consists in monitoring the orbital dynamics in the simulated clusters and testing whether it agrees with discriminating isochrone properties, as the generalized Kepler's third law.



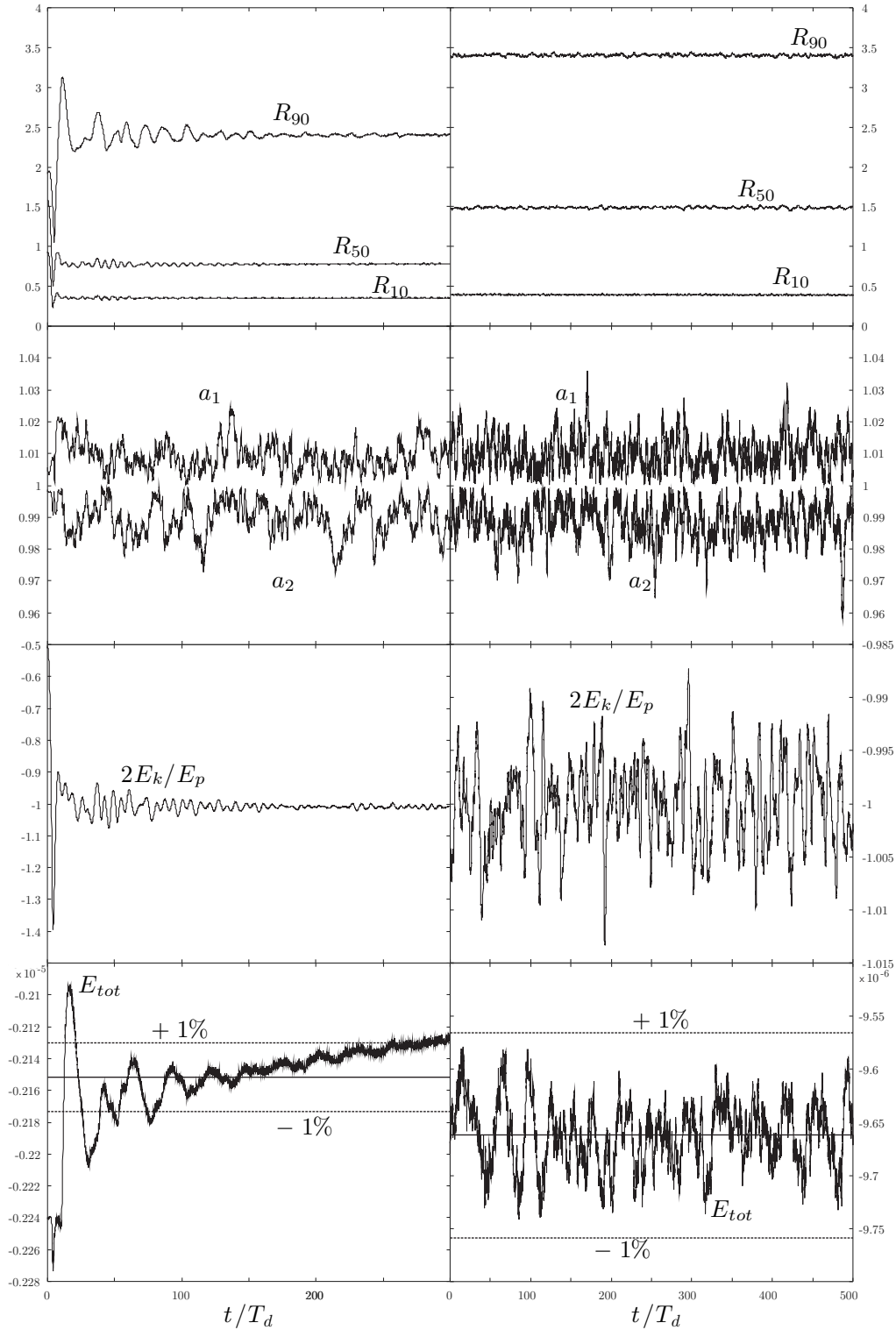


Figure 4.1: Evolution of the mean physical characteristics of the simulation: on the left side, the Hénon sphere with  $\kappa = -0.5$  at  $t = 0$ ; on the right side the King model with  $W_0 = 9$  at  $t = 0$ . Notice the different time scales and the adapted  $y$ -values for each panel.

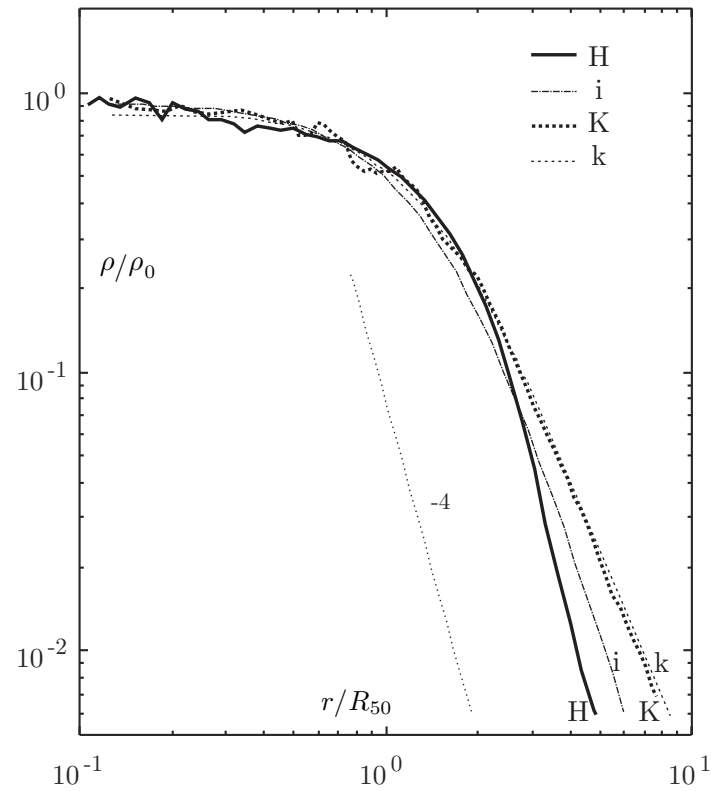


Figure 4.2: Mass density comparison: H represents the Hénon sphere at  $t = 100T_d$ , K the computed King model at  $t = 200T_d$ , i and k are respectively the plots of the isochrone( $b = 0.36$ ) and the King( $W_0 = 9$ ) normalized theoretical mass densities.

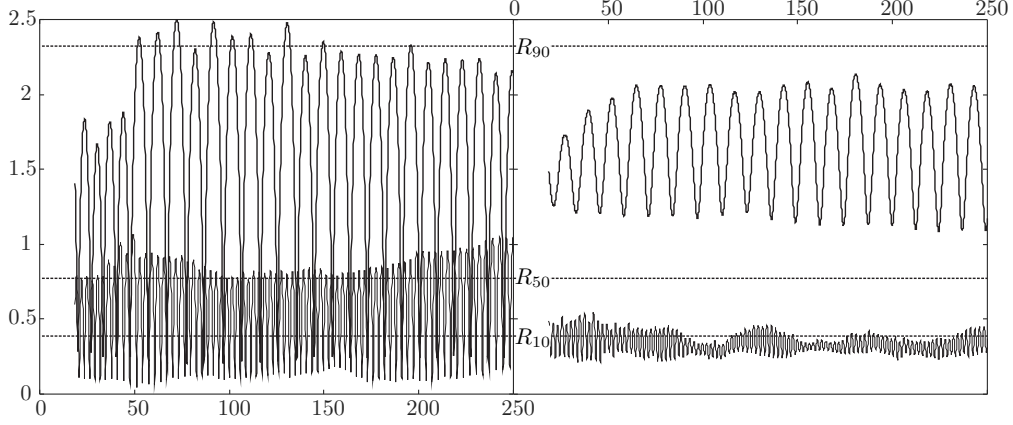


Figure 4.3: Orbits of 4 particles extracted from the H simulation. On  $y$ -axes, the dotted lines indicate the typical lengths  $R_{90}$ ,  $R_{50}$  and  $R_{10}$  of the whole system. The time is indicated on  $x$ -axes in the  $T_d$ -units of the simulation.

In each simulation a subset of  $n = 200$  randomly chosen particles was monitored: three quantities are archived at each time step  $t$ , namely the position  $\mathbf{r}(t)$ , the velocity  $\mathbf{v}(t)$  and the gravitational potential  $\psi(\mathbf{r}, t)$  imposed by the  $N$  bodies of the system at the position  $\mathbf{r}$  at time  $t$ . We point out that we have computed this potential using the Gadget-2 Treecode algorithm, hence with the same softening parameter  $\varepsilon$  defined above. Analyzing these quantities, we can determine, for each monitored particle and when it exists, the period  $\tau_r$  of its radial distance and in all cases its total energy  $e(t) = \frac{1}{2}m\mathbf{v}^2(t) + m\psi(\mathbf{r}, t)$ .

The analysis of the period of particles is a tricky job. *A priori*, we deal with orbits of negative energy particles in a spherical self-gravitating system, and thus in a radial potential. In such conditions, the orbit is planar and the radial distance  $r(t) = |\mathbf{r}(t)|$  is a periodic function of time, i.e. there exists  $\tau_r \in \mathbb{R}^+$  s.t.  $r(t + \tau_r) = r(t)$  as defined in section 2.1. To find this  $\tau_r$  from numerical data and then the values of  $r_a$  and  $r_p$ , the simplest way should consist in the use of the FFT algorithm; but as it can be seen on figure 4.3, in a practical way this method is not precise as it should be expected for several reasons. Depending on the particle properties, its orbit could be concentrated in the deep center of the system (see the lower orbit on the right side of figure 4.3), be spanning only the halo (see the upper orbit on the right side of figure 4.3), be spanning all the system or all its core (see the left side of figure 4.3) or be even more special. When the particle experiences the deep core, the two body effects could influence its dynamics; although the radial distance is periodic this function is modulated both in phase and in amplitude. The phase modulation due to the high density values is weaker when the orbit stays in the outskirts of the system where only large scale oscillations of the potential modulate its amplitude. These effects affect both K and H simulations and introduce various and uncontrollable biases when we compute the period using FFT on the whole data. Instead, in order to get the right value of the period with the smallest significative error, we carry out a hand-made analysis of each orbit. We first check the planar property of the orbit: we determine the mean angular momentum, compute the orthogonal plane to this mean vector and reject orbits with an amplitude of azimuthal oscillation  $\delta$  (see figure 4.4) around this plane less than  $20^\circ$ , such that  $\delta \geq 0.2r_a$ . When the orbit is planar, we determine the coordinates  $(r_{a,i}, t_{a,i})_{i=1, \dots, \mathcal{N}}$  of  $\mathcal{N}$  successive maxima of the function  $r(t)$ . The value of the integer  $\mathcal{N}$  depends on each orbit considered. We set  $\mathcal{N} \geq \mathcal{N}_{\min} = 5$  in order to compute the period at least

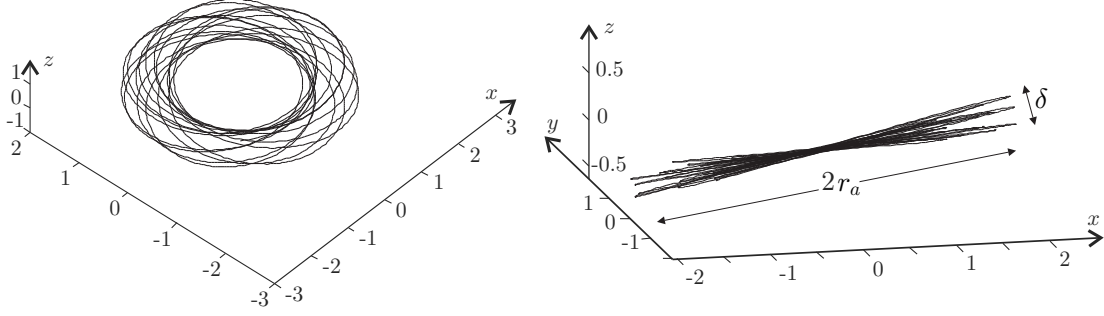


Figure 4.4: 3D representation of an orbit extracted from the K simulation: A view from above is presented in the left panel while the side-on view is presented in the right one.

over  $\mathcal{N}_{\min}$  oscillations. This minimal value allows us to initiate the computation of the period  $\tau_r = \frac{t_{a,\mathcal{N}} - t_{a,1}}{\mathcal{N} - 1}$ , the value of  $\mathcal{N}$  is incremented while  $\sigma_{\tau_r}/\tau_r < 5\%$  where  $\sigma_{\tau_r}$  is the standard deviation of the sequence of instantaneous periods  $\tau_{r,i} = t_{a,i+1} - t_{a,i}$  for  $i = 1, \dots, \mathcal{N} - 1$ . When this algorithm does not converge the orbit is rejected as not periodic. When it gives a unique value this result is compared with the data. When several values of the period are possible during several phases of the orbit, it is rejected as multiperiodic<sup>2</sup>. When the period of the orbit is confirmed, we determine its apocenter  $r_a = \frac{1}{\mathcal{N}} \sum_{i=1}^{\mathcal{N}} r_{a,i}$ . Computing the sequence of the minima of  $r(t)$  in the interval  $[t_{a,1}, t_{a,\mathcal{N}}]$ , we obtain the pericenter of the orbit in the same mean sense. Computing the mean value of the energy  $E = \langle e \rangle_t$  on this same time interval, we get the mean energy of the particle. The standard deviations of  $e$ ,  $\tau_r$ ,  $r_a$ , and  $r_p$  are used for the uncertainty analysis: the amplitude of error bars in the plots are twice the standard deviation.

Using this manufactured but precise algorithm, we are able to extract with a good level of confidence the energy, period, apocenter and pericenter of  $n_H = 155$  orbits for the H simulation and  $n_K = 172$  orbits for the K simulation among the  $n = 200$  monitored for each one.

If each set of orbits is isochrone, then it must fulfill the generalized Kepler third law:

$$\tau_r^2 \times a^{-3} = cst, \quad (4.5)$$

where  $a$  is the isochrone length defined in section 3.4 page 57. We then achieve an analysis in the space  $\mathcal{H}_1 = [\ln(a), \ln(\tau_r)]$ . As the system is neither keplerian, harmonic nor pseudo-Hénon, we guess it should be in a Hénon potential; hence  $a = \frac{1}{2} \left( \sqrt{r_a^2 + b^2} + \sqrt{r_p^2 + b^2} \right)$ . In this formula  $b$  is a macroscopic positive parameter common to all orbits, while  $r_a$  and  $r_p$  are microscopic ones, specific to each orbits. For a given value of  $b$  we can plot the set  $[\ln(a), \ln(\tau_r)]$  containing  $n_X$  points for each simulation  $X = K$  and  $X = H$ . We can then determine the weighted linear fit  $y = s \ln(a) + c$  (see appendix page 126) of these plots and determine the residue of this fit namely

$$\chi_{b,X}^2 = \frac{1}{\ell^2} \sum_{i=1}^{n_X} \{ \ln(\tau_{r,i}) - [s \ln(a_i) + c] \}^2 \text{ with } \ell^2 = \sum_{i=1}^{n_X} \ln(\tau_{r,i})^2. \quad (4.6)$$

The optimal value  $\tilde{b}_X$  of  $b_X$  is obtained by a minimization algorithm applied to this residue computation. Explicitly, we compute the residue for discrete values of  $b$  in the interval  $\mathcal{B} =$

<sup>2</sup>By *several* we mean more dispersed than 5 % around the mean value. This possibility occurs when there is a strong two body interaction in which the characteristics of the orbit (period, apocenter, pericenter) are modified.

X	$\tilde{b}$	$\chi_b^2(\tilde{b})$	$\tilde{s}$	$\delta_{\tilde{s}}$
H	$3.70 \times 10^{-1}$	$2.87 \times 10^{-2}$	1.50	$8.23 \times 10^{-2}$
K	$1.49 \times 10^{-1}$	$1.07 \times 10^{-2}$	1.13	$4.06 \times 10^{-2}$

Table 4.1: Statistical analysis for the sets  $[\ln(a), \ln(\tau_r)]$  in the simulations K and H.

$[0, b_{\max}]$  where  $b_{\max} \simeq R_{50\%}$  as roughly estimated from the isochrone model. We then choose

$$\tilde{b}_X = \min_{b \in \mathcal{B}} \chi_{b,X}^2. \quad (4.7)$$

The plots of  $\chi_{b,K}^2$  and  $\chi_{b,H}^2$  as functions of  $b$  are presented in the small boxes of figure 4.5. When the optimal value  $\tilde{b}_X$  is found, it should correspond to the optimal fit of  $y = \ln(\tau_r)$  by a linear function of  $x = \ln(a)$  for the considered simulation. The best slope  $\tilde{s}_X$  of this best linear fit corresponds to the best power law relation between  $a$  and  $\tau_r$ , it should be  $3/2$  when the system is isochrone. We gather the statistics in table 4.1. The uncertainty of  $s_X$  is evaluated by the dispersion parameter  $\sigma_b$  defined in the annexe page 126. The amplitude of the error bar is equal to this dispersion parameter.

From our orbits analysis we can investigate another space, namely  $\mathcal{H}_2 = [\ln(\tau_r), \ln(-E)]$ . This one is more direct than the previous because it does not need another parameter as  $b$  to build the isochrone length  $a$ . For an isochrone model the Kepler third law applies and gives  $\tau_r^2 \times (-E)^3 = cst$  which implies  $\ln(-E) = -\frac{2}{3} \ln(\tau_r) + cst$ . As we have computed the mean energy  $E$  for each monitored orbit, we can additionally check if K or H should be isochrone in this sense. The results are plotted in figure 4.6.

The result of the isochrone tests is unambiguous. Both spaces  $\mathcal{H}_1$  and  $\mathcal{H}_2$  reveal the isochrone nature of the result of the H simulation and the non isochrone nature of the K one. On the first hand the regression of  $\ln(\tau_r)$  in  $\ln(a)$  is perfectly linear for both simulations for the optimal value of  $b$ , but the value  $\tilde{s}_H = 1,50 \pm 8,23.10^{-2}$  is fully compatible with the isochrone one  $s_{1,\text{iso}} = 3/2$  whereas  $\tilde{s}_K = 1,13 \pm 4,06.10^{-2}$  is definitely not. On the other hand the analysis in  $\mathcal{H}_2$  reveals that there is no unique power law relation between  $\tau_r$  and  $E$  for orbits in a  $W_0 = 9$  King model while this relation clearly exists with the right value  $s_{2,\text{iso}}^2 = -2/3$  for the collapsed Hénon sphere with an initial virial ratio  $\kappa = -0.5$ . The result of the collapsed Hénon sphere is therefore isochrone but not of King type, although both models present adequate density profiles.

## 4.4 An isochrone stage for isolated self-gravitating systems

The presence of an isochrone stage in the evolution of isolated self-gravitating systems is suggested by the precedent isochrone tests. However, this poses some theoretical questions.

Why is the result of violent relaxation isochrone? The answer to this question was certainly proposed sixty years ago by Michel Hénon in his seminal paper [68]. During the mixing of the violent relaxation there is a natural tendency for particles to move toward equipartition in the energy. This is a pillar of statistical mechanics. In this context resonances enable energy exchanges between particles. If stars with the same radial period  $\tau_r$  have different energies, they will exchange energy till they reach the same  $E$ . But the definition of isochrony is precisely that all stars with a given  $\tau_r$  share the same  $E$ .

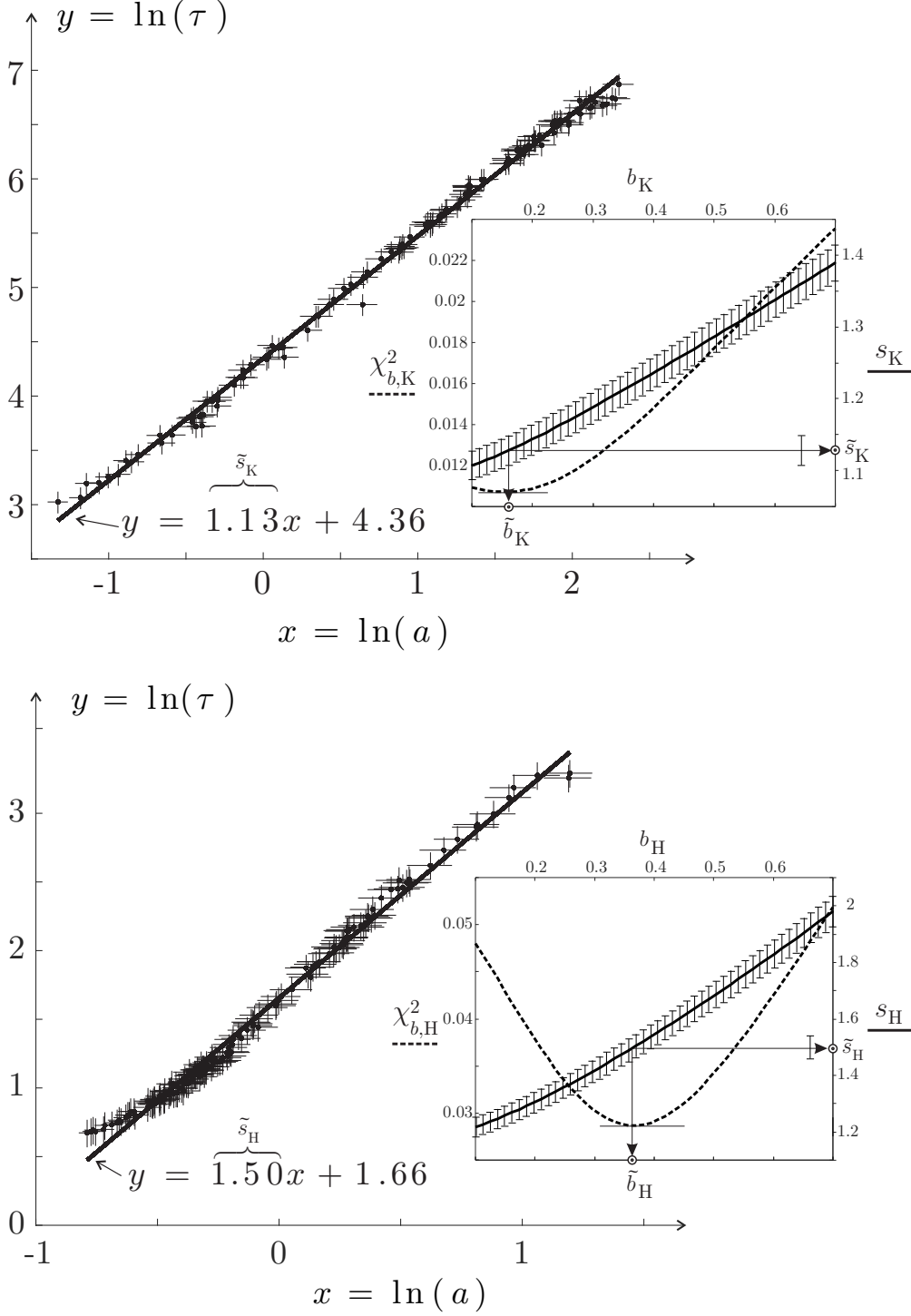


Figure 4.5: Isochrone test 1 for  $X = K$  (upper panel) and  $X = H$  (lower panel). In each panel the small box represents the residue  $\chi^2_{b,X}$  and the slope  $s_X$  of the weighted linear fit as functions of the isochrone parameter  $b$ . The residue plot is the dashed line with values on the left of the small box while the slope is the solid line with values on the right of the small box. The optimal value  $\tilde{b}_X$  of  $b$  is identified as well as the corresponding optimal value of the slope  $\tilde{s}_X$ . The weighted best linear fit of the data  $\{\ln(a), \ln(\tau_r)\}$  for  $b = \tilde{b}_X$  is then plotted.

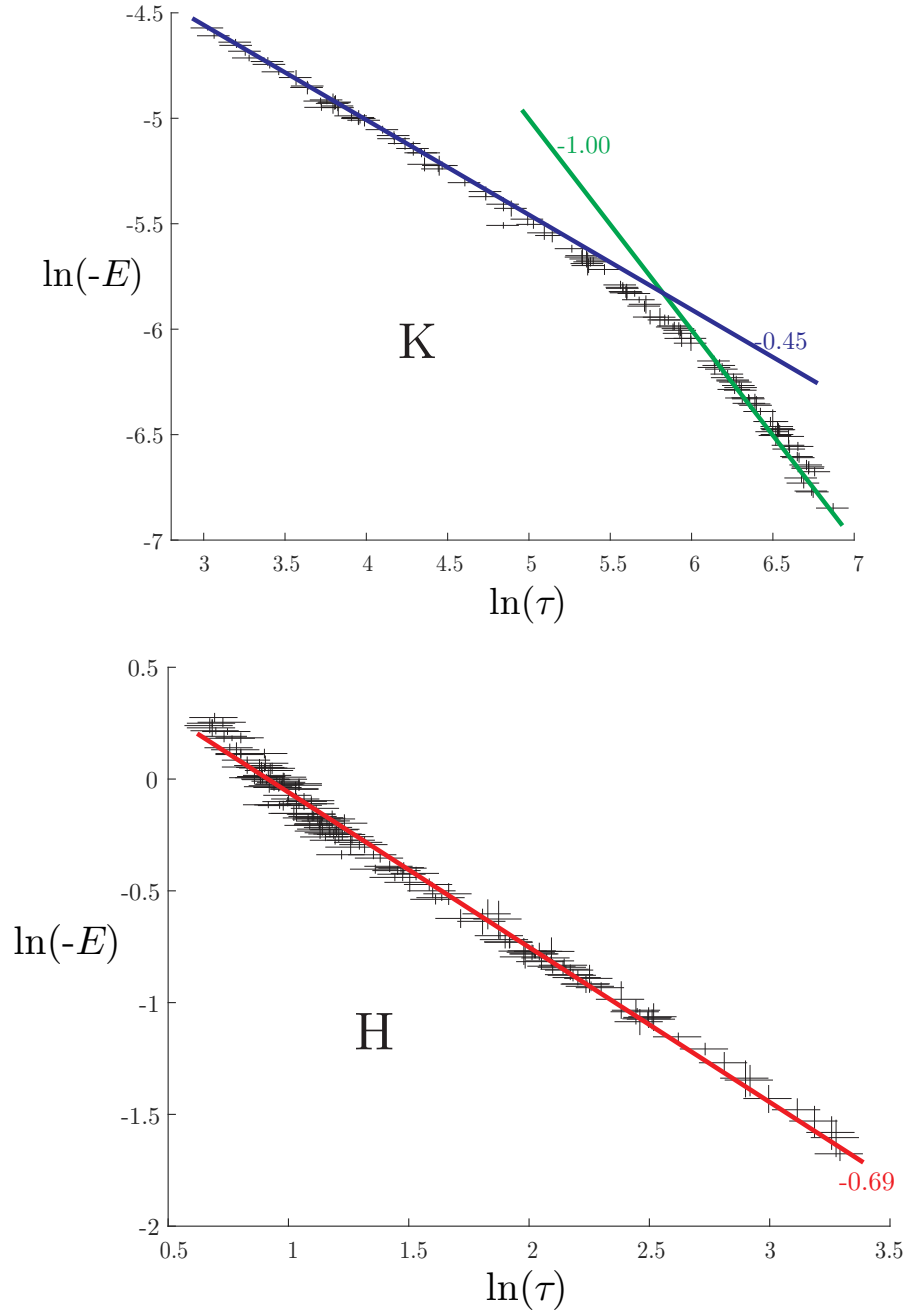


Figure 4.6: Isochrone test 2 for  $X = K$  (top panel) and  $X = H$  (bottom panel). The value of the slopes of the weighted linear fits are indicated near each line.

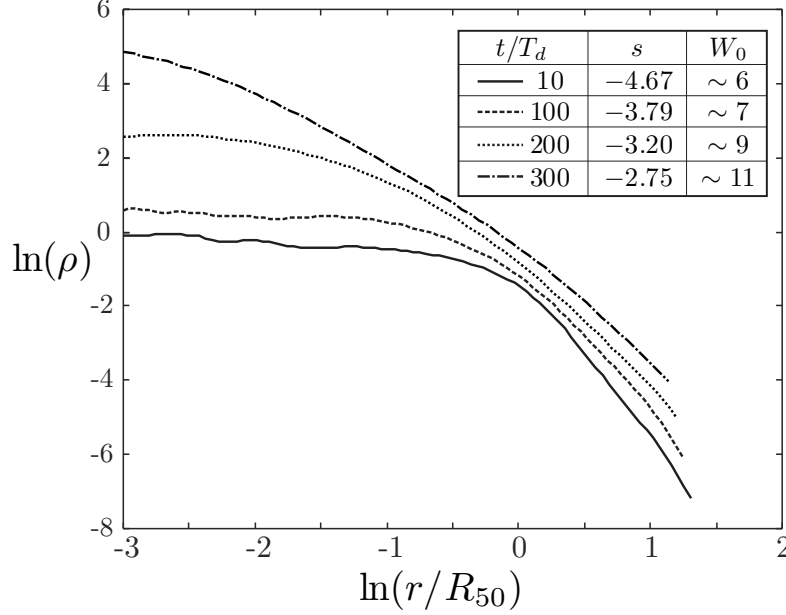


Figure 4.7: Evolution of the density for a Hénon sphere with an initial virial ratio  $\kappa = -0.5$  and a small softening parameter. The slope  $s$  corresponds to the best linear fit of the halo. The value of  $W_0$  is obtained by fitting the halo with a King model.

Why has this old result been progressively forgotten? The response to this question is probably two-fold. First of all, due to the slow relaxation process the initial state obtained after the violent relaxation is progressively changed into a more and more concentrated core-halo system. This gravothermal evolution was studied and understood during the last fifty years. During this process the mass density of the systems changes and it loses its isochrone property. When we let this possibility occur, decreasing the value the softening parameter by, at least, an order of magnitude ( $\varepsilon \rightarrow \varepsilon/50$ ), the simulation of the same Hénon sphere clearly shows this mass density evolution over the same duration (see figure 4.7). Our statistical study is no more possible in this context as the orbital periods evolve with the gravitational potential: when it is similar to a King model with  $W_0 = 9$ , it should have lost part of his isochrone property.

Another simple reason of the isochrone oblivion is the efficiency of the King model: with three free parameters which control the slope of the halo, the size of the core and the concentration of the system, this model is perfect to fit all the evolution of globular clusters evolution regarding the mass density or the luminosity profile. As long as nobody asks for detailed kinematical analysis there is no reason to discredit King model. Otherwise, any dynamical study at a microscopical, i.e. orbital, scale, after gravitational collapses of isolated self-gravitating systems, would certainly gain in accuracy when considering an initial isochrone distribution.

## 4.5 Isochrony in astrophysics

### 4.5.1 Isochrony in self-gravitating systems

The analyzed gravitational collapse process is attainable for isolated self-gravitating systems such as LSB galaxies and globular clusters.



Globular clusters can be considered as isolated during their formation process, since they stand as points in many host galaxies due to their relatively small size (about 1/1000 of the size of the host galaxy). In our Galaxy, almost 80 per cent of the globular clusters show a core-halo structure, see [43] and the numerical results of homogeneous collapses [139].

Low surface brightness (LSB) galaxies are dark-matter dominated galaxies. As explained in the introduction page 18, they dynamically behave as if they were almost isolated and not much influenced by their environment.

Furthermore, at small radii, observational data of LSBs prefer constant density cores rather than cuspy profiles evolving as  $r^{-\alpha}$  with  $\alpha \leq -1$  [38, 86], contrary to the conclusions of cosmological simulations taking into account cold dark matter [115, 116] — this discrepancy is known as the cusp-core problem. Their formation process is certainly not hierarchical as for HSBs which undergo successive merging phases. Thus, as globular clusters, they generally present core-halo structures.

### 4.5.2 Loss of isochrony

After a violent relaxation process, the precedent simulations suggest that a stellar cluster is isochrone. However the observed globular clusters commonly show core-halo structures with a halo slope greater than  $-4$  unlike H  non's isochrone which additionally could not account for rotation curves of LSB galaxies since it is Keplerian at large radii.

The higher values of halo slopes come from the later evolution of the systems. After a collapse, their states evolve towards more concentrated systems in their centers with smoother slopes [131], up to possibly core collapses, and progressively lose the isochrone property. This evolution is driven by the contrast density between the center and system boundary, and thus can be strengthened by the galactic environment.

Therefore, deviations from isochrony constitute dynamical indicators for the evolution of such isolated self-gravitating systems.

### 4.5.3 Conclusion and perspectives

Let us summarize the main results we have presented in this chapter.

The analysis of a self-gravitating system using only its mass density distribution (or luminosity profile) is ambiguous: several models can produce similar mass density profiles. In particular, the King model and its three free parameters can be used to produce a pretty good fit of the mass density profile of a globular cluster at any stage of its dynamical evolution.

The system produced just after the standard<sup>3</sup> violent relaxation process is a core-halo structure compatible with both a King or an isochrone mass density. However, when kinematic data is taken into account, the King model fails where the isochrone succeeds in reproducing the equilibrium state.

The isochrone model is just an initial condition obtained after the formation process of the system. Under slow relaxation processes the system loses its isochrone character as it is confirmed by density profiles.

Such results highlight the isochrone model under a new perspective. More than an aesthetic model, useful because it distinguishes itself by its ability for producing analytic formulas for the

---

<sup>3</sup>By this precision we want to restrict this affirmation to systems which are initially not sufficiently cold to be influenced by the radial orbit instability.

actions and angles of its orbits, the isochrone is in fact a fundamental potential resulting from a homogeneous violent relaxation process.

This process is the one supposed to occur in the formation of isolated self-gravitating systems (globular clusters, LSB galaxies). It is then not surprising that they are characterized by a core-halo structure density profile as long they are not so affected by slow relaxation processes. When the formation process is hierarchical (e.g. HSB galaxies) the continuous merging process is combined with an inhomogeneous violent relaxation. The initial isochrone core-halo structure is no more observable as the core is unstable<sup>4</sup>. This produces their cuspy profile. This could probably also explain the presence of supermassive black holes in the heart of such structures while they are not expected as a rule for globular clusters or LSB galaxies.

Although the isochrone state is explicitly revealed after the homogeneous violent relaxation process, we have no more physical explanations than the one proposed by Michel Hénon in the sixties (resonant coupling arguments). A special investigation on this subject is tricky because it requires to analyse orbits during a non-stationary phase. It deserves to be discussed in a future work.

As we have noticed, the formation process of large-scale structures also has to be considered in its cosmological context. We introduce in part II the grounds of today's standard model of cosmology in order to investigate a physical interaction between dark matter components, in adequacy with large-scale properties of gravitation as described by general relativity.

---

<sup>4</sup>In a inhomogeneous system the critical value of the density contrast could be very low. The collapse of the core could then appear during the merging and virializing phase.



“ Vers un centre commun tout gravite à la fois.

Ce ressort si puissant, l'âme de la nature,  
Etait enseveli dans une nuit obscure :  
Le compas de Newton, mesurant l'univers,  
Lève enfin ce grand voile, et les cieux sont ouverts. ”

“ Towards a common center all gravitates together.

This spring so powerful, the soul of nature,  
was entombed in a dark night:  
the compass of Newton, measuring the universe,  
finally lifts this great veil, and the skies are opened. ”

Voltaire, *A Mme Du Châtelet, Sur la philosophie de Newton, 1736*





# Part II

## Cosmology





# Universe description

CONSTRUCTING an observation-adequate model for the Universe as a whole is a tremendous challenge for researchers. It must appropriately describe the physics we know from experiences at all range of energy and thus correctly take into account the four known interactions: the weak and strong nuclear interactions, and the electromagnetic and gravitational ones.

The widely spread standard model of cosmology considers the Universe as an isotropic (and homogeneous) *cosmic soup* composed of light, neutrinos, baryonic matter, dark matter and dark energy. Those four “fluids” only gravitationally interact one with another, in a manner that is characterized by the general theory of relativity. The standard model is in good agreement with the most recent observational constraints [129]. However, its hypotheses seem quite restrictive.

Let us introduce the general relativity formalism to derive the dynamical system that describes the dynamics of the Universe at large scales, as it is used in the standard model of cosmology. Its origin and restrictions are introduced following historical steps to finely understand the improvement we propose in the last section and the next chapter.

## 5.1 Equations of the dynamics

### 5.1.1 A curved spacetime

In May 1907, as Albert Einstein was an engineer at the Swiss Federal Institute of Intellectual Property, he understood that free-falling bodies do not feel their own weights. Let us give an image: if you were in a small enough<sup>1</sup> closed capsule without windows, you would not be able to feel whether the box is on Earth or in a satellite that is accelerated so that the acceleration in the capsule is the same as on Earth. You would be able to walk in the same manner in both cases. Similarly, it is hard to feel which of your train or the neighbor one is uniformly moving in a station without additional information such as sound or object references.

If you further notice that in a free-falling cabin all objects (umbrellas, bags, etc.) would fall with you in the same manner — nowadays this situation is said to be a state of weightlessness, then we can recover the Galilean equivalence principle: the inertial mass  $m_i$  of a body, that measures its resistance to modify its motion, is also the quantity that rates its interaction with other massive bodies, called gravitational mass,  $m_g$ . A more rigorous argumentation can be found in [47] §2: noting that an increase in energy  $E$  corresponds to an increase in inertial mass as  $E/c^2$ , where  $c$  is the speed of light, as a consequence of special relativity [45]; and then demonstrating that the gravitational mass is also increased with the same quantity  $E/c^2$ . The latter result fortunately preserves the correspondance between the conservation of energy and the conservation of mass, and the proof includes the gravitational redshift description. The equivalence principle,

$$m_i = m_g, \tag{5.1}$$

<sup>1</sup>The larger the body, the greater the tidal forces acting on it.



has been extensively probed and is still under active survey. Galileo perhaps let balls of distinguished masses fall from the Tower of Pisa at the beginning of the XVII<sup>th</sup> century. In 1687 Newton used equal-length pendulums with different hanged-up masses. In 1889 the dutch physicist Eötvös utilized spring pendulums to check the equality up to a billionth. In 1964 Dicke reached a precision of  $10^{-11}$ . Finally, in 2017, the Microscope satellite verified it up to a  $10^{-14}$  relative precision employing differential accelerometers and now aims to test it at the  $10^{-15}$  precision level [152].

The major consequence of (5.1) is revealed when simplifying the fundamental equations of motion in Newtonian mechanics

$$m_i \mathbf{a} = -m_g \nabla \Phi \quad (5.2)$$

by the equal masses  $m_i$  and  $m_g$ . It leads one to

$$\mathbf{a} = -\nabla \Phi, \quad (5.3)$$

where the gravitational potential  $\Phi$  satisfies Poisson's equation

$$\Delta \Phi = 4\pi \mathcal{G} \rho \quad (5.4)$$

in Newton's dynamics and provides, by its gradient  $-m_g \nabla \Phi$ , the force that acts on a particle of acceleration  $\mathbf{a}$  coupled by  $m_g$  to the presence of other masses, with total mass density  $\rho$ . Remembering that, by definition, a force corresponds to a change of velocity, relation (5.3) translates the universality of motion. Any body moves the same way under a given gravitational field ( $\Phi$ ), independently on its mass. Moreover, the equivalence principle can be further interpreted as the equivalence between a system at rest in a gravitational field, as on Earth, and the same system with the counterpart acceleration in vacuum. But what about the behavior of light?

Light is known to propagate in straight lines through media with constant refractive indices. As electromagnetic waves it satisfies Maxwell's equations that are fully integrated into the special theory of relativity [46]. But gravitation is absent from special relativity. The propagation of light is thus not well described in the presence of a gravitational field. In Prague, where he had found an academic research position, Einstein has had a simple and bright thought experiment that suggests an answer.

Consider you are in a lift that is uniformly accelerated upwards. Then you go up with an increasing velocity. Suppose that, at some floor, someone horizontally sends light onto the open or transparent lift shaft. If the lift has a small hole, then light will enter it. But since you are still going up, the light beam will reach the opposite wall of the lift at a vertical position slightly below the height of the hole. Actually, if you are at rest in the lift, you will see the beam with a bent trajectory, see figure 5.1. According to the above interpretation of the equivalence principle, if the acceleration is sufficiently high, then the situation is equivalent to the one in a lift at rest on Earth. Therefore, we should also observe the bending of light motion there. As a consequence, the presence of matter curves light trajectories. But light is intuitively assumed to take the shorter path, that can only be a straight path, be it in a classical Euclidean space or in the Lorentzian geometry of special relativity spacetime. Einstein had thus no other solution than looking for a description of a *curved* spacetime to depict gravitation.

Given the above, the equations of spacetime dynamics have to report how the geometry/metrics curves depending on the distribution of matter, and also how the matter moves provided the geometrical structure. Of course, the travel of energy does deform spacetime at each instant; this latter is now dynamical. This information is transmitted at the speed of light, according to theory [103] and observations [59], and spacetime is progressively kneaded,

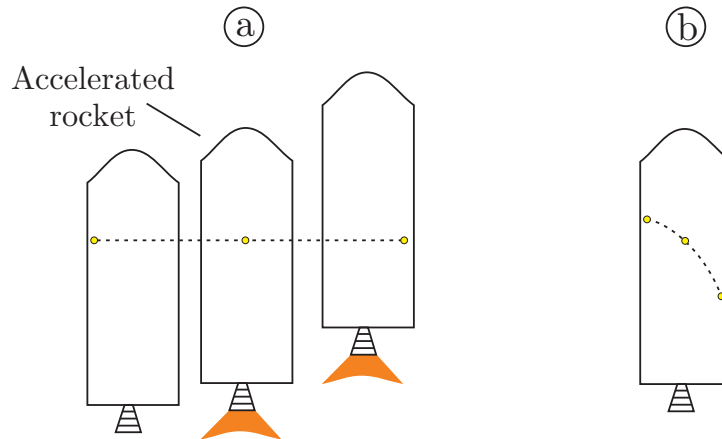


Figure 5.1: Light propagation: (a) observed from an inertial (Galilean) frame, (b) observed in the accelerated frame of an accelerated rocket. When this acceleration corresponds to the  $g$ -force on Earth, the equivalence principle states that the trajectory observed in the accelerated frame of the rocket is the same as the one observed in a frame at rest on Earth. This figure is inspired from an illustration in handwritten notes by J. Heyvaerts.

starting from the region where the deformation or mass modification took place. Gravitational waves are an example of spacetime progressive distortion, they are generated by the combined rotation of two non-symmetric massive bodies, with quadripolar momenta at low order [103].

### 5.1.2 Einstein's equations

Einstein went in Zürich for a few years to mathematically formalize his theory with the help of his friend Marcel Grossman. They based their investigations on two fundamental principles:

- physics is the same in all referential. Consequently, the expression of the equations must be invariant under frame changes, and thus must be written in terms of tensors.
- Newtonian dynamics should be recovered under some appropriate limits.

The first one extends Galileo's and special relativity principles, which assume physics to be identically described in any referential, *if* they are in a uniform translation with respect to a reference one. Such a referential is called a Galilean frame. The second one expresses the desired coherence with classical mechanics, in particular with Poisson's equation (5.4) that relates the gravitational field to the mass distribution in Newtonian dynamics.

In this section, we introduce Einstein's equations with their historical main indices. We first set the covariance notion, needed for the invariance of the equations. Then we look for tensors that can represent geometry and matter distribution, before we can connect them to describe the spacetime dynamics.

#### First principle: why a tensorial formulation?

Tensors locally express a quantity (velocity, acceleration, pressure, curvature, etc.), in a local coordinate system that is adapted at each point of space or spacetime.

In special relativity as in Newtonian mechanics, the change of referential was only possible under uniform rectilinear translations to keep invariant the equations of motion; otherwise, inertial forces appear. The same inertial forces that you can feel on a carousel, and that pulls you towards the rim. In practice, the equations of motion are written as

$$\mathbf{a}_d = \frac{d\mathbf{v}}{dt} = \frac{1}{m}\mathbf{F} \quad (5.5)$$

in a Galilean frame. Whereas they read

$$\mathbf{a}_d = \frac{d\mathbf{v}}{dt} = \frac{1}{m}\mathbf{F} - \mathbf{a}_{ice} - \mathbf{a}_{ico} \quad (5.6)$$

for the same motion described in a rotating frame;  $\mathbf{a}_{ice}$  and  $\mathbf{a}_{ico}$  are the centrifugal and Coriolis fictitious forces. In the tensorial description of special relativity, each component of the 4-acceleration<sup>2</sup> would locally satisfy

$$a_d^\mu = \frac{dv^\mu}{d\tau} = \frac{1}{m}F^\mu - a_{ice}^\mu - a_{ico}^\mu, \quad (5.7)$$

where  $\tau$  is the proper time of the particle, i.e. the time measured in the referential in which the particle is instantaneously at rest, and  $v^\mu = \frac{dx^\mu}{d\tau} = (\gamma c, \gamma \mathbf{v})^\top$  the 4-velocity. The indices  $\mu = 0, 1, 2, 3$  respectively corresponds to temporal and spatial components. The 4-force is generically expressed as  $F^\mu = \left( \frac{\gamma}{c} \mathbf{F} \cdot \mathbf{v}, \gamma \mathbf{F} \right)^\top$ . Then, in a comobile frame, the accelerations simply correspond to  $a^\mu = (0, \mathbf{a})^\top$ . The Lorentz factor

$$\gamma = \frac{dt}{d\tau} = \frac{1}{\sqrt{1 - \frac{v^2}{c^2}}} \quad (5.8)$$

that is involved in the 4-vectors expressions renders the length contraction and time dilatation phenomena in special relativity<sup>3</sup>.

To avoid fictitious forces, the derivative must be correctly redefined. In fact, a differentiation gives the variation of a quantity along a given direction. If we furthermore take into account the deviation of this direction itself, induced by the curvature, then inertial terms coincide with the curvature of spacetime, see page 125 for a proof. Using such a differentiation, equation (5.7) can be written as

$$a_d^\mu + a_{ice}^\mu + a_{ico}^\mu = a_\nabla^\mu = \frac{dv^\mu}{d\tau} + \Gamma_{\kappa\nu}^\mu v^\kappa v^\nu = \frac{1}{m}F^\mu, \quad (5.9)$$

where  $\nabla$  is called a covariant derivative and is defined as in the general theory of relativity in the annexe page 122, with the Christoffel symbols  $\Gamma_{\kappa\nu}^\mu$  that are related to the inertial terms, and  $F^\mu$  contains non-gravitational force terms. As explained in the annexe, see (A.64) and (A.66), equation (5.9) can also be obtained by looking for an extremal-length path in a non-gravitational potential from which the force derives. When  $F^\mu = 0$ , the particle is free and follows a path

<sup>2</sup>The use of 4-vectors is already present in the “Mémoire de Palerme” by Henri Poincaré, but the name of 4-velocity, 4-acceleration, as well as Universe lines appear in an article of Minkowski [108] and especially in his article when drawing Minkowski diagrams [109] after explaining the four-dimensional structure of spacetime in [110]. We then choose the coordinate system  $x^\mu = (ct, x, y, z)^\top$  as defined by (A.49) p. 122, with a  $(+, -, -, -)$  signature of the metrics.

<sup>3</sup>Time dilatation and space contraction can be understood when considering time and space as two correlated notions that both depend on the choice of an observer. These two physical properties describe the perspective view you observe when accelerating with respect to the observed landscape. Please refer to the textbook [62] or to the online second-episode movie (<https://uma.ensta-paristech.fr/conf/expansion/index.php>) that illustrates this accelerated perspective with animated mini-Coopers.

of minimal length called *geodesic*, as does the propagation of light, see equation (A.62). In the relation (5.9),  $a_{\nabla}^{\mu}$  and  $F^{\mu}$  are both tensors, expressed in local basis, therefore their components are transformed exactly as the local coordinates, cf (A.47) and (A.57). The relation is said to be covariant. It holds whatever the choice of referential.

Expressing the physical quantities in those local basis through tensors is thus the most convenient manner to write the equations in a covariant, i.e. invariant, way.

### Spacetime curvature

As intuited by Einstein, see his thought experiment in Prague page 84, the gravitational field curves spacetime, because light follows curved geodesics. The geodesic equation is given by

$$\frac{d^2 x^{\kappa}}{d\tau^2} + \Gamma_{\mu\nu}^{\kappa} \frac{dx^{\mu}}{d\tau} \frac{dx^{\nu}}{d\tau} = 0, \quad (5.10)$$

see (5.9) with  $F^{\mu} = 0$  or (A.62). Its derivation from the least action principle shows that the Christoffel symbols  $\Gamma_{\mu\nu}^{\kappa}$  depend on the first derivatives of the metrics only, see (A.63) — the metrics is a tensor of order two that characterizes the geometry of a curved space, it defines lengths by a scalar product. Locally, a flat spacetime makes these inertial terms vanish. Then, the terms  $\Gamma_{\mu\nu}^{\kappa}$  contain all of the information on the gravitational field. And so, the variations of the metrics translate the variations of the gravitational field.

Now, we need to find a tensor that describes curvature through the derivatives of the metrics only. A computational research leads to the Riemann-Christoffel tensor  $R^{\rho}_{\sigma\mu\nu}$ , defined in the annexe by (A.69), and which renders the properties of curvature in differential geometry. In practice, there are also the Ricci tensor

$$R_{\mu\nu} = -R^{\lambda}_{\mu\lambda\nu} \quad (5.11)$$

and the scalar curvature

$$R = R_{\mu}^{\mu} = g^{\mu\nu} R_{\mu\nu}, \quad (5.12)$$

which are contractions of the Riemann tensor. We notice here that it satisfies the second Bianchi identity (A.75) which implies, after two contractions, that

$$\nabla_{\mu} G^{\mu}_{\nu} = 0, \text{ with } G_{\mu\nu} = R_{\mu\nu} - \frac{1}{2} R g_{\mu\nu}, \quad (5.13)$$

where  $G_{\mu\nu}$  is a symmetric tensor called Einstein tensor.

### Energy and matter source

Curvature depends on the gravitational field, which is sourced by matter. We thus need to generalize the Poisson equation (5.4). But mass is the same as energy, according to special relativity (see Section 5.1.1 and [47]). And mass is described by an energy-momentum tensor. Let us recall some of its properties in the case of an electromagnetic source in a flat spacetime. This provides a description of the source term that can be extended in a curved spacetime, whatever the nature of the energy source, be it empty, electromagnetic or massive.

Maxwell equations work out the spatial and time evolution of the combined electric and magnetic fields,  $\mathbf{E}$  and  $\mathbf{B}$ . These equations write

$$\begin{cases} \nabla \cdot \mathbf{E} = \frac{\rho}{\epsilon_0}, & \frac{1}{c^2} \frac{\partial \mathbf{E}}{\partial t} - \nabla \times \mathbf{B} = -\mu_0 \mathbf{j}, \\ \nabla \cdot \mathbf{B} = 0, & \frac{\partial \mathbf{B}}{\partial t} + \nabla \times \mathbf{E} = 0, \end{cases} \quad (5.14)$$

with  $\rho$  the electric charge density,  $\mu_0$  the vacuum permeability, and  $\epsilon_0$  the vacuum permittivity. The special theory of relativity provides their tensorial expression, that relies on the equivalence principle:

$$\partial_\mu F^{\nu\mu} = \mu_0 J^\nu, \quad \epsilon^{\lambda\mu\nu\rho} \partial_\mu F_{\nu\rho} = 0, \quad (5.15)$$

where  $\epsilon_{\lambda\mu\nu\rho}$  is the totally antisymmetric 4-dimensional tensor with  $\epsilon_{0123} = 1$ , and  $J^\nu = (\rho c, \mathbf{j})^\top$  the 4-current. The first and last Maxwell equations are known to imply the existence of a magnetic potential  $\mathbf{A}$  and an electric potential  $\phi$  defined by

$$\mathbf{B} = \nabla \times \mathbf{A}, \quad \mathbf{E} = -\frac{\partial \mathbf{A}}{\partial t} - \nabla \phi. \quad (5.16)$$

In the relativistic formulation, they can be written as

$$F_{\mu\nu} = \partial_\mu A_\nu - \partial_\nu A_\mu \quad (5.17)$$

by introducing the electromagnetic four-potential

$$A^\mu = \left( \frac{\phi}{c}, \mathbf{A} \right)^\top. \quad (5.18)$$

Taking the divergence of the first equality of (5.15), noting that  $\partial_\mu \partial_\nu F^{\mu\nu} = 0$  because of the antisymmetry of  $F^{\mu\nu}$ , we can express the conservation of the 4-current

$$\partial_\mu J^\mu = 0, \quad (5.19)$$

which translates the classical continuity equation

$$\frac{\partial \rho}{\partial t} + \nabla \cdot \mathbf{j} = 0. \quad (5.20)$$

In a curved spacetime, the local conservation of a scalar electric charge is given by the preservation of the tensor  $J^\mu$  of order 1 with the covariant derivative

$$\nabla_\mu J^\mu = 0, \quad (5.21)$$

when  $J^\mu$  describes both the charge density and its flux. In the same way, the conservation of the 4-momentum, a tensor of order 1, is described by a tensor of order 2 that satisfies

$$\nabla_\mu T^\mu{}_\nu = 0. \quad (5.22)$$

The tensor  $T^{\mu\nu}$  is called energy-momentum tensor and contains the energy and momentum densities, as well as information on their flux; this information translates the stresses present in the matter. The use of the momentum-energy tensor for any type of matter seems to be first used by Max Laue in [92] according to [62] p. 626, and it was also mentioned by Einstein in [51]. The matter and associated energy density in Poisson's equation can thus be replaced in the general relativistic covariance by the symmetric tensor  $T^{\mu\nu}$ .

### Einstein's equations: energy and spacetime dynamics

To summarize, we want to connect spacetime geometry and mass distribution dynamics, in a covariant way. The spacetime energy content can be described by the symmetric tensor  $T^{\mu\nu}$  of order 2. This generalizes the second term of Poisson's equation. Then, the equivalent of the laplacian of the gravitational potential should be a second order symmetric tensor linearly —

for covariance — containing at most second derivatives of the metrics that corresponds to  $\Phi$ . According to the above, it can be obtained by combinations of  $R_{\mu\nu}$ ,  $Rg_{\mu\nu}$ , and a constant  $\Lambda$ . In order to additionally satisfy (5.22), we have to use Einstein's tensor and then get his equations

$$G_{\mu\nu} - \Lambda g_{\mu\nu} = \chi T_{\mu\nu}, \quad (5.23)$$

where the constant  $\chi = \frac{8\pi\mathcal{G}}{c^4}$  is obtained with the first component  $G_{00}$  in the Newtonian limit (with matter velocities  $v \ll c$ ) from Poisson's equations (5.4) when  $\Lambda = 0$ , or transforming this non-relativistic equation into a Helmholtz equation with linear term  $-\Lambda\Phi$  as in [52].

Einstein's and Grossmann's steps were actually more complicated than the above explanation. Many papers have been published after the first clearing work [53] where Marcel Grossmann presented the necessary mathematical tools, while Albert Einstein applied them to a simplified description of gravitational phenomena. It took a few additional years before the general theory of relativity was settled in [48] and the field equations derived in [49]. All this work has implemented the deduction of electrodynamics from electrostatics, with the general Einstein's equations

$$G_{\mu\nu} = \chi T_{\mu\nu}, \quad (5.24)$$

where the constant  $\Lambda$  is taken equal to zero by Einstein, in order to have a vanishing Ricci tensor in vacuum, see [50] p. 804. He reintroduced  $\Lambda$  afterwards, to solve boundary condition problems in his first paper for cosmology [52]. Therefore the constant  $\Lambda$  is called the cosmological constant.

#### A remark on another deduction of Einstein's equations

If we consider gravitation as a constraint on geometry, then it makes sense to look for Einstein's equations as solutions of a least action principle. Variational principles were introduced by Lagrange in the second part of the XVIII<sup>th</sup> century, see [41] or [89]. The first historical chapter of [123] retraces the story of Lagrange equations, and [85] brings a brief history of variational principles. Given a Lagrangian,  $\mathcal{L}$ , that contains the physics of a system, one can derive the equations of the dynamics as critical points of the action

$$S = \int \mathcal{L} dt. \quad (5.25)$$

The adequate Lagrangian density is a scalar — to ensure covariance — that contains the geometry through curvature and its energy sources [25, 123], so that the action is composed of two terms

$$S = S_c + S_m = \int (\mathcal{L}_c + \mathcal{L}_m) \sqrt{-g} d^4x. \quad (5.26)$$

On the first hand the first term can be written as

$$S_c = -\frac{1}{2\chi} \int R \sqrt{-g} d^4x \quad (5.27)$$

with  $\mathcal{L}_c = R$  the simplest scalar related to curvature. On the other hand the matter action is written as

$$S_m = \int \mathcal{L}_m \sqrt{-g} d^4x, \quad (5.28)$$

where  $\mathcal{L}_m$  describes as in special relativity the energy content which affects the geometry. The term  $\sqrt{-g} d^4x$  is the covariant infinitesimal volume of the 4-dimensional spacetime. The variation of  $S_m$  leads to the expression of the energy-momentum tensor as

$$T_{\mu\nu} = 2 \left[ \frac{\partial \mathcal{L}_m}{\partial g^{\mu\nu}} - \frac{1}{2} g_{\mu\nu} \mathcal{L}_m \right]. \quad (5.29)$$

The related lagrangian formalism for the general theory of relativity has been written by Einstein in [51] to assert the previous reasoning of section 5.1 (see [50] p. 804). The action needed to derive the general equations had been given by David Hilbert in 1915 [73], probably after the lectures delivered by Einstein whom he invited in Göttingen and who submitted the gravitation field equations [49] in November 1915, as the result of his lectures, the same month of Hilbert's submission of his article [73].

In this theory, the Universe is now an object in itself, with geometrical properties and energy content. It does not only have local but also global properties: metrics, curvature, etc. It is flexible and dynamical, depending on what happens in it and on the energy it contains. The singularity of the gravitational force due to the equivalence principle on inertial and gravitational masses is justified. Gravitation is no longer a force but coincides with the geometry and models space and time.

## 5.2 The expanding Universe

The intrinsic symmetry of the energy-momentum tensor leaves only 10 distinct equations over the 16 in (5.23) or (5.24), and only 6 are independent because of (5.22). They form a system of 10 coupled non-linear differential equations, which is generally much difficult to solve. Therefore, some hypotheses on the Universe's symmetries are used to simplify them, allowing precise enough results, such as Mercury's or internal planets' perihelion precession, or the variation of the periods of binary pulsars. We derive here the dynamics in the context of the standard model of cosmology.

### 5.2.1 Constraining the geometry

The *cosmological principle* considers that the Universe is homogeneous and spatially isotropic at very large scales. It can be verified for instance with the observations of the cosmic microwave background that reveals a perfect black body radiation at 2,7 K. It is then convenient to write the equations in a synchronous frame. Those are attached to fundamental observers that follow the motion of the universe content, also referred to as comoving observers. For them, the Universe really seems homogeneous and isotropic. In such a frame, the Riemann tensor is maximally symmetric (cf (A.78) p.125), and the metrics can be defined by

$$ds^2 = c^2 dt^2 - R^2(t) \left[ \frac{dr^2}{(1 - kr^2)} + r^2 d\theta^2 + r^2 \sin^2 \theta d\phi^2 \right] \quad (5.30)$$

in a synchronous gauge, see [25] or [74]. The scale factor  $a$  is commonly introduced to decompose the coordinate  $\mathbf{x}$  of any particle with respect to the constant comoving coordinate  $\mathbf{r}$  as

$$\mathbf{x} = a(t)\mathbf{r}. \quad (5.31)$$

Then, it can be expressed in terms of the edge of a sphere as

$$a(t) = \frac{R(t)}{R_0}, \quad (5.32)$$

with  $R_0$  that is generally taken to its value at the present time, and be introduced as a new variable in (5.30). Depending on the sign of  $k$ , which is related to the spatial curvature with a 1/6 factor, the spatial part of the metrics comes in various forms.

- When  $k > 0$ , the geometry is closed as a 3-dimensional sphere.

- When  $k = 0$ , the universe is flat.
- When  $k < 0$ , the universe is opened.

In every case, the spatial geometry is described by a metrics with maximally symmetric hyper-surfaces, because of the cosmological principle, and its evolution is independent from that of the scale factor.

### 5.2.2 Describing the energy content

We assume that the Universe is filled by a continuum of cosmic perfect fluids, see [160, 161] for a discussion on this approximation. The energy-momentum tensor of a perfect fluid is

$$T_{\mu\nu} = \left(\rho + \frac{p}{c^2}\right) u_\mu u_\nu - p g_{\mu\nu}. \quad (5.33)$$

In a synchronous frame, this fluid is at rest, otherwise it would break the spatial isotropy. It is a comoving fluid with a 4-velocity  $u^\mu = (1, 0, 0, 0)^\top$ , constant pressure and uniform density. The trace of its energy tensor is then  $T = T^\mu_\mu = \rho c^2 - 3p$ . If the energy content is described by a set of independent, i.e. only gravitationally interacting, perfect fluids, that we label by indices  $i$ , then the total density is written as

$$\rho = \sum_i \rho_i. \quad (5.34)$$

Each fluid brings a contribution of the type

$$T_{\mu\nu,i} = \left(\rho_i + \frac{p_i}{c^2}\right) u_{\mu,i} u_{\nu,i} - p_i g_{\mu\nu} \quad (5.35)$$

to the total energy-momentum impulse, and independently satisfies the conservation equation (5.22) with

$$\nabla_\mu T^\mu_{\nu,i} = 0. \quad (5.36)$$

In cosmology, it is convenient to introduce barotropic perfect gases, for a simplified distribution of matter, to set the last degree of freedom. Their equations of state

$$p_i = \omega_i \rho_i c^2 \quad (5.37)$$

simplify the integration of the conservation equation in Section 5.2.3, and render a large variety of physical behaviors. Indeed, statistical physics provides such information from a microscopic description of gas and fluids. The Fermi-Dirac statistic accounts for fermionic perfect gas, e.g. electrons, protons, neutrons, neutrinos. In the non-relativistic case, they present an index  $\omega_r = \frac{2}{3}$ , as for a monoatomic perfect gas. Radiation can be described by a perfect fluid of relativistic bosons, namely photons for light, leading to an index  $\omega_r = \frac{1}{3}$ . Pressureless fluids have a vanishing barotropic index  $\omega_m = 0$ , which can describe baryonic and some dark matter. For usual fluids, the barotropic indices are in-between 0 and 1, which corresponds to stiff matter where the sound velocity equals the speed of light. On the other hand, negative barotropic indices allow repulsive behaviors that may correspond to dark matter ( $-\frac{1}{3} < \omega_{DM} \leq 0$ ) or dark energy ( $-1 \leq \omega_{DE} < -\frac{1}{3}$ ). The energy-momentum tensor for a scalar field leads to a pressure  $p = -\rho c^2$  with  $\omega = -1$ , so that it is not affected by any expansion of spacetime, an adequate property of vacuum. We will see in Section 6.2 that the cosmological constant can be interpreted as a fluid of barotropic index  $\omega_\Lambda = -1$ , which is not necessarily associated to vacuum fluctuations. Similarly, curvature will be interpreted as a fluid of index  $\omega_c = -\frac{1}{3}$ .



The cosmological constant, that was taken to 0 in Einstein's field equations (5.23), has been introduced again by Einstein in [52] to solve the boundary conditions problem of (5.24). As a matter of fact, the field equations (5.24) required boundary conditions to accurately determine the metrics. But all natural conditions revealed inconsistent: a degenerate metric at spatial infinity, corresponding to a very high value of the gravitational potential there, could have prevented particles to reach infinity, but this was incompatible with the actual limited value of the potential conditioned by the mass present in the universe. Likewise, a universe asymptotically flat would have suggested a privileged referential to describe physics, and thus was in contradiction with Einstein's fundamental principles for the general theory of relativity. Therefore, Einstein proposed to change his point of view and to consider the universe as a spatially finite (closed) continuum. Then the cosmological constant enabled him to remove the previous problems with a universe with neither center nor border, but of finite spatial extension determined by the total constant density, see [52]. However, his static model was unstable. As suggested by the Hubble law [76], the universe is actually in expansion. When realizing that the Universe was indeed dynamical, and not static, the cosmological constant has been removed. It has been reintroduced again in the nineties to account for the acceleration of the expansion observed by Saul Perlmutter, Adam Riess and their teams [126, 134]. With a barotropic index  $\omega_\Lambda = -1$ , its negative pressure confers a repulsive property to  $\Lambda$  that can explain the acceleration. However, its nature is still uncertain: its various possible origins, e.g. vacuum energy, lack coherence with particle physics' predictions [127] p.226.

### 5.2.3 Friedmann - Lemaître equations

We set here the fundamentals equations of a dynamical universe, which constitutes the grounds of the current standard cosmological model.

Alexandre Friedmann in 1922 and George Lemaître in 1927 derived the form of the metrics (5.30), in agreement with the assumptions of the cosmological principal. They were independently followed by Howard P. Robertson in 1929 and Arthur G. Walker in 1936. With a total density  $\rho$  for a perfect fluid described by (5.35) and the cosmological constant, the temporal and spatial components of Einstein's equations (5.23) give the two Friedmann-Lemaître equations

$$\left\{ \begin{array}{l} \frac{\ddot{a}}{a} = -\frac{4\pi\mathcal{G}}{3} \left( \rho + \frac{3p}{c^2} \right) + \frac{1}{3} \Lambda c^2, \\ \left( \frac{\dot{a}}{a} \right)^2 = \frac{8\pi\mathcal{G}}{3} \rho + \frac{1}{3} \Lambda c^2 - \frac{c^2 K}{a^2}, \end{array} \right. \quad (5.38)$$

where  $K$  is a constant related to the spatial curvature.

The conservation equation (5.13),  $\nabla_\mu G^\mu{}_\nu = 0$ , and equivalently  $\nabla_\mu T^\mu{}_\nu = 0$ , leads to

$$\dot{\rho} + \left( \rho + \frac{p}{c^2} \right) \frac{3\dot{a}}{a} = 0. \quad (5.39)$$

In (5.38) and (5.39), only two equations are independent. The equation of state of the barotropic fluids of Section 5.2.2 facilitates the integration of (5.39), which gives  $\rho \propto a^{-3(1+\omega_i)}$  for a fluid  $i$ . Then, the density of photons, or radiation, of index  $\omega_r = \frac{1}{3}$  decreases as  $\rho_r \propto a^{-4}$ , faster than pressureless matter ( $\omega_m = 0$ ) which decreases as  $\rho_m \propto a^{-3}$ . In the same way, the cosmological constant shows a constant density. At each time, either radiation, dark matter or the cosmological constant dominates the other in terms of densities, see figure 5.2. At late time, the cosmological

constant is preponderant since its density remains constant while the other fluids are diluted by the expansion. The term that contains  $\Lambda$  in (5.38) becomes greater than the others and imply an acceleration of the universe expansion.

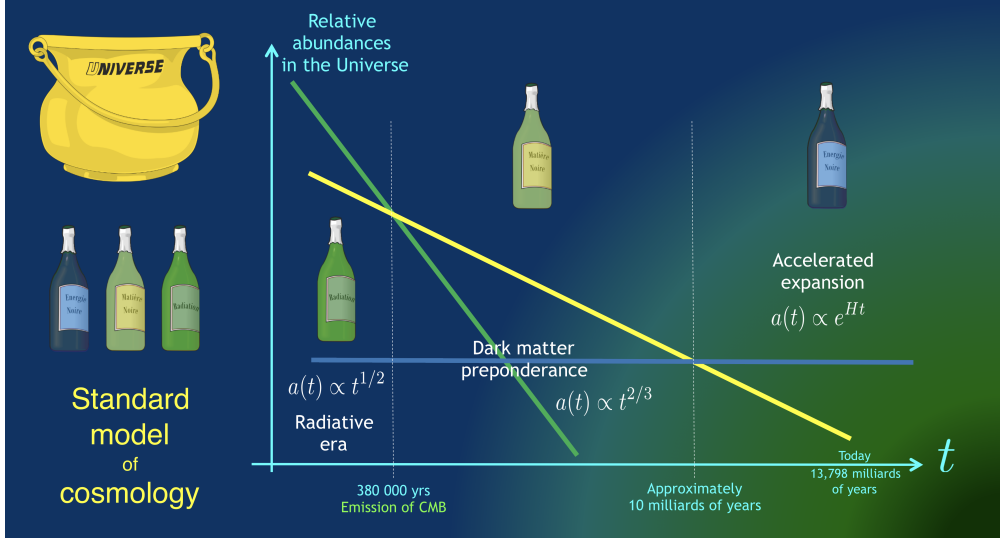


Figure 5.2: Friedmann-Lemaître dynamics for a universe filled by radiation (in green) and pressureless dark matter (in yellow). This illustration of the universe as such a cosmic soup can be found in the third movie of [125]. Asymptotically, the cosmological constant (interpreted as a cosmic fluid in blue) dominates, causing an accelerated expansion of the universe.

The expansion rate of this universe is characterized by the Hubble parameter

$$H = \frac{\dot{a}}{a}. \quad (5.40)$$

Current measurements [128] give today value of the Hubble constant  $H_0 = 67.4 \pm 0.5$  km/s/Mpc. This value generally depends on time but is considered approximately constant for close objects, compared to cosmological distances. Its inverse is commensurable with the age of the Universe, of the order of  $13.799 \pm 0.038$  Gyr.

To summarize, the Friedmann-Lemaître Universes have a local geometry of constant curvature hypersurfaces, which evolution is given by that of the scale factor, depending on the energy content of the Universe. When several fluids are considered, they are assumed to interact only gravitationally one with another. The conservation equation (5.39) is then independently valid for each of them. This Universe's description constitutes the base of today's standard model of cosmology.

### 5.3 The Universe as a gravitational dynamical system

Various scenarios for the future and the past of the Universe can emerge. Among them, the most popular are the Big Chill with an endless cosmic expansion, the Big Rip [23, 11] with a scale factor that becomes infinite at a finite time in the future, the Big Crunch singularity for

spatially closed cosmologies with a small or vanishing cosmological constant, of the same nature as the Big Bang for the early Universe. It reveals more convenient to reformulate the expanding Universe field equations. This enables one to use dynamical systems techniques and allows a global comprehension of the cosmological dynamics.

The dynamics of the Universe depends on the evolution of the scale factor and fluid densities. According to (5.38) and (5.39) for a universe filled by  $\Lambda$  and matter of density  $\rho$  and barotropic index  $\omega$ , it is driven by

$$\frac{\ddot{a}}{a} = -\frac{4\pi\mathcal{G}}{3} \left( \rho + \frac{3p}{c^2} \right) + \frac{c^2}{3} \Lambda \quad (5.41)$$

and

$$\dot{\rho} = - \left( \rho + \frac{p}{c^2} \right) \frac{3\dot{a}}{a}. \quad (5.42)$$

As a dynamical system of order two, the above formulation can be simplified into

$$\dot{x} = f(x), \quad \text{with } x = (a, \dot{a}, \rho). \quad (5.43)$$

This provides a rich framework for a dynamical analysis [158]. An even simpler description appears when introducing relative abundances  $\Omega$  for the barotropic fluids. Given the fluid total density

$$\rho_{tot} = \frac{3}{8\pi\mathcal{G}} H^2, \quad (5.44)$$

the relative abundance of a fluid of density  $\rho$  is defined by

$$\Omega = \frac{\rho}{\rho_{tot}} \quad (5.45)$$

and can be defined by

$$\Omega_\Lambda = \frac{c^2 \Lambda}{3H^2} \quad (5.46)$$

for the cosmological constant, as one can see in (5.41) with the definition (5.45). If one notes that their time derivatives can be expressed by

$$\dot{\Omega} = -2 \frac{\ddot{a}}{a \dot{a}} \Omega, \quad (5.47)$$

then the couple (5.41) and (5.42) gives

$$\begin{cases} \frac{d\Omega}{d\lambda} = \Omega \begin{bmatrix} -1 - 3\omega & + & (1 + 3\omega)\Omega & - & 2\Omega_\Lambda \end{bmatrix} \\ \frac{d\Omega_\Lambda}{d\lambda} = \Omega_\Lambda \begin{bmatrix} 2 & + & (1 + 3\omega)\Omega & - & 2\Omega_\Lambda \end{bmatrix} \end{cases} \quad (5.48)$$

where the independent time variable  $t$  has been changed into the number of e-foldings  $\lambda = \ln(a(t))$ , see e.g. [154]. Therefore, in the standard model of cosmology, even with its five fluids of radiation, baryonic matter, dark matter, dark energy and cosmological constant, the evolving parameters  $x = (a, \dot{a}, \rho)$  can be replaced by relative abundances and densities  $(\Omega, \rho)$  with  $\rho$  defined by (5.34), while  $f$  sets the dynamics of a Lotka-Volterra system [95, 157], as discussed in Chapter 6. Such dynamical systems were introduced in the middle of the 1920's to model the evolution of lynxes and hares based on numerous data, collected by the Hudson's Bay Company during the XIX<sup>th</sup> century [93], and more generally ecological systems.

The future of the Universe is then completely determined by its energy content. Each cosmic fluid, at least matter and cosmological constant, competes with itself and others to survive in terms of density, see Chapter 6. This ecological description and the possibility of a chaotic dynamics when introducing some coupling has led to the name of Jungle Universe, investigated in [124]. The particular case of (5.48) makes the Universe converge towards three possible equilibria, depending on the energy initial distribution. Those equilibria correspond to universes filled by only one cosmological fluid, because of the singular dynamics without coupling. Asymptotically, the Universe can converge towards a Milne Universe that is totally empty, towards the Einstein-de Sitter Universe that is only made of matter, or towards the de Sitter Universe that is dominated by a cosmological constant. This latter is the attractor of the dynamics whenever there is a small amount of dark energy. Consequently, the universe would undergo an endless accelerated expansion in the future.

We shall notice here the degeneracy of the model, only the gravitational interaction is considered! In addition, the cosmological principle imposes a homogeneity and isotropy that is not compulsory at all stages of Universe's history. We will see in Chapter 6 how to possibly remove the interaction restriction. We propose here to glimpse at the possibility to remove the isotropy condition. That allows a description of the possible dynamics of the Universe at early times thanks to a dynamical system analysis developed at the end of the twentieth century.

A scarcely popularized model has been developed by Russian mathematicians under the supervision of Lev Davidovitch Landau to save general relativity from the singularities that can arise as first demonstrated by Roger Penrose and Stephen Hawking in 1970 [67]. It is but of relevant interest, as they proposed an anisotropic dynamical system, with a scale factor per spatial direction. The resulting homogeneous spatial sections were known since 1898 thanks to the classification of Luigi Bianchi [14, 15]. Their metrics can be written as

$$ds^2 = \gamma(\tau) \omega^i \omega^j - N^2(\tau) d\tau^2, \quad (5.49)$$

where  $\tau$  is a conformal time, measuring time through the distance covered by photons in an expanding or contracting universe, and where the spatial components  $\omega^i$  depends on the infinitesimal lengths  $dx^i$  and on the coordinates  $x^i$  through hyperbolic or ordinary trigonometric functions, for instance  $\omega_1 = \cos(x_2) \cos(x_3) dx_1 - \sin(x_3) dx_2$  in Bianchi IX. The spatial part of (5.49) can be diagonalized giving simple access to the volume of the 3-dimensional spatial sections. When inserted in Einstein's equations, sourced by a perfect fluid, these eleven types of Bianchi Universes can account for several schemes: empty or filled universes experiencing successive Kasner eras, which are the fundamental states for such systems.

Kasner states correspond to generic universe solutions in the metrics of Bianchi I. In that state, when  $t \rightarrow 0$ , two spatial directions are in contraction with two different constant rates, while the third direction is in expansion with another fixed rate. In this anisotropic shearing, the volume of a spatial region of the Universe decreases when  $t \rightarrow 0$ . The three rates  $p_1$ ,  $p_2$  and  $p_3$ , satisfy the two conditions

$$p_1 + p_2 + p_3 = p_1^2 + p_2^2 + p_3^2 = 1, \quad (5.50)$$

with  $p_1 < 0$  and  $p_2, p_3 > 0$ . Then the metrics can be rewritten as

$$ds^2 = -c^2 dt^2 + t^{p_1} dx_1^2 + t^{p_2} dx_2^2 + t^{p_3} dx_3^2. \quad (5.51)$$

Furthermore, the dynamics of Bianchi Universes can be decomposed as a finite or infinite sum of transitions between Kasner states.

In particular, the attainable chaotic behavior of Bianchi IX can be considered as an alternative to the Big Bang singularity, as conjectured by the Russians Belinskii, Khalatnikov and Lifschitz [12, 89]. As a matter of fact, the hamiltonian formalism, see e.g. [111, 122], enables one to make a parallel between the propensity of the scale factors to expand or reduce and the motion of a ball on a billard table [36]. Each rebound on the table corresponds to a transition of the Universe between two Kasner states. In a Bianchi IX universe, one may reach the initial singularity by an infinite and chaotic succession of Kasner states, the global volume decreases and the singularity stands as an attractor of any roll-back-time trajectory [137]. A visualization work of the dynamics to understand what expansion means in cosmology can be found in [125]. The third movie illustrates some occurrences for the past and fate of the Universe, based on recent observations and numerical simulations of the Bianchi [122] and Jungle [124, 145] Universes.

As a conclusion, the Universe can be globally described as a dynamical system. The general theory of relativity yields the fundamental grounds for the spacetime dynamics and mainly relies on the equivalence principle. In the standard model of cosmology, the scale factor is an indicator for the expansion of the geometry which is conditioned by the composition of the cosmic soup. However, the cosmological principle from which it stems presents some restrictions, which give rise to alternative models. For a search on the fate of the Universe at large scales, the homogeneity assumption can be retained as a first approximation, according to the small measured fluctuations of the cosmic microwave background [129], as well as the isotropy hypothesis. The remaining interaction limit of the standard model of cosmology is tackled in Chapter 6.



# Jungle interaction in the Universe

THE well-known  $\Lambda$ CDM model is the current concordance model for cosmology. Nevertheless, this standard model still presents limits at both small and large scales [22, 42]. Among them, the unknown nature of dark energy and the coincidence: why do we observe today almost the same order of magnitude for the dark matter and dark energy densities?

In this chapter, we propose a refinement of the standard model of cosmology. After an outline of the fundamental characteristics of Lotka-Volterra systems, we remind how the fields equations of general relativity can be expressed in such an ecological framework. This perspective both offers a more comprehensive dynamics and facilitates the consideration of a natural non-gravitational coupling. We eventually question the origin of dark energy as possibly emerging from a non-gravitational interaction between cosmic fluids. Throughout the chapter, we discuss and complete the major results on the jungle dynamics and effective dark energy that have been published in [124, 145].

## 6.1 Lotka-Volterra systems

Lotka-Volterra systems [95, 157] and competing species are largely studied as dynamical systems in various domains [75, 114, 158, 35, 150]. They commonly model the interactive dynamics of a population of predators  $x_2$  and preys  $x_1$

$$\begin{cases} \dot{x}_1 = x_1 (+r_1 - a_{12}x_2) \\ \dot{x}_2 = x_2 (-r_2 + a_{21}x_1) \end{cases} \quad (6.1)$$

where  $x_1$  and  $x_2$  are two functions of the  $t$  variable, and the other parameters are positive. The capacity vector  $r = (r_1, r_2)$  contains the decay or growth rates of preys and predators, while  $a_{12}$  and  $a_{21}$  are real parameters quantifying the interactions between the two populations. In ecological systems, they can depend on the mobility of the species and their defense or aggressive capacity for instance. When the initial conditions  $x_1(t_0)$  and  $x_2(t_0)$  are positive, then the two functions  $x_1$  and  $x_2$  are periodic. The orbits of the system in the configurations space are confined along concentric closed curves and are centered on the equilibrium point  $(\tilde{x}_1, \tilde{x}_2) = \left(\frac{r_1}{a_{12}}, \frac{r_2}{a_{21}}\right)$ . They correspond to the isovalues of the Lyapunov function of the system  $V(x_1, x_2) = a_{21}x_1 + a_{12}x_2 - (r_2 \ln x_1 + r_1 \ln x_2)$ , which is convex and satisfies  $\frac{dV}{dt} = 0$ .

This dynamics is relatively simple, and allows unlimited growth of populations when  $a_{12} = 0$ . A more realistic dynamics can be obtained with the generalized Lotka-Volterra equations that contain limiting coefficients:

$$\begin{cases} \dot{x}_1 = x_1 (+r_1 - a_{11}x_1 - a_{12}x_2), \\ \dot{x}_2 = x_2 (-r_2 + a_{21}x_1 - a_{22}x_2). \end{cases} \quad (6.2)$$

The matrix  $A = (a_{ij})$  is called the interaction matrix. The sign of its components are related to the properties of the physical system they describe. For an ecological model, many interactions can appear:

- a pure intraspecific competition:  $a_{12} = a_{21} = 0$ ,  $a_{11}, a_{22}, r_1, -r_2 > 0$ , in this decoupled system, each population competes with itself for the same resource;
- an intra- and interspecific competition:  $a_{12} < 0$  and  $a_{21}, a_{11}, a_{22}, r_1, -r_2 > 0$ , both species compete with themselves and the others;
- a cooperation or mutualism:  $a_{12} > 0$  and  $a_{21} < 0$ , the different species benefit from the presence of the others;
- a prey-predator model or parasitism:  $a_{12} < 0$ , and  $a_{21} < 0$ , the first species takes profit from the second one and damages it;
- commensalism:  $a_{12} < 0$ , and  $a_{21} = 0$ , the first species takes advantage of the second one with no damage;
- amensalism:  $a_{12} > 0$ , and  $a_{21} = 0$ , the first species inhibits the other but without any benefit.

When all the constants are positive, then closed curves, solutions of (6.3), are spirals that converge into the equilibrium point  $(\tilde{x}_1 \neq 0, \tilde{x}_2 \neq 0)$  solution of

$$\begin{cases} r_1 = +a_{11}x_1 + a_{12}x_2, \\ r_2 = -a_{21}x_1 + a_{22}x_2. \end{cases} \quad (6.3)$$

If the matrix  $A = (a_{ij})$  is singular — not invertible — then the situation is said to be degenerate and equilibria are on the axes ( $x_1 = 0$ ) or ( $x_2 = 0$ ), depending on which one has the greater capacity  $r_i$ .

This Lotka-Volterra model can be generalized to any  $n$ -dimensional case that describes the cohabitation between  $n$  species. It can be written as

$$\frac{dx_i}{dt} = x_i \left( r_i + \sum_{j=1}^n a_{ij}x_j \right), \quad i = 1, \dots, n. \quad (6.4)$$

The dynamics and equilibria depend on the properties of the interaction matrix and capacity vector. In any case, the disappearance of one of the species is irreversible. In other words, if there exists some time  $t_e$  when  $x_i(t_e) = 0$ , then for all  $t > t_e$ ,  $x_i(t) = 0$ , setting the extinction of the species  $i$ . The dynamics can be more easily understood with Lyapunov functions that are first integrals of the dynamics, i.e. they are invariant at each step along a given trajectory. For an introduction to dynamics in a phase space, the books and articles [7, 30, 31, 17, 18] provide mathematical grounds and applications in celestial mechanics.

## 6.2 An ecological framework for the standard model of cosmology

As presented in [124], the Friedmann-Lemaître cosmology can be directly interpreted as a Lotka-Volterra system. As introduced in Section 5.3, a change of temporal variable  $\lambda = \ln(a(t))$  and the description of  $n$  fluids densities through their relative abundances  $\Omega_i$ ,  $i = 1, \dots, n$ , in the global cosmic soup give the new formulation of Friedmann-Lemaître equations:

$$\forall i = 1, \dots, n+1, \quad \frac{d\Omega_i}{d\lambda} = \Omega_i \left[ -1 - 3\omega_i + \sum_{j=1}^n (1 + 3\omega_j) \Omega_j \right] \quad (6.5)$$

and

$$1 = \sum_{i=1}^{n+1} \Omega_i. \quad (6.6)$$

The relative abundances

$$\Omega_i = \frac{\rho_i}{\rho_{tot}} = \frac{8\pi\mathcal{G}}{3H^2} \rho_i \quad (6.7)$$

are expressed in terms of the total energy density

$$\rho_{tot} = \frac{3}{8\pi\mathcal{G}} H^2 \quad (6.8)$$

and are valid for any cosmic fluid, including curvature for which we define a  $(n+1)^{th}$  fluid of relative abundance

$$\Omega_c = -\frac{c^2 K}{a^2 H^2} \quad (6.9)$$

and barotropic index

$$\omega_c = -\frac{1}{3}. \quad (6.10)$$

The curvature abundance can be seen as an indicator for the rate of the Universe expansion or contraction: if it decelerates then  $\Omega_c$  decreases, if it accelerates then  $\Omega_c$  increases, and vice versa. This effective definition comes from the identification of (6.7) in the first Friedmann-Lemaître equation (5.41). In the same way, the cosmological constant has a relative abundance defined by

$$\Omega_\Lambda = \frac{c^2 \Lambda}{3H^2} \quad (6.11)$$

with a barotropic index

$$\omega_\Lambda = -1. \quad (6.12)$$

The second equation (6.6) expresses the global conservation of energy. Since it is invariant, it can be considered as a constraint on the generalized Lotka-Volterra system established by equations (6.5). This  $(n+1)$ -dimensional set of differential equations constitutes a new framework to work on the fluids' global evolution.

Asymptotically, only one species survives, the one with the greater value of capacity  $-3\omega_i - 1$ , because of the singularity of the community matrix composed of identical rows

$$\begin{bmatrix} 1 + 3\omega_1 & \dots & 1 + 3\omega_n & 0 \\ \vdots & \ddots & \vdots & \vdots \\ 1 + 3\omega_1 & \dots & 1 + 3\omega_n & 0 \\ 1 + 3\omega_1 & \dots & 1 + 3\omega_n & 0 \end{bmatrix}. \quad (6.13)$$

Since the barotropic index  $\omega$  always ranges from  $\omega_{\min} = -1$  for the cosmological constant or frozen scalar field in an unstable vacuum to  $\omega_{\max} = +1$  for a free scalar field or stiff matter where sound velocity equals the speed of light, the surviving species is always the dark energy fluid with  $\omega = \omega_\Lambda = -1$ , equivalent to the cosmological constant. This is true whatever its initial abundance, provided that only the gravitational interaction is considered.

Furthermore, the fundamental equations (6.5) can be rewritten using (6.6) and (6.10) as

$$\forall i = 1, \dots, n+1, \quad \frac{d\Omega_i}{d\lambda} = \Omega_i \left[ \sum_{j=1}^{n+1} 3(\omega_j - \omega_i) \Omega_j \right] \quad (6.14)$$



which redefines the community matrix as

$$\begin{bmatrix} 0 & 3(\omega_2 - \omega_1) & 3(\omega_3 - \omega_1) & \dots & 3(\omega_{n+1} - \omega_1) \\ 3(\omega_1 - \omega_2) & 0 & 3(\omega_3 - \omega_2) & \dots & 3(\omega_{n+1} - \omega_2) \\ \vdots & & \ddots & \ddots & \vdots \\ 3(\omega_1 - \omega_n) & \dots & 3(\omega_{n-1} - \omega_n) & 0 & 3(\omega_{n+1} - \omega_n) \\ 3(\omega_1 - \omega_{n+1}) & \dots & 3(\omega_{n-1} - \omega_{n+1}) & 3(\omega_n - \omega_{n+1}) & 0 \end{bmatrix}. \quad (6.15)$$

The skew-symmetry of (6.15) assures that the differential equations system is conservative, in accordance with the global energy conservation constraint. In this form, we notice that the evolution of the relative abundances mainly depends on the differences between the cosmological indices, and thus on pressure differences for equivalent densities. However the rank of this interaction matrix depends on the values of the parameters  $\omega_i$  and the  $n + 1$ -dimension parity. In the standard cosmological model, it generally equals 2 ( $< 6 = n + 1$ ).

Instead of this idealized dynamics, we propose now to remove the degeneracy of the community matrix by allowing for a non-gravitational coupling between the species.

### 6.3 Jungle interactions enrich the standard model

A coupling between two species has to modify the continuity equations in a perfectly balanced way to guarantee the overall energy-momentum conservation. For two coupled barotropic fluids with indices  $i$  and  $j$ , they can be modified as

$$\begin{cases} \dot{\rho}_i &= -3H\rho_i(1 + \omega_i) + \mathcal{Q}_{ij}, \\ \dot{\rho}_j &= -3H\rho_j(1 + \omega_j) - \mathcal{Q}_{ij}, \end{cases} \quad (6.16)$$

which mirrors the adaptation of the conservation equations

$$\begin{cases} \frac{d\Omega_i}{d\lambda} = \Omega_i [-(1 + 3\omega_i) + \sum_{l=1}^n (1 + 3\omega_l) \Omega_l] + \frac{8\pi\mathcal{G}}{3H^3} \mathcal{Q}_{ij}, \\ \frac{d\Omega_j}{d\lambda} = \Omega_j [-(1 + 3\omega_j) + \sum_{l=1}^n (1 + 3\omega_l) \Omega_l] - \frac{8\pi\mathcal{G}}{3H^3} \mathcal{Q}_{ij}. \end{cases} \quad (6.17)$$

The energy transfer  $\mathcal{Q}_{ij}$  is taken quadratic in densities in order to preserve the Lotka-Volterra structure of the Friedmann-Lemaître system, which is kept globally invariant. Then, we can set

$$\mathcal{Q}_{ij} = \mathcal{Q}(\varepsilon_{ij}) = \varepsilon_{ij} \frac{8\pi\mathcal{G}}{3H} \rho_i \rho_j = \varepsilon_{ij} H \Omega_i \rho_j \quad (6.18)$$

with a positive coupling parameter  $\varepsilon_{ij}$ . In (6.18), the Hubble constant  $H$  factor ensures that the energy transfer varies with the volume of the cosmological fluids. In addition, the symmetric expression of  $\mathcal{Q}$  involves the proportion  $\Omega$  of one of the species. This definition makes possible complex microscopic interactions that take into account agglomeration or saturation behaviors for instance, unlike the simpler expression  $\mathcal{Q}(\eta_{ij}) = \eta_{ij} \rho_i \rho_j$ .

Besides, the coupling term (6.18) removes part of the degeneracy of the community matrix (6.13) of rank 1. As a matter of fact, factorizing by the relative abundance  $\Omega_j$  in (6.5) for the two interacting fluids resets its  $(i, j)$ -th and  $(j, i)$ -th coefficients, increasing its rank to 3. The associated dynamics results in being much richer. An example of coupling between dark energy, dark matter and radiation is given in [124]. It allows cyclic behaviors where transient acceleration and deceleration phases alternate, according to whether dark energy or dark matter dominates, without exotic dark energy of index  $\omega < -1$ . One can see on figure 6.1 the attractive character of the dark plane. The cyclic behavior holds when standard fluids are coupled to dark energy. The period of this oscillation when there is no inflation is of the same order as the age of the universe and thus could be an alternative to the coincidence problem.

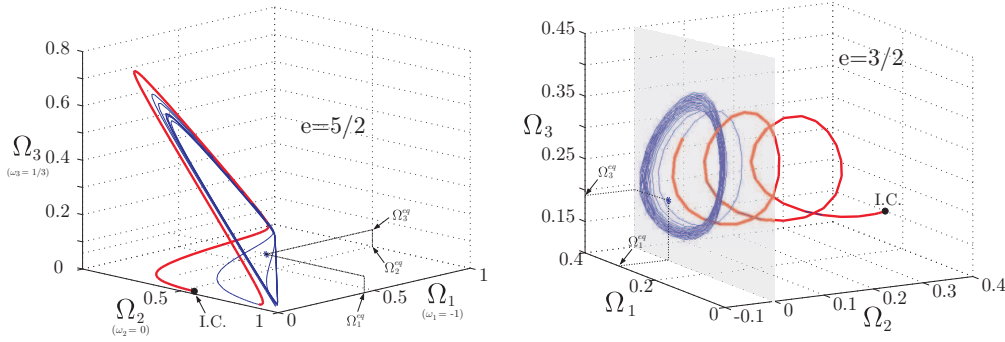


Figure 6.1: Evolution of the three coupled relative abundances, in the 3D phase space, with coupling constants:  $\epsilon_{12} = \epsilon_{13} = \epsilon_{23} = e$ . The starting points of the orbits are marked by a bold red line. Initial conditions are indicated by I.C. and a black dot. Relevant equilibria are indicated by stars [124].

The coupling terms have a tremendous impact on the conservation equations (6.16). Let us consider the density evolution of the first fluid. We may rewrite it as

$$\dot{\rho}_i = -3H \left[ 1 + \omega_i - \varepsilon_{ij} \frac{8\pi\mathcal{G}}{9H^2} \rho_j \right] \rho_i. \quad (6.19)$$

This factorization redefines the equation of state of the fluid  $i$  into

$$p = \omega_i^{\text{eff}} \rho_i c^2, \quad (6.20)$$

which displays an effective barotropic index

$$\omega_i^{\text{eff}} = \omega_i - \varepsilon_{ij} \frac{8\pi\mathcal{G}}{9H^2} \rho_j = \omega_i - \frac{\varepsilon_{ij}}{3} \Omega_j. \quad (6.21)$$

But the scale factor growth or decrease is not altered when taking the interaction into account, as a result of the total energy-momentum preservation. This opens the road to a large variety of physical interplays. The subsequent effective dynamics is developed in section 6.4.

The jungle coupling can be extended to three or more species in interaction. Then the total energy-momentum conservation can be written as

$$\sum_{i,j=1}^{n+1} \mathcal{Q}_{ij} = 0, \quad (6.22)$$

and the effective barotropic indices are generalized by

$$\omega_i^{\text{eff}} = \omega_i - \sum_{j=1}^{n+1} \frac{\varepsilon_{ij}}{3} \Omega_j, \quad \forall i = 1, \dots, n+1, \quad (6.23)$$

with real coupling parameters  $\varepsilon_{ij}$ .

## 6.4 Camouflage in the Jungle

In this section, we question the nature of dark energy as possibly emerging from a jungle coupling. As a matter of fact, the evolution of the scale factor is left unchanged after the introduction of such a coupling. In other words, the first Friedmann equation

$$\frac{\ddot{a}}{a} = -\frac{4\pi\mathcal{G}}{3} \sum_{i=1}^n (1 + 3\omega_i) \rho_i \quad (6.24)$$

is unchanged when taking into account the energy-balanced interactions  $\pm Q_{ij}$ . It can be written as

$$\frac{\ddot{a}}{a} = -\frac{4\pi\mathcal{G}}{3} \sum_{i=1}^n (1 + 3\omega_i^{\text{eff}}) \rho_i. \quad (6.25)$$

Then, an acceleration ( $\ddot{a} > 0$ ) can either result from a dominant dark energy component with  $\omega < -\frac{1}{3}$ , or from other interacting fluids whose effective barotropic indices also imply a positive acceleration of the scale factor.

### Two-fluids interaction in the jungle

Let us first consider the interaction between two fluids of the same nature, i.e. a with  $\omega_1 = \omega_2 = \omega$ . We exclude here the cosmological constant ( $\omega = -1$ ) for which a coupling with itself is not physically relevant and actually does not alter its global observed dynamics. By setting  $8\pi\mathcal{G} = 1$ , we may write their densities evolution as

$$3H^2 = \rho_1 + \rho_2, \quad (6.26)$$

$$\dot{\rho}_1 = -3H(1 + \omega)\rho_1 + \frac{\varepsilon}{3H^2}\rho_1\rho_2, \quad (6.27)$$

$$\dot{\rho}_2 = -3H(1 + \omega)\rho_2 - \frac{\varepsilon}{3H^2}\rho_1\rho_2. \quad (6.28)$$

We introduce the new variable  $u = \rho_1 + \rho_2$  in order to rewrite the equations as

$$\begin{cases} 3H^2 = u, \\ \dot{u} = -3H(1 + \omega)u, \end{cases} \quad (6.29)$$

which leads to

$$\dot{u} = -\sqrt{3}(1 + \omega)u^{3/2}. \quad (6.30)$$

Redefining the origin of time, its solution is given by

$$u(t) = \frac{4}{3(1 + \omega)^2 t^2} \text{ and } H(t) = \frac{2}{3(1 + \omega)t}. \quad (6.31)$$

Then, inserting (6.26) and (6.31) in (6.27) gives the non-linear differential equation

$$\dot{\rho}_1 - \frac{2\varepsilon - 6(1+\omega)}{3(1+\omega)t} \rho_1 = -\frac{\varepsilon(1+\omega)t}{2} \rho_1^2. \quad (6.32)$$

A new change of variable  $z = \frac{1}{\rho_1}$  provides the differential equation

$$\dot{z} + \frac{\alpha}{t} z = \frac{\varepsilon(1+\omega)t}{2} \quad \text{with } \alpha = \frac{2\varepsilon}{3(1+\omega)} - 2. \quad (6.33)$$

The general solution of the homogeneous equation is of the form  $z_0(t) = \lambda t^{-\alpha}$ , and a variation of constants method gives the general solution

$$z(t) = \frac{\varepsilon(1+\omega)}{2(\alpha+2)} t^2 + \sigma t^{-\alpha}, \quad (6.34)$$

where the integration constant  $\sigma$  is assumed not to vanish from now on. Hence we can deduce the following time evolution from the densities  $\rho_1$  and  $\rho_2$ ,

$$\rho_1(t) = \frac{1}{t^2 \left( \frac{3(1+\omega)^2}{4} + \left( \beta t^{+\frac{2\varepsilon}{3(1+\omega)}} \right)^{-1} \right)} \quad \text{and} \quad \rho_2(t) = \frac{1}{t^2 \left( \frac{3(1+\omega)^2}{4} + \beta t^{+\frac{2\varepsilon}{3(1+\omega)}} \right)} \quad (6.35)$$

where  $\beta = \sigma^{-1}$  is the same constant for both densities, because of the constraint (6.26), and is taken positive to assure positive values of  $\rho_1$  when  $t \rightarrow 0$  when  $\varepsilon > 0$  and  $\omega > -1$ . Eventually, the effective barotropic indices can be expressed as

$$\omega_1^{\text{eff}}(t) = \omega - \frac{\varepsilon}{9H^2} \rho_2 = \omega - \frac{\varepsilon}{3 + \frac{4\beta}{(1+\omega)^2} t^{+\frac{2\varepsilon}{3(1+\omega)}}} \quad (6.36)$$

and

$$\omega_2^{\text{eff}}(t) = \omega + \frac{\varepsilon}{9H^2} \rho_1 = \omega + \frac{\varepsilon \beta t^{+\frac{2\varepsilon}{3(1+\omega)}}}{3\beta t^{+\frac{2\varepsilon}{3(1+\omega)}} + \frac{4}{(1+\omega)^2}}. \quad (6.37)$$

Their limit — initial or asymptotic — behavior is the same for all values of  $\varepsilon > 0$  since in our physical context  $1 + \omega > 0$ . When  $\varepsilon > 0$ , then we have

$$\begin{aligned} \lim_{t \rightarrow 0^+} \omega_1^{\text{eff}}(t) &= \omega - \frac{\varepsilon}{3} & \text{and} & & \lim_{t \rightarrow +\infty} \omega_1^{\text{eff}}(t) &= \omega^-, \\ \lim_{t \rightarrow 0^+} \omega_2^{\text{eff}}(t) &= \omega^+ & \text{and} & & \lim_{t \rightarrow +\infty} \omega_2^{\text{eff}}(t) &= \omega + \frac{\varepsilon}{3}, \end{aligned} \quad (6.38)$$

with  $\omega^+$  and  $\omega^-$  the limits obtained by superior and inferior values of  $\omega^{\text{eff}}$ . We understand here that an effective dynamics can emerge in the sense that the coupling has modified the densities and  $\omega^{\text{eff}}$ -indices evolution. But it is not possible to see an emergent dark energy ( $\omega^{\text{eff}} < -\frac{1}{3}$ ) from the coupling of two non-exotic dark matter fluids ( $\omega = 0$ ) nor other ordinary fluids ( $0 \leq \omega < 1$ ) at late times. When  $\varepsilon < 0$ , the role of the two fluids is just interchanged.

### Effective dark energy in the jungle

Let us now illustrate the effective dynamics when three fluids are in interaction. When the first and last two interact with each other, then they satisfy the following system:

$$\begin{cases} H &= \frac{1}{\sqrt{3}}\sqrt{\rho_1 + \rho_2 + \rho_3}, \\ \dot{\rho}_1 &= \rho_1 \left[ -3H(1 + \omega_1) + \frac{\varepsilon_{12}\rho_2}{3H} \right], \\ \dot{\rho}_2 &= \rho_2 \left[ -3H(1 + \omega_2) - \frac{\varepsilon_{12}\rho_1}{3H} + \frac{\varepsilon_{23}\rho_3}{3H} \right], \\ \dot{\rho}_3 &= \rho_3 \left[ -3H(1 + \omega_3) - \frac{\varepsilon_{23}\rho_2}{3H} \right]. \end{cases} \quad (6.39)$$

The numerical integration uses a Matlab solver based on numerical differentiation formulas of orders 1 to 5 [142, 143]. Then the energy may not be preserved. However, the exact preservation of the symplectic property of spacetime does not matter here, since we mainly focus on the qualitative behavior of effective equations of state. We let the system evolve until it reaches its stable asymptotic state. By demanding that  $\varepsilon_{12} = 2$  and  $\varepsilon_{23} = 3$ , the mutual interactions make the first fluid asymptotically dominate the others in terms of density after mimicking a dark energy with an effective barotropic index close to  $-0.4$ , with the initial abundances given in figure 6.2. In the same way, the third and then the second fluids look like monoatomic perfect gas. This behavior holds for the third fluid, even if the others have small abundances.

A large variety of couplings can be considered, leading to various effective dark energies. The conservative condition for energy transfers imposes the presence of some real dark energy for it to dominate others. Indeed, if one rewrites (6.24) in terms of relative abundances and look for a dominant dark energy term, then there should exist some fluid  $i$  such that

$$-\sum_{j \neq i} (1 + 3\omega_j)\Omega_j > \Omega_i + 3\omega_i\Omega_i. \quad (6.40)$$

Taking into account the global conservation  $\Omega_i + \sum_{j \neq i} \Omega_j = 1$ , the inequality becomes

$$-3\sum_{j \neq i} \omega_j\Omega_j - 3\omega_i\Omega_i > 1, \quad (6.41)$$

and thus

$$\sum_{j=1}^n \omega_j\Omega_j < -\frac{1}{3}. \quad (6.42)$$

The necessary condition (6.42) holds for the effective barotropic indices, because of the assumption of balanced energy transfers. An acceleration at large scales can then occur if a small amount of energy with  $\omega < -\frac{1}{3}$  can emerge. Interactions between this energy and other species can then lead to an effective dark energy with a distinct effective barotropic index. These aspects are yet under investigation.

Therefore, the coupling changes the fluids observed behavior and can influence the global dynamics of the universe.

## 6.5 Questioning the nature of dark energy

The most recent observations and analysis from the Planck mission<sup>1</sup> [129] reveal a spacetime of homogeneous geometry, with neither anisotropy nor measurable rotation, and no spatial curvature up to its measures' precision. It should contain dark matter and a cosmological constant of still unknown origin. As from the supernovae observations [118, 126, 134], a cosmic acceleration is confirmed. But Planck's results [130] are still under tension with data from supernovae [136]. In particular, they differ on the determination of the Hubble constant, and thus on the Universe expansion rate and the nature of a possible dark energy.

Theoretically, the model from Einstein's field equations is under-determined, since it does not specify the physical properties of the cosmic fluids. In order to be predictive, we have to provide an equation of state, that relates pressure  $p$  and density  $\rho$ . This degeneracy implies that any scale factor  $a(t)$  can solve the equations given a correct equation of state. They generate energy-momentum tensors  $T_{\mu\nu}$  that are needed to be tested at very large energy scales, which may not be possible for physicists now.

This degeneracy has given rise to a lot of alternative models. Besides (non-scalar) modified gravity theories, numerous propositions of interactions or new types of fluids exist. A large variety of coupling is taken linear in the densities or proportional to  $H\rho$ , see [2, 10] for the most recent proposals. They are broadly used for modeling the decay of heavy matter particles like WIMPS into relativistic particles, particle-antiparticle annihilations into radiation, particle production, inflaton and radiation during reheating e.g. [33], sometimes even the evaporation of a population of primordial black holes [10], the decay of a cosmological vacuum, and energy exchanges between two dark components e.g. [165, 166] (coupled quintessence, a scalar field with varying barotropic index) or with ordinary matter or radiation. More extensive couplings expressed as a product of power laws of two interacting fluids are also proposed, e.g. [104, 9, 5, 162]. However, those probes generally only set up a one-way energy transmission and the proof for the solution to be an attractor of the dynamics is not always possible as in the Lotka-Volterra context [10].

Contrary to the majority of those attempts, the jungle quadratic coupling finds its origin in the natural Lotka-Volterra framework of the Friedmann-Lemaître equations, and allows a simple combined transfer of energy between numerous species. The resulting effective barotropic fluids show dynamical equations of state that are coherent with a dynamical dark energy as in the recent study [164], and that allow one to reconcile different measurements of the Hubble constant [128, 135]. Remarkably, the jungle interaction parameters  $\varepsilon$  provide a meaningful tuning for the variation of the state equation that is otherwise composed of a redshift-dependent barotropic index, which relation  $\omega(z)$  is approached by statistical means.

Furthermore, the interaction product of the density can naturally emerge from microscopic investigation of its nature. Indeed, if the gas approximation holds, i.e. we can describe them by a distribution function, then we may introduce a collision term in the Boltzmann equation and analyze the resulting perturbations. For the early Universe, this approach is already adopted, for instance to figure out electron scattering or annihilation processes [159, 153]. The jungle interaction deserves such a future investigation on its microscopic origin. Obviously, one should also consider a change of dominant interaction type for different cosmic eras.

Cosmological constraints of the  $\Lambda$ CDM standard model and new studies on dark energy as with the installation of the Dark Energy Spectroscopic Instrument (DESI) in 2019 are eventually forthcoming complementary probes of the jungle interactions and possibility of an effective dark energy.

<sup>1</sup>The Planck satellite aims at observing the cosmic microwave background (CMB).

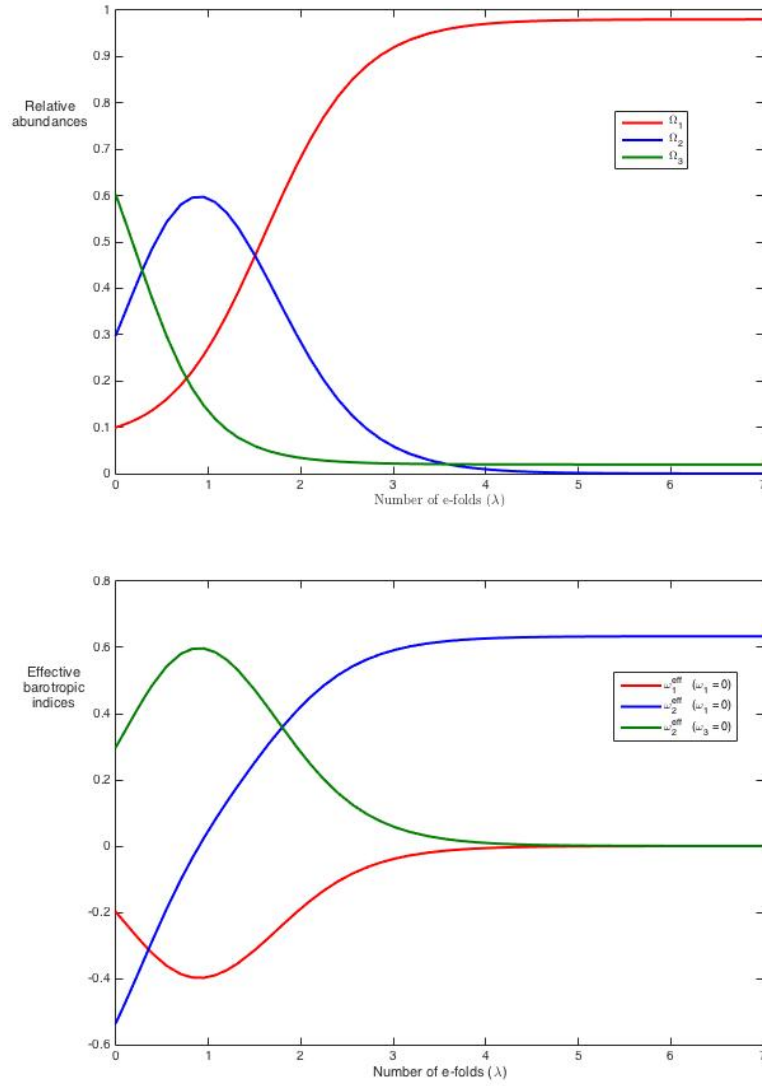


Figure 6.2: Interaction between three dark matter fluids. The evolution of their effective barotropic indices is plotted on the right panel. The left panel contains the evolution of their relative abundances. The coupling constants are such that  $\varepsilon_{12} = 2$  and  $\varepsilon_{23} = 3$ .

“ TERRA : Senti tu questo suono piacevolissimo  
che fanno i corpi celesti  
coi loro moti? ”

“ EARTH : Do you hear, you, this extremely pleasant sound  
that celestial bodies breathe  
by their moves? ”

Giacomo Leopardi, *Dialogo della Terra e della Luna*, 1827









## Conclusion and Perspectives

---

THE dynamical systems considered in the present thesis are governed by gravitation.

The notion of isochrony has arisen with the study of oscillatory motions. Half a century ago, Michel Hénon introduced an extended definition of isochrony to characterize orbital oscillations of stars around the center of the system to which they belong. In that case, the periods of oscillations can depend on the energy of the stars but not on their angular momentum.

By reasoning on the set of all isochrone potentials and on their geometric characterization as parabolas (which proof has been clarified in the complement SPD), we have revisited the set of isochrone orbits in three-dimensional spherical systems. Taking into account very general properties of potentials in physics — i.e. invariance under the addition of a constant, conservation of the energy and angular momentum for isolated radial systems — we have given a geometrical classification of the set of all isochrone orbits and potentials that we have completed. The latter contains the harmonic, Keplerian, Hénon and the new bounded potentials. The physics that occurs in those isochrone systems has been explored along with the explicit expression of orbital characteristics. These analytical results have enabled us to present an original demonstration of the Bertrand's theorem and apprehend common features of isochrones that are at the heart of the isochrone relativity.

Special relativity has been introduced to describe the laws of physics in any inertial referential. For this, special transformations mix temporal and spatial components. In the same way, one can write the isochrone laws of motion in the same way in special reference frames. For this, the new *i*-BOLST transformations generalize the Levi-Civita or Bohlin transformation by exchanging temporal and spatial (energy and potential) components and preserving the orbital differential equation for a given value of the angular momentum. The mathematical group  $\mathbb{B}$  generated by these (symmetric) transformations acts on isochrones and makes explicit their actual Keplerian nature. Kepler's third law is thus generalized to all isochrones. A dictionary summarizing the main correspondences between the isochrone and special relativities has been established. Future works could extend it and possibly use it as a base for a theory of general relativity of central potentials using non-linear transformations. Such theory could relate any orbit in a radial potential to an associated orbit in a Kepler potential.

In astrophysics, the analysis of a self-gravitating system only using its mass density distribution (or luminosity profile) is ambiguous, since several models can produce similar mass density profiles. The system which is produced just after the standard violent relaxation process is a core-halo structure compatible with both a King or an isochrone mass density. However, when kinematic data is taken into account, the King model fails where the isochrone succeeds in reproducing the equilibrium state. As a matter of fact, we have developed an isochrone analysis where the generalized third Kepler law has become a new criterion to characterize such a state of isolated self-gravitating systems.

In the executed numerical experiments, the resulting quasi-stationary state of a violent relaxation process appears to be isochrone. The isochrone model is thus an initial condition obtained after the formation process of the system. Under slow relaxation processes the system loses its isochrone character as confirmed by density profiles. As a consequence for isolated self-gravitating systems, isochrony stands as a dynamical age indicator.

The essence of isochrony is therefore Keplerian and constitutes one of the crucial problems to investigate for the understanding of dynamical systems.

The second part of the thesis is dedicated to cosmology. There, we have constructed a reflexion on an adequate model for the universe from a gravitational point of view. We have derived Einstein's equations emphasizing his historical approach as well as the key reasonings necessary to the foundations of the general theory of relativity. This has enabled us to understand the dynamical picture of the standard model of cosmology along with its restrictions. Its reformulation in terms of a dynamical system opens large perspectives for adequately relieving these restrictions, as do for example the anisotropic models of Bianchi Universes or non-gravitational couplings at cosmological scales as in the Jungle Universes. We have refined the dynamical analysis in the latter by pointing out the conservative structure of the related Lotka-Volterra systems and the possibility of effective dynamics inside the standard model of cosmology. A deeper understanding of such interactions could be favored by further modeling their microscopic physical origins.



## Bibliography

---

- [1] A. Albouy. Lectures on the two-body problem. *Classical and celestial mechanics*, (Recife, 1993/1999):63–116, 2002.
- [2] L. Amendola et al. Cosmology and fundamental physics with the Euclid satellite. *Living Reviews in Relativity*, 21:2, April 2018.
- [3] C. Antón and J. L. Brun. Isochronous oscillations: Potentials derived from a parabola by shearing. *American Journal of Physics*, 76:537, 2008.
- [4] V.A. Antonov. Most probable phase space distribution in spherical star systems and conditions for its existence. *Vestnik Leningrad Univ.*, 7:135 (in Russian, English translation in [61], 1962.
- [5] F. Arévalo, A. P. Bacalhau, and W. Zimdahl. Cosmological dynamics with nonlinear interactions. *Classical and Quantum Gravity*, 29(23):235001, December 2012.
- [6] V. I. Arnold. *Mathematical Methods of Classical Mechanics*. Springer-Verlag, New York, 1978.
- [7] V.I. Arnold. *Mathematical Methods of Classical Mechanics*. Springer-Verlag, 1989.
- [8] V.I. Arnold. Huygens & barrow, newton & hooke. *Birkhäuser Verlag, Basel*, page 95, 1990.
- [9] P. P. Avelino and H. M. R. da Silva. Effective dark energy equation of state in interacting dark energy models. *Phys. Rev. B*, 714:6–10, 2012.
- [10] J. D. Barrow and T. Clifton. Cosmologies with energy exchange. *Physical Review Letter D*, 73(10):103520, May 2006, updated July 2018.
- [11] J.D. Barrow. Sudden Future Singularities. *Class.Quant.Grav.*, 21:L79–L82, 2004.
- [12] V.A. Belinskii, L.M. Khalatnikov, and E.M. Lifschitz. Oscillatory approach to a singular point in relativistic cosmology. *Adv. Phys.*, 19:525, 1970.
- [13] J. Bertrand. Théorème relatif au mouvement d’un point attiré vers un centre fixe. *Comptes Rendus de l’Académie des Sciences de Paris*, 77:849–853, 1873.
- [14] L. Bianchi. Sugli spazi a tre dimensioni che ammettono un gruppo continuo di movimenti. *Memorie di Matematica e di Fisica della Società Italiana delle Scienze, Serie Terza*, 11:267–352, 1898.
- [15] L. Bianchi. Lezioni sulla teoria dei gruppi continui finite di trasformazioni (1902-1903). *Pisa*, pages 550–557, 1918.
- [16] J. Binney and M. Petrou. Structure of box-shaped bulges and other spheroidal components. *Mon. Not. R. Astron. Soc.*, 214:449–462, June 1985.

- [17] D. Boccaletti and G. Pucacco. *Theory of Orbits, Volume 1: Integrable Systems and Non-perturbative Methods*. Astronomy and Astrophysics Library, 1996.
- [18] D. Boccaletti and G. Pucacco. *Theory of Orbits, Volume 2: Perturbative and Geometrical Methods*. Astronomy and Astrophysics Library, 1999.
- [19] K. Bohlin. Bound central orbits. *Bull. Astron. Ser. I*, 28:113, 1911.
- [20] S. V. Bolotin and R. S. MacKay. Isochronous potentials, in “localization and energy transfer in nonlinear systems”, eds l vazquez, rs mackay, m-p zorzano. *World Sci.*, pages 217–224, 2003.
- [21] L. S. Brown. Forces giving no orbit precession. *Am. J. Phys.*, 46:930–931, 1978.
- [22] P. Bull, Y. Akrami, J. Adamek, T. Baker, E. Bellini, J. Beltrán Jiménez, E. Bentivegna, S. Camera, S. Clesse, J. H. Davis, E. Di Dio, J. Enander, A. Heavens, L. Heisenberg, B. Hu, C. Llinares, R. Maartens, E. Mörtzell, S. Nadathur, J. Noller, R. Pasechnik, M. S. Pawlowski, T. S. Pereira, M. Quartin, A. Ricciardone, S. Riemer-Sørensen, M. Rinaldi, J. Sakstein, I. D. Saltas, V. Salzano, I. Sawicki, A. R. Solomon, D. Spolyar, G. D. Starkman, D. Steer, I. Tereno, L. Verde, F. Villaescusa-Navarro, M. von Strauss, and H. A. Winther. Beyond  $\Lambda$  CDM: Problems, solutions, and the road ahead. *Physics of the Dark Universe*, 12:56–99, June 2016.
- [23] R.R. Caldwell, M. Kamionkowski, and N.N. Weinberg. Phantom energy and cosmic doomsday. *Phys. Rev. Let.*, 91:7, 2003.
- [24] J. F. Cariñena, A. M. Perelomov, and M.F. Rañada. Isochronous classical systems and quantum systems with equally spaced spectra. *Journal of Physics: Conference Series*, 87(1):012007, 2007.
- [25] S. Carroll. *An introduction to General Relativity, Spacetime and Geometry*. Pearson Addison Wesley, 2004.
- [26] J. L. Castro-Quilantan, J. L. Del Rio-Correa, and M. A. R. Medina. Alternative proof of Bertrand’s theorem using a phase space approach. *Rev. Mex. Fis.*, 42:867–877, 1996.
- [27] P.H. Chavanis. Gravitational instability of finite isothermal spheres. *A&A*, 381, 340, 2002.
- [28] P.H. Chavanis, M. Lemou, and F. Mehats. Models of dark matter halos based on statistical mechanics: I. the classical King model. *Phys. Rev. D*, 91, 063531, 2015.
- [29] Javier Chavarriga and Marco Sabatini. A survey of isochronous centers. *Qualitative Theory of Dynamical Systems*, 1(1):1, Mar 1999.
- [30] A. Chenciner. Systèmes dynamiques différentiables. *Encyclopedia Universalis*, 1985.
- [31] A. Chenciner. De la Mécanique Céleste à la théorie des Systèmes Dynamiques, aller et retour. *Actes de la conférence "Epistémologie des systèmes dynamiques"*, 1999.
- [32] S. A. Chin. A truly elementary proof of Bertrand’s theorem. *Am. J. Phys.*, 83, 2015.
- [33] T. Clifton and J. D. Barrow. Ups and downs of cyclic universes. *Phys. Rev. D*, 75(4):043515, February 2007.

- [34] G. Contopoulos, S. T. Gottesman, J. H. Hunter, Jr., and M. N. England. Comparison of stellar and gasdynamics of a barred galaxy. *Astrophysical Journal*, 343:608–616, August 1989.
- [35] J. Coste, J. Peyraud, P. Couillet, and A. Chenciner. About the Theory of Competing Species. *Theoretical Population Biology*, 14:165–184, 1978.
- [36] T. Damour, M. Henneaux, and H. Nicolai. Cosmological Billiards. *Class. Quant. Grav.*, 20:R145, 2003.
- [37] G. Darboux. *Comptes rendus hebdomadaires de l’académie des sciences*, 108:449–450, 1889.
- [38] W. J. G. de Blok, A. Bosma, and S. McGaugh. Simulating observations of dark matter dominated galaxies: towards the optimal halo profile. *Mon. Not. R. Astron. Soc.*, 340:657–678, April 2003.
- [39] W. J. G. de Blok and S. S. McGaugh. The dark and visible matter content of low surface brightness disc galaxies. *Mon. Not. R. Astron. Soc.*, 290:533–552, September 1997.
- [40] W. J. G. de Blok, S. S. McGaugh, and J. M. van der Hulst. HI observations of low surface brightness galaxies: probing low-density galaxies. *Mon. Not. R. Astron. Soc.*, 283:18–54, November 1996.
- [41] M. de La Grange. *Mécanique Analytique*. Veuve DESAINT, 2<sup>nd</sup> edition, 1815.
- [42] A. Del Popolo and M. Le Delliou. Small Scale Problems of the  $\Lambda$ CDM Model: A Short Review. *Galaxies*, 5:17, February 2017.
- [43] S. Djorgovski and I. R. King. A preliminary survey of collapsed cores in globular clusters. *ApJ*, 305, L61, 1986.
- [44] J. Dornigac. On the quantum spectrum of isochronous potentials. *Journal of Physics A Mathematical General*, 38:6183–6210, July 2005.
- [45] A. Einstein. Ist die Trägheit eines Körpers von seinem Energieinhalt abhängig? *Annalen der Physik*, 323:639–641, 1905.
- [46] A. Einstein. Zur Elektrodynamik bewegter Körper. *Annalen der Physik*, 17, N. 10:891–921, 1905.
- [47] A. Einstein. Über den Einfluß der Schwerkraft auf die Ausbreitung des Lichtes. *Annalen der Physik*, 340:898–908, 1911.
- [48] A. Einstein. Die formale Grundlage der allgemeinen Relativitätstheorie. *Gesammtsitzung v. 19. Nov. 1914 — Mitth. d. physi.-math. Cl. v. 29. Oct*, pages 1030–1085, 1914.
- [49] A. Einstein. Die Feldgleichungen der Gravitation. *Preussische Akademie der Wissenschaften, Sitzungsberichte*, pages 844–847, 1915.
- [50] A. Einstein. Die Grundlage der allgemeinen Relativitätstheorie. *Annalen der Physik*, IV. Folge. 49:769–822, 1916.
- [51] A. Einstein. HAMILTONsches Prinzip und allgemeine Relativitätstheorie. *Sitzungsberichte der Königlich Preußischen Akademie der Wissenschaften (Berlin)*, pages 1111–1116, 1916.

- [52] A. Einstein. Kosmologische Betrachtungen zur allgemeinen Relativitätstheorie. *Sitzungsberichte der Königlich Preussischen Akademie der Wissenschaften (Berlin)*, pages 142–152, 1917.
- [53] A. Einstein and M. Grossmann. Entwurf einer verallgemeinerten Relativitätstheorie und einer Theorie der Gravitation. *Leipzig, Berlin: Teubner*, 1913.
- [54] N. W. Evans, P. T. de Zeeuw, and D. Lynden-Bell. The flattened isochrone. *Mon. Not. R. Astron. Soc.*, 244:111–129, May 1990.
- [55] A. Fasano and S. Marni. *Analytic Mechanics - An Introduction*. Oxford University Press, Oxford England, 2006.
- [56] J. Féjoz and L. Kaczmarek. Sur le théorème de Bertrand (d’après Michael Herman). *Michael Herman Memorial Issue, Ergodic Theory Dyn. Sys.*, 24:5:1583–1589, 2004.
- [57] D. A. Forbes, N. Bastian, M. Gieles, R. A. Crain, J. M. D. Kruijssen, S. S. Larsen, S. Ploekinger, O. Agertz, M. Trenti, A. M. N. Ferguson, J. Pfeffer, and Gnedin O. Y. Globular cluster formation and evolution in the context of cosmological galaxy assembly: open questions. *Proc.R.Soc.A*, 474, 20170616, 2018.
- [58] P. Garg and A. Banerjee. Origin of low surface brightness galaxies: a dynamical study. *Mon. Not. R. Astron. Soc.*, 472:166–173, November 2017.
- [59] A. Goldstein et al. An ordinary short gamma-ray burst with extraordinary implications: Fermi -gbm detection of grb 170817a. *The Astrophysical Journal Letters*, 848(2):L14, 2017.
- [60] J. Goodman. An instability test for non-rotating galaxies. *Astrophysical Journal*, 329:621, 1988.
- [61] J. Goodman and P. Hut. Dynamics of star clusters. *IAU Symposium 113, Dordrecht, Reidel*, 1985.
- [62] E.ourgoulhon. *Relativité restreinte, Des particules à l’astrophysique*. CNRS Editions, 2010.
- [63] E. Goursat. Les transformations isogonales en mécanique. *Comptes rendus hebdomadaires de l’académie des sciences*, 108:446–448, 1889.
- [64] Y. Grandati, A. Bérard, and F. Ménas. Inverse problem and Bertrand’s theorem. *Am. J. Phys.*, 76:782–787, 2008.
- [65] Goldstein H. *Classical Mechanics*. Addison Wesley, New York, 1981.
- [66] C. Hamilton, J.-B. Fouvry, J. Binney, and C. Pichon. Revisiting relaxation in globular clusters. *Mon. Not. R. Astron. Soc.*, 481:2041–2061, December 2018.
- [67] S. Hawking and R. Penrose. The singularities of gravitational collapse and cosmology. *Proc. Roy. Soc. Lond.*, A314:529, 1970.
- [68] M. Hénon. L’amas isochrone, i. *Annales d’Astrophysique*, 22:126, 1959.
- [69] M. Hénon. L’amas isochrone, ii. — calcul des orbites. *Annales d’Astrophysique*, 22:491, 1959.

- [70] M. Hénon. L'amas isochrone, iii. — fonction de distribution. *Annales d'Astrophysique*, 23:474, 1960.
- [71] M. Hénon. L'évolution initiale d'un amas sphérique. *Annales d'Astrophysique*, Vol. 27, p.83, 1964.
- [72] J. Heyvaerts, J.-B. Fouvry, P.-H. Chavanis, and C. Pichon. Dressed diffusion and friction coefficients in inhomogeneous multicomponent self-gravitating systems. *MNRAS*, 469, 4193, 2017.
- [73] D. Hilbert. Die Grundlagen der Physik. *Gott.Nachr.*, 27:395–407, 1915.
- [74] M.P. Hobson et al. *General relativity: an introduction for physicists*. Cambridge University Press, 2006.
- [75] J. Hofbauer and K. Sigmund. *Evolutionary Games and Population Dynamics*. Cambridge University Press, 1998.
- [76] E. Hubble. A Relation between Distance and Radial Velocity among Extra-Galactic Nebulae. *Proceedings of the National Academy of Science*, 15:168–173, March 1929.
- [77] Binney J. Hénon's isochrone model. “*Une vie dédiée aux systèmes dynamiques*” ed. J.-M. Alimi, R. Mohayaee & J. Perez, Hermann, pages 99–109, 2016.
- [78] Binney J. and Tremaine S. *Galactic Dynamics 2<sup>nd</sup> edition*. Princeton University Press, 2<sup>nd</sup> edition, 2008.
- [79] V. Jovanović. A note on the proof of Bertrand's theorem. *Theoretical and Applied Mathematics*, 42, Issue 1:22–33, 2015.
- [80] M. Joyce, B. Marcos, and F. Sylos Labini. Energy ejection in the collapse of a cold spherical self-gravitating clouds. *MNRAS*, 397, 775, 2009.
- [81] A. J. Kalnajs. Dynamics of Flat Galaxies. III. Equilibrium Models. *Astrophysical Journal*, 205:751–761, May 1976.
- [82] J. Katz. On the number of unstable modes of an equilibrium. *MNRAS*, 183, 765, 1978.
- [83] J. Kepler. *Harmonices Mundi*. 1619.
- [84] I. R. King. The structure of star clusters. III. some simple dynamical models. *AJ*, 71, 64, 1966.
- [85] C. Kopper. *Principes variationnels et Mécanique analytique*. Ecole Polytechnique, 2013.
- [86] R. Kuzio de Naray, S. S. McGaugh, and W. J. G. de Blok. Mass Models for Low Surface Brightness Galaxies with High-Resolution Optical Velocity Fields. *Astrophysical Journal*, 676:920–943, April 2008.
- [87] G.G. Kuzmin and Ü.-I.K. Veltmann. Generalized isochrone models for spherical stellar systems. *Symposium - International Astronomical Union*, 153:363–366, 1993.
- [88] J.-L. Lagrange. *Solution de différents problèmes de calcul intégral, Œuvres complètes, Vol. I, p.573*. Springer-Verlag, New York, 1978.
- [89] L. Landau and E. Lifschitz. *Mécanique*. Éditions Mir, 1970.



- [90] L. Landau and E. Lifshitz. *Mechanics, 2nd ed.* Pergamon Press, NewYork, 1969.
- [91] D. Langlois. *Géométrie et gravitation*. Ecole Polytechnique, 2015.
- [92] M. Laue. Zur Dynamik der Relativitätstheorie. *Annalen der Physik*, 35:524, 1911.
- [93] R. Lehoucq. *La SF sous les feux de la science*. Editions Le Pommier, 2012.
- [94] T. Levi-Civita. Sur la résolution qualitative du problème restreint des trois corps. *Acta Math*, 30:54, 1906.
- [95] A.J. Lotka. Contribution to the theory of periodic reaction. *J. Phys. Chem*, 14 (3):271–274, 1910.
- [96] D. Lynden-Bell. Statistical mechanics of violent relaxation in stellar systems. *Mon. Not. R. Astron. Soc.*, 136:101, 1967.
- [97] D. Lynden-Bell. On a mechanism that structures galaxies. *Mon. Not. R. Astron. Soc.*, 187:101–107, April 1979.
- [98] D. Lynden-Bell. Bound central orbits. *Mon. Not. R. Astron. Soc.*, 447 (2):1962–1972, 2015.
- [99] D. Lynden-Bell and S. Jin. Analytic central orbits and their transformation group. *Mon. Not. R. Astron. Soc.*, 386:245–260, 2008.
- [100] D. Lynden-Bell and R. Wood. The gravo-thermal catastrophe in isothermal spheres and the onset of red-giant structure for stellar systems. *MNRAS*, 138, 495, 1968.
- [101] A. D. Mackey and G. F. Gilmore. Surface brightness profiles and structural parameters for 53 rich stellar clusters in the large magellanic cloud. *MNRAS*, 338, 85, 2003.
- [102] C. MacLaurin. *A treatise on fluxions*. London: W. Baynes, 1801.
- [103] M. Maggiore. *Gravitational Waves, Vol1: Theory and Experiments*. Oxford University Press, 2007.
- [104] G. Mangano, G. Miele, and V. Pettorino. Coupled Quintessence and the Coincidence Problem. *Modern Physics Letters A*, 18:831–842, 2003.
- [105] L. Maréchal and J. Perez. Radial orbit instability: review and perspectives. *Transp. Theor. & Stat. Phys.*, 40, 425, 2012.
- [106] S. S. McGaugh and G. D. Bothun. Structural characteristics and stellar composition of low surface brightness disk galaxies. *Astrophysical Journal*, 107:530–542, February 1994.
- [107] C. McGill and J. Binney. Torus construction in general gravitational potentials. *Mon. Not. R. Astron. Soc.*, 244:634–645, June 1990.
- [108] H. Minkowski. Die Grundgleichungen für die elektromagnetischen Vorgänge in bewegten Körpern. *Nachrichten von der Gesellschaft der Wissenschaften zu Göttingen, Mathematisch-Physikalische Klasse 1908*, pages 53–111, 1907.
- [109] H. Minkowski. Espace et temps. *Annales scientifiques de l'Ecole Normale Supérieure*, 3<sup>e</sup> série, 26:499–517, 1909.
- [110] H. Minkowski. Das Relativitätsprinzip. *Conference given on November 5, 1907 for the Göttinger Mathematischen Gesellschaft; printed in Annalen der Physik*, 47:927, 1915.

- [111] C.W. Misner. Mixmaster Universe. *Phys. Rev. Let.*, 22:1071, 1969.
- [112] C. Mouhot and C. Villani. On Landau damping. *Acta Mathematica*, 207:29–201, 2011.
- [113] W.A. Mulder. Dynamical friction on extended objects . *Astronomy and Astrophysics*, 117:9–16, 1983.
- [114] J.D. Murray. *Mathematical Biology I: An Introduction, 3rd Edition*. Springer, Berlin, 2002.
- [115] J. F. Navarro, C. S. Frenk, and S. D. M. White. The Structure of Cold Dark Matter Halos. *The Astrophysical Journal*, 462:563, May 1996.
- [116] J. F. Navarro, C. S. Frenk, and S. D. M. White. A Universal Density Profile from Hierarchical Clustering. *The Astrophysical Journal*, 490:493–508, December 1997.
- [117] I. Newton. *Philosophiae naturalis principia mathematica*. London, 1756.
- [118] J.T. Nielse, A. Guffanti, and S. Sarkar. Marginal evidence for cosmic acceleration from Type Ia supernovae. *Scientific reports*, 6:35596, 2016.
- [119] E. T. Osypowski and M. G. Olsson. Isynchronous motion in classical mechanics. *Am. J. Phys*, 55 (8):720, 1987.
- [120] T. Padmanabhan. Statistical mechanics of gravitating systems. *Phys. Rep.*, 188, 285, 1990.
- [121] P.L. Palmer and J. Papaloizou. Instability in spherical stellar systems. *Mon. Not. R. Astron. Soc.*, 238:1281, 1989.
- [122] J. Perez. *Essai de Gravitation, des Univers homogènes à la dynamique des systèmes autogravitants*. HDR, ENSTA ParisTech, 2007.
- [123] J. Perez. *Théorie des champs*. Les Presses de l’ENSTA, 2017.
- [124] J. Perez, A. Füzfa, T. Carletti, L. Mélot, and L. Guedezounme. The Jungle Universe: coupled cosmological models in a Lotka-Volterra framework. *Gen. Relativ. Gravit.*, 46:1753, 2014.
- [125] J. Perez, A. Simon-Petit, J. Leys, and B. Rimboux. Expansion, la cyber-mooc conférence, <https://uma.ensta-paristech.fr/conf/expansion/index.php>, 2016.
- [126] S. Perlmutter et al. Measurements of Omega and Lambda from 42 High-Redshift Supernovae. *The Astrophysical Journal*, 517:565–586, 1999.
- [127] P. Peter and J.-P. Uzan. *Cosmologie primordiale*. Editions Belin, 2012.
- [128] Planck Collaboration. Planck 2015 results. XIII. Cosmological parameters. *Astronomy and Astrophysics*, 594:A13, 2016.
- [129] Planck Collaboration. Planck 2018 results. I. Overview and the cosmological legacy of Planck. *arXiv:1807.06205*, 2018.
- [130] Planck Collaboration. Planck 2018 results. VI. Cosmological parameters. *arXiv:1807.06209*, 2018.
- [131] G. Plum. *Dynamique d’une sphère autogravitante isotherme et tronquée*. PhD thesis, École Doctorale Astronomie et Astrophysique d’Île-de-France, 2014.

- [132] R. P. Rartinez-y Romero, H. N. Nunez-Yepez, and A. L. Salas-Brito. Closed orbits and constants of motion in classical mechanics. *Eur. J. Phys.*, 13:26–31, 1992.
- [133] V. P. Reshetnikov, S. S. Savchenko, A. V. Moiseev, and O. V. Egorov. SDSS J170745+302056: A low-surface-brightness galaxy in a group. *Astronomy Letters*, 43:812–819, December 2017.
- [134] A. G. Riess et al. Observational Evidence from Supernovae for an Accelerating Universe and a Cosmological Constant. *The Astrophysical Journal*, 116:1009–1038, 1998.
- [135] A. G. Riess et al. A 2,4% determination of the local value of the Hubble constant. *The Astrophysical Journal*, 826:56, 2016.
- [136] A.G. Riess et al. New Parallaxes of Galactic Cepheids from Spatially Scanning the Hubble Space Telescope: Implications for the Hubble Constant. *The Astrophysical Journal*, 855:136, 2018.
- [137] H. Ringström. The Bianchi IX attractor. *Ann. Inst. H. Poincaré*, 2:405, 2001.
- [138] H. Ringström. *On the Topology and Future Stability of th Universe*. Oxford Mathematical Monographs, 2013.
- [139] F. Roy and J. Perez. Dissipationless collapse of a set of N massive particles. *MNRAS*, 348, 62, 2004.
- [140] P. Saha. Unstable modes of a spherical stellar system. *Mon. Not. R. Astron. Soc.*, 248:494–502, February 1991.
- [141] F. Santos, V. Soares, and A. Tort. Determination of the Apsidal Angle and Bertrand’s theorem. *Phys. Rev. E*, 79, 036605-1–6, 2009.
- [142] L. F. Shampine and M. W. Reichelt. The MATLAB ODE Suite. *SIAM Journal on Scientific Computing*, 18:1–22, 1997.
- [143] L. F. Shampine, M. W. Reichelt, and J.A. Kierzenka. Solving Index-1 DAEs in MATLAB and Simulink. *SIAM Review*, 41:538–552, 1999.
- [144] A. Simon-Petit, J. Perez, and G. Duval. Isochrony in 3D radial potentials. *Communications in Mathematical Physics*, 363(2):605–653, 2018.
- [145] A. Simon-Petit, H.-H. Yap, and J. Perez. Refinements in the Jungle Universes. In *28th Texas Symposium on Relativistic Astrophysics (Geneva)*, 2016.
- [146] V. Springel. The cosmological simulation code gadget-2. *MNRAS*, 364,1105, 2005.
- [147] F. H. Stillinger and D. K. Stillinger. Pseudoharmonic Oscillators and Inadequacy of Semiclassical Quantization. *J. Phys. Chem*, 93:6890–6892, 1989.
- [148] J. Szeftel. *Introduction à la relativité générale d’un point de vue mathématique*. Ecole Polytechnique, 2015.
- [149] P. Terra, R. de Melo e Souza, and C. Farina. Is the tautochrone curve unique? *American Association of Physics Teachers*, 84:917, 2006.
- [150] S. Terracini, G. Verzini, and A. Zilio. Spiraling asymptotic profiles of competition-diffusion systems. *ArXiv e-prints*, July 2017.

- [151] Y. Tikochinsky. A simplified proof of Bertrand's theorem. *Am. J. Phys.*, 56:1073–1075, 1988.
- [152] P. Touboul et al. MICROSCOPE Mission: First Results of a Space Test of the Equivalence Principle. *Physical Review Letters*, 119(23):231101, December 2017.
- [153] J.-P. Uzan. Dynamics of Relativistic Interacting Gases : from a Kinetic to a Fluid Description. *Class.Quant.Grav.*, 15:1063–1088, 1998.
- [154] J.-P. Uzan and R. Lehoucq. A dynamical study of the Friedmann equations. *European Journal of Physics*, 22:371–384, July 2001.
- [155] J. M. van der Hulst, E. D. Skillman, T. R. Smith, G. D. Bothun, S. S. McGaugh, and W. J. G. de Blok. Star formation thresholds in Low Surface Brightness galaxies. *Astrophysical Journal*, 106:548–559, August 1993.
- [156] P.O. Vandervoort. On lagrangian methods for the study of small perturbations in stellar systems. *Astrophysical Journal*, 341:105, 1989.
- [157] V. Volterra. Variazioni e fluttuazioni del numero d'individui in specie animali conviventi. *Mem. Acad. Lincei Roma*, 2):31–113, 1926.
- [158] J. Wainwright and G. F. R. Ellis (Editors). *Dynamical Systems in Cosmology*. Cambridge University Press, 2005.
- [159] S. Weinberg. *Gravitation and Cosmology*. Ed. John Wiley and Sons, 1972.
- [160] D. L. Wiltshire. What is dust? — Physical foundations of the averaging problem in cosmology. *Classical and Quantum Gravity*, 28(16):164006, August 2011.
- [161] D. L. Wiltshire. Cosmic structure, averaging and dark energy. *ArXiv e-prints*, November 2013.
- [162] W. Yang, S. Pan, and J. D. Barrow. Large-scale stability and astronomical constraints for coupled dark-energy models. *Phys. Rev. D*, 97(4):043529, February 2018.
- [163] Y. Zarmi. The Bertrand theorem revisited. *Am. J. Phys.*, 70:446–449, 2002.
- [164] G.-B. Zhao et al. Dynamical dark energy in light of the latest observations. *Nature Astronomy*, 1 (9):627, 2017.
- [165] W. Zimdahl. Models of interacting dark energy. In J. Alcaniz, S. Carneiro, L. P. Chimento, S. Del Campo, J. C. Fabris, J. A. S. Lima, and W. Zimdahl, editors, *American Institute of Physics Conference Series*, volume 1471 of *American Institute of Physics Conference Series*, pages 51–56, October 2012.
- [166] W. Zimdahl. Interactions in the dark sector of the Universe. *ArXiv e-prints*, April 2014.
- [167] A. Zocchi, G. Bertin, and A. L. Varri. A dynamical study of galactic globular clusters under different relaxation conditions. *A&A*, 539, A65, 2012.





## Annexe

---

### Basics for differential geometry

We remind here some fundamentals of differential geometry. A more detailed approach can be found in [148] for a french mathematical introduction, [91] for its application to general relativity, [25] for their english equivalent, and [50] for their historical summary and meaning in the general theory of relativity.

#### Notations

Greek indices  $\mu, \nu, \dots$  refer to either temporal 0 or spatial 1, 2, 3 indices. Latin indices  $i, j, \dots$  are only for spatial components. Then, in the preceding coordinate system,  $x^0 = ct$  and  $x^i$  can refer to  $x^1 = x$ ,  $x^2 = y$ , or  $x^3 = z$ .

In addition, we adopt Einstein's convention for summation: repeating an index in a single expression is equivalent to summing the expression with itself, spanning all possible values of the index. For instance,  $A^\mu B_\mu = A^0 B_0 + A^1 B_1 + A^2 B_2 + A^3 B_3$ .

#### Tensors

Let  $E$  be a vector space, of dimension  $n$ . Its dual vector space  $E^*$  is composed of the linear forms acting on  $E$ ,

$$\Lambda : E \rightarrow \mathbb{R}, \quad \mathbf{u} \mapsto \lambda(\mathbf{u}), \quad (\text{A.43})$$

called covectors. A tensor is a multilinear form defined on the product  $E \times \dots \times E \times E^* \times \dots \times E^*$  by

$$\mathbf{T} : \begin{matrix} E \times \dots \times E \times E^* \times \dots \times E^* \\ (u_1, \dots, u_p, \lambda_1, \dots, \lambda_q) \end{matrix} \rightarrow \mathbb{R}, \quad \mapsto \mathbf{T}(u_A, \dots, u_p, \lambda_1, \dots, \lambda_q). \quad (\text{A.44})$$

Here the transformation is called a  $p$ -covariant and  $q$ -contravariant tensor. The sum  $p + q$  is called the order of the tensor. For instance, a vector, or a linear form on  $E^*$ , is a contravariant tensor of order 1. A covector of  $E^*$ , seen as linear form on  $E$ , is a covariant tensor of order 1. A bilinear form on  $E$ , such as the scalar product  $\mathbf{g}$ , is a covariant tensor of order 2.

When a basis  $\{\mathbf{e}_\mu\}$  of  $E$  is chosen, we write its components on the basis and its dual as

$$T_{\mu_1 \dots \mu_p}^{\nu_1 \dots \nu_q} = \mathbf{T}(\mathbf{e}_{\mu_1}, \dots, \mathbf{e}_{\mu_p}, \mathbf{e}_*^{\nu_1}, \dots, \mathbf{e}_*^{\nu_q}). \quad (\text{A.45})$$

Its decomposition on the basis can be written as

$$\mathbf{T} = T_{\mu_1 \dots \mu_p}^{\nu_1 \dots \nu_q} \mathbf{e}_{\mu_1} \otimes \dots \otimes \mathbf{e}_{\mu_p} \otimes \mathbf{e}_*^{\nu_1} \otimes \dots \otimes \mathbf{e}_*^{\nu_q}. \quad (\text{A.46})$$

When the basis  $\{\mathbf{e}_\mu\}$  is changed into  $\{\mathbf{e}'_\mu\}$ , then the components of the tensor are transformed by

$$T'_{\mu_1 \dots \mu_p}^{\nu_1 \dots \nu_q} = \frac{\partial x^{\rho_1}}{\partial x'^{\mu_1}} \dots \frac{\partial x^{\rho_p}}{\partial x'^{\mu_p}} \frac{\partial x'^{\nu_1}}{\partial x^{\sigma_1}} \dots \frac{\partial x'^{\nu_q}}{\partial x^{\sigma_q}} T_{\rho_1 \dots \rho_p}^{\sigma_1 \dots \sigma_q}. \quad (\text{A.47})$$

## Metrics

The metrics is a tensor of order two, that characterizes the geometry of a curved space by defining a scalar product on it. Omitting the direct product, in a coordinate system  $\{x^\mu\}$ , the metrics is generally noted by

$$\mathbf{g} = g_{\mu\nu} dx^\mu dx^\nu \quad (\text{A.48})$$

Einstein's historical choice of signature for metrics is  $(+, -, -, -)$ , when the first coordinate is temporal and the three latter are spatial in a coordinate system given by

$$x^\mu = (ct, x, y, z)^\top. \quad (\text{A.49})$$

## Covariant derivative

The derivative of a function  $f$  along a direction given by a vector  $\mathbf{v}$  defines a covector  $\mathbf{df}$ . In  $\mathbb{R}^n$ , if  $\mathbf{v} = \mathbf{e}_{\mu_i}$ , the component of the differential  $\mathbf{df}$  are

$$\partial_{\mu_i} = \frac{\partial f}{\partial x^{\mu_i}}. \quad (\text{A.50})$$

In  $\mathbb{R}^n$ , this definition is invariant under coordinate changes. However, the differentiation for tensors in a curved space cannot be so simply defined, since expression (A.50) does not hold when changing the coordinate systems. In fact, using the transformation law (A.47), one gets

$$\frac{\partial v'^\mu}{\partial x'^\nu} = \frac{\partial x^\kappa}{\partial x'^\nu} \frac{\partial}{\partial x^\kappa} \left( \frac{\partial x'^\nu}{\partial x^\lambda} v^\lambda \right) = \frac{\partial x^\kappa}{\partial x'^\nu} \frac{\partial x'^\nu}{\partial x^\lambda} \frac{\partial v^\lambda}{\partial x^\kappa} + \frac{\partial x^\kappa}{\partial x'^\nu} \frac{\partial^2 x'^\mu}{\partial x^\kappa \partial x^\lambda} v^\lambda \quad (\text{A.51})$$

So that the components  $\frac{\partial v'^\mu}{\partial x'^\nu}$  and  $\frac{\partial v^\mu}{\partial x^\nu}$  cannot describe the same tensor since they do not verify (A.47), unless the coordinates are linear as the cartesian coordinates in a Euclidean space, which cancels the second term in the right term of (A.51).

We thus define a *covariant derivative* such that we can decompose any tensor  $\mathbf{T}$  along a vector  $\mathbf{v}$  as

$$\mathbf{T} = \nabla \mathbf{v} = \nabla (v^\kappa \mathbf{e}_\kappa) = \nabla (v^\kappa) \otimes \mathbf{e}_\kappa + v^\kappa \nabla \mathbf{e}_\kappa. \quad (\text{A.52})$$

It must satisfy two constraints: first, it must coincides with the usual differentiation  $\partial$  on functions  $\nabla f = \partial_\mu f \mathbf{e}_*^\mu$ , which gives in particular the differentiation of vectors as

$$\nabla v^\nu = \partial_\mu v^\nu \mathbf{e}_*^\mu, \quad (\text{A.53})$$

second, for each  $\kappa$ ,  $\nabla \mathbf{e}_\kappa$  must be a 1-covariant 1-contravariant tensor which can be decomposed as

$$\nabla \mathbf{e}_\kappa = \Gamma_{\mu\nu}^\kappa \mathbf{e}_*^\mu \otimes \mathbf{e}_\nu. \quad (\text{A.54})$$

The coefficients  $\Gamma_{\mu\nu}^\sigma$  are called *Christoffel symbols*, but are not the components of a tensor. Then, the components of the tensor  $\mathbf{T}$  are given by

$$\mathbf{T} = (\partial_\mu v^\nu + \Gamma_{\mu\kappa}^\nu v^\kappa) \mathbf{e}_*^\mu \otimes \mathbf{e}_\nu, \quad (\text{A.55})$$

so that, if  $\mathbf{T} = \nabla \mathbf{v}$ , then

$$T_\mu^\nu = \nabla_\mu v^\nu = \partial_\mu v^\nu + \Gamma_{\mu\kappa}^\nu v^\kappa. \quad (\text{A.56})$$

More generally, the covariant derivative of a tensor has components given by

$$\nabla_\lambda T_{\nu_1 \dots \nu_q}^{\mu_1 \dots \mu_p} = \partial_\lambda T_{\nu_1 \dots \nu_q}^{\mu_1 \dots \mu_p} + \sum_{\alpha} \Gamma_{\lambda\sigma}^{\mu_\alpha} T_{\nu_1 \dots \nu_q}^{\mu_1 \dots \sigma \dots \mu_p} - \sum_{\alpha} \Gamma_{\lambda\nu_\alpha}^\sigma T_{\nu_1 \dots \sigma \dots \nu_q}^{\mu_1 \dots \mu_p}. \quad (\text{A.57})$$

The same space actually admits several covariant derivatives. In the general theory of relativity, we are interested in the Levi-Civita covariant derivative, uniquely defined by the two conditions:

- Christoffel symbols must verify  $\Gamma_{\mu\nu}^{\kappa} = \Gamma_{\nu\mu}^{\kappa}$ ,
- the derivative does not introduce any torsion when moving in the curved space along its geometry, in other words  $\nabla \mathbf{g} = 0$ .

This defines the Christoffel symbols with the first derivatives of the metrics:

$$\Gamma_{\mu\nu}^{\sigma} = \frac{1}{2} g^{\sigma\rho} (\partial_{\mu} g_{\nu\rho} + \partial_{\nu} g_{\rho\mu} - \partial_{\rho} g_{\mu\nu}). \quad (\text{A.58})$$

## Geodesics

In a Euclidean space, the shorter path between two points draws a segment. Straight lines are the geodesics of flat spaces, i.e. they minimize (or maximize) the length of a trajectory linking the two points. In a four-dimensional spacetime, the length of a time-like trajectory is given by

$$S = \int_{\lambda_0}^{\lambda_1} d\lambda \sqrt{g_{\mu\nu} \frac{dx^{\mu}}{d\lambda} \frac{dx^{\nu}}{d\lambda}}, \quad (\text{A.59})$$

where  $S$  can be considered as the action associated to the lagrangian

$$L \left[ x^{\mu}, \frac{dx^{\mu}}{d\lambda} \right] = \sqrt{g_{\mu\nu} \frac{dx^{\mu}}{d\lambda} \frac{dx^{\nu}}{d\lambda}}. \quad (\text{A.60})$$

The metrics is arbitrary, and the results are valid in special as well as general relativity.

A *geodesic* is a trajectory of extremal length between two points of spacetime. It thus satisfies Euler-Lagrange equations

$$\frac{d}{dt} \left( \frac{\partial L}{\partial \dot{x}^{\mu}} \right) = \frac{\partial L}{\partial x^{\mu}}, \quad \dot{x}^{\mu} \equiv \frac{dx^{\mu}}{d\lambda}. \quad (\text{A.61})$$

The differentiation of these equations leads to the *geodesics equation*

$$\frac{d^2 x^{\kappa}}{d\tau^2} + \Gamma_{\mu\nu}^{\kappa} \frac{dx^{\mu}}{d\tau} \frac{dx^{\nu}}{d\tau} = 0, \quad (\text{A.62})$$

where

$$\Gamma_{\mu\nu}^{\sigma} = \frac{1}{2} g^{\sigma\rho} (\partial_{\mu} g_{\nu\rho} + \partial_{\nu} g_{\rho\mu} - \partial_{\rho} g_{\mu\nu}) \quad (\text{A.63})$$

are the *Christoffel symbols* defined with first derivatives of the metrics. The terms in the left side of (A.62) are the components of the 4-vector acceleration

$$a^{\kappa} = u^{\mu} \nabla_{\mu} u^{\kappa} = \frac{d^2 x^{\kappa}}{d\tau^2} + \Gamma_{\mu\nu}^{\kappa} \frac{dx^{\mu}}{d\tau} \frac{dx^{\nu}}{d\tau}, \quad (\text{A.64})$$

written in any geometry and coordinate system, and where  $u^{\mu} = \frac{dx^{\mu}}{d\tau}$  is the associated 4-velocity and  $\tau$  the proper time of the considered particle.

A time-like geodesic is thus characterized by a vanishing 4-acceleration. Then, the motion of a free particle in a spacetime of any geometry corresponds to a geodesic.



### Equation of motion in a curved spacetime

The general equation of motion of a particle can also be derived from the least action principle with the lagrangian

$$L \left[ x^\mu, \frac{dx^\mu}{d\lambda} \right] = g_{\mu\nu} \frac{dx^\mu}{d\lambda} \frac{dx^\nu}{d\lambda} - V(x^\mu) \quad (\text{A.65})$$

which gives

$$\frac{d^2 x^\kappa}{d\tau^2} + \Gamma_{\mu\nu}^\kappa \frac{dx^\mu}{d\tau} \frac{dx^\nu}{d\tau} = \frac{1}{m} \partial^\kappa g_{00}. \quad (\text{A.66})$$

### Riemann tensor

The *Riemann tensor* locally describes the curvature of a differential manifold by quantifying the parallel transport of vectors along infinitesimal closed loops. This operation is evaluated by the Lie bracket of two covariant derivatives, the reader can find the construction in [25]. In fact, torsion and curvature tensors enable us to quantify the deviation introduced by the non-commutativity of covariant derivatives. Riemann tensor is defined by

$$R(u, v)w = \nabla_u \nabla_v w - \nabla_v \nabla_u w - \nabla_{[u, v]} w \quad (\text{A.67})$$

for all vector fields  $u$ ,  $v$ , and  $w$ , where  $[\cdot, \cdot]$  is the Lie bracket. In a given coordinate system, its components are given by

$$\nabla_\nu \nabla_\mu v_\sigma - \nabla_\mu \nabla_\nu v_\sigma = R_{\sigma\mu\nu}^\rho v_\rho \quad (\text{A.68})$$

so that

$$R_{\sigma\mu\nu}^\rho = \partial_\mu \Gamma_{\sigma\nu}^\rho - \partial_\nu \Gamma_{\sigma\mu}^\rho + \Gamma_{\lambda\mu}^\rho \Gamma_{\sigma\nu}^\lambda - \Gamma_{\lambda\nu}^\rho \Gamma_{\sigma\mu}^\lambda \quad (\text{A.69})$$

where the *Christoffel symbols* satisfy (A.58). We can then define the symmetric *Ricci tensor*, which is a contraction of Riemann's one

$$R_{\mu\nu} = -R_{\mu\lambda\nu}^\lambda \quad (\text{A.70})$$

and the *scalar* or *Ricci curvature* as follows

$$R = R_\mu^\mu = g^{\mu\nu} R_{\mu\nu}. \quad (\text{A.71})$$

It is used to describe the dynamics from Einstein's equations.

Riemann tensor has the following properties:

- antisymmetry on the first two indices,

$$R_{\sigma\mu\nu}^\rho = -R_{\mu\sigma\nu}^\rho \quad (\text{A.72})$$

- antisymmetry on the last two indices,

$$R_{\sigma\mu\nu\rho} = -R_{\sigma\mu\rho\nu}; \quad (\text{A.73})$$

- first Bianchi identity,

$$R_{[\sigma\mu\nu]}^\rho = 0; \quad (\text{A.74})$$

- second Bianchi identity,

$$\nabla_{[\lambda} R_{\sigma\mu]\nu}^\rho = 0. \quad (\text{A.75})$$

Here above, we have used brackets to define the antisymmetry on indices. A bracket acts on two indices as

$$F_{[\mu\nu]} = \frac{1}{2} (F_{\mu\nu} - F_{\nu\mu}), \quad (\text{A.76})$$

on three indices as

$$T_{[\mu\nu\rho]} = \frac{1}{3!} (T_{\mu\nu\rho} - T_{\nu\mu\rho} + T_{\nu\rho\mu} - T_{\rho\nu\mu} + T_{\rho\mu\nu} - T_{\mu\rho\nu}), \quad (\text{A.77})$$

and can be generalized to any number of indices.

In a three-dimensional space, the antisymmetric curvature tensor generally possesses 6 independent components, which depend on the coordinates and which are required to describe the geometrical properties of space. They are additionally constrained by the symmetries imposed by the cosmological principle, i.e. homogeneity and spatial isotropy at very large scales. First, time and space can be decorrelated when considering a synchronous frame in which the metrics is a block diagonal matrix. Second, the spatial part of Riemann tensor satisfies the relation

$${}^{(3)}R_{ijkl} = 2K\gamma_{i[k}\gamma_{l]j} = 2K(\gamma_{ik}\gamma_{jl} - \gamma_{il}\gamma_{jk}) \quad (\text{A.78})$$

in a *maximally symmetric* space. Spatial sections of such a spacetime have constant curvature  ${}^{(3)}R = -6K$ , where  $K$  gives its sign. This is used in Section 5.2.1 page 90.

## Geodesics, gravitation and curvature

Consider two geodesics of spacetime starting at two neighbor points. The first geodesic is given by  $\{x^\mu(\cdot)\}$  coordinates and the second one by  $\{y^\mu(\cdot)\}$ , both satisfy the geodesics equation (A.62) with  $y^\mu(\tau) = x^\mu(\tau) + \delta x^\mu(\tau)$ . In fact, we have

$$\frac{d^2 x^\kappa}{d\tau^2} + \Gamma_{\mu\nu}^\kappa(x^\kappa) \frac{dx^\mu}{d\tau} \frac{dx^\nu}{d\tau} = 0, \quad (\text{A.79})$$

and

$$\frac{d^2 y^\kappa}{d\tau^2} + \Gamma_{\mu\nu}^\kappa(y^\kappa) \frac{dy^\mu}{d\tau} \frac{dy^\nu}{d\tau} = 0. \quad (\text{A.80})$$

The difference of (A.79) and (A.80) at first order gives

$$\frac{d^2(\delta x^\kappa)}{d\tau^2} + (\delta_\rho \Gamma_{\mu\nu}^\kappa) \delta x^\rho \frac{dx^\mu}{d\tau} \frac{dx^\nu}{d\tau} + 2\Gamma_{\mu\nu}^\kappa \frac{d(\delta x^\mu)}{d\tau} \frac{dx^\nu}{d\tau} = 0. \quad (\text{A.81})$$

Using the covariant derivative along the first trajectory parametrized by  $\tau$ , equation (A.81) can be written as

$$\nabla^2(\delta x^\kappa) = -R_{\nu\rho\mu}^\kappa \delta x^\rho \frac{dx^\mu}{d\tau} \frac{dx^\nu}{d\tau}, \quad (\text{A.82})$$

where  $R_{\nu\rho\mu}^\kappa$  are the components of Riemann tensor, defined in (A.69). They contain information on the spacetime curvature.

According to the geodesics equation (A.62), we remark that a particle moving on the first geodesic is either at rest or has 4-velocity such that  $\nabla u^\mu = 0$ . By comparing with equation (A.82), the curvature tensor appears as a force that constraints the particle to stay on the geodesic, by recalling the particle if it deviates from the geodesic. In other words,

- geodesics appear as the natural trajectories of free falling bodies, see the solution of the least action principle from (A.59) and (A.62) or the above comparison from (A.82),

- if the presence of matter or gravitational force curves spacetime, then it curves geodesics, see (A.62),
- reciprocally, the curvature of spacetime acts as a force that bends geodesics, see (A.82).

This sets the equivalence between spacetime curvature and gravitational field.

## Weighted least squares

Let us remind here the essential formulae for a weighted linear regression.

The linear fit of a given sequence  $\{x_i; y_i \pm \sigma_i\}_{i=1, \dots, n}$ , we have to compute values for  $c$  and  $s$  which minimize the quantity

$$d^2 = \sum_{i=1}^n [y_i - (c + sx_i)]^2. \quad (\text{A.83})$$

The uncertainty on  $y_i$ , namely  $\sigma_i$ , allows us to define the weight  $w_i = \sigma_i^{-2}$  of the  $i$ -th value of  $y$ . The  $d^2$ -minimization problem gives

$$c = \frac{1}{\Delta} \left( \sum_{i=1}^n w_i x_i^2 \right) \left( \sum_{i=1}^n w_i y_i \right) - \frac{1}{\Delta} \left( \sum_{i=1}^n w_i x_i \right) \left( \sum_{i=1}^n w_i x_i y_i \right) \quad (\text{A.84})$$

and

$$s = \frac{1}{\Delta} \left( \sum_{i=1}^n w_i \right) \left( \sum_{i=1}^n w_i x_i y_i \right) - \frac{1}{\Delta} \left( \sum_{i=1}^n w_i x_i \right) \left( \sum_{i=1}^n w_i y_i \right) \quad (\text{A.85})$$

where

$$\Delta = \left( \sum_{i=1}^n w_i \right) \left( \sum_{i=1}^n w_i x_i^2 \right) - \left( \sum_{i=1}^n w_i x_i \right)^2. \quad (\text{A.86})$$

The uncertainty on  $c$  and  $s$  are given by

$$\sigma_c = \sqrt{\frac{1}{\Delta} \sum_{i=1}^n w_i x_i^2} \text{ and } \sigma_s = \sqrt{\frac{1}{\Delta} \sum_{i=1}^n w_i}. \quad (\text{A.87})$$

These relations are used in chapter 4 for the isochrone analysis.



## Résumé en français

---

La gravitation, classique et relativiste, est présente à toutes les échelles cosmologiques. A l'échelle des systèmes planétaires comme à celle de l'univers dans son ensemble, elle est à l'origine de systèmes dynamiques riches tant du point de vue physique que du point de vue mathématique. La présente thèse de doctorat a pour objet la modélisation et l'analyse de systèmes dynamiques gouvernés par la gravitation.

La notion d'isochronie caractérise des mouvements oscillatoires dès le XVII<sup>ème</sup> siècle, lorsque Galilée observe les oscillations de lustres puis de pendules dans le champ localement uniforme de la Terre. Pour de petites amplitudes d'oscillations, le temps requis pour effectuer une oscillation est identique quelqu'en soit l'amplitude. A la même époque, Johannes Kepler étudiait le mouvement des planètes autour du Soleil à partir des observations commandées par Tycho Brahé, et mettait en évidence des trajectoires elliptiques. Ces dernières vérifient la troisième loi de Kepler, laquelle définit la période de révolution en fonction uniquement de l'étendue (demi grand axe) de l'ellipse et indépendante de son épaisseur (demi petit axe). La distance Soleil-Planète effectue alors des oscillations entre périhélies et aphélie que l'on peut qualifier d'isochrones.

En 1958, l'astronome et mathématicien Michel Hénon remarqua que ces deux champs de gravitation, uniforme et engendré par une masse ponctuelle respectivement, sont susceptibles de rendre compte de la dynamique dans le cœur pour le premier et à la périphérie pour le second d'un même amas stellaire, appelé amas globulaire. Il chercha et mit en évidence un potentiel capable de décrire le champ de gravitation de tels amas et isochrone, au sens où les trajectoires au sein du système oscillent entre des péricentres et apocentres avec une période indépendante de leur "épaisseur". Dans ce cas, la période des oscillations peut dépendre de l'énergie des particules considérées mais pas de leur moment cinétique, leur second degré de liberté.

Par un raisonnement sur l'ensemble des potentiels isochrones et leur caractérisation géométrique à l'aide de paraboles, obtenues par le changement de variable (2.13) et caractérisées par une démonstration présentée dans le complément de ce manuscrit, nous avons revisité l'ensemble des orbites isochrones dans les systèmes à symétrie sphérique. Nous avons alors proposé une classification géométrique de l'ensemble des potentiels et trajectoires isochrones que nous avons en outre complété. Cet ensemble est partitionné sous l'action d'un sous-groupe affine en quatre orbites de groupe engendrées par les potentiels harmonique, de Kepler, de Hénon et le nouveau potentiel dit borné. La physique décrite dans ces systèmes isochrones est également explorée dans le chapitre 2, avec des interprétations possibles tant à l'échelle quantique qu'à celles astrophysiques. Ces résultats analytiques nous ont permis de proposer une démonstration originale du théorème de Bertrand et de comprendre certaines particularités communes aux isochrones, au cœur de la relativité isochrone.

La relativité restreinte a été élaborée afin de décrire les lois de la physique de la même manière dans tous les référentiels inertiels. Pour cela, les transformations de Lorentz effectuent un mélange entre les coordonnées spatiales et temporelles. De manière analogue, il est possible d'écrire les lois des mouvements isochrones de la même manière dans des référentiels isochrones propres. Pour cela, les nouvelles transformations appelées  $i$ -BOLST généralisent

la transformation de Bohlin ou la transformation de Levi-Civita en effectuant un mélange entre coordonnées temporelles et spatiales (contenant l'énergie et des potentiels isochrones), lequel préserve la structure des équations différentielles du mouvement étant donné une loi des aires ou un moment cinétique. Le groupe mathématique  $\mathbb{B}$  engendré par ces transformations conformes (symétriques) agit sur l'ensemble des isochrones et explicite leur nature keplerienne sous-jacente. Un dictionnaire résume les principales correspondances entre les relativités restreinte et isochrone. Cette dernière est construite au chapitre 3 grâce à l'analyse des relations entre les systèmes isochrones. De futures recherches pourront généraliser le dictionnaire et l'utiliser comme socle pour une théorie de la relativité générale pour des potentiels centraux à l'aide de transformations non-linéaires. Une telle théorie pourrait relier toute orbite dans un potentiel central à sa description keplerienne.

A l'échelle intermédiaire d'amas stellaires et à l'échelle galactique, la dynamique des systèmes auto-gravitants est un domaine d'étude observationnel, théorique et numérique. Cependant, les modèles théoriques en adéquation avec certaines données observationnelles manquent parfois de justification physique. C'est pourquoi la compréhension des mécanismes en jeu lors de la formation et de l'évolution de ces systèmes dynamiques est cruciale. En effet, l'analyse en astrophysique de systèmes auto-gravitants par le seul profil de luminosité (ou densité de masse) est ambiguë, car plusieurs modèles peuvent produire la même distribution de masse. Le système issu du processus de formation standard de relaxation violente est une structure de type cœur-halo compatible à la fois avec un profil de densité issu d'un modèle de King ou d'un modèle d'amas isochrone. En revanche, la prise en compte des propriétés dynamiques à petite échelle, comme la troisième loi de Kepler généralisée, nous a permis de construire une analyse isochrone permettant de discriminer les modèles comme celui de King au profit du modèle isochrone pour caractériser le résultat d'un effondrement gravitationnel numérique.

Cette propriété repose sur l'étude du mouvement de rotation des étoiles composant un système à symétrie sphérique isochrone. Dans cette analyse isochrone, la troisième de Kepler généralisée est devenue un nouveau critère pour caractériser l'évolution de systèmes auto-gravitants. Dans les expériences numériques effectuées au chapitre 4, l'état quasi-stationnaire résultant d'un processus de formation rapide et non hiérarchique de type relaxation violente apparaît isochrone. Le modèle isochrone de Michel Hénon constitue donc une condition initiale obtenue après la formation de ces systèmes. Sous l'effet de relaxations plus lentes, les systèmes perdent leur caractère isochrone comme confirmé par les profils de densité. Par conséquent, l'isochronie représente un indicateur de l'âge dynamique de tels systèmes auto-gravitants.

L'essence de l'isochronie est en conclusion keplerienne et constitue l'un des problèmes fondamentaux pour la compréhension des systèmes dynamiques à de nombreuses échelles.

A l'échelle de l'univers, l'expansion accélérée de l'univers est communément attribuée à la présence d'énergie noire. Plusieurs alternatives ont été proposées pour compléter le modèle standard de la cosmologie ou modifier la description relativiste de la gravitation à grande échelle. Dans le cadre du modèle cosmologique standard, la structure naturelle du système dynamique que représente l'univers permet de prendre en compte des interactions non-gravitationnelles entre les différentes formes d'énergie présentes dans l'univers.

La construction historique de la relativité générale présentée au chapitre 5 permet en effet de comprendre l'absence de telles interactions au sein du modèle standard de la cosmologie. La structure sous-jacente du modèle cosmologique de Friedmann-Lemaître, à savoir un système de Lotka-Volterra, permettant de pallier ce manque par la mise en évidence d'un couplage non-gravitationnel naturel à grande échelle. De même que ce système modélise en écologie

la dynamique de populations, il décrit également l'évolution de  $n$  fluides cosmologiques distincts décrits par leurs densités relatives  $\Omega_i$ , conformément à la dynamique décrite par (6.15) au chapitre 6. Dans ce formalisme, l'univers prend le nom d'univers jungle. L'introduction du couplage conduit alors à une dynamique effective de l'expansion de l'univers et de l'abondance des fluides cosmologiques.

De nombreuses perspectives ressortent de la prise en compte de ces interactions entre diverses formes d'énergie, parmi lesquelles une analyse plus poussée de leur origine physique et une analyse de la dynamique induite en confrontation avec les données observationnelles à venir.

Une annexe synthétise les éléments de géométrie riemannienne nécessaires au chapitre 5, tandis qu'un complément reproduit l'article original contenant les résultats et démonstrations portant sur l'isochronie en physique telle qu'expliquée par une approche intuitive aux chapitres 2 et 3 de la présente thèse de doctorat.



Complement  
Isochrony in 3D central potentials  
(SPD)





## Isochrony in 3D radial potentials

### From Michel Hénon's ideas to isochrone relativity: classification, interpretation and applications

Alicia Simon-Petit · Jérôme Perez ·  
Guillaume Duval

Received: 13 October 2017 / Accepted: 31 May 2018  
Springer-Verlag GmbH Germany, part of Springer Nature 2018

**Abstract** Revisiting and extending an old idea of Michel Hénon, we geometrically and algebraically characterize the whole set of isochrone potentials. Such potentials are fundamental in potential theory. They appear in spherically symmetrical systems formed by a large amount of charges (electrical or gravitational) of the same type considered in mean-field theory. Such potentials are defined by the fact that the radial period of a test charge in such potentials, provided that it exists, depends only on its energy and not on its angular momentum. Our characterization of the isochrone set is based on the action of a real affine subgroup on isochrone potentials related to parabolas in the  $\mathbb{R}^2$  plane. Furthermore, any isochrone orbits are mapped onto associated Keplerian elliptic ones by a generalization of the Bohlin transformation. This mapping allows us to understand the isochrony property of a given potential as relative to the reference frame in which its parabola is represented. We detail this isochrone relativity in the special relativity formalism. We eventually exploit the completeness of our characterization and the relativity of isochrony to propose a deeper understanding of general symmetries such as Kepler's Third Law and Bertrand's theorem.

**Keywords** Theoretical Astrophysics; Potential Theory (Mathematics); Integrable Systems; Differential Equations; Classical Gravitation.

## Contents

1 Introduction . . . . .	2
--------------------------	---

---

Alicia Simon-Petit  
Ensta ParisTech, Paris Saclay University, Applied Mathematics Laboratory, France  
E-mail: alicia.simon-petit@ensta-paristech.fr

Jérôme Perez  
Ensta ParisTech, Paris Saclay University, Applied Mathematics Laboratory, France  
E-mail: jerome.perez@ensta-paristech.fr

Guillaume Duval  
INSA Rouen, Mathematics & Informatics Laboratory, France

2	The isochrone geometry . . . . .	5
2.1	Hénon's parabola . . . . .	5
2.2	General properties of isochrone parabolas . . . . .	7
2.3	Classification of isochrone potentials . . . . .	11
2.4	Some physical meaning of this classification . . . . .	14
2.5	The affine group action on the Isochrone set . . . . .	15
3	Isochrone orbits and isochrone transformations . . . . .	18
3.1	Introduction and motivation . . . . .	18
3.1.1	Isochrone orbits transformations . . . . .	18
3.1.2	The bolst as the generalized Bohlin transformation . . . . .	20
3.1.3	The bolst, a key to isochrony . . . . .	24
3.2	Isochrone relativity . . . . .	24
3.2.1	The ibolst Algebra . . . . .	25
3.2.2	Lengths and spaces . . . . .	26
3.2.3	Orbits relativity . . . . .	27
3.2.4	Potentials relativity . . . . .	31
3.2.5	Isochrone orbits construction . . . . .	32
4	Applications . . . . .	33
4.1	Physical properties of isochrone potentials . . . . .	33
4.2	Period and precession of periastron for isochrones . . . . .	35
4.3	Generalization of Kepler's Third Law . . . . .	38
4.4	The Bertrand theorem . . . . .	41
5	Conclusion . . . . .	42
A	Isochrone characterization . . . . .	44
B	Proof of a parabola property . . . . .	44
C	Useful Lemmas . . . . .	47
D	Isochrone integrals . . . . .	48
D.1	Computation of $\mathcal{A}_r^{\text{ke}}$ , $\mathcal{A}_r^{\text{ha}}$ and physical deduction of $\mathcal{I}_1$ . . . . .	48
D.2	Proof for the expression of $\mathcal{I}_2$ . . . . .	49

## 1 Introduction

Macroscopic properties of self-gravitating systems can be derived from the orbits of their components, e.g. stars. These orbits are designed by the potential – density pair  $(\psi - \rho)$  involved in Poisson's equation  $\Delta\psi = 4\pi G\rho$ . This pair forms a steady-state model for such astrophysical systems and there are essentially two ways to produce a physically relevant model — one depending on empirical input, the other on theoretical input.

By compiling observational data, one can look for the emergence of an *empirical* model. For example, consider de Vaucouleur's law for elliptical galaxies in the middle of the twentieth century [40]. In that paper, the author remarks that the projection  $I(R)$  of the luminosity onto the plane of the sky of elliptical galaxies varies as a function of an apparent distance  $R$  from the center as  $I(R) \propto \exp(-R^{1/4})$ . From  $I(R)$ , assuming a given mass-to-light ratio, one can build the mass density  $\rho$  of the system and, solving Poisson's equation, obtain a gravitational potential for elliptical galaxies. This problem is generally ill-posed: as a matter of fact, after the projection, a lot of “good” potentials (Jaffe [22], Hernquist [21], Dehnen [11] or NFW [34]) produce  $R^{1/4}$ -compatible luminosity profiles. Apart from this empirical property all these famous models are poorly justified physically.

The reverse approach is much less investigated. The mass density is a marginal velocity law of the one-particle distribution function  $f$  associated with a self-gravitating system. This function  $f(t, \mathbf{r}, \mathbf{p})$  describes the statistical properties of a

test particle of mass  $m$ , position  $\mathbf{r}$  and momentum  $\mathbf{p}$  in the mean field gravitational potential  $\psi(t, \mathbf{r})$ . These two functions satisfy the Collisionless-Boltzmann and Poisson system

$$\begin{cases} \frac{\partial f}{\partial t} + \{f, E\} = 0, \\ \Delta\psi = 4\pi G\rho = 4\pi mG \int f d\mathbf{p}, \end{cases}$$

where  $E = \frac{\mathbf{p}^2}{2m} + m\psi$  is the total energy of the test particle and  $\{, \}$  stands for the Poisson bracket. Using basic properties of these brackets, one can see that the simplest steady states are described by  $f(E)$ : this is the simplest case of Jeans' theorem (see e.g. [6]). Involving Gidas-Nirenberg theorem [14], one can show ([35] sect. 2) that, if their total mass is finite, the corresponding self-gravitating systems are spherical and isotropic and thus their gravitational potentials are radial,  $\psi = \psi(r)$  with  $r = |\mathbf{r}|$ . Stability analysis can restrict possible steady states to decreasing and positive  $f$  but nothing general can be said anymore about the choice of an equilibrium in this context. Adding thermodynamic considerations, Lynden-Bell [28] has initiated a long debate. Based on the fact that in three spatial dimensions there is no regular isothermal steady states with finite mass, this debate is often summarized by the fact that isolated self-gravitating systems could settle down in a truncated isothermal state with a core-halo density distribution. The size of the core and the slope of the halo depend on structural dissipation which can occur in the system. This point will be discussed in a forthcoming paper.

In a singular and seminal paper in French, Hénon [20] (for an English translation see [5]) followed another way to address this problem. Radial potentials confer to any of their confined test particles the property to have a periodic radial distance from the center of the system. This radial period  $\tau_r$  depends generically on the two physical parameters of this test particle: its energy  $E$  and the modulus  $L^2$  of its squared angular momentum. Hénon remarks that orbits confined around the center of the system (which evolve generically in a harmonic potential) and orbits confined to the outer parts (which evolve generically in a Keplerian potential) have a radial period that depends only on  $E$ . He then proposed looking for a general potential which could be characterized by this property. He succeeded by finding his famous isochrone potential. Although his potential gives a mass density in pretty good accordance with some of the observed globular clusters at the time, history has decided to follow another direction. In his conclusion, Michel Hénon proposed a mechanism based on resonances that could lead to the formation of an isochrone. This mechanism needed to be considered more accurately and proved substantially [20, 5], but it has not been further investigated. In addition to Lynden-Bell's work on violent relaxation and the above-mentioned debate that followed, the observational data refinement and the development of numerical simulations revealed a great variety of profiles for self-gravitating systems and Hénon's isochrone became one among them. Recent works (in a paper in preparation by Simon-Petit, A., Perez, J., and Plum, G.) reveal that, as suggested by Hénon [20] in his conclusion, isochrony could in fact be inherited from the formation process of isolated self-gravitating systems. Hence there could be a fundamental initial state from which, after the initial collapse, the observed diversity could arise.

For all of these reasons, we have decided to revisit in detail isochrony in radial potential-governed systems. Inspecting Hénon ideas we have found that his work is far from exhaustive in a mathematical sense even if the potential he has found

might be one of the most important for physical applications. We propose in this paper to characterize the whole set of isochrone potentials in a rigorous way. This characterization will help for a global understanding of the importance of the isochrone property and will clarify some important physical symmetries occurring in gravitation like Kepler's Third law or Bertrand's theorem.

The paper is organized as follows. In the spirit of Michel Hénon, section 2 is devoted to geometry. In sec. 2.1 we first recall the basics of the problem of potential isochrony, general definitions and the Hénon link between isochrony and parabolas. In addition, we call for a rigorous proof of this parabola property which is given in appendix B. Taking into account very general physical properties, we introduce in sec. 2.2 appropriate transformations and prove three lemmas which allow us to restrict the study to parabolas passing through the origin with a vertical or a horizontal tangent. As these transformations leave invariant vertical lines, these three lemmas will make clear the decomposition of parabolas into four families: ones with a vertical symmetry axis (straight parabolas) and others (tilted parabolas) that are classified in three different types depending on the parabola orientation and vertical tangent position. These transformations and hence this distinction were not identified by Hénon who also missed some elements of the isochrone set. Thanks to this geometric decomposition, we deduce in sec. 2.3 the whole set of isochrone potentials. It is a modulus space in which each point is a potential from one of the four classes of equivalence of parabolas under the action of the previous transformations. This algebraic representation classifies the four isochrone potential types but separates them in a partition of four equivalence classes. However, isochrone potentials are unified, linking orbits together.

In section 3, we focus on the isochrone orbits. Based on the fundamental differential orbital equation, we present in sec. 3.1 the most general transformation which preserves isochrony and angular momentum when applied to a given orbit. This linear application is then identified as a generalization of the well-known Bohlin transformation ([7,3]) as well as the brilliant idea of Donald Lynden-Bell [30]. It continuously maps isochrone orbits onto their Keplerian associates. This Keplerian character of a given isochrone orbit is developed in sec. 3.2. Adapting the time, energy and angular momentum of a given isochrone orbit in an isochrone potential, it is shown in detail how to map this orbit onto its associated Keplerian one in the appropriate frame.

The last section is devoted to physical applications of this isochrony classification and interpretation. We first present in sec. 4.1 the physical properties of systems associated with isochrone potentials. In particular, we give in table 50 the explicit formulation of  $\tau_r(E)$  and  $n_\varphi(L^2)$  for all isochrone potentials. The properties of  $\tau_r(E)$  allow us to give a generalization of Kepler's third law in sec. 4.3. Eventually we show in sec. 4.4 that the famous Bertrand's theorem about closed orbits in radial potentials is just a corollary of a general property of isochrone orbits.

Four appendices detail important results for isochrony used in the paper.

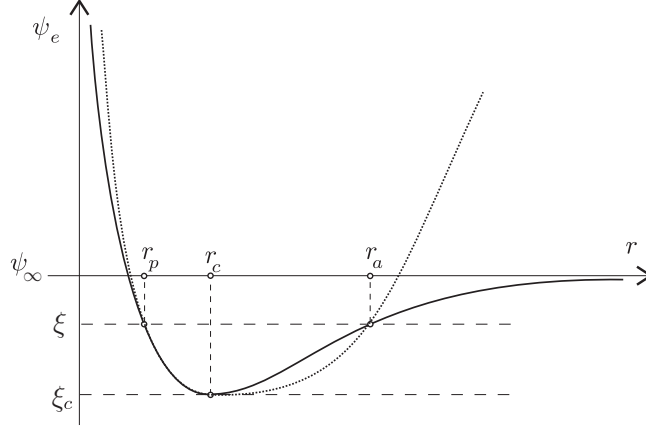


**Fig. 1** Physical effective potentials that allow Periodic Radial Orbits. The solid curve corresponds to a finite  $\psi_\infty$  and the dashed curve corresponds to an infinite  $\psi_\infty$ .

## 2 The isochrone geometry

### 2.1 Hénon's parabola

We consider a stellar system described by a gravitational potential  $\psi(\mathbf{r}) = \psi(r)$ , where  $\mathbf{r}$  is the position vector of a test particle of mass  $m$  confined in this system. The orbit of this test particle is contained in a plane. In this plane, the two parameters of this orbit are its energy  $E = m\xi$  and the norm of its angular momentum  $L = m\Lambda$ . Both these two parameters contribute to the definition of the gravitational potential of the cluster  $\psi(r)$  and to the computation of the distance  $r$  between the star and the center of mass of the cluster at each time  $t$ . This contribution is summarized in the definition of the energy of the star,

$$\xi = \frac{1}{2} \left( \frac{dr}{dt} \right)^2 + \frac{\Lambda^2}{2r^2} + \psi(r) = \text{cst.} \quad (1)$$

We are interested in increasing<sup>1</sup> potentials  $\psi(r)$  for which the ODE (1) admits periodic solutions, named hereafter Periodic Radial Orbits (PROs). The effective potential  $\psi_e(r) = \frac{\Lambda^2}{2r^2} + \psi(r)$  then reaches a global minimum and diverges to  $+\infty$  when  $r \rightarrow 0$  as shown in figure 1. When they exist, the apoastron at distance  $r_a$  and periastron at  $r_p$  of a PRO are given by the two intersections of the graph of  $\psi_e$  with constant  $\xi$ -lines. For a given energy  $\xi_c$  corresponding to the minimum of  $\psi_e$ , the distance  $r_a = r_p$  and the orbit is circular.

In order to clarify the vocabulary we will use, let us define two fundamental potentials in this context.

**Definition 1** The harmonic potential is defined by  $\psi_{\text{ha}}(r) = \frac{1}{2}\omega^2 r^2$  with  $\omega \neq 0$ . We call the potential  $\psi_{\text{ke}}(r) = -\frac{\mu}{r}$  with  $\mu > 0$  a Keplerian potential.

<sup>1</sup> This restriction characterizes the gravitational interaction for which Gauss' theorem in spherical symmetry indicates that  $\frac{d\psi}{dr} = \frac{GM(r)}{r^2} > 0$ .

To get the existence of a global minimum of the effective potential  $\psi_e$  and hence of PRO's, we have to specify the behavior of the potential  $\psi$  when  $r \rightarrow 0$ . This is the objective of the following lemma.

**Lemma 1** *If for some  $\Lambda \geq 0$ , the effective potential  $\psi_e(r) \rightarrow +\infty$  when  $r \rightarrow 0$ , then  $\lim_{r \rightarrow 0} r^2 \psi(r) = \ell < \infty$ . Conversely, if  $\lim_{r \rightarrow 0} r^2 \psi(r) = \ell < \infty$ , then for any  $\Lambda \geq 0$  the effective potential  $\psi_e(r) \rightarrow +\infty$  when  $r \rightarrow 0$  provided that  $\ell > -\Lambda^2$ .*

*Proof* The converse claim is obvious since  $\lim_{r \rightarrow 0} r^2 \psi_e(r) = \Lambda^2 + \ell > 0$  if  $\ell > -\Lambda^2$ . For the first claim, let us assume that  $\lim_{r \rightarrow 0} r^2 \psi(r)$  is infinite. Then  $\lim_{r \rightarrow 0} \psi(r)$  is also infinite. But since  $r \mapsto \psi(r)$  is increasing we must have  $\lim_{r \rightarrow 0} \psi(r) = -\infty$ . So for any  $\Lambda > 0$ , by choosing  $r$  close enough to 0, we would get

$$r^2 \psi(r) < -\Lambda^2 \implies \psi(r) < -\frac{\Lambda^2}{r^2} \implies \psi_e(r) < -\frac{\Lambda^2}{2r^2}$$

which implies  $\lim_{r \rightarrow 0} \psi_e(r) = -\infty$ . The claim follows by contraposition.  $\square$

These restrictions allow a PRO provided that  $\xi \in [\xi_c, \psi_\infty)$ , where  $\psi_\infty = \lim_{r \rightarrow +\infty} \psi(r)$  may be infinite. The total and/or the central mass of such systems could be infinite but the radial period

$$\tau_r = 2 \int_{r_p}^{r_a} \frac{dr}{\sqrt{2[\xi - \psi(r)] - \frac{\Lambda^2}{r^2}}} \quad (2)$$

is always finite. This period corresponds to the total duration of the transfer from  $r_a$  to  $r_p$  and back, and it is also related to the  $\xi$ -derivative of the radial action  $\mathcal{A}_r$ , which gives the radial pulsation (see for example [6] p. 221)

$$\Omega_r^{-1} = \frac{\tau_r}{2\pi} = \frac{\partial \mathcal{A}_r}{\partial \xi} \text{ with } \mathcal{A}_r = \frac{1}{\pi} \int_{r_p}^{r_a} \sqrt{2[\xi - \psi(r)] - \frac{\Lambda^2}{r^2}} dr. \quad (3)$$

This radial action also generates the increment of the azimuthal angle  $\Delta\varphi$  during the transfer from  $r_a$  to  $r_p$  and back given by

$$\frac{\Delta\varphi}{2\pi} = n_\varphi = -\frac{\partial \mathcal{A}_r}{\partial \Lambda}. \quad (4)$$

Both  $\tau_r$  and  $\Delta\varphi$  are clearly two functions of the two variables  $\xi$  and  $\Lambda$ . In May 1958, Michel Hénon pointed out that two fundamental potentials, i.e. the Keplerian and harmonic ones, have  $\tau_r$  which only depends on  $\xi$ . One year later, in a seminal article in French [20] (for an English translation see [5]), he found a family of physical potentials for which this property remains valid. We propose to complete this characterization of isochrony by an equivalent property on the azimuthal angle:  $\Delta\varphi$  only depends on  $\Lambda$ , see theorem 6 in appendix A. This family is known as Hénon's Isochrone. We propose now to follow his steps to recover his result and eventually extend it by exhibiting the whole set of possible isochrones.

Introducing Hénon's variables,

$$x = 2r^2 \quad \text{and} \quad Y(x) = x\psi\left(\sqrt{x/2}\right), \quad (5)$$

one can see that the corresponding  $x$ -values of the periastron and apoastron, namely  $x_a$  and  $x_p$ , are the roots of the equation  $Y(x) = \xi x - \Lambda^2$ . As it is detailed in figure 2, for a fixed value  $\xi$  of the energy, the set of all points  $(P_{a,i}; P_{p,i})$  on the lines  $y_i(x) = \xi x - \Lambda_i^2$  with corresponding abscissa  $x_{a,i}$  and  $x_{p,i}$  form the graph of  $Y$ . Using a clever analysis Michel Hénon shows that  $\tau_r$  only depends on  $\xi$  if and only if  $P_0 I$  is proportional to  $(x_{p,1} - x_{a,1})^2$  when  $\Lambda^2$  is varying. After a much more involved analysis Hénon was able to prove that this property characterizes parabolas. This original proof is very technical and we give a new version of it in theorem 7 of appendix B highlighting the analytical property of the potentials.

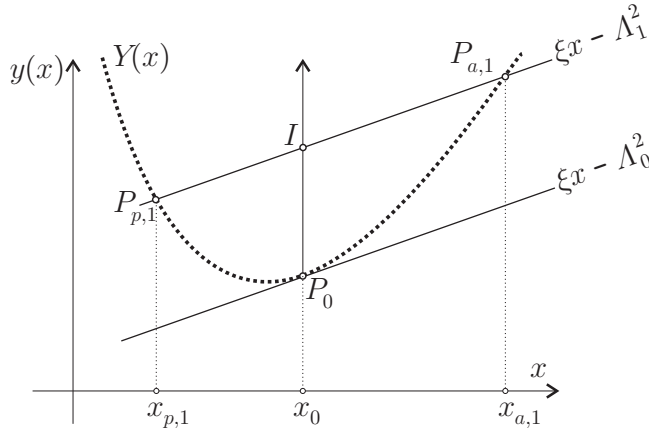


**Fig. 2** Geometric view of Hénon's variables.

## 2.2 General properties of isochrone parabolas

The general equation for a parabola in Hénon's variables is written as

$$(ax + bY)^2 + cx + dY + e = 0. \quad (6)$$

The expressions of the constants  $a$ ,  $b$ ,  $c$ ,  $d$  and  $e$  in terms of the problem parameters are given in the original Hénon paper [20], where  $a$  and  $b$  cannot simultaneously vanish. From now on, the function defined by  $\psi : x \mapsto Y(x)/x$  represents an isochrone potential according to the previous result. Two remarks allow us to simplify the parabola equation. First, any potential is defined up to a constant  $\epsilon$  which enables us to map  $\psi \rightarrow \psi + \epsilon$  or  $Y \rightarrow Y + \epsilon x$  without loss of generality. This transformation is named an  $\epsilon$ -transvection  $(x, Y) \rightarrow (x, Y + \epsilon x)$ . Second, by inspection of equation (1), one can see that if  $\psi$  is isochrone then the potential  $\psi^*(r) = \psi(r) + j_\lambda(r)$  where  $j_\lambda(r) = \frac{\lambda}{2r^2}$  is also isochrone with a new value



of the angular momentum  $\Lambda'^2 = \Lambda^2 + \lambda > 0$ . In terms of  $Y$  this allows the transformation  $Y \rightarrow Y^* = Y + \lambda$ . Let us call this translation of the parabola a  $\lambda$ -gauge transformation of an isochrone potential. The action of a  $\lambda$ -gauge or  $\epsilon$ -transvection could be synthesized in an affine transformation which is denoted as

$$J_{\epsilon, \lambda} : \mathbb{R}^2 \rightarrow \mathbb{R}^2 \\ (x, Y) \mapsto (x, Y + \epsilon x + \lambda).$$

If we denote by  $\mathbb{A}$  the set of these affine transformations  $J_{\epsilon, \lambda}$  and by observing that  $J_{\epsilon, \lambda} \circ J_{\epsilon', \lambda'} = J_{\epsilon + \epsilon', \lambda + \lambda'}$ , we see that it is a subgroup of affine transformations of the real plane, isomorphic to  $(\mathbb{R}^2, +)$ . Affine transformations in Hénon's variables correspond to physical transformations which preserve the isochrone property. From this, we arrive at three short lemmas to organize the discussion.

**Lemma 2** *With a vertical translation  $J_{0, \lambda} : Y \rightarrow Y^* = Y + \lambda$ , the Hénon Parabola can be reduced to a non-degenerate parabola passing through the origin of the  $(x, y)$ -axis.*

*Proof* According to lemma 1,  $\ell = \lim_{r \rightarrow 0} r^2 \psi(r)$  is a real number. By plugging the potential in equation (6) with the Hénon change of variables, we get

$$\left[ 2ar^2 + 2br^2 \psi(r) \right]^2 + 2cr^2 + 2dr^2 \psi(r) + e = 0.$$

Taking the limit as  $r \rightarrow 0$  we get

$$4b^2 \ell^2 + 2d\ell + e = 0. \quad (7)$$

Now, the  $\lambda$ -translation  $Y \rightarrow Y^* = Y + \lambda$  changes the potential to  $\psi^*(r) = \psi(r) + \frac{\lambda}{2r^2}$  and hence  $\ell^* = \lim_{r \rightarrow 0} r^2 \psi^*(r) = \ell + \frac{\lambda}{2}$ . So by taking  $\lambda = -2\ell$  we have  $\ell^* = 0$ . Therefore, according to (7), we have  $e^* = 0$  for the new parabola. In other words, the translated parabola passes through the origin of the  $(x, y)$ -axis. The degenerate cases of parabolas, where  $a/b$  (resp.  $b/a$ ) is proportional to  $c/d$  (resp.  $d/c$ ) or  $d = c = 0$  or  $a = b = 0$ , are not of interest in our study since they lead to constant potentials up to a gauge.  $\square$

Considering the result of lemma 2, it is now possible to consider the asymptotic behavior of the isochrone potential  $\psi$  associated with  $Y$ , which is given by the relation

$$(A + B\psi)^2 = \frac{C\psi + D}{2r^2}. \quad (8)$$

Let  $\mathcal{D}_\psi \subset \mathbb{R}^+$  be the domain on which the potential is defined physically. Then, let us introduce

$$\mathcal{R} = \sup_{\mathbb{R}} [\mathcal{D}_\psi], \quad (9)$$

where a priori  $\mathcal{R}$  is finite and positive if  $\mathcal{D}_\psi$  is bounded or  $\mathcal{R} = +\infty$  if not. We additionally define  $\psi_\infty = \lim_{r \rightarrow \mathcal{R}} \psi(r)$ . We now have the following lemma:

**Lemma 3** *In the context of the above reduction given by (8) we have the following equivalences:  $\psi_\infty$  is infinite if and only if  $B = 0$  if and only if  $\psi$  is harmonic up to an additive constant.*

- Proof* – If  $B = 0$  then, according to lemma 2,  $C \neq 0$  and from (8) we get  $\psi(r) = 2\frac{A^2}{C}r^2 - \frac{D}{C}$ . As we are only interested in increasing potentials,  $C$  is positive and  $\psi(r) = \psi_{\text{ha}}(r) = \frac{1}{2}\omega^2 r^2$  with  $\omega \neq 0$  — up to an additive constant. This potential is defined on  $[0, +\infty)$  so  $\mathcal{R} = +\infty$  and  $\psi_\infty = +\infty$ .
- Let us assume conversely that  $\psi_\infty$  is infinite. As the potential is increasing, there exists an  $r_0$  in the neighborhood of  $\mathcal{R}$  such that for all  $r > r_0$ ,  $\psi(r) > 0$ . By dividing equation (8) by  $\psi$  for  $r > r_0$ , we get

$$\frac{1}{\psi}(A + B\psi)^2 = \frac{1}{2r^2} \left( C + \frac{D}{\psi} \right).$$

The right hand side of this equality tends to the finite limit  $\frac{C}{2\mathcal{R}^2}$  when  $r \rightarrow \mathcal{R}$  (that is to zero if  $\mathcal{R} = +\infty$ ). If  $B \neq 0$ , since  $\psi_\infty = +\infty$ , the left hand side tends to  $+\infty$  when  $r \rightarrow \mathcal{R}$ . Therefore,  $\psi_\infty$  infinite implies that  $B = 0$  and  $\psi$  is harmonic by the first part of this analysis.  $\square$

The quantity  $\psi_\infty$  indicates the asymptotic direction of the parabola. When  $\psi_\infty = +\infty$ , then the symmetry axis of the parabola is parallel to  $(Oy)$ . We do not consider the case  $\psi_\infty = -\infty$  because it corresponds to bottom-oriented parabolas which are always associated with decreasing harmonic potentials  $\psi_{\text{ha}}^-(r) = -\frac{1}{2}\omega^2 r^2$ . In this case the effective potential never has global nor local minima and no orbit could ever be periodic.

Before exhibiting the isochrone potentials we can say a little more about the tangent to the parabola at the origin.

**Lemma 4** *For a potential given by (8), two cases may happen concerning the tangent at the origin of the isochrone parabola:*

1. *It is vertical and the reduced potential is Keplerian up to an additive constant. This corresponds to  $C = 0$  in (8).*
2. *It is not vertical and modulo a transvection we can manage to get a horizontal tangent corresponding to  $D = 0$  in the transvected version of (8).*

*Proof* With a gauge transformation we may write the isochrone parabola equation as  $(Ax + BY)^2 = CY + Dx$ . Let us apply to it a transvection with a parameter  $\epsilon$ . The new equation is then

$$(A'x + B'Y)^2 = C'Y + D'x \quad \text{with} \quad \begin{cases} A' = A + B\epsilon, & C' = C \\ B' = B & \text{and } D' = D + C\epsilon. \end{cases} \quad (10)$$

By considering the gradient of the function  $f(x, y) = (A'x + B'y)^2 - C'y - D'x$  at the origin, we get the equation of the tangent to the parabola at the origin,  $D'x + C'y = 0$ . Depending on its direction, two cases may be distinguished:

1. When  $C = 0$ , the parabola passes through the origin with a vertical tangent. One may further simplify the parabolic equation choosing  $\epsilon$  to cancel  $A'$  since  $B$  should be non-zero according to lemma 2. We eventually obtain  $(B')^2 Y^2 = D'x$ . This equation implies that  $D' > 0$ . Making explicit Hénon variables with (5), we get  $\psi(r) = \psi_{\text{ke}}(r) = -\frac{\mu}{r}$  where  $\mu = \sqrt{\frac{D'}{2B'^2}}$  is a positive constant since  $r \mapsto \psi(r)$  is increasing.

2. When  $C \neq 0$ , it is possible to choose the parameter  $\epsilon$  of the transvection to cancel  $D'$  so that the parabola passes through the origin with a horizontal tangent. In other words, we choose the arbitrary constant of the potential to simplify the study of its corresponding parabola, which may be described by  $(A'x + B'Y)^2 = C'Y$  with  $A' \neq 0$ .  $A'$  cannot vanish unless  $\epsilon = -\frac{A}{B} = -\frac{D}{C}$  which is forbidden by lemma 2.  $\square$

Let us summarize the situation at this point (see figure 3).

Any parabola in the plane  $(x, y)$  is associated with an isochrone potential. Combining lemmas 2, 3 and 4 we can only study the family of parabolas passing through the origin and belonging to one of the two following classes:

- Straight parabolas, which possess a vertical symmetry axis and thus never admit any vertical tangent. As we have explained before we are only interested in straight up-oriented parabolas. Using affine transformations, straight parabolas could be moved in such a manner that their apices are the origin of the  $(x, y)$ -plane. They correspond to harmonic potentials.
- Tilted parabolas, whose symmetry axes are inclined from the vertical ones and possess a horizontal or vertical tangent at the origin. This tilted parabola family is composed of three categories:
  - Laid parabolas, with a vertical tangent at the origin corresponding to Kepler potentials;
  - Right-oriented parabolas, with a horizontal tangent at the origin;
  - Left-oriented parabolas, with a horizontal tangent at the origin.

In figure 3, we have plotted in the  $(xOy)$  plane the four *reduced* classes of parabolas. A precise definition of the corresponding potentials is given in definition 2 p.15.

The reduced isochrone potential contained in each reduced parabola is emphasized in this figure and it corresponds to a limited part of the parabola. As a matter of fact, the variable of the potential is the radial distance, a positive real number. Each isochrone potential is then included in the  $x$ -positive right plane. This remark excludes left-oriented laid parabolas. For any non-straight parabolas there are two functions  $x \mapsto y_1(x)$  and  $x \mapsto y_2(x)$  into which the  $x$ -positive part of the graph of the parabola could be decomposed (see figure 3). The slope of the chord between the origin and a point  $M$  of abscissa  $x > 0$  on the graph of  $y_1$  or  $y_2$  is given by the ratio  $\frac{y_1(x)}{x}$  or  $\frac{y_2(x)}{x}$  which is precisely the definition of the potential  $\psi$ . This remark shows that  $\psi$  is an increasing (resp. decreasing) function if the graph of  $y$  is convex (resp. concave), i.e. the chord between two points is above (resp. below) the function. As we look for increasing potentials in order to have PRO's, we have to consider the convex part of the parabola graph. This part is named  $y_1$  in figure 3.

Tilted parabolas have a symmetry axis with a finite slope. Any  $\epsilon$ -transvection adds  $\epsilon$  to this slope, modifying the orientation of these parabolas. Nevertheless, we cannot jump from a left-oriented parabola to a right-oriented one using an affine transformation. However, according to lemma 4 and conserving its orientation, we can morph any tilted parabola with a horizontal tangent or a vertical tangent at the origin. In the latter case, the symmetry axis is parallel to  $(Ox)$ . The morphing from the reduced parabolas to the whole set of isochrone ones is detailed in figure 5 following our analysis of the concerned potentials in the next section.

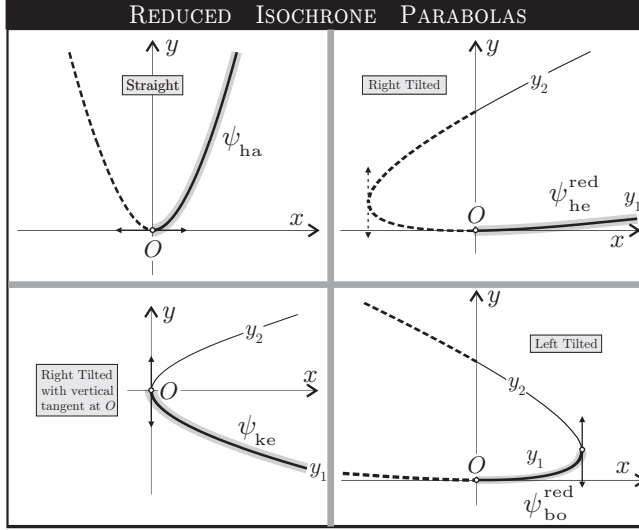


**Fig. 3** The four classes of reduced parabolas corresponding to the reduced isochrone potentials. The part of the parabola associated with the increasing potential is highlighted ( $y_1$ ). The dashed part of the parabola corresponds to potentials with an imaginary distance argument ( $x < 0$ ). The unhighlighted solid line part of the parabola ( $y_2$ ) in the  $x > 0$  half-plane corresponds to decreasing potentials.

Our reduction to four families of parabolas and their corresponding potentials enables us to obtain the whole set of isochrone potentials. In his historical study, Michel Hénon did not remark on the crucial role of these affine transformations. He dismissed out-of-origin parabolas and forgot left-oriented tilted ones.

Let us now determine explicitly the isochrone potentials of the reduced families.

### 2.3 Classification of isochrone potentials

From the previous analysis we will now state and prove the following classification result.

**Theorem 1** *The isochrone potentials are classified by these two properties:*

1. *There are essentially four types of reduced isochrone potentials:*
  - The Keplerian potential  $\psi_{ke}$  for which the reduced parabola has a horizontal symmetry axis and a vertical tangent at the origin.
  - The harmonic potential  $\psi_{ha}$  for which the reduced parabola is straight with a horizontal tangent at the origin.
  - Two other potentials  $\psi_{he}^{red}$  and  $\psi_{bo}^{red}$  for which the reduced parabolas have horizontal tangents at the origin and are respectively right and left oriented. They are given by the formulae

$$\psi_{he}^{red} := \frac{\mu}{2b} - \frac{\mu}{b + \sqrt{b^2 + r^2}}, \quad \psi_{bo}^{red} := -\frac{\mu}{2b} + \frac{\mu}{b + \sqrt{b^2 - r^2}},$$

where  $\mu$  and  $b$  are positive constants.

2. Any isochrone potential  $\psi$  is equivalent under an affine transformation to one of the previous types. That is to say there exist two constants  $\epsilon$  and  $\lambda$  and some reduced potential  $\psi^{\text{red}} \in \{\psi_{\text{ke}}, \psi_{\text{ha}}, \psi_{\text{he}}^{\text{red}}, \psi_{\text{bo}}^{\text{red}}\}$  such that  $\psi(r) = \psi^{\text{red}}(r) + \epsilon + \frac{\lambda}{2r^2}$ .

The potential  $\psi_{\text{he}}$  is the original potential discovered by Michel Hénon. From our knowledge, the potential  $\psi_{\text{bo}}$  is a new one. We call it the *bounded* potential for reasons appearing in sec. 2.4.

*Proof* Let  $\mathcal{P}$  be the parabola associated with an isochrone potential  $\psi$  which is neither Keplerian nor harmonic. According to lemmas 2, 3 and 4 we are left to consider the case where  $\mathcal{P}$  passes through the origin, has a horizontal tangent and has a symmetry axis which is not vertical. According to (8) and the previous lemmas, this corresponds to having an equation of the form

$$2r^2 = \frac{n\psi}{(\psi - m)^2},$$

for some constant  $m$  and  $n$  both non zero. As a consequence, we see here that the potential  $\psi$  will depend on two constants. Normalizing the potential by setting  $\psi = mV$ , we are led to the functional equation

$$q = q(V) = \frac{V}{(V-1)^2}, \quad \text{with} \quad q = \kappa x = 2\kappa r^2,$$

where  $\kappa = m/n$  is another non zero constant. The inversion of the function  $q$  gives two solutions  $V(q)$  of the quadratic equation

$$qV^2 - (2q+1)V + q = 0. \quad (11)$$

They are of the form

$$\begin{cases} V^+(q) := \frac{2q+1+\sqrt{4q+1}}{2q} = 1 - \frac{2}{1+\sqrt{4q+1}}, \\ V^-(q) := \frac{2q+1-\sqrt{4q+1}}{2q} = 1 - \frac{2}{1-\sqrt{4q+1}}. \end{cases} \quad (12)$$

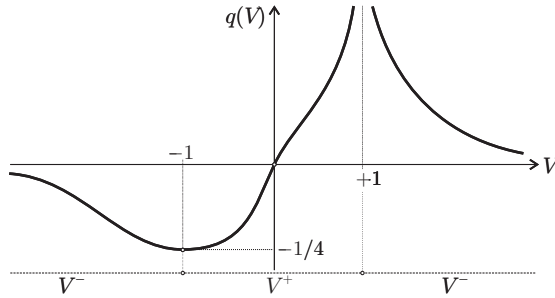


**Fig. 4** The potential  $V^+$  and  $V^-$  as functions of  $q$ .

These two functions  $q \mapsto V(q)$  are defined on the real interval  $q \geq -1/4$ . As shown in figure 4, the  $\pm$  signs of  $V$  are chosen in such a way that  $q \mapsto V^+(q)$

is increasing on  $[-1/4, +\infty)$  and  $q \mapsto V^-(q)$  is decreasing on both  $[-1/4, 0)$  and  $]0, +\infty)$ . From the quadratic equation (11) we have

$$V^+(q) + V^-(q) = 2 + \frac{1}{q} \quad \text{and} \quad V^+(q)V^-(q) = 1. \quad (13)$$

Now we compute the potential. From the expression  $q = \kappa x = 2\kappa r^2$ , we will classify the potentials by the sign of the constant  $\kappa$ .

1. **When  $\kappa < 0$** , then  $q$  is necessarily negative. Therefore  $-1/4 \leq q \leq 0$  which implies

$$r^2 \leq \frac{1}{8|\kappa|}.$$

Setting a new constant  $b := \frac{1}{\sqrt{8|\kappa|}}$  in such a way that the previous inequality becomes  $r \leq b$ , we have  $q = \frac{-r^2}{4b^2}$ . Therefore,

$$\psi(r) = mV(q) = mV\left(\frac{-r^2}{4b^2}\right).$$

This gives us two possible potentials  $\psi^\pm$ . But to have a PRO, the function  $r \mapsto \psi(r)$  must be ultimately increasing. That is,

$$\frac{-mr}{2b^2} \frac{dV}{dq} \left( \frac{-r^2}{4b^2} \right) > 0.$$

Since  $q \mapsto V^+(q)$  is increasing we must choose  $m = -\frac{\mu}{2b}$  for some positive constant  $\mu$ . The factor  $\frac{1}{2b}$  is just here for simplicity of the final result. Similarly in the formula for  $\psi^-$  we must choose  $m = \frac{\mu}{2b} > 0$ . This leads to the two potentials

$$\begin{cases} \psi_{\text{bo}}^+(r) := -\frac{\mu}{2b} V^+\left(\frac{-r^2}{4b^2}\right) = -\frac{\mu}{2b} + \frac{\mu}{b+\sqrt{b^2-r^2}}, \\ \psi_{\text{bo}}^-(r) := \frac{\mu}{2b} V^-\left(\frac{-r^2}{4b^2}\right) = \frac{\mu}{2b} - \frac{\mu}{b-\sqrt{b^2-r^2}}. \end{cases}$$

From (13), we get that

$$\psi_{\text{bo}}^-(r) - \psi_{\text{bo}}^+(r) = \frac{\mu}{2b} \left[ V^+\left(\frac{-r^2}{4b^2}\right) + V^-\left(\frac{-r^2}{4b^2}\right) \right] = \frac{\mu}{b} - \frac{2b\mu}{r^2}. \quad (14)$$

As a consequence, the left-oriented parabolas associated with  $\psi_{\text{bo}}^+$  and  $\psi_{\text{bo}}^-$  are exchanged by an affine transformation. This is the meaning of the word *essentially* in the statement of the theorem since the group orbits of  $\psi_{\text{bo}}^{\text{red}} := \psi_{\text{bo}}^+$  and of  $\psi_{\text{bo}}^-$  under the action of the affine group are the same.

2. **When  $\kappa > 0$** , setting  $b := 1/\sqrt{8\kappa}$  again, we similarly get  $\psi = mV(q) = mV\left(\frac{r^2}{4b^2}\right)$ . And by setting again  $\frac{\mu}{2b} := |m|$  we get two new isochrone potentials

$$\begin{cases} \psi_{\text{he}}^+(r) := \frac{\mu}{2b} V^+\left(\frac{r^2}{4b^2}\right) = \frac{\mu}{2b} - \frac{\mu}{b+\sqrt{b^2+r^2}}, \\ \psi_{\text{he}}^-(r) := -\frac{\mu}{2b} V^-\left(\frac{r^2}{4b^2}\right) = -\frac{\mu}{2b} + \frac{\mu}{b-\sqrt{b^2+r^2}}. \end{cases}$$

Again from (13), we have that

$$\psi_{\text{he}}^+(r) - \psi_{\text{he}}^-(r) = \frac{\mu}{2b} \left[ V^+\left(\frac{r^2}{4b^2}\right) + V^-\left(\frac{r^2}{4b^2}\right) \right] = \frac{\mu}{b} + \frac{2b\mu}{r^2}. \quad (15)$$

Therefore,  $\psi_{\text{he}}^{\text{red}} := \psi_{\text{he}}^+$  and  $\psi_{\text{he}}^-$  are also exchanged by the affine group and their respective group orbits under this group action will coincide. These potentials are defined for all values of  $r \in [0, +\infty)$  so that their parabolas are then right-oriented.

To conclude the proof of the theorem we only have to observe that according to lemmas 2, 3 and 4, any isochrone is in the orbit of a reduced one under the affine subgroup generated by the  $J_{\epsilon, \lambda}$  transformations.  $\square$

These reduced potentials can be visualized in figure 3.

Using natural notations taken from the proof of theorem 1, from (14) and (15) we can write

$$\begin{cases} \psi_{\text{bo}}^- = J_{+\epsilon, \lambda}(\psi_{\text{bo}}^+) \\ \psi_{\text{he}}^- = J_{-\epsilon, \lambda}(\psi_{\text{he}}^+) \end{cases} \quad \text{with } \epsilon = \frac{\mu}{b} \text{ and } \lambda = -4b\mu. \quad (16)$$

The tilted parabolas presented in figure 3 are the ones associated with  $\psi_{\text{he}}^+$  for the right (called  $\mathcal{P}_{\text{he}}^+$ ) parabola and with  $\psi_{\text{bo}}^+$  for the left one (called  $\mathcal{P}_{\text{bo}}^+$ ). These two parabolas both open to the top, i.e. in the direction where  $y$  increases. Using property (16) or by direct representation, one can verify that, using natural notations,  $\mathcal{P}_{\text{he}}^-$  (resp.  $\mathcal{P}_{\text{bo}}^-$ ) is the image of  $\mathcal{P}_{\text{he}}^+$  (resp.  $\mathcal{P}_{\text{bo}}^+$ ) by the symmetry under the  $(O, x)$ -axis. Thus, these two “negative” parabolas both open to the bottom.

## 2.4 Some physical meaning of this classification

The potential  $\psi_{\text{he}}^{\text{red}}$  defined by

$$\psi_{\text{he}}^{\text{red}}(r) := \frac{\mu}{2b} - \frac{\mu}{b + \sqrt{b^2 + r^2}}$$

is the original isochrone potential discovered by Michel Hénon. Similarly, the potential

$$\psi_{\text{bo}}^{\text{red}} := -\frac{\mu}{2b} + \frac{\mu}{b + \sqrt{b^2 - r^2}}$$

defines another type of isochrone potential. The index *bo* means *bounded potential*. Indeed, from the above formula the mappings  $r \mapsto \psi_{\text{bo}}^{\text{red}}(r) + \epsilon$  are only defined for bounded values of

$$r \in \mathcal{D}_{\psi_{\text{bo}}} = [0, b]. \quad (17)$$

The fact that such potentials are associated with a *bounded* system give them special features which are very different from the three other types of isochrone potentials. Up to our knowledge, such bounded potentials do not seem to have appeared in the literature before.

The potential of Michel Hénon is equivalent to a Keplerian one when  $r \rightarrow \infty$ . Using relation (12), we can readily see that  $V^+(q) \sim q$  when  $q \rightarrow 0$ . The roots product in (13) then implies  $V^-(q) \sim q^{-1}$  in the same limit. Then both  $\psi_{\text{bo}}^{\text{red}}$  and  $\psi_{\text{he}}^{\text{red}}$  come from  $V^+$ . Hence we can assert that they are harmonic near their center:  $\psi_{\text{bo}}^{\text{red}} \sim \psi_{\text{he}}^{\text{red}} \sim \psi_{\text{ha}}$  when  $r \rightarrow 0$ .

From a physical point of view,  $\epsilon$ -transvections  $J_{\epsilon,0} : \psi \rightarrow \psi + \epsilon$  add a constant to the potential, hence they do not change anything for the dynamics in the considered potential, changing only the value of the energy attributed to the trajectories.

When the  $\lambda$ -gauge  $J_{0,\lambda} : \psi \rightarrow \psi + \frac{\lambda}{2r^2}$  is applied to a reduced potential, it makes it divergent as  $r^{-2}$  when  $r \rightarrow 0$ . As we said at the beginning of sec. 2.2, such transformations correspond to a change of the value of the angular momentum in the corresponding isochrone orbit.

Geometrically, when the physical convex part of the parabola starts from the origin, then, when  $r \rightarrow 0$ , the corresponding potential is finite (if it is  $\psi_{bo}$ ,  $\psi_{he}$  or  $\psi_{ha}$ ) or diverges like  $r^{-1}$  (if it is Keplerian). This behavior is not perturbed by  $\epsilon$ -transvections. In all other cases isochrone potentials diverge like  $r^{-2}$  when  $r \rightarrow 0$ ; but, using a  $\lambda$ -translation, we can manage this physical problem.

These remarks enable us to define three classes of isochrone potentials. They are classes of equivalence under the action of  $J_{\epsilon,\lambda}$  affine transformations as detailed in sec. 2.5. Definition 2 sets their names in addition to the name of the four isochrone potential types.

**Definition 2** 1. We call the four isochrone potentials

$$\begin{aligned} \psi_{ke}(r) &= -\frac{\mu}{r}, & \psi_{ha}(r) &= \frac{1}{2}\omega^2 r^2, \\ \psi_{he}(r) &= -\frac{\mu}{b + \sqrt{b^2 + r^2}}, & \text{and } \psi_{bo}(r) &= \frac{\mu}{b + \sqrt{b^2 - r^2}}, \end{aligned}$$

the Kepler, the harmonic, the Hénon and the bounded potential, respectively.

2. We call *reduced isochrone* potentials  $\psi_{iso}^{red}$  one of the four potentials

$$\psi_{ke}, \psi_{ha}, \psi_{he}^{red} = J_{\frac{\mu}{2b},0}(\psi_{he}) = \frac{\mu}{2b} + \psi_{he} \text{ or } \psi_{bo}^{red} = J_{-\frac{\mu}{2b},0}(\psi_{bo}) = -\frac{\mu}{2b} + \psi_{bo}.$$

3. We call *physical isochrone* potentials  $\psi_{iso}^{phy}$  the result of a transvection applied to a reduced isochrone:  $\psi_{iso}^{phy} = J_{\epsilon,0}(\psi_{iso}^{red}) = \psi_{iso}^{red} + \epsilon$ .

4. We call *gauged isochrone* potentials  $\psi_{iso}^{gau}$  the result of a vertical translation applied to a physical isochrone:  $\psi_{iso}^{gau} = J_{0,\lambda}(\psi_{iso}^{phys}) = \psi_{iso}^{phys} + \frac{\lambda}{2r^2}$ .

Physical isochrones possess interesting physical properties which are presented and studied in section 4. They all confine a finite mass in a finite radius  $r < \mathcal{R}$  (see equation (9), page 8). Reduced isochrones are special cases of physical ones: their parabolas pass through the origin with a horizontal or a vertical tangent.

Due to their  $r^{-2}$  divergence in the potential, when  $\lambda \neq 0$ , gauged isochrone potentials have an infinite mass at their center and thus possess poor physical meaning. However, they are essential to the completeness of the isochrone set.

## 2.5 The affine group action on the Isochrone set

Let us denote respectively  $\mathbb{I}_{pot}$  and  $\mathbb{I}_{par}$  the set of isochrone potentials and parabolas. These two sets are in bijection and theorem 1 states that, from a mathematical point of view, they are four-dimensional manifolds. As a matter



of fact, each isochrone potential is uniquely determined by four real parameters  $(\mu, b, \epsilon, \lambda)$  with  $\mu > 0$ ,  $b \geq 0$  and  $(\epsilon, \lambda) \in \mathbb{R}^2$  — n.b. for  $\psi_{bo}$ ,  $b > 0$ .

We have also seen that the two-dimensional affine group  $\mathbb{A} \simeq (\mathbb{R}^2, +)$ , generated by the affine transformations  $J_{\epsilon, \lambda}$  with  $(\epsilon, \lambda) \in \mathbb{R}^2$ , acts on both sets, either on potentials or on the corresponding parabolas. Since the dimension of  $\mathbb{A}$  is less than the dimension of  $\mathbb{I}_{pot}$  and  $\mathbb{I}_{par}$  ( $2 < 4$ ), the action is not transitive and each group orbit  $\mathbb{A} \cdot \psi$  or  $\mathbb{A} \cdot \mathcal{P}$  for corresponding potential  $\psi$  or parabola  $\mathcal{P}$  is a two-dimensional sub-manifold of  $\mathbb{I}_{pot}$  or  $\mathbb{I}_{par}$ . This translates the second part of theorem 1: we have four types of group orbits under the action of  $\mathbb{A}$ , one for each type of isochrone potential.

Let us now see more precisely this action of the affine group and its corresponding group orbits.

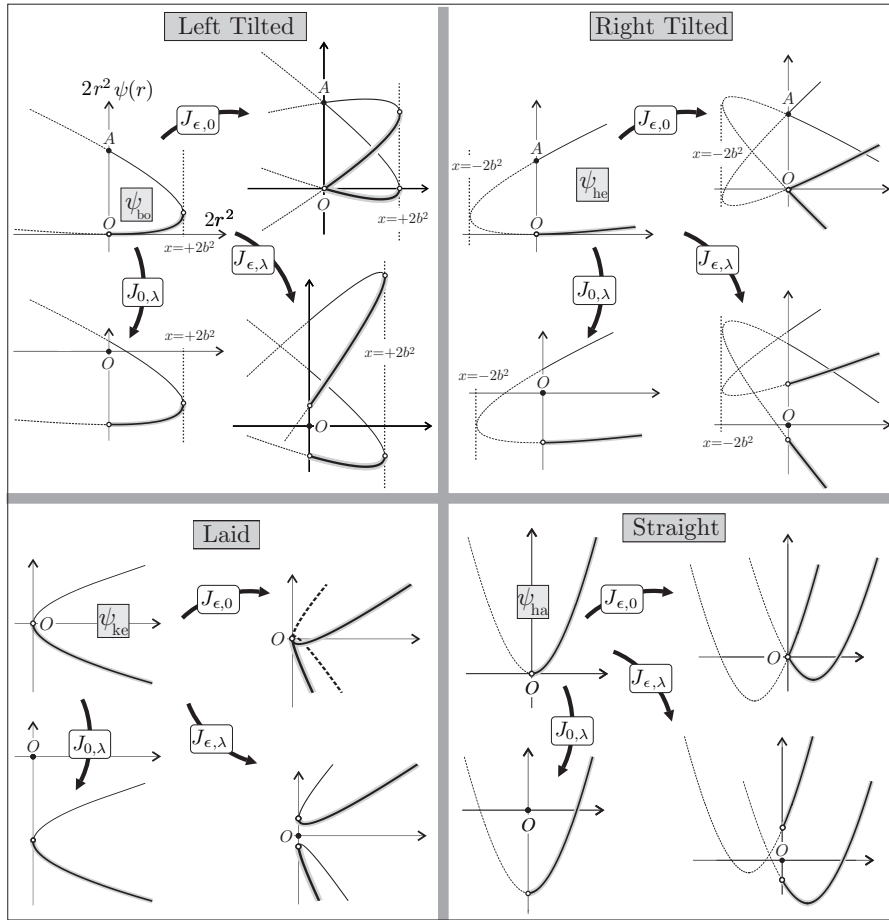


**Fig. 5** The action of affine transformations on reduced parabolas and their corresponding potentials.

Each parabola is associated with an isochrone potential and vice-versa. Each isochrone parabola belongs to one of the four classes of reduced parabolas we have presented in figure 3 and is associated with one of the four reduced isochrone potentials made explicit in theorem 1. In order to geometrically understand the morphing of parabolas associated with the action of affine transformations, we propose the general picture of figure 5.

We do not represent in this figure either the bottom-oriented straight parabolas or the left-oriented laid ones because they respectively correspond to decreasing and non-physical potentials. We specify that it is always possible to have  $(Oy)$ -axis crossing the parabola: this corresponds to a horizontal translation of the parabola associated with a good choice of the origin of the physical referential.

Transvections correspond to  $J_{\epsilon,0}$ . They are associated with a swivel combined with a deformation of the parabola: the points of the parabola lying on the  $(Oy)$ -axis are invariant as is the abscissa of the vertical tangent.

General affine transformations  $J_{\epsilon,\lambda}$  swivel, deform and translate a reduced parabola. They affect both the energy and the angular momentum of the considered isochrone orbit. Any parabola obtained from the action of  $J_{\epsilon,\lambda}$  on a reduced one corresponds to an isochrone potential in the same group orbit of the reduced potential under the action of the Affine Group. In this sense we can claim that there are only four different isochrone potentials up to an affinity on its parabola.

We note that relations exist between the isochrone potentials. As a matter of fact,  $\psi_{ke}$  and  $\psi_{ha}$  come from  $\psi_{he}$  when  $b \rightarrow 0$  and  $b \rightarrow +\infty$ , respectively. Furthermore, known relations exist between  $\psi_{ke}$  and  $\psi_{ha}$ , such as the Bohlén transformation ([7], [3], [31], see also the footnote 3 p.20) which maps the harmonic orbits onto Keplerian ones and vice versa. All these relations are not in the scope of the affine group action and do not affect the parameters  $(\mu, b)$  or  $\omega$  of the concerned potentials.

Nevertheless, making use of rotations  $R_\theta$  of an angle  $\theta$  in the  $(x, y)$ -frame and starting, for instance, from the laid Kepler parabola, we can obtain a new parabola with an arbitrarily oriented axis of symmetry. Then, acting with  $J_{\epsilon,\lambda}$ , we can recover the corresponding reduced parabola in one of the four families. This operation is graphically illustrated in figure 6 in the case of the morphing from the Kepler isochrone to the Hénon isochrone.

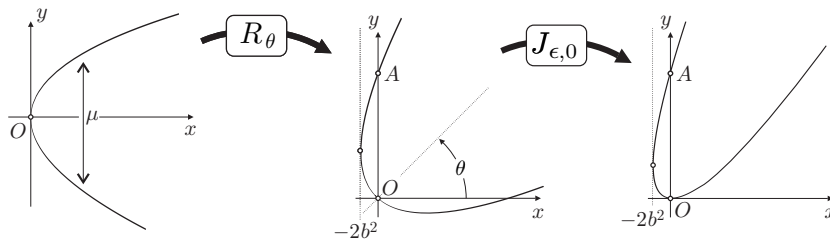


**Fig. 6** Rotation and transvection of the Kepler parabola to the Hénon one.

Varying the unique parameter  $\mu$  of the Kepler potential, written as

$$y_{\text{ke}}(x) = -\mu\sqrt{2x} \quad (18)$$

in Hénon's variables, the aperture of its laid parabola varies and produces a variation of the  $b$  parameter of the Hénon potential corresponding to the negative part of the rotated parabola. Using this process one can easily understand that when  $\theta \in (-\frac{\pi}{2}, +\frac{\pi}{2})$ , we recover a Hénon potential  $\psi_{\text{he}}$ ; when  $\theta \in (\frac{\pi}{2}, +\frac{3\pi}{2})$ , we recover the bounded potential  $\psi_{\text{bo}}$ ; and for  $\theta = +\frac{\pi}{2}$ , we obtain the harmonic  $\psi_{\text{ha}}$  from the Kepler potential  $\psi_{\text{ke}}$ . More generally, any isochrone potential is contained in the group orbit of a Kepler potential under the action of the group  $\text{SO}(2) \ltimes \mathbb{A}$ .

As we have completely classified  $\mathbb{I}_{\text{pot}}$  and  $\mathbb{I}_{\text{par}}$ , we can now return to the study of isochrone PRO's. We will see that relevant isochrone rotations are not Euclidian but hyperbolic.

### 3 Isochrone orbits and isochrone transformations

#### 3.1 Introduction and motivation

From the geometrical classification of the isochrone potentials established through the action of the Affine Group in section 2, we propose now to investigate isochrone orbits<sup>2</sup>.

For this purpose, we generalize a transformation that originates in the work of Newton, Karl Bohlin [7] and Donald Lynden-Bell [30] who recently passed away and to whom we dedicate this work. He explored a remarkable property of Michel Hénon's isochrone, namely  $\psi_{\text{he}}$  is equivalent to a harmonic potential at small distances and to a Keplerian potential at larger ones, see section 4. In those two potentials, the orbits are closed ellipses. Newton showed, in the later edition of the Principia, how to map a Keplerian elliptical orbit onto a harmonic one and vice versa. His methods relied on a total exchange of energy and potential between a Kepler and a Hooke system. Pointing out a freedom that involves partial exchange of energy and potential, Donald Lynden-Bell derived Hénon's isochrone as a convex interpolation of Kepler and Hooke potentials. Let us detail now their mathematical analysis and generalize it to isochrone orbits transformations.

##### 3.1.1 Isochrone orbits transformations

A Periodic radial orbit (PRO)  $r_0(t_0)$  in a radial potential  $\psi_0$  is governed by the ordinary differential equation

$$\frac{1}{2} \left( \frac{dr_0}{dt_0} \right)^2 + \frac{\Lambda_0^2}{2r_0^2} = \xi_0 - \psi_0(r_0).$$

In Hénon variables  $x_0 = 2r_0^2$  and  $y_0 = x_0\psi_0(x_0)$ , it can be written as

$$\frac{1}{16} \left( \frac{dx_0}{dt_0} \right)^2 + \Lambda_0^2 = x_0\xi_0 - y_0(x_0). \quad (19)$$

---

<sup>2</sup> When not specified, orbit refers to the trajectory of the considered test particle in the considered potential and no more to the group orbit of a potential or parabola under a group action.

Since the force derived from a radial potential is radial, the motion of a test particle takes place in a fixed plane and this particle is described by its polar coordinates  $(r_0, \varphi_0)$  in this plane.

When the potential is isochrone,  $y_0$  is a parabola. This property is preserved by linear transformations of parabolas (see lemma 8 in appendix C) and consequently for the orbits they contain. Placing the origin of the  $(x, y)$ -plane at the center of the system described by  $\psi_0$ , linear transformations relate isochrone orbits together. There exists then a change of variables  $(r_0, t_0) \mapsto (r_1, t_1)$  mapping an isochrone orbit onto another one that satisfies an orbital equation in the new potential  $y_1$ , i.e.

$$\frac{1}{16} \left( \frac{dx_1}{dt_1} \right)^2 + A_1^2 = x_1 \xi_1 - y_1(x_1). \quad (20)$$

As Donald Lynden-Bell explained ([31] sect. 3 or [30] sect. 2), it is convenient to study orbits of identical angular momentum

$$A_1 = A_0 = A. \quad (21)$$

This hypothesis allows one to get the same Kepler's area law for both orbits, in their respective radial potentials.

At this point, no constraints specify how each of the three remaining terms  $\left( \frac{dx_0}{dt_0} \right)^2$ ,  $x_0 \xi_0$ , and  $y_0$  in (19) is transformed in the mapping. For instance, the Bohlin transformation (see [7] for the original reference or [3] for a modern presentation) consists of a full exchange between energy and potential terms. As underlined by Lynden-Bell, the exchange can also be partial: only part of the potential term  $y_0$  is then mapped onto the energy  $\xi_1$  and vice versa. We thus propose to conserve

$$x_1 \xi_1 - y_1(x_1) = x_0 \xi_0 - y_0(x_0). \quad (22)$$

The two conditions (21) and (22) imply

$$\frac{dx_1}{dt_1} = \frac{dx_0}{dt_0} \quad \text{and} \quad 2A = x_0 \frac{d\varphi_0}{dt_0} = x_1 \frac{d\varphi_1}{dt_1} \quad (23)$$

for the radial and angular velocities of the orbits in the mapping.

The more general linear transformation of  $\mathbf{w} = (\xi x, y)^\top$  satisfying the constraint (22) is given by

$$\mathbf{w}_1 = B_{\alpha, \beta}(\mathbf{w}_0) \quad \text{with} \quad B_{\alpha, \beta} = \begin{bmatrix} \alpha & \beta \\ \alpha - 1 & \beta + 1 \end{bmatrix}, \quad (\alpha, \beta) \in \mathbb{R}^2. \quad (24)$$

Lynden-Bell transformation only depends on one parameter with  $\beta = 1 - \alpha$ . From now on, we will assume  $\det(B_{\alpha, \beta}) = \alpha + \beta \neq 0$  because the corresponding singular transformation leads to constant potentials or not well-defined image orbits. As a consequence,  $B_{\alpha, \beta}$  will be invertible and can be used to change the reference frame. In this case we call  $B_{\alpha, \beta}$  a *bolst* in the general case or an *ibolst* when it is symmetric. Reasons for these names will become clear later.

### 3.1.2 The bolst as the generalized Bohlin transformation

A bolst  $B_{\alpha,\beta}$  maps two orbits in two isochrone potentials. It induces a change of time which can be made explicit: using (23) and (24) we get

$$\frac{dt_1}{dt_0} = \frac{dx_1}{dx_0} = \frac{\alpha\xi_0}{\xi_1} + \frac{\beta}{\xi_1} \frac{dy_0}{dx_0}. \quad (25)$$

We assume  $\xi_1 \neq 0$  since associated orbits are not well-defined in the coordinates of  $\mathbf{w}$ . To deal with  $\xi_1 = 0$  one may apply first a transvection  $J_{\epsilon,0}$  to  $\mathbf{w}$ , then study the orbit with  $\xi_1 + \epsilon \neq 0$ .

In order to ensure a bijective time transformation  $t_0 \rightarrow t_1(t_0)$ , we need to impose a fixed sign on  $\frac{dt_1}{dt_0}$ . For instance, we assume it to be positive. Combining its expression (25) with the second condition of (23), the time evolution can be expressed in terms of the polar angles of the two orbits in their respective planes of motion. They are linked through

$$\left[ \frac{\alpha\xi_0}{\xi_1} + \frac{\beta}{\xi_1} \frac{y_0}{x_0} \right] \frac{d\varphi_1}{d\varphi_0} = \frac{\alpha\xi_0}{\xi_1} + \frac{\beta}{\xi_1} \frac{dy_0}{dx_0} > 0. \quad (26)$$

As we will see below, this ODE gives  $\varphi_1$  as a function of  $\varphi_0$ , i.e.  $\varphi_1(\varphi_0)$ , when  $y_0(x_0)$  is specified. When it is solved, the orbit can be plotted in polar coordinates  $(x_1, \varphi_1)$ . In the next proposition we solve this equation when a bolst is applied to a Keplerian orbit. In theorem 2, we call system a potential - orbit couple.

**Theorem 2** *Only the harmonic and Keplerian potentials can exchange their radial orbits with a linear change of polar angle. The transformation of a Kepler system into a scaled Kepler system is given by  $B_{\alpha,0}$ . On the other hand,  $B_{0,\beta}$  maps a Kepler system onto a harmonic one by fully exchanging the energy and potential. This is the classical Bohlin transformation<sup>3</sup>.*

*Otherwise, when  $\alpha\beta \neq 0$ , the image of a Keplerian PRO by  $B_{\alpha,\beta}$  is an isochrone orbit. Its azimuthal angle is given by*

$$\varphi_1(\varphi_0) = \frac{\varphi_0}{2} + \frac{\chi}{\sqrt{(1+\chi)^2 - e^2}} \arctan \left[ \sqrt{\frac{1+\chi-e}{1+\chi+e}} \tan \left( \frac{\varphi_0}{2} \right) \right] \quad \text{with } \chi = \frac{p\alpha|\xi_0|}{\mu\beta}, \quad (27)$$

where  $p$  and  $e$  are respectively the semilatus rectum and excentricity of the primary Keplerian orbit. The expression holds when  $\alpha \rightarrow 0$  and for the neutral bolst  $B_{\alpha,0}$  when  $\beta \rightarrow 0$ . The precession  $\Delta\varphi_1$  of the transformed polar angle during the transfer from the periastron to the apoastron and back is given by

$$\Delta\varphi_1 = \pi \left( 1 + \frac{\chi}{\sqrt{(1+\chi)^2 - e^2}} \right).$$

*Proof* Assume potential  $\psi_0$  to be  $\psi_{\text{ke}}$ . If the primary orbit is a PRO, then the radial distance is known by

$$\frac{1}{r_0} = \frac{1 + e \cos \varphi_0}{p},$$

---

<sup>3</sup> This transformation is also known as the transformation of Levi-Civita [27] and was already introduced by C. MacLaurin in [32] and then E. Goursat in [17] as excellently remarked by Alain Albouy and Niccolò Guicciardini.

where  $p$  and  $e$  are respectively the semilatus rectum and the excentricity of the Keplerian elliptic orbit of energy  $\xi_0 < 0$  that we consider. Moreover, from equation (18), we have  $y_0(x_0) = -\mu\sqrt{2x_0}$ . Hence,

$$\frac{y_0}{x_0} = \psi_0 = -\frac{\mu}{r_0} \text{ and } \frac{dy_0}{dx_0} = -\frac{\mu}{\sqrt{2x_0}} = -\frac{\mu}{2r_0}.$$

In this case, the ODE (26) becomes

$$\left[ \alpha\xi_0 - \frac{\mu\beta}{p} (1 + e \cos \varphi_0) \right] \frac{d\varphi_1}{d\varphi_0} = \alpha\xi_0 - \frac{\mu\beta}{2p} (1 + e \cos \varphi_0)$$

for  $\xi_1 \neq 0$ . Two cases appear to be trivial:

1. When  $\alpha = 0$  and  $\beta \neq 0$ , then

$$\frac{d\varphi_1}{d\varphi_0} = \frac{1}{2}.$$

The system (24) can be directly inverted and gives

$$\begin{cases} r_1^2 = -\frac{\beta\mu}{\xi_1} r_0, \\ \psi_1(r_1) = \beta_1 + \frac{1}{2}\omega_1 r_1^2, \end{cases} \quad \text{where } \omega_1^2 = \frac{2|\xi_0|\xi_1^2}{\mu^2\beta^2} \text{ and } \beta_1 = \frac{\beta+1}{\beta}\xi_1.$$

This duality between the harmonic and the Keplerian potentials is the same as that described by a Bohlin transformation [19]. In order to get a real  $r_1$ , the quantity  $\frac{\beta}{\xi_1}$  must be negative. The angle  $\varphi_0$  of the Keplerian orbit is twice that of the corresponding  $\varphi_1$  of the harmonic one, as represented in figure 7. The focus  $F$  of the Keplerian ellipse is the center of the harmonic one.

2. When  $\alpha \neq 0$  and  $\beta = 0$ , then

$$\frac{d\varphi_1}{d\varphi_0} = 1.$$

The system can still be inverted as

$$\begin{cases} r_1^2 = \frac{\alpha\xi_0}{\xi_1} r_0^2, \\ \psi_1(r_1) = \alpha_1 - \frac{\mu_1}{r_1}, \end{cases} \quad \text{where } \alpha_1 = \frac{(\alpha-1)}{\alpha}\xi_1 \text{ and } \mu_1 = \mu\sqrt{\frac{\xi_1}{\alpha\xi_0}}.$$

The quantity  $\frac{\xi_1}{\alpha\xi_0}$  must be positive when  $x_{0,1} = 2r_{0,1}^2 > 0$ . This transformation maps the primary Keplerian ellipse onto a scaled confocal one. The two moving points are always aligned with the common focus of the two ellipses. As  $\xi_1$  needs to be negative to ensure bounded bolsted orbit, this imposes  $\alpha > 0$ .

These two special cases are represented in figure 7.

To show that only the harmonic and Keplerian potentials can exchange their radial orbit with a linear change of polar angles, we assume that

$$\varphi_1(t_1) = m\varphi_0(t_0) \quad \text{with } m = \text{cst.} \quad (28)$$

Combining (23) with the derivative of (28) one can verify that  $y_0$  satisfies the ODE

$$\frac{dy}{dx_0} - \frac{m}{x_0}y = \xi_0 \frac{\alpha}{\beta} (m-1), \quad (29)$$

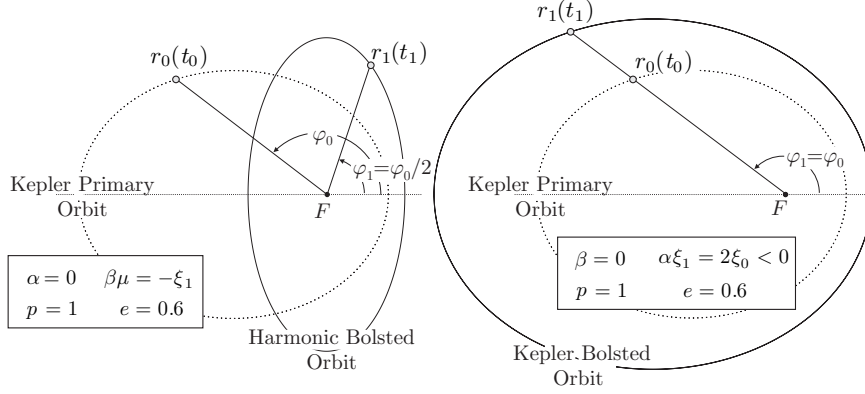


**Fig. 7** The transformation  $B_{0,\beta}$  of a Keplerian PRO gives a harmonic PRO when  $\beta\xi_1 < 0$ , as represented on the left panel. The transformation  $B_{\alpha,0}$  of a Keplerian PRO gives a Keplerian PRO when  $\alpha > 0$  and  $\xi_1 < 0$ , as represented on the right panel.

which holds for  $\beta \neq 0$ . The solution of (29) is given by

$$y_0(x_0) = kx_0^m - \xi_0 \frac{\alpha}{\beta} x_0.$$

But  $y_0$  must describe a parabola, so either

- $m = 1$  or  $m = 0$ . Then the potential is constant or constant with a gauge, and no PRO exists.
- $m = \frac{1}{2}$ . Then  $y_0$  represents a Keplerian potential up to a constant. Inserting the solution  $y_0$  in  $(\xi_1 x_1, y_1)^\top$ ,  $y_1$  is a harmonic potential with a constant.
- $m = 2$ . Then  $y_0$  represents a harmonic potential up to a constant and  $y_1$  a transvected Keplerian potential.

Let us examine now the more general case when  $\alpha\beta \neq 0$ . The ODE for phases is written as

$$\frac{d\varphi_1}{d\varphi_0} = \frac{N(\varphi_0)}{D(\varphi_0)} \quad \text{where} \quad \begin{cases} N(\varphi_0) = \frac{dx_1}{dx_0} = \frac{1}{\xi_1} \left[ \alpha\xi_0 - \frac{\mu\beta}{2p} (1 + e \cos \varphi_0) \right], \\ D(\varphi_0) = \frac{x_1}{x_0} = \frac{1}{\xi_1} \left[ \alpha\xi_0 - \frac{\mu\beta}{p} (1 + e \cos \varphi_0) \right]. \end{cases} \quad (30)$$

We first remark that the denominator function  $\varphi \rightarrow D(\varphi)$  is strictly positive as both  $x_0 = 2r_0^2$  and  $x_1 = 2r_1^2$  are positive functions. In (25) we have seen that the sign of  $N(\varphi)$  cannot change; as a consequence the function  $\varphi_0 \rightarrow \varphi_1(\varphi_0)$  is monotone. In our hypothesis where  $N(\varphi) \geq 0$ ,  $\varphi_1$  is an increasing function of  $\varphi_0$ . After a little rearrangement, from (30) we obtain

$$\varphi_1 = \int_0^{\varphi_0} \frac{\eta + \cos \varphi}{\delta + 2 \cos \varphi} d\varphi \quad \text{where} \quad \eta = \frac{\mu\beta - 2p\alpha\xi_0}{\mu\beta e} \geq 1 \quad \text{and} \quad \delta = \frac{2\mu\beta - 2p\alpha\xi_0}{\mu\beta e} > 2.$$

We notice that the particular case when the primary Keplerian orbit is circular, i.e.  $e = 0$ , linearly links  $\varphi_0$  and  $\varphi_1$ . The integral for  $\varphi_1$  can be made explicit: introducing  $u = \tan(\varphi/2)$  we get  $\cos \varphi = \frac{1-u^2}{1+u^2}$ ,  $d\varphi = \frac{2du}{1+u^2}$  and thus

$$\varphi_1 = 2 \int_0^{u_0} \frac{\ell + 2 + \ell u^2}{(m + 4 + mu^2)(1 + u^2)} du \quad \text{where} \quad \begin{cases} \ell = \eta - 1 \geq 0, \\ m = \delta - 2 > 0. \end{cases}$$

A partial fraction decomposition gives

$$\varphi_1 = \int_0^{u_0} \frac{1}{1+u^2} du + \frac{2\ell-m}{\sqrt{m(m+4)}} \int_0^{v_0} \frac{dv}{1+v^2},$$

where  $v = \sqrt{\frac{m}{m+4}}u$ . The integration leads to

$$\varphi_1 = \frac{\varphi_0}{2} + \frac{2\ell-m}{\sqrt{m(m+4)}} \arctan \left[ \sqrt{\frac{m}{m+4}} \tan \left( \frac{\varphi_0}{2} \right) \right],$$

and so

$$\varphi_1 = \frac{\varphi_0}{2} + \frac{\chi}{\sqrt{(1+\chi)^2 - e^2}} \arctan \left[ \sqrt{\frac{1+\chi-e}{1+\chi+e}} \tan \left( \frac{\varphi_0}{2} \right) \right] \quad \text{with } \chi = \frac{p\alpha|\xi_0|}{\mu\beta}.$$

If  $\alpha = 0$  we would recover the relation  $\varphi_1 = \frac{\varphi_0}{2}$  previously mentioned. In the same way, when  $\beta \rightarrow 0$ , then  $\varphi_1 \rightarrow \varphi_0$ . When the bolsted orbit is a PRO, we can easily compute the increment of the azimuthal angle  $\Delta\varphi$  during the transfer from  $r_a$  to  $r_p$  and back. In the Keplerian case, from figure 8, we see that the transfer for  $r_0 : r_{0,p} \rightarrow r_{0,a}$  corresponds to  $\varphi_0 : 0 \rightarrow \pi$ . Hence, using (27) one gets

$$\begin{aligned} \varphi_1 : 0 \rightarrow \frac{1}{2}\Delta\varphi_1 &= \frac{\pi}{2} + \frac{\chi}{\sqrt{(1+\chi)^2 - e^2}} \arctan(\infty) \\ &= \frac{\pi}{2} \left( 1 + \frac{\chi}{\sqrt{(1+\chi)^2 - e^2}} \right). \end{aligned}$$

Since

$$p = \frac{\Lambda^2}{\mu} \quad \text{and} \quad e = \sqrt{1 + \frac{2\Lambda^2\xi_0}{\mu^2}},$$

we see that  $\Delta\varphi_1$  depends on  $\Lambda^2$  but not on  $\xi_1$ . This is a characterization of isochrone orbits (see theorem 6 in appendix A). Given a point  $(\varphi_0, r_0)$  on the primary Keplerian ellipse, its image on the bolsted orbit has a polar angle  $\varphi_1$  given by the formula (27) and a distance  $r_1$  given by the relation (24), i.e.

$$x_1 = 2r_1^2 = 2\alpha \frac{\xi_0}{\xi_1} r_0^2 - 2\mu \frac{\beta}{\xi_1} r_0 \implies r_1^2 = \frac{\alpha\xi_0 r_0^2 - \mu\beta r_0}{\xi_1}.$$

When  $\alpha, \beta$  and  $\xi_1$  are such that  $r_1^2 > 0$  for all  $r_0$  on the Keplerian orbit, this corresponds to an isochrone PRO.  $\square$

Theorem 2 shows that any Keplerian PRO can be transformed into a particular isochrone one by a suitable bolst  $B_{\alpha,\beta}$ . When  $\alpha = 0$ , the bolst coincides with a Bohlin transformation. In the other cases, it generalizes it; we have plotted an example of such a bolst in figure 8.

Reciprocally, we will see in sec. 3.2.5 that any isochrone PRO could be connected to a Keplerian ellipse.



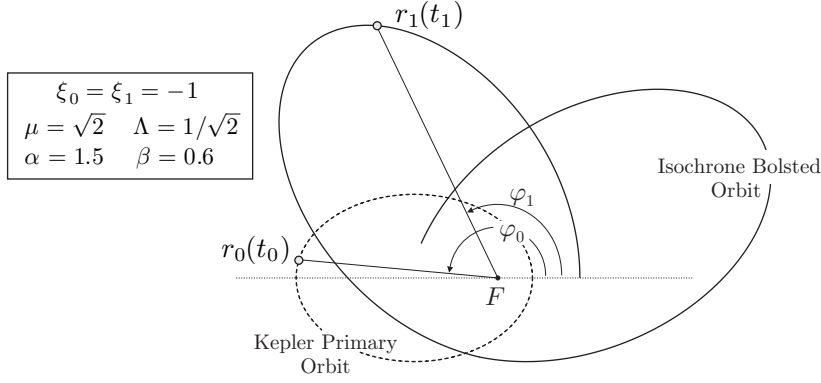


**Fig. 8** The  $\alpha = 1.5$  and  $\beta = 0.6$  bolst of a Keplerian ellipse ( $e \simeq 0.7$ ;  $p \simeq 0.35$ ) which gives an isochrone orbit with the same energy ( $\xi_0 = \xi_1 = -1$ ).

### 3.1.3 The bolst, a key to isochrony

Geometrically, a Keplerian parabola in a frame  $\mathcal{R}_O = (O, \mathbf{i}, \mathbf{j})$  is laid (see sec. 2.2, p. 10), i.e. its tangent at the origin is  $\mathbb{R}\mathbf{j}$  and its axis of symmetry is  $\mathbb{R}\mathbf{i}$ . According to lemma 9 in appendix C, its image by a bolst  $B_{\alpha, \beta}$  remains laid, and so Keplerian, in the image frame  $B_{\alpha, \beta}(\mathcal{R}_O)$ . But, in  $\mathcal{R}_O$ , the image parabola has two distinct intersections with  $\mathbb{R}\mathbf{j}$  and thus appears to be a non-Keplerian isochrone. Therefore, it appears that to be or not to be Keplerian depends on the choice of the reference frame. This is an aspect of the isochrone relativity that we will discuss in what follows.

For this discussion, we will not consider the general case of any bolst  $B_{\alpha, \beta}$ . With only technical restrictions, we will consider the case where the bolst is symmetric: according to (24),  $B_{\alpha, \beta}$  is a symmetric matrix if and only if  $\alpha - 1 = \beta$ . Introducing the parameter  $\gamma = \alpha + \beta$  which is the variable eigenvalue of  $B_{\alpha, \beta}$ , with the other 1, the general bolst  $B_{\alpha, \beta}$  then becomes the symmetric  $B_\gamma$  that we call an *ibolst* for which the isochrone relativity appears to be clear.

We have seen that bolsts generalize the Bohlin transformation, and we will see now that ibolsts are the boosts of the isochrone relativity. Names appear to be clarified: *bolst* stands for bohlin boost and *ibolst* for symmetric bohlin boost.

## 3.2 Isochrone relativity

The special theory of relativity has two pillars:

1. The Einstein principle of special relativity imposes that the laws of physics can be written in the same way in all Galilean frames;
2. The length of any space-time interval is conserved through changes of Galilean frames, aka Lorentz frames.

These principles make time and length relative to a given Galilean frame. These two physical quantities are linearly exchanged during changes of Galilean frames.

In the same way, the linear exchange between  $\xi x$  and  $y$  proposed in the previous section conserves the “*isochrone interval*”  $\xi x - y$  in equation (22). This

conservation is imposed by that of the fundamental orbital law (19) which renders the conservation of the energy along the orbit. The linearity of the transformation is associated with the isochrony preservation. The conservations of the “isochrone interval” and isochrone law are the two pillars of the isochrone relativity.

For the sake of simplicity, we restrict our attention to symmetric exchanges between  $\xi x$  and  $y$ : the bolst  $B_{\alpha,\beta}$  is then reduced to the ibolst  $B_{\gamma=\alpha+\beta}$ , choosing  $\alpha - 1 = \beta$ ,

$$B_\gamma = \frac{1}{2} \begin{bmatrix} \gamma + 1 & \gamma - 1 \\ \gamma - 1 & \gamma + 1 \end{bmatrix}.$$

### 3.2.1 The ibolst Algebra

Let  $\mathcal{R} = (\mathbf{i}, \mathbf{j})$  be the canonical basis of  $\mathbb{R}^2$ . Any vector  $\mathbf{z} \in \mathbb{R}^2$  has affine coordinates  $(z_1, z_2)$  in the frame  $\mathcal{R}_O = (O, \mathbf{i}, \mathbf{j})$ , i.e. there exists a unique point  $Z$  in the  $Oz_1z_2$  plane such that  $\mathbf{z} = \overrightarrow{OZ} = z_1\mathbf{i} + z_2\mathbf{j}$ . We do not use the usual upper index for contravariant components because, as we are in  $\mathbb{R}^2$ , we do not use Einstein notation for sums and we prefer to conserve the upper index for powers. The orthonormality is defined in the Euclidian sense, i.e. with natural notations

$$\|\mathbf{z}\|^2 = (\mathbf{z}|\mathbf{z}) = z_1^2 + z_2^2 \quad \text{then} \quad (\mathbf{i}|\mathbf{i}) := \|\mathbf{i}\|^2 = \|\mathbf{j}\|^2 =: (\mathbf{j}|\mathbf{j}) = 1 \quad \text{and} \quad (\mathbf{i}|\mathbf{j}) = 0.$$

The  $\mathcal{R}$  basis is then orthonormal for the Euclidian scalar product. We will also use the Minkowski scalar product for which

$$\|\mathbf{z}\|_m^2 = (\mathbf{z}|\mathbf{z}) = z_1^2 - z_2^2 \quad \text{then} \quad \langle \mathbf{i}|\mathbf{i} \rangle := \|\mathbf{i}\|_m^2 = 1, \quad \langle \mathbf{j}|\mathbf{j} \rangle := \|\mathbf{j}\|_m^2 = -1 \quad \text{and} \quad \langle \mathbf{i}|\mathbf{j} \rangle = 0.$$

Consider the two eigenvectors  $\mathbf{k} = \frac{1}{\sqrt{2}}(\mathbf{i} - \mathbf{j})$  and  $\mathbf{l} = \frac{1}{\sqrt{2}}(\mathbf{i} + \mathbf{j})$  of the ibolst  $B_\gamma$  such that

$$B_\gamma(\mathbf{k}) = \mathbf{k} \quad \text{and} \quad B_\gamma(\mathbf{l}) = \gamma\mathbf{l}. \quad (31)$$

The basis  $\tilde{\mathcal{R}} = (\mathbf{k}, \mathbf{l})$  is just  $\mathcal{R}$  rotated by an angle of  $-\frac{\pi}{4}$ . It is thus orthonormal for the Euclidian scalar product. Moreover, we see that for the Minkowski scalar product, we have

$$\langle \mathbf{k}|\mathbf{k} \rangle = \langle \mathbf{l}|\mathbf{l} \rangle = 0 \quad \text{and} \quad \langle \mathbf{k}|\mathbf{l} \rangle = \langle \mathbf{l}|\mathbf{k} \rangle = 1. \quad (32)$$

From (31), let us remark that the set  $\mathbb{B} = \{B_\gamma, \gamma \in \mathbb{R}^*\}$  forms a commutative linear group since

$$\forall (\gamma, \gamma') \in \mathbb{R}^* \times \mathbb{R}^*, \quad B_\gamma \circ B_{\gamma'} = B_{\gamma'} \circ B_\gamma = B_{\gamma\gamma'} \in \mathbb{B}.$$

For this law,  $B_1$  is an identity element. The inverse of a transformation  $B_\gamma$  for  $\gamma \in \mathbb{R}^*$  is  $B_{\frac{1}{\gamma}}$ .

As expected, any ibolst is symmetric, i.e. for the Euclidian scalar product and for any vectors  $\mathbf{w}$  and  $\mathbf{z}$ , we have

$$(B_\gamma(\mathbf{w})|\mathbf{z}) = (\mathbf{w}|B_\gamma(\mathbf{z})). \quad (33)$$

As a matter of fact, since the matrix  $B_\gamma$  is symmetric, considering the expansion of these vectors in the basis  $\tilde{\mathcal{R}}$  noted with a tilde, we get directly from (31) that

$$\begin{aligned} (B_\gamma(\mathbf{w})|\mathbf{z}) &= (\tilde{w}_1 B_\gamma(\mathbf{k}) + \tilde{w}_2 B_\gamma(\mathbf{l})|\tilde{z}_1 \mathbf{k} + \tilde{z}_2 \mathbf{l}) = \tilde{w}_1 \tilde{z}_1 + \gamma \tilde{w}_2 \tilde{z}_2 \\ &= \tilde{z}_1 \tilde{w}_1 + \gamma \tilde{z}_2 \tilde{w}_2 = (B_\gamma(\mathbf{z})|\mathbf{w}) = (\mathbf{w}|B_\gamma(\mathbf{z})). \end{aligned}$$

However this symmetry property does not generally hold for the Minkowski scalar product.

### 3.2.2 Lengths and spaces

Let us consider  $\xi$  and  $\Lambda$  as two fixed parameters. We can define in  $\mathcal{R}_O$  the affine coordinates system ( $w_1 = \xi x, w_2 = y$ ). Using these coordinates we set

$$\mathbf{w}' = B_\gamma(\mathbf{w}).$$

The symmetry (33) of the ibolst for the Euclidian scalar product gives

$$\forall \alpha \in \mathbb{R}, (\mathbf{w}' | \alpha \mathbf{l}) = (B_\gamma(\mathbf{w}) | \alpha \mathbf{l}) = (\mathbf{w} | B_\gamma(\alpha \mathbf{l})) = \gamma(\mathbf{w} | \alpha \mathbf{l}).$$

With  $\alpha = \sqrt{2}$ , this relation corresponds to the equality

$$\xi' x' + y' = \gamma(\xi x + y). \quad (34)$$

This same symmetry, but in the direction given by  $\mathbf{k}$ , gives the conservation of the isochrone interval

$$\forall \alpha \in \mathbb{R}, (\mathbf{w}' | \alpha \mathbf{k}) = (\mathbf{w} | \alpha \mathbf{k}) \Rightarrow \xi' x' - y' = \xi x - y. \quad (35)$$

By multiplication of these two relations we get directly<sup>4</sup>

$$(\xi' x')^2 - y'^2 = \gamma \left[ (\xi x)^2 - y^2 \right]. \quad (36)$$

This relation corresponds to the fact that an ibolst is not an isometry using the Minkowskian norm

$$\langle \mathbf{w}' | \mathbf{w}' \rangle = \gamma \langle \mathbf{w} | \mathbf{w} \rangle. \quad (37)$$

As a consequence, the radial cone

$$\mathcal{C} = \left\{ \mathbf{z} \in \mathbb{R}^2, \langle \mathbf{z} | \mathbf{z} \rangle = 0 \right\}$$

is preserved by the ibolst as  $\mathcal{C} = \mathbb{R}\mathbf{k} \cup \mathbb{R}\mathbf{l}$ . Its name comes from the fact that the line  $y = \xi x$  defines a radial orbit ( $\Lambda = 0$ ) of energy  $\xi$  in the potential  $\psi(r)$ . In a Kepler potential  $\psi_{\text{ke}}(r) = -\frac{\mu}{r}$  a test particle of energy  $\xi < 0$  with a radial orbit moves on a segment from  $r_a = \frac{\mu}{|\xi|}$  at  $t = 0$  to  $r \rightarrow 0$  when  $t \rightarrow +\infty$ . As its period should be infinite, a radial orbit is not a PRO but we can say that it is a maximal time-bounded orbit.

In this relativistic formulation of the problem we can then define periodic-like vectors lying in the periodic space

$$\mathcal{P} = \left\{ \mathbf{z} \in \mathbb{R}^2, \langle \mathbf{z} | \mathbf{z} \rangle < 0 \right\}$$

and aperiodic-like vectors lying in the aperiodic space

$$\mathcal{A} = \left\{ \mathbf{z} \in \mathbb{R}^2, \langle \mathbf{z} | \mathbf{z} \rangle > 0 \right\}.$$

As the convex  $x$ -positive part of parabolas containing PRO in the coordinates system  $(\xi x, y)$  is delimited by the radial cone and exactly contained in  $\mathcal{P}$ , the names  $\mathcal{P}$  and  $\mathcal{A}$  are natural.

<sup>4</sup> The relation (35) holds for any bolst  $B_{\alpha, \beta}$ . This is not the case for (34) which requires the  $B_\gamma$ -symmetry. As a consequence, the relation (36) is simple only in the symmetric case.

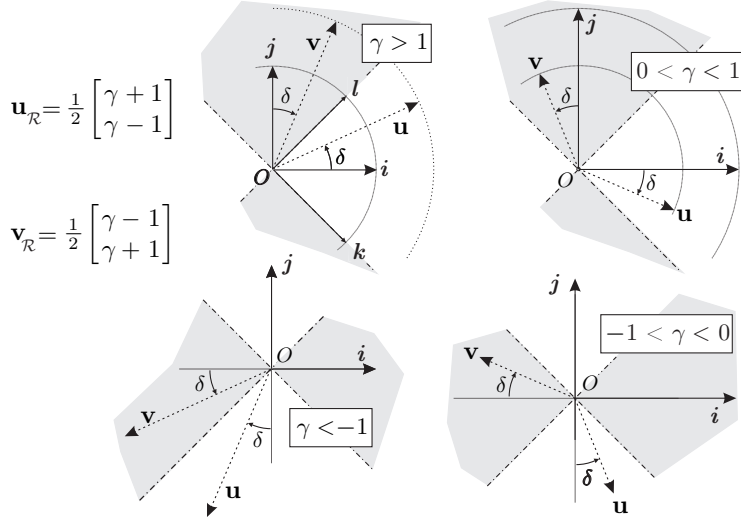


**Fig. 9** The bolsted frame  $\mathcal{R}'_O = (O, \mathbf{u}, \mathbf{v})$ , when  $\xi\xi' > 0$ . Its periodic space  $\mathcal{P}'$  is represented in grey, while its aperiodic one  $\mathcal{A}'$  is in white.

### 3.2.3 Orbits relativity

Let us define the ibolsted frame  $\mathcal{R}'_O = (O, \mathbf{u}, \mathbf{v})$  such that

$$\begin{cases} \mathbf{u} = B_\gamma(\mathbf{i}) = B_\gamma\left(\frac{\mathbf{l} + \mathbf{k}}{\sqrt{2}}\right) = \frac{\gamma\mathbf{l} + \mathbf{k}}{\sqrt{2}} \\ \text{and} \\ \mathbf{v} = B_\gamma(\mathbf{j}) = B_\gamma\left(\frac{\mathbf{l} - \mathbf{k}}{\sqrt{2}}\right) = \frac{\gamma\mathbf{l} - \mathbf{k}}{\sqrt{2}} \end{cases} \implies \mathbf{k} = \frac{\mathbf{u} - \mathbf{v}}{\sqrt{2}}. \quad (38)$$

**Definition 3** The reference frame of a given parabola  $\mathcal{P}$  is the frame  $(O, \mathbf{t}, \mathbf{n})$  where the tangent to the parabola at the origin is  $\mathcal{T}_O(\mathcal{P}) = \mathbb{R}\mathbf{t}$  and the symmetry axis is  $\mathcal{S}(\mathcal{P}) = \mathbb{R}\mathbf{n}$ .

A reference frame geometrically defines a parabola up to a scale factor. For instance,  $\mathcal{R}_O$  is the reference frame of the Keplerian parabola containing  $\psi_{\text{ke}}$  up to the scale factor  $\mu$ . According to lemma 9 in appendix C, the line  $\mathbb{R}\mathbf{v}$  is tangent to the bolsted parabola and  $\mathbb{R}\mathbf{u}$  is its symmetry axis. Thus,  $\mathcal{R}'_O$  is the reference frame of the bolsted parabola and characterizes it up to a scale factor.

All possibilities are represented in figure 9, when the primary energy  $\xi$  and the image energy  $\xi'$  share the same sign. When  $\xi\xi' < 0$ , the direction of  $\mathbf{u}$  has to be inverted.

Depending on the value of  $\gamma \neq 1$ , we can define the angle  $\delta$  given by

$$\tan \delta = \left| \frac{\gamma + 1}{\gamma - 1} \right|$$

which is useful to construct  $\mathcal{R}'_O$  from  $\mathcal{R}_O$  by simple composition of a homothety and a hyperbolic rotation (see [8] p.28 for a nice description in French or [16] for general properties of rotation in special relativity).

As with  $\mathbf{i}$  and  $\mathbf{j}$ , the two ibolsted basis vectors  $\mathbf{u}$  and  $\mathbf{v}$  have the same Euclidian norm

$$\|\mathbf{u}\|^2 = \|\mathbf{v}\|^2 = \frac{\gamma^2 + 1}{2}$$

and opposed Minkowskian lengths

$$\|\mathbf{u}\|_m = \gamma = -\|\mathbf{v}\|_m.$$

Moreover, from (32) and (38), the primary and the ibolsted basis are orthogonal in the Minkowskian scalar product:  $\langle \mathbf{i} | \mathbf{j} \rangle = \langle \mathbf{u} | \mathbf{v} \rangle = 0$ . Depending on  $\gamma$  and on the frame  $\mathcal{R}_O$  or  $\mathcal{R}'_O$  used to define the scalar product, one vector is aperiodic-like and the other is periodic-like, see figure 9.

In the canonical frame  $\mathcal{R}_O$ , using the isochrone relativity formalism and introducing the proper time  $d\tau = \xi dt$  of an orbit of energy  $\xi$  and angular momentum  $\Lambda$ , the orbital differential equation (19) in the affine coordinates  $(\xi x, y)$  can be written as

$$\frac{1}{16} \left[ \frac{d}{d\tau} (\mathbf{w} | \mathbf{i}) \right]^2 = (\mathbf{w} | \mathbf{i} - \mathbf{j}) + (\mathbf{w}_\Lambda | \mathbf{j}), \quad (39)$$

where  $\mathbf{w}_\Lambda = -\Lambda^2 \mathbf{j}$ . The vector  $\mathbf{w}$  describes the potential of parabola  $\mathcal{P}$  and the orbit which corresponds to an arc of  $\mathcal{P}$ . When this orbit is a PRO, this arc is finite. When  $\mathbf{w}$  describes a Keplerian orbit, its ibolsted image  $\mathbf{w}'$  is characterized by theorem 3.

**Theorem 3** *A vector  $\mathbf{w}'$  describes an isochrone orbit  $(\xi', \Lambda')$  on its arc of parabola if and only if it is the image, by an ibolst  $B_\gamma \in \mathbb{B}$ , of a vector  $\mathbf{w}$  which describes a Keplerian orbit  $(\xi, \Lambda)$  on a Keplerian parabola. In the Keplerian frame  $\mathcal{R}_O = (O, \mathbf{i}, \mathbf{j})$ , the orbit  $(\xi', \Lambda')$  is isochrone but generally not Keplerian. In its natural bolsted frame  $\mathcal{R}'_O = (O, \mathbf{u}, \mathbf{v})$  it is a Keplerian orbit with angular momentum  $\Lambda$ . If  $\xi \xi' > 0$  then<sup>5</sup>*

$$\Lambda' = \sqrt{\gamma} \Lambda$$

else

$$\Lambda' = \Lambda.$$

*Proof* In the affine coordinate system  $(w_1 = |\xi|x, w_2 = y)$ , an orbit of energy  $\xi < 0$  and angular momentum  $\Lambda$  corresponds to an arc of the parabola  $\mathcal{P}$ . When this orbit is a PRO, the two extremities  $A$  and  $P$  of this parabolic arc are associated with the two solutions apostron  $\mathbf{w}_A$  and periastron  $\mathbf{w}_P$  of the equation  $\frac{d}{d\tau} (\mathbf{w}, \mathbf{i}) = 0$ , with  $d\tau = |\xi|dt$ . Considering the orbital differential equation (39) in the coordinates  $(|\xi|x, y)$ , these two extremal points of the orbit are on the extremal line

$$\Delta = \left\{ \mathbf{w} \in \mathbb{R}^2, \sqrt{2} (\mathbf{w} | \mathbf{k}) = \Lambda^2 \right\}.$$

Trivially we then note that  $\Delta$  is parallel to  $\mathbb{R}\mathbf{k}$ . As the vectors  $\mathbf{w}$  defining this PRO satisfy  $\left[ \frac{d}{d\tau} (\mathbf{w}, \mathbf{i}) \right]^2 \geq 0$ , they are periodic-like vectors. Defining

$$K = \mathcal{T}_O(\mathcal{P}) \cap \Delta,$$

---

<sup>5</sup> When  $\gamma < 0$ ,  $\Lambda$  is imaginary and does not correspond to a PRO.

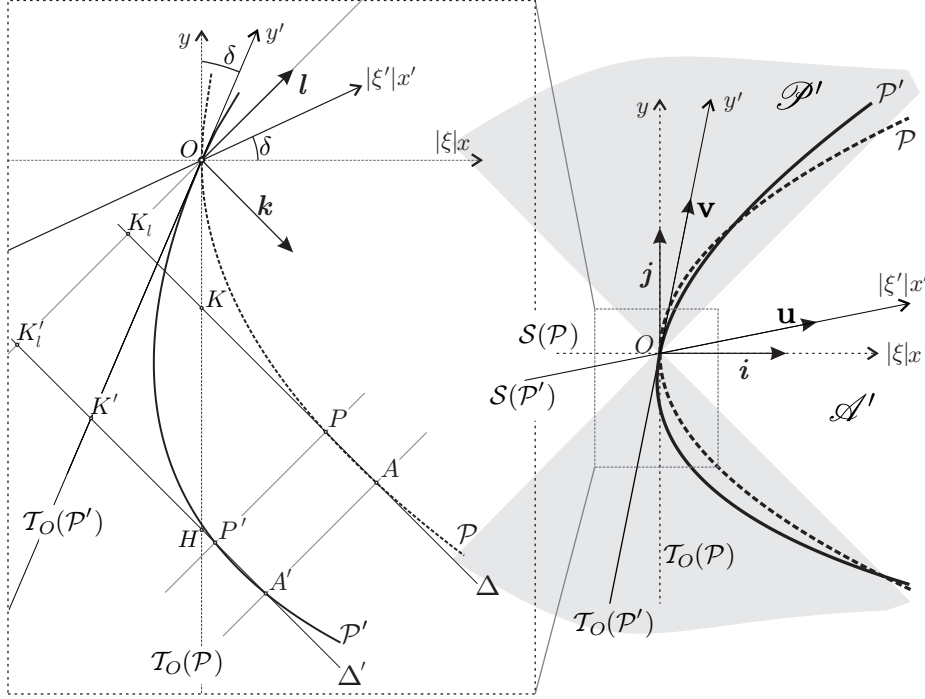


**Fig. 10** The  $\gamma > 1$  ibolst of the Kepler parabola when  $\xi\xi' > 0$ .

the point  $K$  is the  $\mathbf{k}$  parallel projection of  $A$  and  $P$  on  $\mathbb{R}\mathbf{j}$  and trivially,

$$\overrightarrow{OK} = -\Lambda^2 \mathbf{j}. \quad (40)$$

When  $\gamma > 1$ , the ibolst of the Kepler parabola is represented in figure 10; the other values of  $\gamma$  can be deduced directly from figure 9 and the analysis we will give below. With natural notations, we set  $\mathcal{P}' = B_\gamma(\mathcal{P})$  and  $\Delta' = B_\gamma(\Delta)$ . As  $\Delta$  is parallel to  $\mathbb{R}\mathbf{k}$ , which is an invariant direction of the ibolst,  $\Delta'$  is also parallel to  $\mathbb{R}\mathbf{k}$ . Let us consider  $K' = B_\gamma(K)$ . According to lemma 9 we have

$$\begin{aligned} K' &= B_\gamma(\mathcal{T}_O(\mathcal{P}) \cap \Delta) \\ &= B_\gamma(\mathcal{T}_O(\mathcal{P})) \cap B_\gamma(\Delta) \\ &= \mathcal{T}_O(\mathcal{P}') \cap \Delta' \end{aligned}$$

and quantitatively, as  $\overrightarrow{OK} = -\Lambda^2 \mathbf{j}$ , after an ibolst, we get

$$\overrightarrow{OK'} = -\Lambda^2 \mathbf{v}. \quad (41)$$

This relation clearly indicates that  $\Lambda$  is the same angular momentum for the Keplerian orbit and for the ibolsted orbit when it is considered in the reference frame of its ibolsted parabola, where it is also a Keplerian one. In addition,

$$\Delta' = K' + \mathbb{R}\mathbf{k} = B_\gamma(K) + \mathbb{R}B_\gamma(\mathbf{k}). \quad (42)$$

Therefore, each point of the isochrone orbit on its arc of parabola is directly linked by the ibolst to its  $\mathbf{l}$ -parallel projection on the Keplerian parabola. We can determine the angular momentum  $\Lambda'$  of the isochrone orbit in the Keplerian coordinates. Combining (38), (40) and (41) we get

$$\overrightarrow{KK'} = -\Lambda^2 (\mathbf{v} - \mathbf{j}) = -\frac{\Lambda^2}{\sqrt{2}} (\gamma - 1) \mathbf{l}.$$

If we introduce now the two orthogonal projections  $K_l$  and  $K'_l$  of  $K$  and  $K'$  on  $\mathbb{R}\mathbf{l}$ , we have  $\overrightarrow{KK'} = \overrightarrow{K_l K'_l}$  and  $\overrightarrow{OK'_l} = B_\gamma(\overrightarrow{OK_l})$  by (42). Since  $K_l = \Delta \cap \mathbb{R}\mathbf{l}$ ,  $K'_l = \Delta' \cap \mathbb{R}\mathbf{l}$  and  $B_\gamma$  sends  $\Delta$  to  $\Delta'$  and  $\mathbf{l}$  to  $\gamma\mathbf{l}$ , we get

$$\overrightarrow{OK'_l} = B_\gamma(\overrightarrow{OK_l}) = \gamma \overrightarrow{OK_l}.$$

And finally by Thales theorem,

$$\frac{OK'_l}{OK_l} = \frac{OH}{OK} = \gamma \quad \text{where } H = \mathcal{T}_O(\mathcal{P}) \cap \Delta'. \quad (43)$$

The length  $OH$  is the squared angular momentum  $\Lambda'^2$  of the ibolsted orbit considered in the reference frame of the Keplerian parabola. As  $OK$  is the squared angular momentum of the Keplerian orbit in its natural frame, we have

$$\Lambda'^2 = \gamma \Lambda^2.$$

When  $\xi\xi' < 0$ , the orientation of  $\mathbf{u}$  is inverted. The line  $\Delta'$  is  $\Delta' = K' + \mathbb{R}\mathbf{l}$ , and since  $\overrightarrow{OK'_l}$  is directed by  $\mathbf{k}$ , then  $\Lambda' = \Lambda$ .  $\square$

The bolsted orbital differential equations follow from theorem 3. As we can see from (45), in isochrone relativity, orbital laws are the same in all reference frames.

**Corollary 1** *In the canonical frame  $\mathcal{R}_O$ , the bolsted orbital differential equation is*

$$\frac{1}{16} \left[ \frac{d}{d\tau} (\mathbf{w}'|\mathbf{i}) \right]^2 = (\mathbf{w}'|\mathbf{i} - \mathbf{j}) + (\mathbf{w}_{\Lambda'}|\mathbf{j}) \quad (44)$$

with  $\mathbf{w}_{\Lambda'} = -\Lambda'^2 \mathbf{j}$ .

In the bolsted frame  $\mathcal{R}'_O$  with affine coordinates  $(\xi'x', y')$  and proper time  $d\tau' = \xi' dt'$ , the bolsted orbital differential equation is

$$\frac{1}{16} \left[ \frac{d}{d\tau'} (\mathbf{w}'|\mathbf{u}) \right]^2 = (\mathbf{w}'|\mathbf{u} - \mathbf{v}) + (\mathbf{w}'_{\Lambda'}|\mathbf{v}) \quad (45)$$

with  $\mathbf{w}'_{\Lambda'} = -\Lambda'^2 \mathbf{v}$ .

Isochrone PRO are contained in the periodic-space of their parabola reference frame. But in the Keplerian primary frame this periodic-space appears vertical when  $\gamma > 0$  and horizontal otherwise. In some cases, the PRO is then associated with an arc of parabola which is concave or located in the negative part of the Keplerian frame. Those image orbits are not physical.

### 3.2.4 Potentials relativity

The Keplerian nature of an isochrone potential is revealed in the reference frame  $\mathcal{R}'_O$  of its parabola, cf. theorem 3. An ibolst can also bolst a harmonic potential and then exactly provide the appropriate primary frame which characterizes the radial oscillation of a PRO in the image isochrone potential. In such a frame, all periods of PRO have indeed the same value.

We give hereafter an explicit formulation of the parameters of all the image potentials. They can be obtained by direct resolution of quadratic equations.

When the primary potential is Keplerian  $\psi_{\text{ke}}(r) = -\frac{\mu}{r}$ , the primary orbits are such that  $\xi < 0$  in order to be bounded. If  $\gamma > 0$ , the ibolsted potential  $\psi'(r')$  is always a transvection of a Hénon or a bounded isochrone potential introduced in sec. 2.3. Using the notations of reduced potentials, coming from the proof of theorem 1 and equation (16), one can verify that

	$\text{sign}(\xi') = -\text{sign}(\xi) > 0$	$\text{sign}(\xi') = \text{sign}(\xi) < 0$	
$\gamma > 1$	$J_{\epsilon,0}(\psi_{\text{bo}}^+) = \psi_{\text{bo}}^+ + \epsilon$	$J_{\epsilon,0}(\psi_{\text{he}}^-) = \psi_{\text{he}}^- + \epsilon$	(46)
$0 < \gamma < 1$	$J_{-\epsilon,0}(\psi_{\text{bo}}^-) = \psi_{\text{bo}}^- - \epsilon$	$J_{-\epsilon,0}(\psi_{\text{he}}^+) = \psi_{\text{he}}^+ - \epsilon$	

where

$$\epsilon = \frac{\mu'(\gamma+1)^2}{8\gamma b} > 0, \quad \mu' = \left| \frac{8\mu\xi'\gamma}{(\gamma+1)\sqrt{|8\xi\xi'(\gamma+1)|}} \right| \quad \text{and} \quad b = \left| \frac{\mu(\gamma-1)}{\sqrt{|8\xi\xi'(\gamma+1)|}} \right|.$$

Then, when the primary potential  $\psi(r)$  is the harmonic  $\psi_{\text{ha}}(r) = +\frac{1}{2}\omega^2 r^2$ , the primary energy is positive  $\xi > 0$  in order to get bounded orbits. When  $\gamma > 0$ , the ibolst leads to the four increasing potentials  $\psi'(r')$ ,

	$\text{sign}(\xi') = \text{sign}(\xi) > 0$	$\text{sign}(\xi') = -\text{sign}(\xi) < 0$	
$\gamma > 1$	$J_{\epsilon,0}(\psi_{\text{he}}^+) = \psi_{\text{he}}^+ + \epsilon$	$J_{\epsilon,0}(\psi_{\text{bo}}^-) = \psi_{\text{he}}^+ + \epsilon$	(47)
$0 < \gamma < 1$	$J_{-\epsilon,0}(\psi_{\text{bo}}^+) = \psi_{\text{bo}}^+ - \epsilon$	$J_{-\epsilon,0}(\psi_{\text{bo}}^+) = \psi_{\text{bo}}^+ - \epsilon$	

where

$$\epsilon = \frac{\mu'(\gamma-1)^2}{8b\gamma}, \quad \mu' = \left| \frac{4\xi'\xi\gamma}{\omega(\gamma-1)\sqrt{|\xi'(\gamma-1)|}} \right| \quad \text{and} \quad b = \frac{(\gamma+1)|\xi|}{2\omega\sqrt{|\xi'(\gamma-1)|}}.$$

The classical Bohlin transformation  $B_{-1}$  exchanges the two potentials  $\psi_{\text{ke}}$  and  $\psi_{\text{ha}}$ , cf. theorem 2 p.20. The commutative structure and associative property of the group  $\mathbb{B}$  then provide the image of any isochrone potential by  $B_\gamma$  when  $\gamma < 0$ .

A transvection  $J_{\epsilon,0}$  swivels a parabola when it only adds the constant  $\epsilon$  to the corresponding potential. This constant has no particular role and we can neglect it in a potential diagram summarizing the effect of the ibolst on isochrone potentials. This is the purpose of figure 11.

Using this diagram and the group property of the ibolst, we can recover all ibolsted potentials only from the Keplerian one. Isochrone potentials form the group orbit of Kepler potentials under the action of  $\mathbb{B}$ .



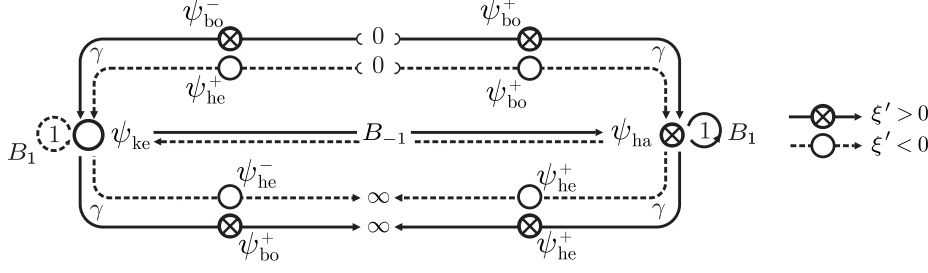


**Fig. 11** Diagram of the set of all possible ibolsted potentials up to an additive constant. The nomenclature used is the one defined in the isochrone classification of sec. 2.3.

### 3.2.5 Isochrone orbits construction

Isochrone is a Keplerian property seen from an appropriate reference frame. Theorem 3 gives a method to find the relative isochrone reference frame from a Keplerian potential. From any isochrone potential one may reciprocally construct its isochrone orbits and find their related Keplerian description graphically using parabolas.

In order to be concrete, we build now the complete *back to the Kepler* process when the needed ibolst has  $\gamma > 1$  for  $\xi\xi' > 0$  in figure 12.

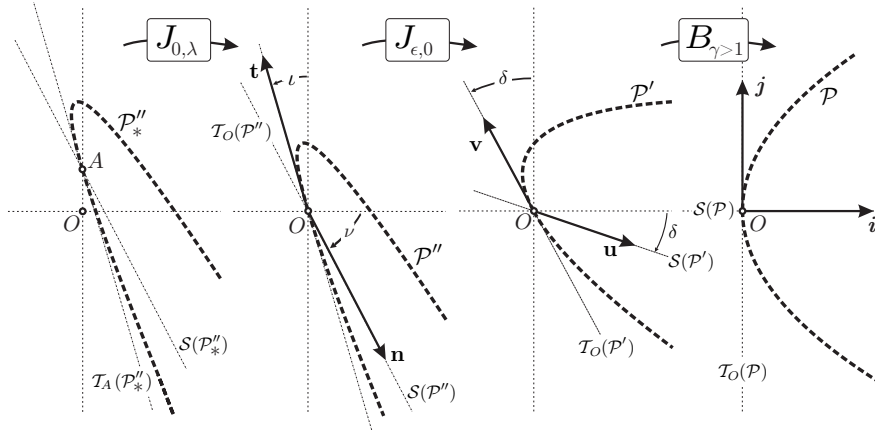


**Fig. 12** Graphical determination of the Keplerian reference frame of an isochrone parabola. Here isochrone orbits have negative energy.

Consider a parabola  $\mathcal{P}''$ . From definition 2 p.15, we retrieve a *physical* parabola from a vertical translation  $J_{0,\lambda}(\mathcal{P}'') = \mathcal{P}''$ . Then, by definition 3 p.27, we find the natural frame  $(O, \mathbf{t}, \mathbf{n})$  attached to  $\mathcal{P}''$ . While the angles  $\iota$  and  $\nu$  are not equal, we adjust the parabola with a transvection  $J_{\epsilon,0}$  to prepare it for a bolst. We then debolst the parabola with the ibolst  $B_\gamma$  given by the angle  $\delta = \iota = \nu$ , with  $\delta < \frac{\pi}{2}$ . Given  $\mathcal{P}$  and  $\mathcal{P}'$ , the isochrone orbit can be related to its Keplerian description as in figure 10.

This geometrical construction gives the radial distances

$$r_0 = \frac{1}{2\sqrt{|\xi_0|}} \sqrt{(\mathbf{w}|\mathbf{i})} \quad \text{and} \quad r_1 = \frac{1}{2\sqrt{|\xi_0|}} \sqrt{(\mathbf{w}'|\mathbf{i})}$$

of the Keplerian and isochrone orbits in the  $(|\xi_0|x, y)$ -coordinates of the Keplerian frame. The angles  $\varphi_0$  and  $\varphi_1$  are provided by theorem 2 p.20 and given by

$$a = \frac{1}{2}(r_{0,p} + r_{0,a}), \quad \frac{|\xi_0|}{\mu} = \frac{1}{2a}, \quad e = \frac{r_{0,a} - r_{0,p}}{2a}, \quad p = (1 - e^2)a, \quad \text{and} \quad \frac{\alpha}{\beta} = \frac{\gamma + 1}{\gamma - 1}.$$

They can also be geometrically determined. In fact, the precession of the isochrone apocenters or pericenters  $n_\varphi$  depends on  $A$  and the ordinate of the intersection of the convex part of the parabola and  $\mathbb{R}\mathbf{j}$ , see proposition 1. This intersection is given by the vertical translation parameter  $\lambda$  and the aperture of the parabola; more precisely, by the distance  $4b\mu$  between the two intersections of the parabola and the axis  $\mathbb{R}\mathbf{j}$ , just as one can deduce from (16) and its following properties on page 14.

This construction does not explicitly depend on the hypothesis  $\gamma > 1$ , and can be generalized to other values of  $\gamma$  as long as the considered initial orbit is a PRO, i.e.  $\mathbf{w}'$  remains a periodic-like vector on the convex part of a parabola. It is also possible to construct positive energy ibolsted orbits from negative energy Keplerian orbits.

This procedure can also be generalized using a bolst  $B_{\alpha,\beta}$ , which is a transvection of an ibolst  $B_\gamma$  when expressed in the basis  $(\mathbf{l}, \mathbf{k})$ . In the same way, the first translation  $J_{0,\lambda}$  is not compulsory.

## 4 Applications

### 4.1 Physical properties of isochrone potentials

Up to an affine transformation, there are four different increasing potentials which are isochrone, i.e. in which the radial periods  $\tau_r$  only depend on the energy of the considered radially oscillating particles. Two of them are very well known: the Kepler potential  $\psi_{\text{ke}}$  is associated with a Dirac density distribution and the harmonic potential  $\psi_{\text{ha}}$  is sourced by a constant density distribution of matter in the considered volume. In figure 13 we present the plot of the two other ones, i.e.  $\psi_{\text{bo}}$  and  $\psi_{\text{he}}$ . Notice their harmonic quadratic behavior at small radial distances.

The Hénon potential  $\psi_{\text{he}}$  has important physical properties in gravitational stellar dynamics: in a forthcoming paper in preparation by Simon-Petit et al., we will show that it appears to be a fundamental equilibrium state where stellar systems settle down after violent relaxation (e.g. [28] for the original contribution and [6] p. 380-382 for a modern review). The corresponding density is a core-halo structure: the typical size of the core is the length  $b$  and the surrounding halo falls like a  $r^{-4}$  power law. This property ensures that the mass  $M_{\text{he}}(r)$  contained in any ball of radius  $r$  in a Hénon potential is finite. As a matter of fact, by Gauss' theorem, we have  $GM_{\text{he}}(r) = r^2 \frac{d\psi_{\text{he}}}{dr}$  and  $\lim_{r \rightarrow \infty} GM_{\text{he}}(r) = \mu$ . Recalling definition 2, this finite mass property is trivially conserved for the reduced version of the Hénon potential  $\psi_{\text{he}}^{\text{red}} = \psi_{\text{he}}^+ = \psi_{\text{he}} + \frac{\mu}{2b}$  and for all physical Hénon's  $\psi_{\text{he}}^{\text{phy}} =$

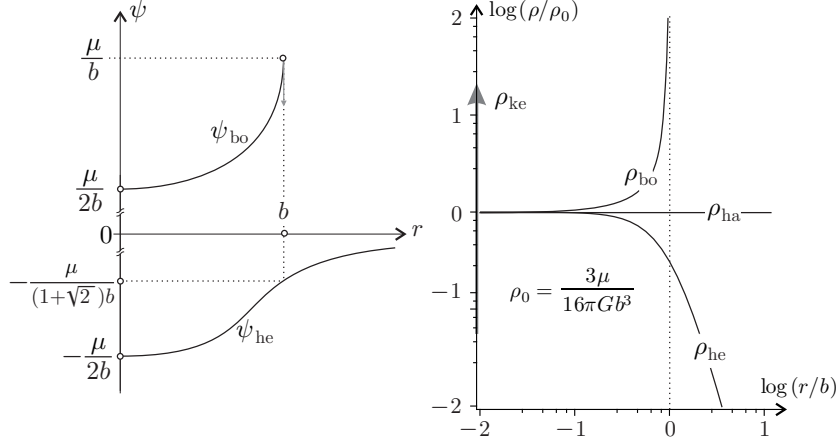


**Fig. 13** The bounded and the Hénon isochrone potential (left). The mass density of isochrones (right).

$\psi_{\text{he}} + \epsilon$  for any real  $\epsilon$ . However, the gauged Hénon  $\psi_{\text{he}}^{\text{gau}} = \psi_{\text{he}}^{\text{phy}} + \frac{\lambda}{2r^2}$  contains an infinite mass in its center and has poor physical meaning. Nevertheless, this latter potential is still isochrone. As we said in the classification of the sec. 2.3, gauged potentials are essential for the completeness of the isochrone set.

The properties of systems associated with the  $\psi_{\text{bo}}$  potential are more unusual. When it is considered on its whole domain  $\mathcal{D}_{\psi_{\text{bo}}} = [0, b]$ , the systems have an infinite total mass. As a matter of fact,  $GM_{\text{bo}}(r) \sim \mu \sqrt{\frac{b}{2(b-r)}}$  when  $r \rightarrow b$ . This property holds for any physical bounded potential. In fact these systems are self-confined because there exists an infinite repulsive force at their boundaries in  $r = b$ . Perhaps  $\psi_{\text{bo}}$  potentials might be used as classical models for structurally confined systems like, for example, quarks in the nucleon. Indeed, such fundamental particles are confined in the nucleon (here of size  $b$ ) and are characterized by asymptotic freedom, i.e. they do not feel any force at the center of the nucleon. Gauged bounded potentials are even more unusual with their infinite central mass!

The repartition of mass in physical isochrones is progressive: the mass is concentrated into a point in the center of a Kepler system, while in a Hénon one, the mass is equally distributed up to a characteristic length settled by the parameter  $b$ , and in a less concentrated decreasing repartition after the characteristic radius. When  $b$  increases, the first dense harmonic part grows and the Hénon potential eventually behaves like a harmonic potential since

$$\psi_{\text{he}}^{\text{red}} \underset{b \rightarrow \infty}{\sim} \frac{\mu}{8b^3} r^2, \quad (48)$$

i.e. the physical Hénon isochrone is changed into the physical harmonic when  $b \rightarrow +\infty$ . This property can be easily seen on the mass density distribution in the right panel of the figure 13. Subsequently, since

$$\psi_{\text{bo}}^{\text{red}} \underset{b \rightarrow \infty}{\sim} \frac{\mu}{8b^3} r^2 \quad (49)$$

we can say in a converse manner that when the infinite mass of the unbounded harmonic is concentrated into a finite domain of size  $b$ . We can recover the bounded isochrone by controlling  $b$ .

Let us revisit the properties of orbits.

#### 4.2 Period and precession of periastron for isochrones

Proposition 1 gathers the properties  $\tau_r$  and  $n_\varphi$  of isochrone orbits and reveals the interesting similarities of isochrone radial periods. Their form in  $\psi_{\text{he}}$  and  $\psi_{\text{bo}}$  is the same as in the Keplerian potential. We will use this remark to generalize Kepler's third law in the next subsection. In a harmonic potential,  $\tau_r$  is the same regardless of the energy of the massive particles. Moreover, in  $\psi_{\text{ke}}$  and  $\psi_{\text{ha}}$ ,  $n_\varphi$  is rational and all orbits are closed.

**Proposition 1** *Given a PRO  $(\xi, \Lambda)$  in an isochrone potential, its radial and azimuthal periods are*

	$\psi_{\text{ke}}$	$\psi_{\text{ha}}$	$\psi_{\text{he}}$	$\psi_{\text{bo}}$
$\tau_r$	$2\pi\mu  2\xi ^{-3/2}$	$\pi\omega^{-1}$	$2\pi\mu  2\xi ^{-3/2}$	$2\pi\mu  2\xi ^{-3/2}$
$n_\varphi$	1	$\frac{1}{2}$	$\frac{1}{2} + \frac{\Lambda}{2\sqrt{4b\mu + \Lambda^2}}$	$\frac{1}{2} - \frac{\Lambda}{2\sqrt{4b\mu + \Lambda^2}}$

(50)

*Proof* Using isochrone potential expressions, the radial period (2) and increment  $n_\varphi$  of the azimuthal angle (4) come from the computation of the radial action

$$\mathcal{A}_r = \frac{1}{\pi} \int_{r_p}^{r_a} \sqrt{2[\xi - \psi(r)] - \frac{\Lambda^2}{r^2}} dr.$$

For a Keplerian orbit of energy  $\xi_k < 0$  in  $\psi_{\text{ke}}(r) = -\frac{\mu}{r}$  and a harmonic orbit of energy  $\xi_h > 0$  in  $\psi_{\text{ha}}(r) = \frac{1}{2}\omega^2 r^2$ , we have

$$\mathcal{A}_r^{\text{ke}} = \frac{\sqrt{2|\xi_k|}}{\pi} \int_{r_p}^{r_a} \frac{\sqrt{(r-r_p)(r_a-r)}}{r} dr \text{ with } \begin{cases} r_p + r_a = \frac{\mu}{|\xi_k|} \\ r_p r_a = \frac{\Lambda^2}{2|\xi_k|} \end{cases} \quad (51)$$

and

$$\mathcal{A}_r^{\text{ha}} = \frac{\sqrt{\mu}}{2\pi} \int_{r_p^2}^{r_a^2} \frac{\sqrt{(u-r_p^2)(r_a^2-u)}}{u} du \text{ with } \begin{cases} r_p^2 + r_a^2 = \frac{2\xi_h}{\omega^2} \\ (r_p r_a)^2 = \frac{\Lambda^2}{\omega^2} \end{cases}. \quad (52)$$

The computation of these radial actions can be done by meticulous integration to recover  $\tau_r$  and  $n_\varphi$  in  $\psi_{\text{ke}}$  and  $\psi_{\text{ha}}$ . Conversely, knowing the radial and azimuthal periods, one recovers the expression of  $\mathcal{A}_r^{\text{ke}}$  and  $\mathcal{A}_r^{\text{ha}}$ . Indeed, for  $\psi_{\text{ke}}$ ,  $\tau_r$  follows from the classical Kepler's third law, and  $n_\varphi = 1$  because the center of attraction of a Keplerian ellipse is located at one of its foci (see figure 7). For the harmonic potential,  $\tau_r = \frac{\pi}{\omega}$  and  $n_\varphi = \frac{1}{2}$  because harmonic ellipses are centered at their centers of attraction, see figure 7. As it is shown in appendix D, one gets

$$\mathcal{A}_r^{\text{ke}} = \frac{\mu}{\sqrt{2|\xi_k|}} - \Lambda \text{ and } \mathcal{A}_r^{\text{ha}} = \frac{\xi_h}{2\omega} - \frac{\Lambda}{2}.$$

For the two non classical isochrones  $\psi_{\text{he}}^{\text{bo}}(r) = \pm \frac{\mu}{b} \left(1 + \sqrt{1 \mp \frac{r^2}{b^2}}\right)^{-1}$ , generalizing [6] p.152, we introduce  $s = 1 + \sqrt{1 \mp \frac{r^2}{b^2}}$ . For the Hénon potential,  $s > 2$  and the PRO has  $\xi_- < 0$  according to its effective potential, see sec. 2.1 p.5. In the same way, for the bounded potential,  $2 > s > 0$  and its PRO has positive energy  $\xi^+ > 0$ . Then, for  $s_p < s_a$ , the radial actions are

$$\mathcal{A}_{r,\text{he}}^{\text{bo}} = \mp \frac{b\sqrt{2|\xi_-^+|}}{\pi} \int_{s_p}^{s_a} \frac{(s-1)}{s(s-2)} \sqrt{(s-s_p)(s_a-s)} ds$$

with

$$\begin{cases} s_p + s_a = 2 + \frac{\mu}{b|\xi_-^+|} \\ s_a s_p = \frac{4b\mu + \Lambda^2}{2b^2|\xi_-^+|}. \end{cases} \quad (53)$$

Hence, using  $\mathcal{I}_2$  from appendix D, one gets

$$\mathcal{A}_{r,\text{he}}^{\text{bo}} = \mp \frac{\mu}{\sqrt{2|\xi_-^+|}} - \frac{1}{2} \left( \Lambda \mp \sqrt{4b\mu + \Lambda^2} \right).$$

The results follow by derivation.  $\square$

The dynamics is unchanged when adding constants to potentials, i.e.  $\psi \rightarrow \psi + \epsilon$ . However, the expression of the periods are modified and can be deduced from propositions 1 and 2 for the reduced, physical and gauged isochrones.

**Proposition 2** *Let  $\psi$  and  $\psi^*$  be two potentials related by an affine transformation  $\psi^* = J_{\epsilon,\lambda}(\psi) = \psi + \epsilon + \frac{\lambda}{2r^2}$ .*

*An orbit defined in  $\psi$  and its affine transformation in  $\psi^*$  share the same orbital properties  $\tau_r$  and  $n_\varphi$ .*

*Provided that  $\lambda + \Lambda^2 > 0$ , the radial action and its derivatives are transformed as follows:*

1.  $\mathcal{A}_r^*(\xi; \Lambda) = \mathcal{A}_r(\xi - \epsilon; \sqrt{\lambda + \Lambda^2})$ ,
2.  $\tau_r^*(\xi; \Lambda) = \tau_r(\xi - \epsilon; \sqrt{\lambda + \Lambda^2})$ ,
3.  $n_\varphi^*(\xi; \Lambda) = n_\varphi(\xi - \epsilon; \sqrt{\lambda + \Lambda^2}) \frac{\Lambda}{\sqrt{\lambda + \Lambda^2}}$ .

*Proof* The radial action of an orbit of energy  $\xi$  and angular momentum  $\Lambda$  in  $\psi^*$  is given by

$$\begin{aligned} \mathcal{A}_r^*(\xi; \Lambda) &= \frac{1}{\pi} \int_{r_p^*(\xi; \Lambda)}^{r_a^*(\xi; \Lambda)} \sqrt{2(\xi - \psi^*(r)) - \frac{\Lambda^2}{r^2}} dr \\ &= \frac{1}{\pi} \int_{r_p^*(\xi; \Lambda)}^{r_a^*(\xi; \Lambda)} \sqrt{2(\xi - \epsilon - \psi(r)) - \frac{\lambda + \Lambda^2}{r^2}} dr \\ &= \frac{1}{\pi} \int_{r_p(\xi - \epsilon; \sqrt{\lambda + \Lambda^2})}^{r_a(\xi - \epsilon; \sqrt{\lambda + \Lambda^2})} \sqrt{2(\xi - \epsilon - \psi(r)) - \frac{\lambda + \Lambda^2}{r^2}} dr \\ \mathcal{A}_r^*(\xi; \Lambda) &= \mathcal{A}_r(\xi - \epsilon; \sqrt{\lambda + \Lambda^2}), \end{aligned}$$

where  $r$  is the radial distance in the reference frame associated with  $\psi$ , and  $r^*$  is the image in the same frame by the affine transformation. For the second relation we use the definition  $\frac{\tau_r^*(\xi; \Lambda)}{2\pi} = \frac{\partial A_r^*}{\partial \xi}(\xi; \Lambda)$ . For the third one, we get

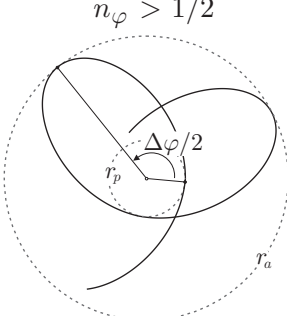
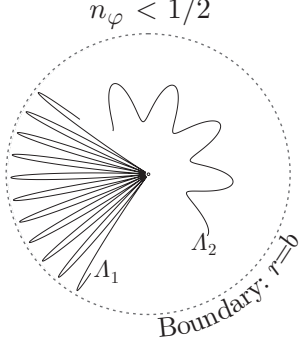
$$\begin{aligned} n_\varphi^*(\xi; \Lambda) &= -\frac{\partial A_r^*}{\partial \Lambda}(\xi; \Lambda) \\ &= -\frac{\partial}{\partial \Lambda}(\mathcal{A}_r(\xi - \epsilon; \sqrt{\lambda + \Lambda^2})) \\ &= -\frac{\partial \mathcal{A}_r}{\partial \Lambda}(\xi - \epsilon; \sqrt{\lambda + \Lambda^2}) \times \frac{\Lambda}{\sqrt{\lambda + \Lambda^2}}. \end{aligned}$$

And the third relation follows.

Eventually, a transformation  $J_{\epsilon, \lambda}$  maps an orbit  $(\xi, \Lambda)$  onto another one of parameters  $(\xi + \epsilon, \sqrt{\Lambda^2 - \lambda})$  when  $\Lambda^2 - \lambda > 0$ . Inserting them in the previous relations, we recover the invariance of  $\tau_r$  and  $n_\varphi$  under  $J_{\epsilon, \lambda}$ : the radial period of the image orbit  $\tau^*(\xi + \epsilon, \sqrt{\Lambda^2 - \lambda})$  is that of the primary orbit  $\tau(\xi, \Lambda)$ . In the same way,  $n_\varphi^*(\xi + \epsilon; \sqrt{\Lambda^2 - \lambda}) = n_\varphi(\xi, \Lambda)$ .  $\square$

Eventually, the radially periodic orbits are rosettes, [6] sect. 3. The number  $n_\varphi$  of revolutions to reach a periastron from the preceding one can be greater or lower than for a harmonic or Keplerian potential. A gauge introduces orbits that spiral into the origin [29], as it happens for orbits of the extremal line defining an imaginary radial distance on its parabola at the pericenter. The gauged harmonic presents a similarity with  $\psi_{\text{he}}$  and  $\psi_{\text{bo}}$ , as described in proposition 3. The precession of orbits that emerge when adding a  $\frac{1}{r^2}$ -term to the potential corresponds to the one described in Proposition XLIV of Newton's *Principia* [33] for the Kepler force.

**Proposition 3** *Bounded, Hénon and gauged harmonic PRO's are rosettes with azimuthal precessions  $n_\varphi$  such that:*

$\psi_{\text{he}}$ and $J_{0, \lambda}(\psi_{\text{ha}})$ with $\lambda > 0$	$\psi_{\text{bo}}$ and $J_{0, \lambda}(\psi_{\text{ha}})$ with $\lambda < 0$
$n_\varphi > 1/2$ 	$n_\varphi < 1/2$ 

*Proof* Let us illustrate the case of a harmonic oscillator and its gauge transform  $\psi^* = J_{0, \lambda}(\psi_{\text{ha}}) = \psi_{\text{ha}} + \frac{\lambda}{2r^2}$ . From proposition 2, we get that for the modified potential,

$$\tau_r^* = \tau_r = \frac{\pi}{\omega}, \quad n_\varphi^* = \frac{\Lambda}{2\sqrt{\lambda + \Lambda^2}}.$$

Thus, for harmonic potentials, adding a gauge modifies  $n_\varphi$ , whereas the period never changes. Moreover we get the dynamical consequence that  $n_\varphi^* < 1/2$  when  $\lambda > 0$  and  $n_\varphi^* > 1/2$  when  $\lambda < 0$ .

The parallel property exists for  $\psi_{\text{he}}$  and  $\psi_{\text{bo}}$ . According to (50) in proposition 1,  $n_{\varphi}^{\text{bo}} = \frac{1}{2} - \frac{\Lambda}{2\sqrt{4b\mu + \Lambda^2}}$  where  $\frac{\Lambda}{2\sqrt{4b\mu + \Lambda^2}} > 0$ , and then  $n_{\varphi}^{\text{bo}} < \frac{1}{2}$ . In the same way,  $n_{\varphi}^{\text{he}} > \frac{1}{2}$ .

This  $n_{\varphi}$  property shapes the corresponding orbits. On the one hand, when  $n_{\varphi} > \frac{1}{2}$ , the azimuthal precession  $\Delta\varphi/2$  during the transfer from apoastron ( $r = r_a$ ) to the periastron ( $r = r_p$ ) is greater than  $\pi$ . Thus the orbit must turn around the center of the system as it is indicated on the left panel of the proposition. On the other hand, when  $n_{\varphi} < \frac{1}{2}$ , the transfer  $r_p \rightarrow r_a \rightarrow r_p$  cannot turn around the center; such orbits oscillate between  $r_a$  and  $r_p$ , precessing around the center, as is plotted on the right panel of the proposition. The smaller the value of the angular momentum, the tighter the oscillation is. On this right panel we have  $0 \simeq \Lambda_1 < \Lambda_2$ .  $\square$

Let us conclude this section remarking that the extension ( $r_a$  and  $r_p$ ) of an isochrone orbit is managed by its energy (see the expression of  $\xi$  in (51), (52) and (53)) when the thickness of its oscillation is governed by its angular momentum. More precisely, radial (thin) orbits are obtained when  $\Lambda \rightarrow 0$  and circular (fat) orbits when  $\Lambda = \Lambda_c$ , the largest value possible of the angular momentum for the considered energy.

### 4.3 Generalization of Kepler's Third Law

The Kepler potential  $\psi_{\text{ke}}(r) = -\frac{\mu}{r}$  is sourced by a point of mass  $M$  such that  $\mu = GM$  where  $G$  is the Newton constant. Radially periodic orbits close after one radial period  $\tau_r$  and form ellipses with semi major axes  $a = -\frac{\mu}{2\xi}$ . In his last major book *Harmonices Mundi* [24], Johannes Kepler proposed in 1619 his third law claiming that  $\tau_r^2 \times a^{-3}$  is constant for all ellipses. Isaac Newton, half a century later, proved this empirical observation using his laws of dynamics and his gravitational force. This law appears to become a cornerstone of celestial mechanics because the Kepler constant appears to be  $\tau_r^2 a^{-3} = \frac{4\pi^2}{\mu}$  and thus gives the mass of the attracting body.

In this paper we have shown that Kepler potential generates the isochrone group and we remark that Kepler's third law could be generalized. As a matter of fact, considering the specific energy  $\xi$  associated with a given PRO in an isochrone potential  $\psi \in \{\psi_{\text{ke}}, \psi_{\text{he}}, \psi_{\text{bo}}\}$ , we see that according to proposition 1, except for the harmonic potential, all isochrone orbits are such that

$$\tau_r^2 |\xi|^3 = \frac{\pi^2 \mu^2}{2} = \text{cst.} \quad (54)$$

Nevertheless, the law (54) expressed in terms of the specific energy is not stable under transvections of the potential,  $\psi \mapsto \psi^* = \psi + \epsilon$ , and has to be slightly modified for physical potentials when adding a constant. As mentioned in proposition 2, a PRO  $(\xi, \Lambda)$  in  $\psi^*$  will satisfy

$$\tau_r^2 |\xi - \epsilon|^3 = \frac{\pi^2 \mu^2}{2} = \text{cst.} \quad (55)$$

In these relations,  $\xi$  is the specific energy of the test particle moving on a PRO with period  $\tau_r$ . The parameter  $\mu$  is directly related to the total mass of the system

which sources the potential when it is finite i.e.  $\psi_{\text{ke}}$  and  $\psi_{\text{he}}$ . For the other non classical isochrone  $\psi_{\text{bo}}$ , the total mass is infinite but equation (54) always holds with a less physically comprehensive  $\mu$  constant. The modification of the law (54) into (55) somehow hides the symmetry of the considered system. We thus propose a geometric formulation of Kepler's Third Law for isochrones.

The formulation of Kepler  $\tau_r^2 \propto a^{-3}$  in terms of the geometric parameter  $a$  is more appropriate for conveying the symmetry of the potential. In fact, the Lagrangian  $L = T - U$ , with  $T$  the specific kinetic energy of a particle and  $U = \psi_{\text{ke}}$ , is invariant, under a time  $t \rightarrow \tilde{t} = \zeta t$  and space  $\mathbf{r} \rightarrow \tilde{\mathbf{r}} = \varpi \mathbf{r}$  rescaling, if

$$\zeta^2 \propto \varpi^3$$

because  $\psi_{\text{ke}}$  is a homogeneous function of degree  $-1$ , i.e.  $\psi_{\text{ke}}(\tilde{\mathbf{r}}) = \varpi^{-1} \psi_{\text{ke}}(\mathbf{r})$ . In order to geometrically express Kepler's Third law, we introduce in definition 4 "semi major axes", relevant to all isochrone potentials, and directly related to their Keplerian relative description. These characteristic lengths, generally related to specific energies by (51), (52) and (53), provide a method to determine the mass of an isochrone system as mentioned at the end of this section.

**Definition 4** Let  $r_p$  and  $r_a$  be the peri- and apoastron radial distance of a given isochrone periodic orbit. We call the *isochrone semi-major axis* of this orbit by the following lengths:

1. in a Kepler potential,

$$a = \frac{1}{2} (r_a + r_p),$$

2. in a homogeneous box of radius  $R$ ,

$$a = \left(\frac{1}{2}\right)^{2/3} R,$$

3. in a Hénon potential,

$$a = \frac{1}{2} \left( \sqrt{b^2 + r_a^2} + \sqrt{b^2 + r_p^2} \right),$$

4. in a bounded potential,

$$a = \frac{1}{2} \left( \sqrt{b^2 - r_a^2} + \sqrt{b^2 - r_p^2} \right).$$

In definition 4, we have considered a homogeneous box to include the description of its elliptic trajectories with the Third Law. In fact, the situation of the harmonic potential needs more attention since  $\psi_{\text{ha}}$  is degenerate. In such a potential all test particles share the same period but different specific energies, hence relation (54) cannot hold for each specific energy.

The harmonic potential is not exactly representative of a real system because of its constant density and infinite spatial extension, which imply an infinite mass. Instead, the potential associated with a finite homogenous repartition of masses in



a ball of radius  $R$  with constant density (while the outside region is empty) does represent a real system and can be written as

$$\psi_{\text{ha}}^R(r) = \begin{cases} \frac{1}{2}\omega^2 r^2 - \frac{3}{2}\omega^2 R^2 & \text{if } r < R \\ -\frac{GM}{r} & \text{if } r > R. \end{cases}$$

We call it a finite harmonic potential. Additionally, either Gauss' theorem or the continuity of the force at the boundary of the ball leads to the following relation:

$$\mu = GM = \omega^2 R^3. \quad (56)$$

As mentioned on page 17, the harmonic potential corresponds to the limit of an isochrone potential  $\psi_{\text{he}}$  or  $\psi_{\text{bo}}$  when  $b \rightarrow \infty$ . This result holds for the finite harmonic potential  $\psi_{\text{ha}}^R$ . In figure 13, we see the confluence of these potentials and their densities when the parameter  $b$  is large, as written in proposition 4. As it will be proven in theorem 4, the characteristic length for the finite harmonic also naturally appears in the expression of Kepler's Third Law.

**Proposition 4** *The finite harmonic potential satisfies*

$$\psi_{\text{he}}(r) \underset{b \rightarrow \infty}{\sim} \psi_{\text{ha}}^R(r) \quad \text{and} \quad \psi_{\text{bo}}(r) \underset{b \rightarrow \infty}{\sim} \psi_{\text{ha}}^R(r) \quad \text{with} \quad R = 2^{2/3}b \quad \text{for any fixed } r.$$

*Proof* As already mentioned, the potential  $\psi_{\text{ha}}^R$  is continuous in  $r = R$  if and only if  $\mu = GM = \omega^2 R^3$ .

We assume the potentials vanish at  $r = 0$  without loss of generality. We consider then the reduced potentials and their equivalents from (48) and (49) as  $\psi_{\text{he}}^{\text{red}} \underset{b \rightarrow \infty}{\sim} \frac{\mu}{8b^3} r^2$  and  $\psi_{\text{bo}}^{\text{red}} \underset{b \rightarrow \infty}{\sim} \frac{\mu}{8b^3} r^2$ .

In this limit, the Hénon and bounded potentials behave as homogeneous spheres inside a radius  $R = 2^{2/3}b$ .  $\square$

Now, Kepler's third law can be generalized to all isochrone potentials in theorem 4.

**Theorem 4** *For any radially periodic orbit in an isochrone potential, the square of the radial period is proportional to the cube of the isochrone semi-major axis by*

$$\tau_r^2 = \frac{4\pi^2}{\mu} a^3, \quad (57)$$

where  $\mu$  is the mass parameter of  $\psi_{\text{ke}}$ ,  $\psi_{\text{he}}$ ,  $\psi_{\text{bo}}$  and  $\mu = \omega^2 R^3$  for  $\psi_{\text{ha}}^R$ .

*Proof* In  $\psi_{\text{ke}}$ , it is Kepler's third law. In  $\psi_{\text{he}}$ , for a PRO of energy  $\xi < 0$ , the radial variable  $s$  introduced in the proof of proposition 1 satisfies (53) as

$$s_a + s_p = 2 - \frac{\mu}{\xi b} = 2 + \sqrt{\left(\frac{r_a}{b}\right)^2 + 1} + \sqrt{\left(\frac{r_p}{b}\right)^2 + 1}$$

and

$$\xi = -\frac{\mu}{2a} \quad \text{with} \quad a = \frac{\sqrt{r_a^2 + b^2} + \sqrt{r_p^2 + b^2}}{2}.$$

Inserting this expression of  $\xi$  in (54) gives (57).

Similarly, in  $\psi_{\text{bo}}$  the variable  $s$  satisfies

$$s_{\min} + s_{\max} = 2 + \frac{\mu}{\xi b} = 2 + \sqrt{1 - \left(\frac{r_p}{b}\right)^2} + \sqrt{1 - \left(\frac{r_a}{b}\right)^2}$$

and

$$\xi = \frac{\mu}{2a} > 0 \quad \text{with} \quad a = \frac{1}{2} = \sqrt{b^2 - r_p^2} + \sqrt{b^2 - r_a^2}.$$

By inserting this expression in (54), we recover the law (57).

In  $\psi_{\text{ha}}$ , all orbits have the same radial period  $\tau_r = \frac{\pi}{\omega}$ . When a harmonic system is compacted into a ball of radius  $R$  of constant density, then  $\mu = \omega^2 R^3$  according to (56). Hence, the period could be related to the radius of the ball through the relation  $\tau_r = \frac{\pi}{\sqrt{\mu}} R^{3/2}$ . Introducing the length  $a = \left(\frac{1}{2}\right)^{2/3} R$ , one has

$$\mu \tau_r^2 = 4\pi^2 a^3. \quad \square$$

Thus, Kepler's third law appears to be generalized through the isochrone group. Kepler's third law is mainly used for mass determination, as in, for example, the post-newtonian approximation to estimate the mass of black holes. For a Kepler potential, only one orbit is theoretically necessary to determine the mass of the central attractive body given by  $\mu$ . For other isochrone potentials, using (4), only two orbits would be necessary to determine the parameter  $b$  and mass  $\mu$  described by their isochrone potential.

#### 4.4 The Bertrand theorem

In 1873, J. Bertrand published a fascinating theorem: *There are only two central potentials for which all orbits with an initial velocity below a certain limit are closed, namely the Keplerian and the harmonic potentials.* While this fascinating result was proved more than 140 years ago, the proof of this theorem has been retaining the attention. According to the most recent reviews [38] and works on this topic [1, chap. 3], it has been proven using very different techniques: [4, 2, 25, 23, 10], using global methods, sometimes stemming from the analysis of the precession rate as initiated in proposition XLV of [33]; [9, 15, 41, 12], developing perturbative expansions; [39, 18, 37], using inverse transformations methods; [36], by searching for additional constants of motion; and [13], mainly using Birkhoff invariants along circular orbits in a generic potential. Furthermore, the original proof does not mention the case of collision orbits. We will therefore consider the result of Bertrand's theorem under the hypotheses of orbits that are bounded in position and bounded away from 0. We propose here to show that, in fact, Bertrand's theorem is a refined property of the isochrone one.

**Theorem 5** *In a given radial potential  $\psi$ , if all non-circular orbits that are bounded in position and bounded away from 0 are closed, then  $\psi$  is isochrone.*

*Proof* In a given radial potential  $\psi$ , if all bounded and bounded away from 0 orbits are closed, the increment of the azimuthal angle  $\Delta\varphi$  during the transfer from  $r_a$

to  $r_p$  is a fractional multiple of  $2\pi$ , i.e. the quantity  $n_\varphi = \frac{\Delta\varphi}{2\pi} \in \mathbb{Q}$ . But, for a given radial potential  $\psi(r)$ , we have that

$$n_\varphi = -\frac{\partial \mathcal{A}_r}{\partial \Lambda} = \frac{1}{\pi} \int_{r_p}^{r_a} \frac{\Lambda}{r^2 \sqrt{2[\xi - \psi(r)] - \frac{\Lambda^2}{r^2}}} dr$$

is a continuous mapping  $(\xi, \Lambda) \mapsto n_\varphi$ . By continuity, because the set  $\mathbb{R} \setminus \mathbb{Q}$  is dense in  $\mathbb{R}$ , one can conclude that in order to only have closed orbits,  $n_\varphi = cst \in \mathbb{Q}$ . In these conditions we then have

$$0 = \frac{\partial n_\varphi}{\partial \xi}.$$

This characterizes an isochrone potential according to theorem 6 of appendix A. The potentials of the form  $-\frac{\mu}{r^\alpha}$  with  $\alpha > 2$  are excluded because all orbits that are bounded in position either collide at the origin or are circular.  $\square$

Using our study we can go further because we have obtained a geometric and algebraic description of the whole set of isochrone potentials. More specifically, we have obtained in table (50) the explicit value of  $n_\varphi$  for all isochrone potentials. The completeness of our description and this table enable us to claim that Bertrand's theorem is a corollary of theorem 5.

**Corollary 2** *The Bertrand Theorem ! There are only two central potentials for which all non-circular orbits that are bounded in position and bounded away from 0 are closed, namely the Keplerian and the harmonic potentials.*

*Proof* As the quantities  $\frac{\Lambda}{2\sqrt{4b\mu + \Lambda^2}}$  and  $\frac{\Lambda}{\sqrt{\lambda + \Lambda^2}}$  in proposition 1 and 2 cannot be rational for each value of  $\Lambda$ , among all isochrone potentials, only  $\psi_{ke}$  and  $\psi_{ha}$  have rational  $n_\varphi$  for all orbits, i.e. for all values of  $(\xi, \Lambda)$ .  $\square$

In a given potential, the fact that all bounded orbits are closed, namely Bertrand's property, is then a supplementary restriction to the isochrone one.

## 5 Conclusion

In this paper we have revisited the set of isochrone orbits in radial 3D potentials. These models concern self-organised radial systems with long-range interactions like gravitation or electrostatics with one kind of electric charge. Let us summarize the main results we have obtained:

1. We have clarified the original proof by Michel Hénon [20] that isochrone potentials are contained in a branch of a parabola in adapted coordinates (theorem 7). These parabolas characterize the property of isochrony.
2. Taking into account very general properties of potentials in physics — i.e. invariance under the addition of a constant, conservation of the energy and angular momentum for isolated radial systems — we have given a geometrical characterization and classification of the set of all isochrone orbits/potentials that we have completed. This characterization (theorem 1) is based on a subgroup  $\mathbb{A}$  of the real affine group.

3. We have shown (theorem 1 and sec. 2.5) that under the group action of  $\mathbb{A}$ , any isochrone potential is in the orbit of one of the four fundamental potentials: Kepler, Hénon, Bounded or Harmonic (definition 2).
4. Focusing on orbits, we have proposed a mapping which generalizes the Bohlin transformation to all isochrone potentials. This mapping, summarized in theorem 2, connects any Keplerian elliptic orbit to a particular isochrone radially periodic orbit. Reciprocally, by theorem 3, we have shown how to construct the elliptic Keplerian orbit connected to any isochrone periodic orbit. This mapping is based on a particular linear transformation, that we call a bolst, which preserves the orbital differential equation for a given value of the angular momentum.
5. With the set of symmetric bolsts, namely Ibolsts, we have revealed the relative behavior of the isochrone property of orbits/potentials. We have detailed in sec. 3.2 a lot of similarities between the special theory of relativity and the isochrony of orbits in radial potentials. In this view, a given orbit in an isochrone potential is seen as a Keplerian orbit in its special frame. This is the Isochrone Relativity presented in sec. 3.2. The time and energy are relative to each orbit which defines a frame of reference. Various examples were presented and illustrated to construct isochrone orbits in isochrone potentials.
6. The explicit expression of the radial ( $\tau_r$ ) and azimuthal ( $n_\varphi$ ) periods was calculated for all fundamental isochrone potentials. These results are presented in proposition 1. The computation of these periods in physical or gauged isochrones is possible using the results presented in proposition 2.
7. We have proposed a generalization of the quadricentennial Kepler's Third Law in theorem 4. While this classic law involves the semi major axis of *closed* Keplerian orbits, we define characteristic lengths in each isochrone potential that are related to the radial period in the famous  $3/2$  power equation. This rational value  $3/2$  is well known to be related to the mechanical similarity involved in the Kepler potential and its  $-1$  homogeneity property (e.g. [26] p. 22-24). In this view, the generalization of the Kepler's Third Law to any isochrone is not surprising since we have seen that any isochrone is a Kepler in the adequate referential.
8. Noting that both the radial period  $\tau_r$  and the precession rate  $n_\varphi$  are partial derivatives of the same quantity, i.e. the radial action  $\mathcal{A}_r$ , we observed that the famous Bertrand's theorem is a specific property of isochrones. Once again this property could be interpreted as a consequence of the isochrone relativity.

The essence of isochrony is Keplerian. As isochrony is characterized by the parabolic property in Hénon's variables, we understand the linear transformations that act on these parabolas and are shaped by the bolst  $B_{\alpha,\beta}$  play crucial roles. Merging these ideas, we conjecture that a theory of general relativity of radial potentials could be formulated using non-linear transformations. This theory could relate any orbit in a radial potential to an associated orbit in a Kepler potential.

In a forthcoming paper we will explain the physical importance of the isochrone potential during the formation and evolution process of self-gravitating systems.

## Appendix

### A Isochrone characterization

Let us recall that the radial action  $\mathcal{A}_r$  gives the radial period  $\tau_r$  and the increment of the azimuthal angle  $n_\varphi$  through (3) and (4) in sec. 2.1:

$$\frac{\partial \mathcal{A}_r}{\partial \xi} = \frac{\tau_r}{2\pi} \quad \text{and} \quad -\frac{\partial \mathcal{A}_r}{\partial \Lambda} = \frac{\Delta\varphi}{2\pi} = n_\varphi.$$

The exclusive  $\xi$ -dependency of  $\tau_r$  is the fundamental isochrone property used by Michel Hénon to define isochrone potentials. After his analysis, he remarked the exclusive  $\Lambda$ -dependency of  $n_\varphi$  for his potential. The following theorem establishes the equivalence of properties which can characterize isochrone potentials as a whole.

**Theorem 6** *Consider a central potential  $\psi$ . Then the following properties are equivalent:*

1. For any orbit  $(\xi, \Lambda)$  in  $\psi$ ,  $\tau_r$  only depends on  $\xi$ .
2. For any orbit  $(\xi, \Lambda)$  in  $\psi$ ,  $n_\varphi$  only depends on  $\Lambda$ .
3. There exist two function  $f$  and  $g$  such that for any  $(\xi, \Lambda)$  the radial action is  $\mathcal{A}_r(\xi, \Lambda) = f(\xi) + g(\Lambda)$ .

*Proof* The separation of variables in the radial action expressed in 3 implies the two properties 1 and 2 by direct differentiation with respect to  $\xi$  for 1 and  $\Lambda$  for 2. Assume 2 is true for any orbit in the central potential  $\psi$ . Then  $\frac{\partial \mathcal{A}_r}{\partial \xi} = \frac{\tau_r(\xi)}{2\pi}$  and by integration there exists a function  $g$ , constant with respect to  $\xi$ , such that  $\mathcal{A}_r(\xi, \Lambda) = f(\xi) + g(\Lambda)$ , where  $f$  is a primitive of  $\frac{\tau_r}{2\pi}$ . We thus recover 3. In the same way, assuming 2 implies 3.  $\square$

### B Proof of a parabola property

Michel Hénon has shown in [20] the equivalence between the isochrony of a potential  $\psi$  and the parabolic property of the graph  $\mathcal{C}$  of  $f : x \rightarrow x\psi$  associated with it. We propose here a different proof based on the analyticity of the potential.

We call  $(\mathcal{P})$  this parabolic property, and it can be formulated as follows.

A function  $f : I \rightarrow \mathbb{R}$  has the property  $(\mathcal{P})$  if and only if :

1.  $f$  is either convex or concave on the real interval  $I$ , i.e.  $f'' > 0$  or  $f'' < 0$  on  $I$ .
2. For any  $P_0$  belonging to its graph  $\mathcal{C}$ , and for any line  $\mathcal{L}$  parallel to the tangent  $\mathcal{T}_{P_0}(\mathcal{C})$ , the square length of the projected chord  $|x_{a,1} - x_{p,1}|$  is proportional to the distance between the chord and the tangent to the curve that is parallel to the chord. The proportional relation holds equivalently with the vertical distance  $P_0I$  between  $\mathcal{T}_{P_0}(\mathcal{C})$  and  $\mathcal{L}$ . In figure 2 we have  $\mathcal{T}_{P_0}(\mathcal{C}) : y = \xi x - \Lambda_0^2$  and  $\mathcal{L} : y = \xi x - \Lambda_1^2$ .

In terms of function, this last point translates as follows:

$$(\mathcal{P}) : \begin{cases} \forall x_0 \in I, \exists \varpi(x_0) \in \mathbb{R}_+ \text{ such that } \forall \lambda > 0, \text{ when they exist,} \\ \text{the two solutions } x_p \text{ and } x_a \text{ of the equation} \\ f(x) - f(x_0) = \lambda + f'(x_0)(x - x_0) \\ \text{satisfy the relation } (x_a - x_p) = \varpi(x_0)\sqrt{\lambda} \text{ with } x_a > x_p. \end{cases}$$

Michel Hénon's equivalence then corresponds to the following theorem.

**Theorem 7** *Let  $f : I \rightarrow \mathbb{R}$  be an analytic real function on an interval  $I \subset \mathbb{R}$ . Then the graph of  $f$  is a parabola if and only if  $f$  has the property  $(\mathcal{P})$ .*

The proof of this result will be done in several steps. The first one is a reduction procedure given by the following lemma.

**Lemma 5** *Let  $g : I \rightarrow \mathbb{R}$  be a real analytic function satisfying property  $(\mathcal{P})$ . Then we have*

1. *For any real constant  $a \neq 0$ ,  $f := ag$  satisfies  $(\mathcal{P})$ ;*
2. *For any constants  $(\varepsilon, \lambda) \in \mathbb{R}^2$ ,  $f(x) = g(x) + \varepsilon x + \lambda$  satisfies  $(\mathcal{P})$ ;*
3. *For any constants  $(\varepsilon, \lambda) \in \mathbb{R}^2$ , with  $\varepsilon \neq 0$ ,  $f(x) := g(\varepsilon x + \lambda)$  satisfies  $(\mathcal{P})$ .*

This statement indicates that property  $(\mathcal{P})$  is stable by affine transformations acting on the graph of the considered function. Its proof is quite obvious and is left to the reader.

Any graph of a parabola can be obtained by the transformations of lemma 5 of the graphs of  $x \mapsto \sqrt{x}$  or  $x \mapsto x^2$ . It follows that, if the graph of  $f$  is a parabola, then  $f$  satisfies the simple implication of the theorem.

In order to have the converse implication, i.e.  $(\mathcal{P}) \implies \mathcal{C}$  is a parabola, we now consider the simple case where, in figure 2,  $\mathcal{T}_{P_0}(\mathcal{C})$  is horizontal.

**Lemma 6** *If  $\varphi : I \rightarrow \mathbb{R}$  is a real analytic function and if at  $x_0 \in I$  we have  $\varphi'(x_0) = 0$  and  $\varphi''(x_0) = 2$ , then*

$$5 \left[ \varphi^{(3)}(x_0) \right]^2 = 6 \varphi^{(4)}(x_0). \quad (\text{B1})$$

*Proof* Let  $\varphi(x) = g(z)$  with  $z = x - x_0$ . Then, since  $\varphi$  is analytic,  $g$  has a convergent Taylor expansion at  $x_0$  of the form  $g(z) = z^2 + g_3 z^3 + g_4 z^4 + \dots$ , such that

$$g(z) = z^2 \left( 1 + \sum_{n \geq 3} g_n z^{n-2} \right) = z^2 (1 + R(z)),$$

where  $R(z)$  is a convergent series that vanishes at  $z = 0$ . Then, we may expand

$$\sqrt{1 + R(z)} = 1 + \frac{1}{2}R + \frac{1}{2!} \left( \frac{1}{2} \right) \left( \frac{1}{2} - 1 \right) R^2 + \dots$$

and insert it in

$$\sqrt{g(z)} = G(z) = z \sqrt{1 + R(z)} = z + G_2 z^2 + G_3 z^3 + \dots$$

Because  $G(0) = 0$  and  $G'(0) = 1$ ,  $G$  is locally bijective in the neighborhood of  $z = 0$ ; the analytic inverse function theorem assures that its inverse  $H$  is also a convergent power series  $H(z) = z + \sum_{n \geq 2} h_n z^n$ .

The fact that  $\varphi$  satisfies  $(\mathcal{P})$  means that for any small enough  $\lambda > 0$  the two solutions  $z_1$  and  $z_2 > z_1$  of  $g(z) = \lambda$  satisfy  $z_2 - z_1 = \varpi(x_0) \sqrt{\lambda}$ . However,

$$\begin{aligned} g(z) = \lambda &\Leftrightarrow G^2(z) = \lambda \\ &\Leftrightarrow G(z) = \pm \lambda \\ &\Leftrightarrow z = H(\pm \lambda). \end{aligned}$$

More precisely,  $z_2 = H(\sqrt{\lambda})$  and  $z_1 = H(-\sqrt{\lambda})$  if  $\lambda \geq 0$  is small enough because  $H$  locally increases. The second condition from  $(\mathcal{P})$  gives  $H(\sqrt{\lambda}) - H(-\sqrt{\lambda}) = \varpi(x_0)\sqrt{\lambda}$  for sufficiently small  $\lambda \geq 0$  and

$$H(t) - H(-t) = \varpi t, \quad (\text{B2})$$

since all members of the previous equation are power series. Inserting the expression of  $H(t) = \sum_{n \geq 1} h_n t^n$  in (B2), noting that the even terms disappear, one finds  $2h_1 = 2 = \varpi$  and  $h_{2m+1} = 0$  if  $m \geq 1$ . In other words,

$$H(t) = t + h_2 t^2 + h_4 t^4 + \dots$$

Identifying the terms of the equality given by  $H \circ G(z) = z$ , one specifically finds  $G_2 = -h_2$  and  $G_3 = -2h_2 G_2 = 2h_2^2$ . Hence the expansion of  $g$  is written as

$$\begin{aligned} g(z) = G^2(z) &= z^2 - 2h_2 z^3 + 5h_2^2 z^4 + \dots \\ &= \frac{1}{2}g''(x_0)z^2 + \frac{1}{6}g^{(3)}(x_0)z^3 + \frac{1}{24}g^{(4)}(x_0)z^4 + \dots, \end{aligned}$$

where the identification between each term leads to  $\left(g^{(3)}(x_0)\right)^2 = 12^2 h_2^2 = \frac{6}{5}g^{(4)}(x_0)$  which is exactly (B1).  $\square$

We now exploit this particular case to characterize the property  $(\mathcal{P})$  in terms of a differential equation.

**Lemma 7** *Let  $f : I \rightarrow \mathbb{R}$  be a real analytic function satisfying  $(\mathcal{P})$ . Then  $f$  also satisfies*

$$\forall x_0 \in I, 5 \left[ f^{(3)}(x_0) \right]^2 = 3f^{(4)}(x_0) f''(x_0). \quad (\text{B3})$$

*Proof* For any point  $x_0 \in I$  with  $f''(x_0) \neq 0$ , the function

$$\varphi(x) = \frac{2}{f''(x_0)} [f(x) - f(x_0) - f'(x_0)(x - x_0)]$$

satisfies the property  $(\mathcal{P})$  according to lemma 5. Moreover we have that  $\varphi'(x_0) = 0$  and

$$\begin{cases} \varphi''(x) = \frac{2f''(x)}{f''(x_0)} \implies \varphi''(x_0) = 2 \\ \varphi^{(3)}(x) = \frac{2f^{(3)}(x)}{f''(x_0)} \implies \varphi^{(3)}(x_0) = \frac{2f^{(3)}(x_0)}{f''(x_0)} \\ \varphi^{(4)}(x) = \frac{2f^{(4)}(x)}{f''(x_0)} \implies \varphi^{(4)}(x_0) = \frac{2f^{(4)}(x_0)}{f''(x_0)}. \end{cases}$$

As a consequence,  $\varphi$  satisfies the assumptions of lemma 6 and therefore (B1)  $\implies$  (B3).  $\square$

Let us observe that (B3) was obtained under the condition that  $f''(x_0) \neq 0$ . By analytic continuation the relation is still satisfied at the isolated points where  $f''$  could vanish.

We are therefore led to solve (B3), which is in fact the *universal differential equation for parabolas*. Setting  $w = f''$ , (B3) becomes

$$5(w')^2 = 3w''w. \quad (\text{B4})$$

Two cases may occur:

1. If  $w' = f^{(3)} := 0$  on  $I$ :  
then  $f''$  is constant and  $f$  is a second-degree polynomial and its graph  $\mathcal{C}$  is a parabola.
2. If  $w' = f^{(3)}$  do not vanish everywhere on  $I$ :  
then on any subset where  $w' \neq 0$ , equation (B4) becomes

$$\frac{5w'}{w} = \frac{3w''}{w'},$$

which gives by integration

$$5 \ln |w| = 3 \ln |w'| + cst \implies w' w^{-5/3} = cst.$$

Hence  $w^{-2/3}$  is a linear function of  $x$ , namely  $w(x) = f''(x) = (\varepsilon x + \lambda)^{-3/2}$ . By integrating this equation twice, we get that  $f$  is proportional to  $f_0(x) = \sqrt{\varepsilon x + \lambda} + ax + b$  whose graph is a parabola too.

This concludes the proof of theorem 7.

## C Useful Lemmas

Consider

- a frame  $\mathcal{R}_O = (O, \mathbf{i}, \mathbf{j})$  with coordinates  $(x, y)$  for each point  $M$ ;
- a linear application  $L : \mathbb{R}^2 \rightarrow \mathbb{R}^2$  such that  $L(\mathbf{i}) = \mathbf{u}$  and  $L(\mathbf{j}) = \mathbf{v}$ ;
- a curve  $\mathcal{C}$  of equation  $f(x, y) = 0$  in the frame  $\mathcal{R}$ .

The linearity of  $L$  ensures the two properties below.

**Lemma 8** *The cartesian equation of curve  $\mathcal{C}' = L(\mathcal{C})$  in the frame  $\mathcal{R}'_O = (O, \mathbf{u}, \mathbf{v})$  remains  $f(x, y) = 0$ .*

*Proof* Consider  $\overrightarrow{OM} = x\mathbf{i} + y\mathbf{j}$ . Then  $M \in \mathcal{C} \Leftrightarrow f(x, y) = 0$ . But  $L(\overrightarrow{OM}) = xL(\mathbf{i}) + yL(\mathbf{j}) = x\mathbf{u} + y\mathbf{v} \in \mathcal{C}'$  by definition. Thus  $f(x, y) = 0$  also defines  $\mathcal{C}'$  in  $\mathcal{R}'_O$ .

Define

- $\mathcal{T}_O(\mathcal{P})$  the tangent at the origin  $O$  to a parabola  $\mathcal{P}$ ;
- $\mathcal{S}(\mathcal{P})$  the symmetry axis of parabola  $\mathcal{P}$ .

Then we have the following lemma:

**Lemma 9** *If  $\mathcal{P}' = L(\mathcal{P})$  then  $\mathcal{T}_O(\mathcal{P}') = L(\mathcal{T}_O(\mathcal{P}))$  and  $\mathcal{S}(\mathcal{P}') = L(\mathcal{S}(\mathcal{P}))$ .*

*Proof* According to lemma 8,  $\mathcal{P}$  and  $\mathcal{P}'$  have the equation  $(ax + by) + e = (cx + dy)^2$  in their respective frames. Then the tangent  $\mathcal{T}_O$  has the direction vector  $\mathbf{t} = -b\mathbf{i} + a\mathbf{j}$  and the symmetry axis  $\mathcal{S}(\mathcal{P})$  has the vector  $\mathbf{n} = -d\mathbf{i} + c\mathbf{j}$ . In the same way, with natural notations,  $\mathbf{t}' = -b\mathbf{u} + a\mathbf{v}$  and  $\mathbf{n}' = -d\mathbf{u} + c\mathbf{v}$ . Thus  $\mathbf{t}' = L(\mathbf{t})$  and  $\mathbf{n}' = L(\mathbf{n})$ .



## D Isochrone integrals

**Lemma 10** *The Keplerian and harmonic radial actions are given by*

$$\mathcal{A}_r^{\text{ke}} = \frac{\mu}{\sqrt{-2\xi}} - \Lambda \quad \text{and} \quad \mathcal{A}_r^{\text{ha}} = \frac{\xi}{2\omega} - \frac{\Lambda}{2}.$$

For any pair of positive real  $(u_1, u_2)$  such that  $u_1 < u_2$ , we have

$$\mathcal{I}_1(u_1, u_2) = \int_{u_1}^{u_2} \frac{\sqrt{(u-u_1)(u_2-u)}}{u} du = \frac{\pi}{2} (u_1 + u_2 - 2\sqrt{u_1 u_2})$$

and

$$\begin{aligned} \mathcal{I}_2(u_1, u_2) &= \int_{u_1}^{u_2} \frac{(u-1)\sqrt{(u-u_1)(u_2-u)}}{u(u-2)} du \\ &= \begin{cases} \frac{\pi}{2} \left[ u_1 + u_2 - \sqrt{u_1 u_2} - \sqrt{(u_1-2)(u_2-2)} - 2 \right] & \text{if } 2 < u_1 \\ \frac{\pi}{2} \left[ u_1 + u_2 - \sqrt{u_1 u_2} + \sqrt{(u_1-2)(u_2-2)} - 2 \right] & \text{if } u_2 < 2. \end{cases} \end{aligned}$$

The result of  $\mathcal{I}_1$  can be obtained by a direct meticulous computation; instead, we propose to deduce it from the physical computation of the Keplerian radial action.

In a second step, we will deduce  $\mathcal{I}_2$  from  $\mathcal{I}_1$ .

### D.1 Computation of $\mathcal{A}_r^{\text{ke}}$ , $\mathcal{A}_r^{\text{ha}}$ and physical deduction of $\mathcal{I}_1$

The radial action for an orbit of negative energy  $\xi$  and momentum  $\Lambda$  in a Keplerian potential  $\psi_{\text{ke}}(r) = -\frac{\mu}{r}$  is given by

$$\mathcal{A}_r^{\text{ke}} = \frac{1}{\pi} \int_{r_p}^{r_a} \sqrt{2[\xi - \psi_{\text{ke}}(r)] - \frac{\Lambda^2}{r^2}} dr \quad (\text{D5})$$

$$= \frac{\sqrt{-2\xi}}{\pi} \int_{r_p}^{r_a} \frac{\sqrt{(r-r_p)(r_a-r)}}{r} dr \quad \text{with} \quad \begin{cases} r_p + r_a = -\frac{\mu}{\xi} \\ r_p r_a = -\frac{\Lambda^2}{2\xi} \end{cases} \quad (\text{D6})$$

as in (51). The radial period and the azimuthal precession are just partial derivatives of the radial action according to (3) and (4):

$$\frac{\partial \mathcal{A}_r}{\partial \xi} = \frac{\tau_r}{2\pi} \quad \text{and} \quad \frac{\partial \mathcal{A}_r}{\partial \Lambda} = -\frac{\Delta\varphi}{2\pi} = -n_\varphi.$$

For a negative energy, the Kepler orbit is an ellipse with semi-major axis  $a = \frac{1}{2}(r_a + r_p)$ , where  $r_a$  and  $r_p$  are respectively the apoastron and the periastron of the trajectory (hence  $r_a \geq r_p$ ). For this Keplerian ellipse we trivially have  $\Delta\varphi = 2\pi$  and then  $n_\varphi = 1$ . By integration, one gets in this case

$$\frac{\partial \mathcal{A}_r^{\text{ke}}}{\partial \Lambda} = -1 \implies \mathcal{A}_r^{\text{ke}} = -\Lambda + f(\xi).$$

The unknown function  $f(\xi)$  could be expressed in terms of the radial period through the relation

$$\tau_r = 2\pi \frac{\partial \mathcal{A}_r^{\text{ke}}}{\partial \xi} = 2\pi f'(\xi).$$

From the classical Kepler's third law, we have  $\tau_r = \frac{\pi\mu}{\sqrt{2}(-\xi)^{3/2}}$ , which gives

$$f(\xi) = \frac{\mu}{2\sqrt{2}} \int (-\xi)^{-3/2} d\xi + c = \frac{\mu}{\sqrt{-2\xi}} + c \implies \mathcal{A}_r^{\text{ke}} = \frac{\mu}{\sqrt{-2\xi}} - \Lambda + c, \quad (\text{D7})$$

where  $c$  is a constant. On the one hand, for a circular Keplerian orbit we have  $r_a = r_p$ , so that  $\mathcal{A}_r^{\text{ke}}$  given by (D6) vanishes in this case. On the other hand, a circular Keplerian orbit is characterized by  $\Lambda = \frac{\mu}{\sqrt{-2\xi}}$ . Combining these two remarks in (D7) gives  $c = 0$ . Plugging this result into (D6), one obtains

$$\mathcal{I}_1(r_p, r_a) = \frac{\pi}{\sqrt{-2\xi}} \mathcal{A}_r^{\text{ke}} = \frac{\pi}{2} \left( \frac{\mu}{(-\xi)} - \frac{2\Lambda}{\sqrt{-2\xi}} \right), \quad (\text{D8})$$

where we recognize the values of the sum and the product of  $r_a$  and  $r_p$  given by (D6). Hence,

$$\mathcal{I}_1(r_p, r_a) = \frac{\pi}{2} (r_p + r_a - 2\sqrt{r_p r_a}).$$

Since the above formula holds for any arbitrary positive numbers  $r_p \leq r_a$ , we deduce the explicit expression of  $\mathcal{I}_1$  given in the lemma.

In the same way, given  $\tau_r = \frac{\pi}{\omega}$  and  $n_\varphi = \frac{1}{2}$  to compute the radial action with (3) and (4), the proof can be done similarly for a harmonic potential.

## D.2 Proof for the expression of $\mathcal{I}_2$

The result for  $\mathcal{I}_2(u_1, u_2)$  simply comes from the relation

$$\frac{2(u-1)}{u(u-2)} = \frac{1}{u} + \frac{1}{u-2}$$

from which we have

$$2\mathcal{I}_2(u_1, u_2) = \mathcal{I}_1(u_1, u_2) + \int_{u_1}^{u_2} \frac{\sqrt{(u-u_1)(u_2-u)}}{u-2} du. \quad (\text{D9})$$

Two cases are of interest:

1. If  $2 < u_1 < u_2$ , then plugging  $v = u - 2$  into the last integral of (D9), we get  $2\mathcal{I}_2(u_1, u_2) = \mathcal{I}_1(u_1, u_2) + \mathcal{I}_1(u_1 - 2, u_2 - 2)$  which gives

$$\mathcal{I}_2(u_1, u_2) = \frac{\pi}{2} \left[ u_1 + u_2 - \sqrt{u_1 u_2} - \sqrt{(u_1 - 2)(u_2 - 2)} - 2 \right].$$

2. If  $0 < u_1 < u_2 < 2$ , then plugging  $v = 2 - u$  into the last integral of (D9), we get  $2\mathcal{I}_2(u_1, u_2) = \mathcal{I}_1(u_1, u_2) - \mathcal{I}_1(2 - u_1, 2 - u_2)$  which gives

$$\mathcal{I}_2(u_1, u_2) = \frac{\pi}{2} \left[ u_1 + u_2 - \sqrt{u_1 u_2} + \sqrt{(u_1 - 2)(u_2 - 2)} - 2 \right].$$

This completes the proof for  $\mathcal{I}_2$ .

**Acknowledgment** This work is supported by the “IDI 2015” project funded by the IDEX Paris-Saclay, ANR-11-IDEX-0003-02. JP especially thanks Jean-Baptiste Fouvry for helpful discussions about Bertrand's theorem. ASP especially thanks Alain Albouy for his great remarks on Bertrand's theorem and for sharing his deep historical knowledge. The authors are grateful to Faisal Amlani for his detailed copy-editing of the paper and thank the referees of the article for their helpful comments and fruitful suggestions.

## References

1. Albouy A., Lectures on the two-body problem, Classical and celestial mechanics (Recife, 1993/1999), pp.63-116, 2002
2. Arnold V. I., Mathematical Methods of Classical Mechanics, Springer-Verlag, New York, 1978
3. Arnold V.I., Huygens & Barrow & Newton & Hooke, Birkhäuser Verlag, Basel, p.95, 1990
4. Bertrand J., Théorème relatif au mouvement d'un point attiré vers un centre fixe. Comptes Rendus de l'Académie des Sciences de Paris, 77, p. 849–853, 1873
5. Binney J., Hénon's Isochrone Model, in “Une vie dédiée aux systèmes dynamiques” ed. J.-M. Alimi, R. Mohayaee & J. Perez, Hermann, 2016, p.99–109 - arxiv astro-ph 1411.4937
6. Binney J., Tremaine S., Galactic Dynamics 2<sup>nd</sup> edition, Princeton University Press, 2008
7. Bohlin K., Bull. Astron. Ser. I, 28, 113, 1911
8. Borel E., Introduction géométrique à quelques théories physiques, Gauthier-Villars, 1914
9. Brown L. S., Forces giving no orbit precession, Am. J. Phys. 46, p. 930–931, 1978
10. Castro-Quilantan J. L., Del Rio-Correa J. L. & Medina M. A. R., Alternative proof of Bertrand's theorem using a phase space approach, Rev. Mex. Fis., 42, p. 867–877, 1996
11. Dehnen W., A Family of Potential-Density Pairs for Spherical Galaxies and Bulges, Mon. Not. R. Astron. Soc, 265, p.250, 1993
12. Fasano A. & Marni S., Analytic Mechanics - An Introduction, Oxford University Press, Oxford England, 2006
13. Féjóz, J., Kaczmarek, L., Sur le théorème de Bertrand (d'après Michael Herman), Michael Herman Memorial Issue, Ergodic Theory Dyn. Sys.24:5, 1583–1589, 2004
14. Gidas B., Ni W.-M., Nirenberg L., Symmetry of positive solutions of nonlinear elliptic equations in  $\mathbb{R}^n$ , Math. Analysis & App., 79, pp. 369-402, 1981
15. Goldstein H., Classical Mechanics, Addison Wesley, New York, p. 601–605, 1981
16. Gourgoulhon, E., Special Relativity in General Frames, Graduate Texts in Physics, Springer, 784 pages, 2013
17. Goursat E., Les transformations isogonales en Mécanique, Comptes rendus hebdomadaires de l'académie des sciences, 108, pp. 446–448, 1889
18. Grandati Y., Bérard A. & Ménas F., Inverse problem and Bertrand's theorem, Am. J. Phys. 76, p. 782–787, 2008
19. Grandati Y., Bérard A., and Mohrbach H., Complex representation of planar motions and conserved quantities of the Kepler and Hooke problems. Journal of Nonlinear Mathematical Physics, Vol.17, No. 2, 213-225, 2010
20. Hénon M., L'amas isochrone, Annales d'Astrophysique, Vol. 22, p.126, 1959
21. Hernquist L., An analytical model for spherical galaxies and bulges, Ap. J, . 356, pp. 359-364, 1990
22. Jaffe W., A simple model for the distribution of light in spherical galaxies, Mon. Not. R. Astron. Soc, 202, p.995–999, 1983
23. Jovanović V., A note on the proof of Bertrand's theorem, Theoretical and Applied Mathematics, Vol. 42, Issue 1, pp.27-33, 2015
24. Kepler J., Harmonices Mundi, 1619
25. Lagrange J.-L., Solution de différents problèmes de calcul intégral, Œuvres complètes, Vol. I, p.573
26. Landau L.D., Lifshitz E.M., Mechanics - Volume 1 of A Course of Theoretical Physics, Pergamon Press, 1969
27. Levi-Civita T., Sur la résolution qualitative du problème restreint des trois corps, Acta Math., 30, 1906
28. Lynden-Bell D., Statistical mechanics of violent relaxation in stellar systems, Mon. Not. R. Astron. Soc, 136,p.101,1967
29. Lynden-Bell, D., Bound central orbits, Mon. Not. R. Astron Soc, 447 (2): 1962-1972, 2015
30. Lynden-Bell D., Variations on the theme of Michel Hénon's Isochrone, in “Une vie dédiée aux systèmes dynamiques” ed. J.-M. Alimi, R. Mohayaee & J. Perez, Hermann, 2016, pp.81–86 - arxiv astro-ph 1411.4926
31. Lynden-Bell D., Jin S., Analytic central orbits and their transformation group, Mon. Not. R. Astron. Soc, 386, pp. 245-260, 2008
32. MacLaurin C., A treatise on fluxions, London : W. Baynes, 1801
33. Newton I., Philosophiae naturalis principia mathematica, London, 1756
34. Navarro J., Frenk C., White S., The Structure of Cold Dark Matter Halos, Ap.J, 463, p. 563, 1996

35. Perez J., Aly J.-J., Stability of spherical self-gravitating systems I: Analytical results, *Mon. Not. R. Astron. Soc.*, 280, p. 689, 1996
36. Rartinez-y-Romero R. P., Nunez-Yepez H. N. & Salas-Brito A. L., Closed orbits and constants of motion in classical mechanics, *Eur. J. Phys.* 13, p. 26–31, 1992
37. Santos F., Soares V. & Tort A., Determination of the Apsidal Angle and Bertrand's theorem, *Phys. Rev. E*, 79, 036605-1–6, 2009
38. Siu A. Chin, A truly elementary proof of Bertrand's theorem, *Am. J. Phys.* , 83, 2015
39. Tikochinsky Y., A simplified proof of Bertrand's theorem, *Am. J. Phys.* 56, p.1073–1075, 1988
40. de Vaucouleurs G., Recherches sur les Nebuleuses Extragalactiques, *Ann. Astroph.*, 11, p.247, 1948
41. Zarmi Y., The Bertrand theorem revisited, *Am. J. Phys.* 70, p. 446–449, 2002





© Jean-Charles Spindler, *Somewhere — The dance of the star*







**Title** Gravitational Dynamical Systems

**Keywords** Gravitation, dynamics, cosmology.

**Abstract** Dynamical systems have a centuries-long history with roots going back to the mathematical development for astronomy. In the modern formalism, the present thesis investigates dynamical properties of gravitation at different astrophysical or cosmological scales.

In potential theory, isochrony often refers to harmonic oscillations of pendulums. In 1959, the mathematician and astronomer Michel Hénon introduced an extended definition of isochrony to characterize orbital oscillations of stars around the center of the system which they belong to. In that case, the period of oscillations can depend on the energy of the star. Today, Michel Hénon's isochrone potential is mainly used for its integrable property in numerical simulations, but is not widely known. In this thesis, we revisit his geometrical characterization of isochrony and complete the family of isochrone potentials in physics. The classification of this family under different mathematical group actions highlights a particular relation between the isochrones. The actual Keplerian nature of isochrones is pointed out and stands at the heart of the new isochrone relativity, which are presented together.

The consequences of this relativity in celestial mechanics — a generalization of Kepler's Third law, Bohlin or Levi-Civita transformation, Bertrand's theorem — are applied to analyze the result of a gravitational collapse. By considering dynamical orbital properties, an isochrone analysis is developed to possibly characterize a quasi-stationary state of isolated self-gravitating systems, such as dynamically young stellar clusters or galaxies.

At a cosmological scale, the dynamics of the universe depends on its energy content. Its evolution can be expressed as an ecological dynamical system, namely a conservative generalized Lotka-Volterra model. In this framework of a spatially homogeneous and isotropic spacetime, named Jungle Universe, the dynamical impact of a non-gravitational interaction between the energy components is analyzed. As a result, effective dynamical behaviors can arise.

**Titre** Systèmes Dynamiques Gravitationnels

**Mots clefs** Gravitation, dynamique, cosmologie.

**Résumé** L'histoire séculaire des systèmes dynamiques puise ses origines dans le développement du cadre mathématique en astronomie. L'objet de cette thèse est l'étude de propriétés de la gravitation de ce point de vue de la dynamique à différentes échelles cosmologiques.

Dans la théorie du potentiel, l'isochronie définit généralement le mouvement d'oscillation harmonique de pendules. En 1959, le mathématicien et astronome Michel Hénon étend cette définition afin de caractériser les oscillations orbitales d'étoiles, autour du centre du système à symétrie sphérique auquel elles appartiennent. Dans ce cas, la période d'oscillation peut dépendre de l'énergie de l'étoile. Aujourd'hui, son potentiel isochrone est majoritairement utilisé en simulation numérique pour ses propriétés analytiques d'intégrabilité, mais demeure par ailleurs souvent méconnu. Dans cette thèse, nous revisitons la caractérisation géométrique de l'isochronie comme initiée par Michel Hénon et complétons ainsi la famille des potentiels isochrones en physique. La classification de cet ensemble sous l'action de divers groupes mathématiques met en évidence une relation privilégiée entre les isochrones. Nous montrons alors la nature keplérienne intrinsèque aux isochrones, laquelle est au cœur de la nouvelle relativité isochrone que nous présentons.

Les conséquences de cette relativité en mécanique céleste, à savoir la généralisation de la troisième loi de Kepler, celle de la transformation de Bohlin ou Levi-Civita, et le théorème de Bertrand, conduisent à l'analyse du résultat d'un effondrement gravitationnel. Une analyse isochrone est développée pour caractériser un état de quasi-équilibre de systèmes auto-gravitants isolés, comme certains amas stellaires ou galaxies dynamiquement jeunes, à partir de propriétés orbitales de leurs étoiles ou contenu physique.

A l'échelle cosmologique, la dynamique de l'univers dépend de sa composition énergétique. Elle peut s'exprimer sous forme d'un système dynamique conservatif, bien connu en écologie pour décrire la dynamique de populations variées. Ce modèle dit de Lotka-Volterra est exploité pour décrire un espace-temps globalement homogène et isotrope, dont les composantes peuvent être en interaction non uniquement gravitationnelle. Dans cet univers jungle, des comportements dynamiques effectifs à grande échelle peuvent alors se développer.